CONVERSION OF C_5 HYDROCARBONS TO AROMATICS, CYCLIC OLEFINS, AND LIGHT HYDROCARBONS

NIPAT PEAMAROON

A THESIS SUBMITTED IN PARTIAL FULFILLMENT
OF THE REQUIREMENT FOR THE DEGREE OF
DOCTOR OF PHILOSOPHY IN APPLIED CHEMISTRY
FACULTY OF SCIENCE
KING MONGKUT'S INSTITUTE OF TECHNOLOGY LADKRABANG
2011

KMITL-2011-SC-D-010-027

หัวข้อวิทยานิพนธ์	การเปลี่ยนเพนเทนเป็นสารอะโรมาติกส์ ไซคลิกโอเลฟินส์และไฮโดรคาร์บอนเบา
นักศึกษา	นายนิภัทร เปี่ยมอรุณ
รหัสประจำตัว	49067151
ปริญญา	ปรัชญาดุษฎีบัณฑิต
สาขาวิชา	เคมีประยุกต์
พ.ศ.	2554
อาจารย์ผู้ควบคุมวิทยานิพนธ์	รศ.ดร. ตะวัน สุขน้อย

บทคัดย่อ

งานวิจัยนี้ศึกษาการเปลี่ยนเพนเทน ได้แก่ นอร์มัลเพนเทน ไอโซเพนเทน และไซโคลเพนเทนเป็นสารที่มีมูลค่าสูงขึ้น เพนเทนถูกเปลี่ยนเป็นอะโรมาติกส์ (BTX) ได้บนตัวเร่งปฏิกิริยาแกลเลียมและสังกะสีในซีโอไลต์ชนิด ZSM-5 ที่อุณหภูมิ 500 องศาเซลเซียส ในบรรยากาศของไฮโดรเจน โดยตำแหน่งกัมมันตร์ของโลหะในซีโอไลต์ (GaO^+/GaH_2 และ Zn/Zn^{2+}) สามารถกระตุ้นเพนเทน ด้วยปฏิกิริยาดีไฮโดรจีเนชัน แต่อย่างไรก็ตามกลไกการเกิดปฏิกิริยาขึ้นอยู่กับโครงสร้างของเพนเทน โดยหลังจากถูกกระตุ้นแล้วนอร์มัลและไอโซเพนเทนจะรวมเป็นกลุ่มโอเลฟินไฮโดรคาร์บอนที่มีโครงสร้างเป็นกิ่ง (branch hydrocarbon pool) ซึ่งจะเปลี่ยนเป็นสารประเภท C_1-C_4 จากนั้น C_1-C_4 จะรวมตัวกันเป็นกลุ่มไฮโดรคาร์บอนที่มีโครงสร้างคล้ายอะโรมาติกส์ (aromatics pool) ซึ่งจะถูกปลี่ยนเป็น BTX และอัลคิลอะโรมาติกส์ ส่วนไซโคลเพนเทนจะถูกเปลี่ยนเป็นกลุ่มโอเลฟินส์ไฮโดรคาร์บอนที่มีโครงสร้างเป็นวง (cyclic hydrocarbon pool) ซึ่งจะเปลี่ยนเป็นอะโรมาติกส์โมเลกุลใหญ่ ที่มีวง C_5 อยู่ในโครงสร้าง ในที่สุดจะถูกเปลี่ยนเป็น C_1-C_4 และ BTX ปริมาณอะโรมาติกส์สามารถเพิ่มขึ้นได้ด้วยการใช้ซีโอไลต์ที่มีอัตราส่วนระหว่างซิลิกอนและอะลูมิเนียมต่ำ เพราะจะทำให้โปรตอนและตำแหน่งกัมมันตร์ของโลหะอยู่ใกล้กัน โดยจะช่วยให้เกิดกลุ่มไฮโดรคาร์บอนซึ่งเป็นแหล่งของอะโรมาติกส์มากขึ้น อุณหภูมิที่ใช้ทำปฏิกิริยามีผลต่ออะโรมาติกส์ด้วย โดยหากทำปฏิกิริยาที่อุณหภูมิสูง (มากกว่า 500 องศาเซลเซียส) จะได้อะโรมาติกส์น้อยลง เพราะกลุ่มไฮโดรคาร์บอนจะถูกเปลี่ยนเป็น C_1-C_4 มากขึ้น ในสภาวะที่ไม่มีไฮโดรเจน GaO^+/Ga^+ ทำหน้าที่เป็นตำแหน่งกัมมันตร์ ที่มีความสามารถในการเร่งปฏิกิริยาสูงกว่า GaO^+/GaH_2 จึงได้อะโรมาติกส์มาก แต่ก็จะทำให้เกิดโค้กบนตัวเร่งปฏิกิริยามากขึ้นตามไปด้วย นอร์มัลเพนเทนถูกเปลี่ยนเป็นไซคลิกโอเลฟินส์ได้ด้วยปฏิกิริยาไซไคลเซชันบนตัวเร่งปฏิกิริยาแพลทินัมบนซิลิกา ที่อุณหภูมิ 500 องศาเซลเซียส เมื่อแคลไซน์ตัวเร่งปฏิกิริยาที่อุณหภูมิสูง (500 องศาเซลเซียส) พบว่าแพลทินัมสปีชีส์บางชนิดสามารถแพร่ลงไปในซิลิกาได้ ดังนั้นเพื่อให้มีโลหะแพลทินัมบนพื้นผิวซิลิกาในปริมาณมาก จึงต้องแคลไซน์ที่อุณหภูมิต่ำ (300 องศาเซลเซียส)

นอกจากนี้ยังพบว่ามีคลอไรด์ตกค้างอยู่ในตัวเร่งปฏิกิริยา การรีดิวส์ตัวเร่งปฏิกิริยาในบรรยากาศของแก๊สไฮโดรเจนที่อุณหภูมิสูง (500 องศาเซลเซียส) นอกจากจะช่วยทำให้เกิดโลหะแพลทินัมแล้วยังช่วยลดปริมาณคลอไรด์ นอกจากนี้ยังทำให้โลหะแพลทินัมรวมตัวเป็นกลุ่มขนาดใหญ่ ซึ่งมีผลให้ปฏิกิริยาไซไคลเซชันเกิดได้ดีขึ้น และเพื่อมิให้เกิดปฏิกิริยาไฮโดรจิโนไลซิส อุณหภูมิในการทำปฏิกิริยาต้องไม่เกิน 500 องศาเซลเซียส นอกจากนี้แก๊สไฮโดรเจนยังมีความจำเป็นต่อปฏิกิริยาเพราะช่วยเพิ่มการดูดซับเพนเทนและลดโค้กบนพื้นผิวของตัวเร่งปฏิกิริยา โครงสร้างของเพนเทนมีผลต่อปฏิกิริยา โดยพันธะคาร์บอน-คาร์บอนของไอโซเพนเทนที่มีความเกะกะในโครงสร้างถูกกระตุ้นได้น้อย ดังนั้นปฏิกิริยาไอโซเมอไรเซชัน ไซไคลเซชันและปฏิกิริยาไฮโดรจีโนไลซิส จึงเกิดได้น้อย ส่วนพันธะคาร์บอน-คาร์บอนของไซโคลเพนเทนสามารถถูกกระตุ้นและสามารถเปิดวงกลายเป็นนอร์มัลเพนเทนได้ ในปฏิกิริยาสุดท้ายนอร์มัลเพนเทนถูกเปลี่ยนเป็นไฮโดรคาร์บอนเบาด้วยปฏิกิริยาไฮโดรจีโนไลซิส ที่ 300 องศาเซลเซียส บนตัวเร่งปฏิกิริยาแพลทินัมบนไททาเนีย ซึ่งพบว่าโลหะแพลทินัมมีการกระจายตัวเป็นอย่างดี เมื่อแคลไซน์ตัวเร่งปฏิกิริยาที่อุณหภูมิต่ำ (300 องศาเซลเซียส) จะช่วยลดการแพร่ของแพลทินัมสปีชีส์ไปยังไททาเนีย ทำให้มีโลหะแพลทินัมบนพื้นผิวไททาเนียในปริมาณมาก แต่เมื่อรีดิวส์ตัวเร่งปฏิกิริยาที่อุณหภูมิสูง (500 องศาเซลเซียส) จะทำให้เกิดฟิล์มของ TiO_x ปกคลุมพื้นผิวของโลหะแพลทินัม ดังนั้นเพื่อป้องกันการเกิดฟิล์มดังกล่าวจึงต้องรีดิวส์ตัวเร่งปฏิกิริยาที่อุณหภูมิต่ำ (300 องศาเซลเซียส) อีกทั้งยังพบว่ามีคลอไรด์ ($TiCl_x$ และ/หรือ $PtCl_x$) ตกค้างอยู่ในตัวเร่งปฏิกิริยา ส่งผลให้ตัวเร่งปฏิกิริยามีความเป็นกรด และอาจมีผลต่อโลหะแพลทินัมให้ขาดอิเล็กตรอน จึงช่วยให้เกิดปฏิกิริยาไฮโดรจีโนไลซิสได้ดี นอกจากนี้แก๊สไฮโดรเจนยังมีความจำเป็นต่อปฏิกิริยา เพราะช่วยเพิ่มการดูดซับเพนเทนและลดโค้กบนพื้นผิวของตัวเร่งปฏิกิริยา โครงสร้างของเพนเทนมีผลต่อปฏิกิริยา โดยไอโซเพนเทนที่มีความเกะกะในโครงสร้างไม่ถูกดูดซับบนตัวเร่งปฏิกิริยา จึงไม่สามารถเกิดปฏิกิริยาได้ แต่ไซโคลเพนเทน ถูกดูดซับบนตัวเร่งปฏิกิริยาได้ดี ทำให้พันธะคาร์บอน-คาร์บอนถูกกระตุ้นและเปิดวงออกกลายเป็นนอร์มัลเพนเทน

Thesis Title	Conversion of C_5 to Aromatics, Cyclic Olefins, and Light Hydrocarbons
Student	Mr. Nipat Peamaroon
Student ID	49067151
Degree	Doctor of Philosophy (Ph.D.)
Program	Applied Chemistry
Year	2011
Thesis Advisor	Assoc. Prof. Dr. Tawan Sooknoi

ABSTRACT

This thesis has studied the conversion of pentanes (*n*-pentane, isopentane, and cyclopentane) to valuable products. Pentanes can be converted to aromatics (BTX) over GaZSM-5 and ZnZSM-5 catalysts at 500°C in H_2 atmosphere. With the dehydrogenation activity of GaO^+/GaH_2^+ or Zn/Zn^{2+}, pentanes are readily activated. However, the reaction pathway for aromatics formation depends on the structure of pentanes. After activation, *n*-pentane and isopentane would oligomerize to branch hydrocarbon pool that further cracks to C_1-C_4. The produced C_1-C_4 can be oligomerized to aromatics pool that further cracks to BTX and C_{9+} alkyl aromatics. Whereas, cyclopentane is primarily converted to cyclic hydrocarbon pool that further cracks to C_{9+} indane derivatives. The produced C_{9+} indane derivatives are later dealkelated/ cracked to C_1-C_4 and BTX. Higher aromatics content can be obtained by using low Si/Al ratio. This creates the proton and metal (Ga or Zn) sites proximity leading to higher aromatics source (hydrocarbon pool) formation. Moreover, high reaction temperature (> 500°C) can decrease the aromatics selectivity because the hydrocarbon pools prefer to crack to C_1-C_4. In the absence of H_2, GaO^+/Ga^+ would be the active sites whose possesses higher activity than that of GaO^+/GaH_2^+. Therefore, higher aromatics and coke formation are proportionally obtained. *n*-Pentane can be cyclized to cyclic olefins over Pt/SiO_2 catalyst at 500°C. After calcination at high temperature (500°C), some of Pt species can diffuse into silica. To obtained high available Pt metal surface; therefore, the Pt/SiO_2 must be calcined at low temperature (300°C). The chlorine species can be retained in the catalyst. The H_2 reduction at high temperature (500°C) is required not only for creating the active Pt metal but also chlorine scavenging. In addition, reduction at high temperature (500-650°C) would larger the Pt metal cluster that facilitates cyclization. To avoid hydrogenolysis, the reaction temperature would be kept not higher than 500°C. The H_2 is

required in the reaction to promote pentanes adsorption and reduce coke accumulation. The structure of pentanes can affect to the reaction. The C-C bond activation of isopentane (whose possesses the steric structure) may not be facilitated; therefore, lower isomerization and cyclization activities are obtained. While, C-C bond activation of cyclopentane can be facilitated leading to ring disclosure to *n*-pentane. In the last reaction, *n*-pentane can be stoichiometically hydrogenolyzed to light hydrocarbons over Pt/TiO_2 catalyst at 300°C. The small Pt clusters are highly dispersed over the support. After calcination at high temperature (500°C), some of Pt species can diffuse into titania. To obtained high available Pt metal surface; therefore, the Pt/TiO_2 must be calcined at low temperature (300°C). However, after reduction at high temperature, the TiO_x film can be generated covering the Pt metal leading to loss of active site and lower in activity. Therefore, reduction at low temperature (300°C) is required. The chlorine species can be retained in the catalyst likely in the form of $TiCl_x$ or $PtCl_x$ which possesses the acidity. This presumably affects to the Pt metal to be the electron deficient promoting hydogenolysis activity. In addition, the H_2 is required in the reaction to promote pentanes adsorption and reduce coke accumulation. The structure of pentanes also affect to the hydrogenolysis reaction. Isopentane with its steric structure cannot adsorb over the catalyst; therefore, no further reaction can be taken place. While, cyclopentane is able to adsorb. Its C-C bond activation is facilitated leading to ring disclosure to *n*-pentane.

ACKNOWLEDGEMENTS

I would like to thank my advisor, Assoc. Prof. Dr. Tawan Sooknoi for his supervisions in catalysis, skill coaching, helpful suggestions, encouragements, and patience for any mistakes and doubtfulness. I am also grateful to Asst. Prof. Dr. Vanchat Chuenchom, Dr. Sutha Sutthiruangwong, Assoc. Prof. Dr. Nurak Grisdanurak, and Asst. Prof. Dr. Siriporn Jongpatiwut for serving as the chairperson and the committee, and valuable comments.

I wish to thank Prof. Dr. Jumras Limtrakul and Asst. Prof. Dr. Piboon Pantu for their help in temperature programmed desorption-mass spectrometry, Dr. Wantana Klysubun for her help in X-ray absorption spectroscopy.

I would like to thank all of my teachers and my colleague for the impressive supports and encouragements.

Sincere thanks are due to Rambhai Barni Rajabhat University for giving me a higher educational development scholarship to continue this degree. I acknowledge the SCG chemicals Co., Ltd. for additional financial support.

The support in work place, equipments, chemicals, and public utilities are obtained form the Faculty of Science, King Mongkut's Institute of Technology Ladkrabang with a kindly assist from the officers.

I wish to express thanks to my parent and younger sister for their constant supports and encouragements.

Nipat Peamaroon

CONTENTS

CONTENTS (Continued)

CONTENTS (Continued)

CONTENTS (Continued)

CONTENTS (Continued)

LIST OF TABLES

Table **Page**

CHAPTER 2

CHAPTER 3

CHAPTER 4

CHAPTER 5

LIST OF TABLES (Continued)

Table **Page**

LIST OF FIGURES

Figure **Page**

CHAPTER 2

CHAPTER 3

LIST OF FIGURES (Continued)

Figure **Page**

CHAPTER 4

LIST OF FIGURES (Continued)

LIST OF FIGURES (Continued)

LIST OF FIGURES (Continued)

LIST OF FIGURES (Continued)

LIST OF FIGURES (Continued)

APPENDIX B

CHAPTER 1

INTRODUCTION

1.1 Statement and significant problems

Nowadays, the consumption of hydrocarbon energy for vehicles and industries has been greatly increased. These affect to the petroleum stock that has been decreased annually [1,2,3]. Moreover, the petrochemical feed stocks which are normally based on such petroleum resource are also proportionally reduced. Many efforts are made to produce additional hydrocarbons from other sources, in particular the biomass. However, oxygen content in such resource may lead to a difficulty for the production of some petrochemicals.

In fact, there are futile hydrocarbons in recycled stream that can be converted into other valuable petrochemical feedstock. These include C_5 hydrocarbons stream from the fractionation of naptha cracking unit. Such C_5 hydrocarbons referred to *n*-pentane, isopentane and cyclopentane, are being used as blending to gasoline and input for synthesis gas production. Typically, *n*-pentane possesses low research octane number (61.7) and hence its usage is rather limited. Isopentane gives high research octane number (92.3); nevertheless, it increases gasoline volatility (RVP of *n*-pentane = 15.6; RVP of isopentane = 20.4) which may be a factor for limiting the use of isopentane as gasoline blender. Although cyclopentane showed an octane number higher than that of *n*-pentane and isopentane (as shown below [4,5]), its value may be too high to be used in actual engines. Therefore, the large amounts of C_5 hydrocarbons are still remained in recycle stream.

C_5 Hydrocarbons	RON	RVP	B.P. (^{o}C)
n-Pentane	61.7	15.6	36.1
Isopentane	92.3	20.4	27.7
Cyclopentane	101.3	9.9	49.0

Accordingly, it is of great interest to convert these C_5 hydrocarbons into other valuable hydrocarbons such as aromatics (benzene, toluene, and xylene), cyclic olefins (cyclopentene and cyclopentadiene) and light hydrocarbons (methane, ethane, propane and butane).

Due to a relatively high stability of such C_5 saturated hydrocarbons, a catalyst that possesses acidic and/or dehydrogenating function is required to activate C-C and C-H cleavages. Among heterogeneous catalyst, zeolite and supported metal surface are the most attractive [6]. The advantages of zeolites are its porous and modifiable structure. Acidic zeolite exhibites high activity for converting paraffinic hydrocarbons to aromatics via complex reactions of carbocation such as dehydrogenation, oligomerization, isomerization, disproportionation, cracking, and cyclization reaction [7,8]. Moreover, dehydrogenation activity can be improved after metal (especially Ga and Zn) incorporation and higher aromatics yield can be achieved [9,10]. Alternatively, metal (i.e., Pt) supported on the inert supports (i.e., silica (SiO_2) and titania (TiO_2)) are able to convert paraffinic hydrocarbons to various olefins by dehydrogenation [11,12,13], and also promotes cracking, isomerization, cyclization and hydrogenolysis via akylidyne intermediates [6,14]. Without acid sites on the support, the catalyst would selectively give no high molecular weight products. It is expected that C_5 hydrocarbons can be readily activated and converted to aromatics, cyclic olefins or light hydrocarbons depending on a particular designed catalyst.

In this thesis, ZSM-5 is chosen because of its shape selectivity toward aromatics formation [15]. The gallium and zinc metals are incorporated with HZSM-5 as a bifunctional catalyst to enhance aromatics formation. To convert C_5 hydrocarbons to cyclic olefins and light hydrocarbons, Pt/SiO_2 and Pt/TiO_2 are employed, respectively. The active sites responsible to the observed activity will be studied and proposed. Reaction pathways of C_5 isomers transformation over such catalysts will be investigated. The effect of C_5 structure on the reaction pathway will also be discussed.

1.2 Objectives

1.2.1 To understand the nature of active sites, especially Ga species responsible to the aromatics formation.

1.2.2 To understand the reaction pathway of C_5 hydrocarbons conversion to aromatics over GaZSM-5 and ZnZSM-5 catalysts.

1.2.3 To understand the nature of Pt sites over the SiO_2 and TiO_2 which are responsible to the catalytic activity.

1.2.4 To understand the reaction pathway of C_5 hydrocarbons conversion to cyclic olefins and light hydrocarbons over Pt/SiO_2 and Pt/TiO_2 catalysts.

1.2.5 To understand the effect of reaction condition including temperature and H_2 partial pressure on the reaction of C_5 hydrocarbons conversion over GaZSM-5, Pt/SiO_2 and Pt/TiO_2.

1.3 Scope of the study

1.3.1 C_5 hydrocarbons conversion over metal loaded zeolite

1.3.1.1 Preparation of the catalysts by modification of HZSM-5 zeolite (Si/Al = 28, 45, 180, and 500) with gallium and zinc by impregnation method using gallium (III) nitrate and zinc (II) nitrate as metal precursors.

1.3.1.2 Characterization of the GaZSM-5 and ZnZSM-5 catalysts using X-ray powder diffraction (XRD), scanning electron microscopy-energy dispersive analysis (SEM-EDX), Inductively Coupled Plasma-Atomic Emission Spectroscopy (ICP-AES), gas adsorption analyzer, temperature programmed reduction (H_2-TPR), temperature programmed ammonia desorption (NH_3-TPD), and temperature programmed hydrogen evolution (TPHE).

1.3.1.3 Catalytic activity testing of the GaZSM-5 and ZnZSM-5 i.e., study effect of reactant structure, contact time, reaction pathway, Si/Al ratio of catalyst, reaction and reduction temperature, and H_2 partial pressure.

1.3.2 C_5 hydrocarbons conversion over Pt supported catalysts

1.3.2.1 Preparation of the Pt/SiO_2 and Pt/TiO_2 catalysts by impregnation of chloroplatinic acid ($H_2PtCl_6 \cdot 6H_2O$) onto SiO_2 and TiO_2.

1.3.2.2 Characterization of the Pt/SiO_2 and Pt/TiO_2 catalysts using X-ray powder diffraction (XRD), transmission electron microscopy (TEM), X-ray fluorescent spectrometry (XRF), gas adsorption analyzer, temperature programmed reduction (H_2-TPR), temperature programmed ammonia desorption (NH_3-TPD), temperature programmed pyridine desorption (Pyd-TPD), temperature programmed chlorine desorption (Cl_2-TPD), thermal gravimetric analyzer (TGA), electron spin resonance spectroscopy (ESR), and X-ray absorption near edge spectroscopy (XANES).

1.3.2.3 Catalytic activity testing of the Pt/SiO_2 and Pt/TiO_2 i.e., study the effect of contact time and reaction path way using *n*-pentane as modeled feed, effect of reaction temperature, H_2 partial pressure, and reactant structure.

1.3.2.4 Characterization of the coke formed after reaction by thermogravimetric analyzer (TGA) and temperature programmed desorption-mass spectrometry (TPD-MS).

1.4 Expected results

1.4.1 This research would be guidance for converting C_5 hydrocarbons to aromatics, cyclic olefins and light hydrocarbons in industrial application.

1.4.2 This C_5 hydrocarbons conversion would be an example for converting other saturated hydrocarbons to aromatics, cyclic olefins and light hydrocarbons demanded for various petrochemical industries.

1.5 Overview of this thesis

This thesis has studied the catalytic processes for converting the low-value C_5 alkanes, as *n*-pentane, cyclopentane and isopentane to aromatics (BTX), cyclic olefins (cyclopentene and cyclopentadiene) and light hydrocarbons (methane, ethane, propane, butane) which are valuable products. To produce aromatics, the Ga and Zn metals incorporated with a shape selective HZSM-5 zeolite are employed, as it has been reported the high dehydrogenation and aromatization activities of these metal species [9,10]. Whereas, these zeolite catalysts cannot produce cyclopentene and cyclopentadiene because the olefins can readily undergo isomerization and cracking over acid sites. Moreover, low yield of light hydrocarbon could be obtained over zeolite catalyst because the other products are competitively formed over acid sites. To avoid any acidity, inert support such as silica and titania are employed as support for Pt metal that has been reported to possess high dehydrocyclization and hydrogenolysis activities [12,13]. *n*-Pentane is preliminary used as a modeled feed together with cyclopentane and isopentane for production of cyclic olefins and light hydrocarbons over these Pt supported catalysts.

General information of all pentane reactants is given in CHAPTER 2. The theory concepts of zeolite and metal surface catalysis are also reviewed together with some related literatures.

In CHAPTER 3, the experimental procedures are mentioned step by step from the catalyst preparation, catalyst characterization, catalytic activity testing, and analysis of products and coke in the catalysts. The reactor set up and the analytical processes are explained schematically in details.

Conversions of pentanes to aromatics over GaZSM-5 and ZnZSM-5 catalysts are discussed in CHAPTER 4. Before activity testing, an elemental analysis is performed by ICP/AES techniques to obtain the Ga and Zn loading (~0.7 wt.%). Moreover, XRD, SEM, and BET surface area of such catalysts are also examined. To observe the reducible metal oxide

species in the catalysts, TPR is performed. For GaZSM-5 and ZnZSM-5, the obtained reduction peaks can be related to the type of metal oxide species (Ga_2O_3, GaO^+, Ga^+, and ZnO) presented in the catalyst. Accordingly, the active site of the catalyst can be estimated. After metal loading, the acid site of HZSM-5 would be decreased because the metal can be located at the exchangeable site of zeolite. The NH_3-TPD is employed to speculate the acidity and acid strength of such zeolite catalysts. In the activity testing, conversion of pentanes over HZSM-5 (support) is primarily examined. The role of acid site and pore size of zeolite on the *n*-pentane, isopentane, and cyclopentane conversion are discussed together with their products distribution. Then, the conversion of pentanes over GaZSM-5 and ZnZSM-5 is performed. The role of metal species on the aromatics formation depending on the structure of pentanes is discussed. To validate the reaction pathway, conversion of pentanes with different contact time is performed. Subsequently, the reaction pathways for *n*-pentane, isopentane, and cyclopentane conversion to aromatics are proposed. For characterization of the high molecular weight (hydrocarbon pool) formed during the aromatics formation, the FTIR of the extract from the used catalyst and TPD-MS are performed. The effect of Si/Al ratio of the catalyst, reaction temperature, reduction temperature, and H_2 partial pressure on the aromatics formation are discussed in details.

Conversion of pentanes to cyclic olefins over Pt/SiO_2 catalysts are discussed in CHAPTER 5. The Pt/SiO_2 is characterized for elemental analysis, surface area, crystal structure, and morphology. The reducible platinum oxide species obtained after calcination are examined by TPR. The Cl_2-TPD-MS and TGA are employed as well as ESR technique to speculate the chlorine species retained in the catalyst. The NH_3-TPD and pyridine-TPD are employed to depict the acid sites. The catalytic activity of the Pt/SiO_2 is examined in a fixed bed flow reactor. The role of Pt metal on *n*-pentane conversion to cyclic olefins is discussed. The *n*-pentane conversion over Pt/SiO_2 with different contact time is performed. The reaction pathway for *n*-pentane conversion to cyclic olefins is proposed. Effect of calcination temperature, reaction temperature, reduction temperature, and H_2 partial pressure are discussed. To speculate the high molecular weight compounds formed during the reaction, TPD-MS and TGA are examined. Moreover, isopentane and cyclopentane conversion over this catalyst are tested to observe the effect of feed structure on the catalytic activity and product selectivity.

Hydrogenolysis of pentanes over Pt/TiO_2 to light hydrocarbons is investigated in CHAPTER 6. The Pt/TiO_2 is characterized for elemental analysis, surface area, crystal structure, and morphology. The platinum oxide species obtained after calcination are examined by TPR and

XANE. The Cl_2-TPD-MS, TGA and XANE are employed to speculate the chlorine species retained in the catalyst. The pyridine-TPD is employed to depict the acid sites. The catalytic activity of the Pt/TiO_2 is examined in a fixed bed flow reactor. The role of Pt metal on *n*-pentane hydrogenolysis is discussed. The *n*-pentane conversion over Pt/TiO_2 with different contact time is performed. The reaction pathway for *n*-pentane hydrogenolysis is proposed. Effect of calcination temperature, reaction temperature, reduction temperature, and H_2 partial pressure are discussed. To speculate the high molecular weight compounds formed during the reaction, TPD-MS and TGA are examined. Moreover, isopentane and cyclopentane conversion over this catalyst are tested to observe the effect of feed structure on the catalytic activity and product selectivity.

1.6 References

[1] International Energy Agency (IEA). 2009. "Oil Market Report."

[2] U.S. Department of Energy. 2009. "International Energy Outlook."

[3] World Energy Council. 2004. "Survey of Energy Resource."

[4] Dessau, R.M. "Upgrading of normal pentane to cyclopentene." U.S. Patent no. 5284986, February 1994.

[5] Dessau, R.M. "Upgrading of normal pentane to cyclopentane." U.S. Patent no. 5283385, February 1994.

[6] Gates, B.C. 1992. **Catalytic chemistry.** New York: John Wiley & Son.

[7] Guisnet, M., and Gnep, N.S. 1996. "Mechanism of short-chain alkane transformation over protonic zeolites. Alkylation, disproportionation and aromatization." **Applied Catalysis A: Ganeral.** 146: 33-64.

[8] Sanati, M., Hornell, C., and Jaras, S.G. 1999. "The oligomerization of alkenes by heterogeneous catalysts." **Catalysis.** 14: 236-287.

[9] Caeiro, G., Carvalho, R.H., Wang, X., Lemos, M.A.N.D.A., Lemos, F., Guisnet, M., and Ribeiro, F.R. 2006. "Activation of C_2-C_4 alkanes over acid and bifunctional zeolite catalysts." **Journal of Molecular Catalysis A: Chemical.** 255: 131-158.

[10] Guisnet, M., and Gnep, N.S. 1996. "Mechanism of short-chain alkane transformation over protonic zeolites. Alkylation disproportionation and aromatization." **Applied Catalysis A: General.** 146: 33-64.

[11] Cortright, R.D., and Dumesic, J.A. 1995. "L-zeolite-supported platinum and platinum/tin catalysts for isobutene dehydrogenation." **Applied Catalysis A: General.** 129: 101-115.

[12] Davis, B.H. 1999. "Alkane dehydrocyclization mechanism." **Catalysis Today.** 53: 443-516.

[13] Wang, Y., and Davis, B.H. 2005. "Effect of pressure on H/D exchange during n-octane conversion with Pt-SiO2 catalysts." **Applied Catalysis A: General.** 289: 28-36.

[14] Hagen, J. 2006. **Industrial Catalysis.** Weinheim: WILEY-VCH Verlag GmbH & Co. KGaA.

[15] Bartholomew, C.H., and Farrauto, R.J. 2006. **Fundamentals of industrial catalytic processes.** New York: John Wiley & Son.

CHAPTER 2

THEORY AND LITERATURE REVIEW

This chapter provides the general information of related background and knowledge of catalysis which are important for this thesis. The topics mention about the physical properties of pentanes, background of catalysis, catalysis by zeolite, catalysis by metal surface, and literature review.

2.1 Physical Properties of pentane isomers

Pentane alkanes which are reactants for the aromatization, dehydrocyclization, and hydrogenolysis are saturated hydrocarbons with five carbons composition. Their boiling points are not too high and not too low (in the range of 35-50 ^{o}C). Other physical properties are summarized in Table 2.1., and the explosive limits of these C_5 are summarized in APPENDIX A.

Table 2.1 Physical properties of *n*-pentane, isopentane, and cyclopentane [1, 2, 3].

C_5	*n*-pentane	isopentane	cyclopentane
Formula	C_5H_{12}	C_5H_{12}	C_5H_{10}
Chemical structure	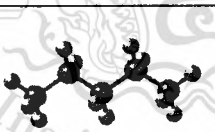		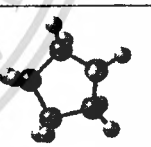
Molar mass (g/mol)	72.15	72.15	70.1
Appearance	Colorless liquid	Colorless liquid	Colorless liquid
Density (g/cm^3)	0.626	0.616	0.751
Melting point (^{o}C)	-129.8	-159.9	-94.0
Boiling point (^{o}C)	36.1	27.7	49.0
Vapor pressure at 20^{o}C (mmHg)	440	570	250

2.2 Catalysis: general background

The rates of many reactions are influenced by the presence of a substance called catalyst which remains unchanged at the end of the process [4]. In 1836 the reaction related to the catalyst were classified by the Swedish chemist, Jon Jakob Berzelius (1779-1848) under the title of catalysis. It is convenient to classify catalyzed reaction according to whether they occurred homogeneously (in a single phase) or heterogeneously (at an interface between two phase).

Various definitions of catalysis have been proposed. An early definition, suggested in 1895 by Wilhelm Ostwald (1853-1932), was that a catalyst is "any substance that alters the velocity of a chemical reaction without modification of the energy factors of the reaction". Another definition is that "a catalyst alters the velocity of a chemical reaction and is both a reactant and a product of the reaction". These definitions were intended to exclude substances that accelerated the rate of a reaction by entering into reaction, thus disturbing the position of equilibrium; such substances are reactants in the ordinary sense. The most satisfactory definition of a catalyst is "a substance that increases the rate of a reaction without modifying the overall standard Gibbs energy change in the reaction".

Although by definition the amount of a catalyst must be unchanged at the end of the reaction, the catalyst is invariably involved in the chemical process. In the case of a single reacting substance (R_1), a complex may be formed between this reactant and the catalyst (R_1--C). If there is more than one reactant, the complex may involve one or more molecules of substance combined to the catalyst. These complexes are formed only as intermediates and decompose to give the products of the reaction (P), with the regeneration of the catalyst molecule (C) [5], as shown in Figure 2.1.

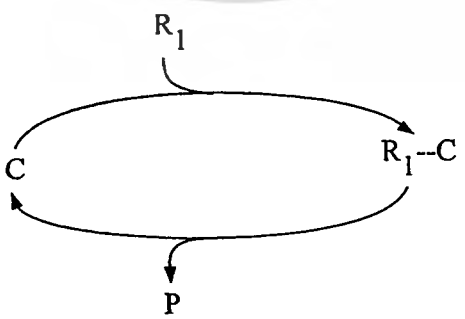

Figure 2.1 Catalytic cycle for the reaction $R_1 \rightarrow P$.

Since the catalyst is unchanged at the end of the reaction, it gives no energy to the system; therefore it can have no influence on the position of equilibrium. It follows that since the equilibrium constant K_c is, at equilibrium, the ratio of the rate constants in the forward and reverse directions (i.e., $K_c = k_1/k_{-1}$), a catalyst must influence the forward and reverse rates in the same proportion.

The activation energy of a catalyzed reaction is almost always lower than that of the same reaction when it is uncatalyzed [6]. In other word, catalysts generally work by permitting the reaction to occur by another reaction path that has lower energy barrier. This is shown schematically in Figure 2.2.

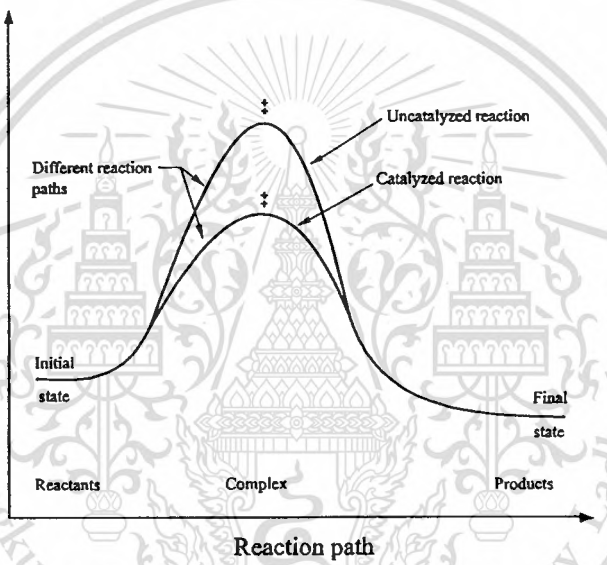

Figure 2.2 Action of a catalyst.

The suitable catalyst depends on these three properties. These are activity, selectivity, and stability (deactivation behavior) of the catalysts [7].

2.2.1 Activity

Activity is a measure of how fast of one or more reaction proceed in the presence of the catalyst. Activity can be defined in terms of kinetics or more practical viewpoint, such as reaction rate (r), rate constant (k) and activation energy (E_a).

In practice, readily determined measures of activity are often sufficient. For comparative measurements, such as catalyst screening, determination of process parameters,

optimization of catalyst production conditions, and deactivation studies, the following activity measures can be used:

2.2.1.1 Conversion under constant reaction conditions

Catalysts are often investigated in continuously operated test reactors, in which the conversions attained at constant space velocity are compared. The conversion (X_A) is the ratio of the amount of reactant A that has reacted to the amount that was introduced into the reactor. For batch reactor, conversion of reactant A is defined as in Eq. (2.1).

$$X_A = \frac{n_{A0} - n_A}{n_{A0}} \quad \text{(mol/mol or \%)} \tag{2.1}$$

Where, n_{A0} = mole of reactant A at initial

n_A = mole of reactant A at final

2.2.1.2 Space velocity for a given constant conversion

The space velocity is the volume flow rate V_0, relative to the catalyst mass m_{cat}, as in Eq. (2.2). If the catalyst mass is replaced with the catalyst volume, then the space velocity is proportional to the reciprocal of the residence time (Eq. (2.3)).

$$\text{Space velocity} = \frac{V_0}{m_{cat}} \quad (m^3\, kg^{-1}\, s^{-1}) \tag{2.2}$$

$$\text{Residence time} = \frac{V}{V_0} \quad (s) \tag{2.3}$$

Figure 2.3 compares two catalysts with different activity. It is found that at a given space velocity, catalyst A is better than catalyst B.

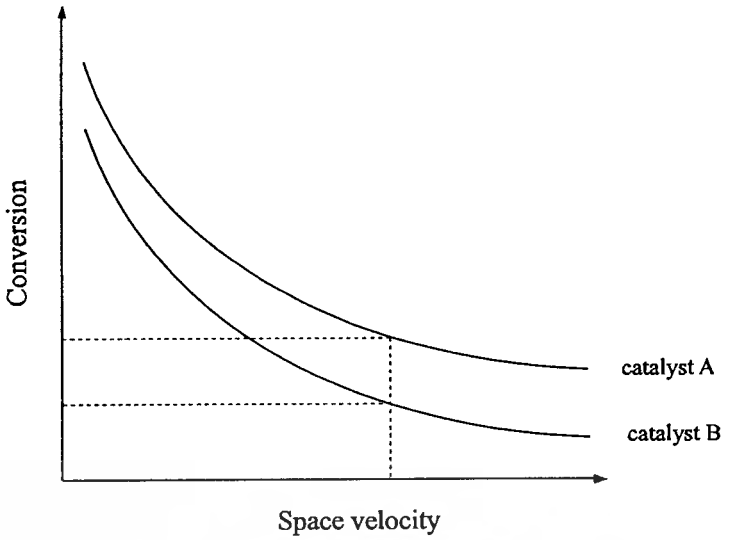

Figure 2.3 Comparison of catalyst activities.

2.2.1.3 Space-time yield

Often the performance of a reactor is given relative to the catalyst mass or volume, so that reactors of different size or construction can be compared with one another. This quantity is known as the space time yield, STY.

$$STY = \frac{\text{Desired product quantity}}{\text{Catalyst volume} \cdot \text{time}} \quad (\text{mol } L^{-1} h^{-1}) \qquad (2.4)$$

2.2.1.4 Temperature required for a given conversion

Determination of the temperature required for a given conversion is another method of comparing catalysts. The best catalyst is the one that gives the desired conversion at a lower temperature. This method can not, however, be recommended since the kinetics are often different at higher temperature, making misinterpretations likely. This method is better suited to carry out deactivation measurements on catalysts in pilot plants.

2.2.1.5 Turn over frequency

The turnover frequency (TOF) quantifies the specific activity of a catalytic center for a special reaction under defined reaction conditions by the number of molecular reactions or catalytic cycles occurring at the center per unit time. For heterogeneous catalysts the number of active centers is derived usually from sorption methods.

$$TOF = \frac{\text{volumetric rate of reaction}}{\text{number of centers / volume}} \quad (\text{time}^{-1}) \qquad (2.5)$$

2.2.2 Selectivity

In the catalytic process, not only desired product (P) can be occurred, but the side products (P_1,P_2) can also be taken place, as shown in Figure 2.4.

Figure 2.4 General chemical reactions.

The selectivity of product P is the fraction of the starting material that is converted to the desired product P. It is expressed by the ratio of the amount of desired product P to the reacted quantity of a reaction partner A. Since this quantity compares starting materials and products, the stoichiometric coefficients (v_i) of the reactants must be taken into account, which gives rise to the following equation.

$$S_p = \frac{n_p / v_p}{(n_{A0} - n_A)/|v_A|} \quad (\text{mol/mol or \%}) \qquad (2.6)$$

In comparative selectivity studies, the reaction conditions of temperature and conversion or space velocity must be kept constant.

2.2.3 Stability

The chemical, thermal, and mechanical stability of a catalyst determines its lifetime in industrial reactors. Catalyst stability is influenced by numerous factors, including decomposition, coking, and poisoning. Catalyst deactivation can be followed by measuring activity or selectivity as a function of time.

Catalysts that lose activity during a process can often be regenerated before they ultimately have to be replaced. The total catalyst lifetime is of crucial importance for the economics of a process.

Today the efficient use of raw materials and energy is of major importance, and it is preferable to optimize existing processes than to develop new ones. For various reasons, the target quantities should be given the following order of priority:

Selectivity > Stability > Activity

2.3 Catalysis by shape selective zeolites

Shape selective catalysis differentiates between reactants, products, or reaction intermediates according to their shape and size. If almost all of the catalytic sites are confined within the pore structure of a zeolite and if the pores are small, the transformation of reactant molecules and the probability of forming products molecules are determined by molecular dimensions and configurations as well as by the types of catalytically active sites present. Only molecules whose dimensions are less than a critical size can enter the pores, have access to internal catalytic sites, and react there [8, 9]. Furthermore, only molecules that can leave appear in the final product [8, 9]. Shape selective catalysis can be used to increase yield of desired products or to hinder undesirable reactions.

The phenomenon of shape selectivity can be distinguished into three types, depending on whether pore size limits the entrance of the reacting molecule, the departure of the product molecule, or the formation of certain transition state [9]:

(1) Reactant selectivity occurs when some of the molecules in a reactant mixture are too large to diffuse through the catalyst pores (Figure 2.5(a)).

(2) Product selectivity occurs when some of the products formed within the pores are too bulky to diffuse out as observed products. They are either converted to less bulky molecules (e.g., by equilibration or cracking) or eventually deactivate the catalyst by blocking the pores (Figure 2.5(b).

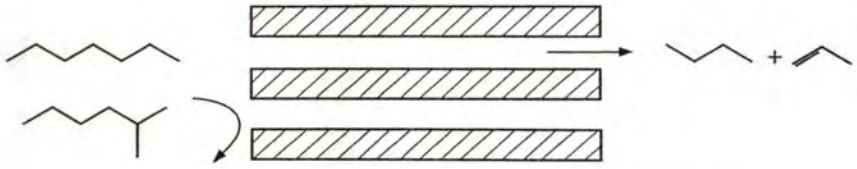

(a) Reactant selectivity

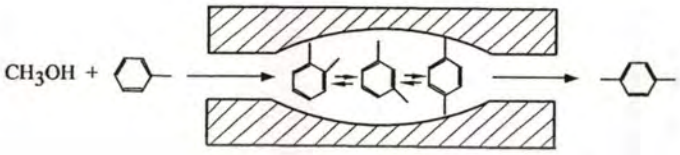

(b) Product selectivity

Figure 2.5 (a) Reactant and (b) product selectivities [10].

(3) Restricted transition state selectivity occurs when certain reactions are prevented because the corresponding transition state would require more space than available in the cavities or pores. Reactions requiring smaller transition state proceed unhindered (Figure 2.6).

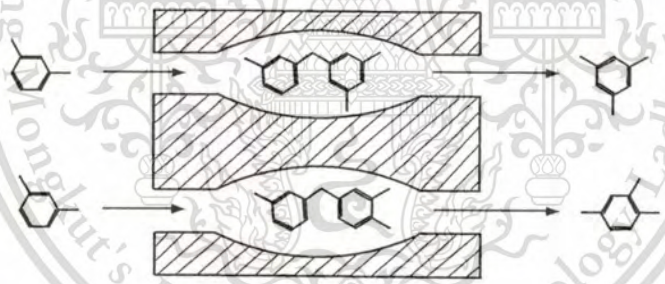

Figure 2.6 Restricted transition state selectivity [10].

2.3.1 Zeolite

Most shape selective catalysts today are molecular sieve zeolites. Zeolites are porous aluminosilicate crystalline materials [7,8,10]. They have the chemical formula of $M_{2/n}OAl_2O_3 \cdot xSiO_2 \cdot yH_2O$, where the charge balancing non-framework cation (M) has valence n, x is 2 or more, and y is the mole of water in the voids. The Al and Si tetrahedral atom, or T atoms form a three dimensional (3D) framework of AlO_4 and SiO_4 tetrahedra linked by bridging oxygen. Although an SiO_4 is charge balanced, an AlO_4 tetrahedra has a negative charge balanced by a

positive charge on M. Related pure SiO_2 frameworks such a silicalite-1 (MFI), are charge balanced and do not need non-framework cation.

The geometrical arrangement of the T atoms relative to each other forms a secondary structure superposed on the primary tetrahedron structure. Because the T atoms are interlinked by bridging oxygen atoms rings of alternating T and oxygen atoms are formed. Zeolites can be considered to be structured assemblies of such rings. Because of the large variation in ring sizes and possible ways of connecting them, numerous structures can be formed (so far 133 structures have been reported) [11]. The arrangement of the rings may give rise to pores and cages, as can be seen in Figure 2.7 which represents the frameworks of zeolites.

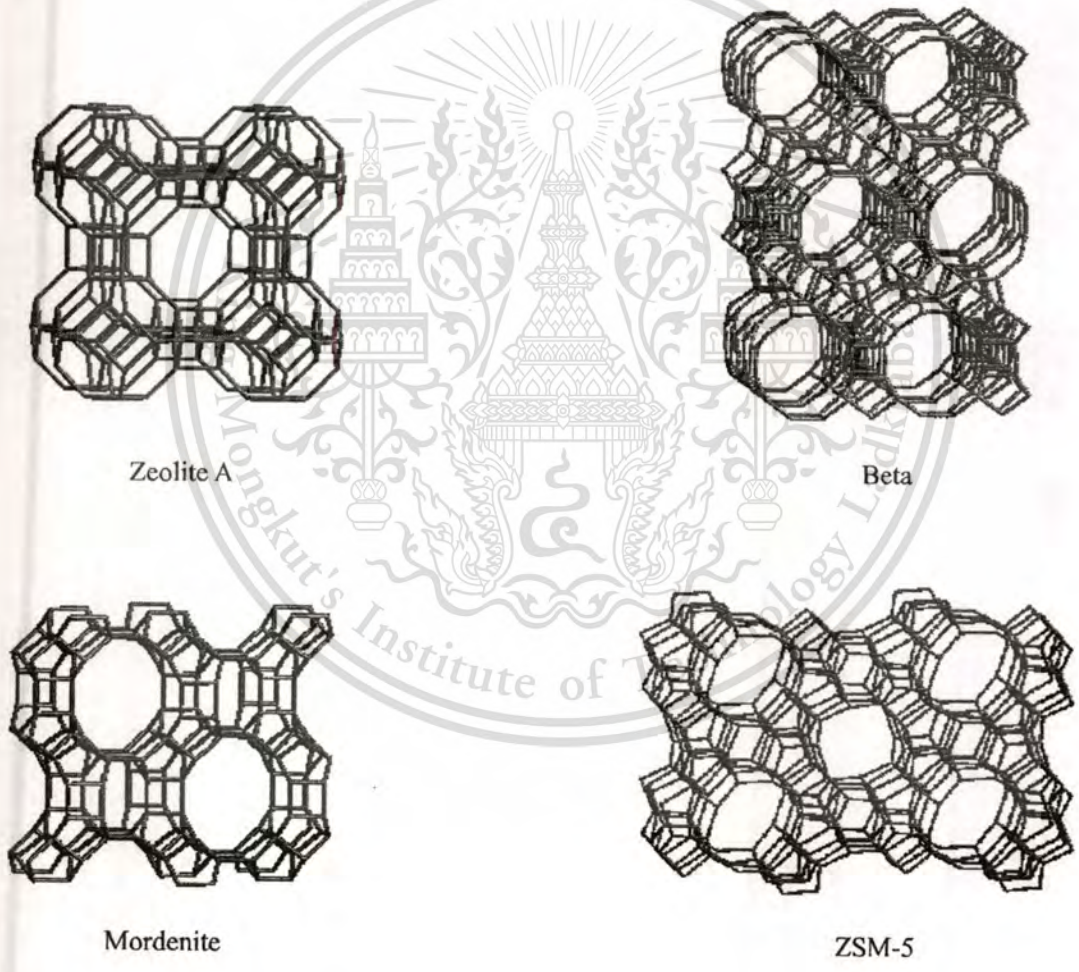

Figure 2.7 Example of zeolite structures [12].

Variants involve Ge substitution for Si in the framework or involve substitution of Ga, Fe, Co, Mn, Zn, Ti, or Mg for Al. In the related aluminophosphates ($AlPO_4$), each negatively charged AlO_4 tetrahedron is balanced by positively charged PO_4 tetrahedron, and non-framefork cations are not needed. Still other variants include the silicoaluminophosphate (SAPO) structures in which Si substitutes some P in the $AlPO_4$ framework; each added Si needs a non framework cation to balance the charge on the framework.

Zeolites have four properties which make them interesting and valuable for heterogeneous catalysis [9]: (1) they have exchangeable cations, allowing the introduction of different cations with various catalytic properties; (2) if these cationic sites are exchanged to H^+, they can have a very high number of very strong acid sites; (3) they have pore diameters with one or more discrete sizes; and (4) they have pore diameters that are in the order of molecular dimension, i.e., less than 1 nm. Properties 1 and 2 account for catalytic activity and properties 3 and 4 are responsible for the molecular sieving action.

Pore diameters in molecular sieves depend on the number of tetrahedra in a ring (Table 2.2). Zeolites with 8 tetrahedra are commonly called small-pore zeolites, those with 10 tetrahedra are medium-pore, and those with 12 tetrahedra are large-pore zeolites. Most industrial applications of shape selectivity today employ medium-pore zeolites. If the plane of the ring is not perpendicular to the axis of the pore, or if the elements forming the ring are not in the same plane (i.e, puckered) then the pore diameter is less than the possible maxima shown in Table 2.2.

Table 2.2 Pore diameter of zeolites [10].

Number of tetrahedra in a ring	Maximum diameter, Å	Example
6	2.8	
8	4.3	Erionite, A, P, Rho
10	6.3	ZSM-5, Ferrierite
12	8.0	L, X, Y, Beta
18	15	ALPO-VPI
20	18	Cloverite

The actual pore size also depends on the type of cation present [9]. Type A sieves have cubic structure with pores just about big enough to allow normal paraffins through. Cations, however, occupy positions which block part of the pores. Monovalent cations (e.g., sodium, potassium) reduce the actual pore size to below ~0.4 nm. With the exception of methane, no organic molecule can penetrate Li-A or Na-A zeolites. Divalent cations, however, occupy only every other cationic site and leave enough space for normal paraffins to diffuse through. Isobutane is slightly larger than normal butane and therefore cannot enter Ca-A (Figure 2.8).

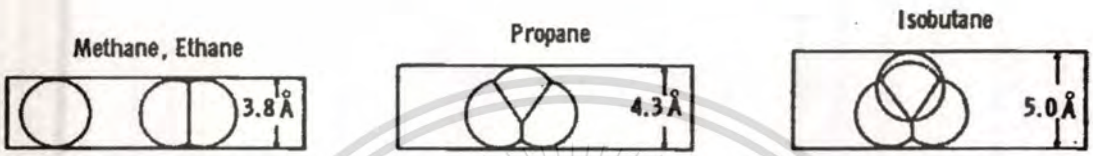

Figure 2.8 Molecular diameters [10].

At higher temperatures the pores enlarge slightly and the diffusing molecules have higher kinetic energy to overcome repulsion forces at pore entrances. These, and molecular vibration allow molecules to wiggle through somewhat narrower pores than expected. Thus, dimensions presented within two decimal points are not meaningful; molecules about 5 Å too large can sometimes make their way through pores because they (and the atoms forming the pores) vibrate. In addition, bond cleavage, followed by reconstruction of the broken bond could facilitate the diffusion of larger molecules through narrow pores [9].

One medium-pore size zeolite family is called "pentasils" because their framework is composed of five-member oxygen rings, and because they can contain more silicon than most other zeolites. ZSM-5 is by far the most important member of the pentasil family because of its catalytic activity, stability, acid strength, many commercial applications, and other remarkable properties. It would not be an exaggeration to say that today commercial shape selective catalysis is the catalysis of ZSM-5.

The structure of ZSM-5 is described by Kokotailo, Lawton, and Olson [13] and Olson, Haag, and Lago [14]. Thomas et al. and Dominguez, Acosta, and Schifter have published high resolution electron microscope images of ZSM-5 together with selected area diffraction studies which show that ZSM-5 has a high degree of crystallinity and a uniform pore distribution [15,16,17,18].

ZSM-5 and silicalite (related pentasil zeolite with a very high silica/alumina ratio) have two types of pores. Both are composed of ten membered rings. One is sinusoidal with a nearly circular cross section (5.4 Å x 5.6 Å). The other system has elliptical pores (5.2 Å x 5.8 Å). These are straight and perpendicular to the first system (Figure 2.9) [19,20].

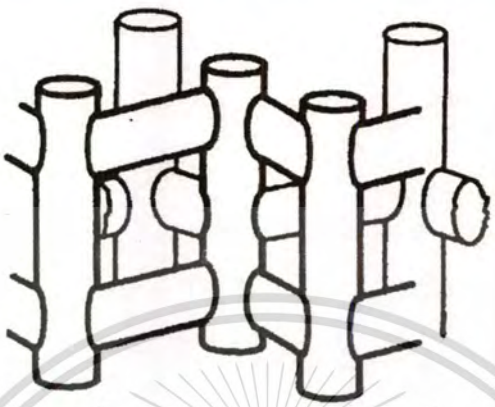

Zig-Zag Channels = 5.4 Å × 5.6 Å
Straight Channels = 5.2 Å × 5.8 Å

Figure 2.9 The pore structure of ZSM-5.

The silica/alumina ratio in ZSM-5 varies from the teens to the thousands. High silica/alumina ratios have several important consequences: hydrophobicity, very strong acid strength, thermal stability, and acid stability. Hydrophobicity depends on the aluminum concentration and it is independent of the structure. Very low alumina ZSM-5 and silicalite are therefore more hydrophobic than most other crystalline and amorphous oxide catalysts. Acid sites are associated with framework aluminum atoms. In most zeolites, including ZSM-5, the strength of the acid sites is inversely proportional to the concentration of framework aluminum up to about a silica/alumina ratio of 10. Above this ratio the aluminum level does not affect acid strength. The number of the acid sites is directly proportional to the concentration of framework aluminum. In ZSM-5, the acid sites are probably located at pore intersections.

One of the most important advantages of ZSM-5 over other crystalline and amorphous catalysts is low coking rate. Because coking is low in ZSM-5, it deactivates much more slowly than other catalysts. This longer life made the commercialization of a number of processes possible [21,22,23,24,25].

Coking is less severe in ZSM-5 than in most other catalysts because the pores lack enough space for the polymerization of coke precursors. In ZSM-5, coke is deposited on the outer surface of crystals; whereas in large-pore zeolites, such as mordenite or offretite, most of the coke forms within the pores [21]. Activity is barely affected in the first case but decreases rapidly in the second. Figure 2.10 shows an oversimplified picture of these phenomena.

(a) Pentasil Zeolites

(b) Mordenite and other large pore zeolites

Figure 2.10 Coke formation in zeolites [21].

2.3.2 Acidity of zeolite

Acidity in zeolites is generated by isomorphous substitution of lattice Si^{4+} cations by trivalent cations such as Al^{3+}, Fe^{3+} or Ga^{3+}. Such a substitution results in a negative lattice charge which must be compensated by a further cation (for instance alkali cations). Bronsted acidity can be introduced by using protons as compensating ion. These can be generated

by subsequently exchanging the original compensating cations with ammonium ions and decomposing the ammonium ions to ammonia at high temperature. The protons thus retained can be expected to be strongly acidic due to the high formal charge excess (+3/4 [26]) of the bridging oxygen atom to which it is attached. Such protons acted as the Bronsted acid sites of zeolite, as shown in Figure 2.11.

A common way to characterize the acid strength of solid acids is the Hammett indicator method. Hammett introduced the acidity function H_0, as a means to be able to compare the acid strength of different solvents:

$$H_0 = pK_{BH^+} - \log \frac{c_{BH^+}}{c_B} \qquad (2.7)$$

Where c_B and c_{BH^+} are respectively the concentrations of a base B and its conjugated acid. pKa is a measure of the base strength of B and is defined by:

$$pK_{BH^+} = \log \frac{a_{BH^+}}{a_H + a_B} \qquad (2.8)$$

Where a_i denotes the activity of species i. The H_0 value of an acid can be determined by measuring c_{BH^+} / c_B for a particular indicator and using a literature value for pK_{BH^+} (these are available for a variety of indicators). Originally, this method was developed to characterize the strength of strong liquid acids [27]. Walling [28] suggested to extend this method to solid acids and Umansky et al. later applied it to characterize the acid strength of zeolites [29]. He found for H-Mordenite a H_0 value somewhat higher than that of 100 % H_2SO_4.

When hydrogen form zeolite is heated to high temperature, water is driven off and coordinatetively unsaturated Al^{3+} ions are formed (Figure 2.11). These are strong Lewis acid; a base like pyridine is typically more strongly bounded to these Lewis acid sites (electron acceptor) than to Bronsted acid site (proton donor), as shown by infrared spectroscopy and temperature programmed desorption [5,8].

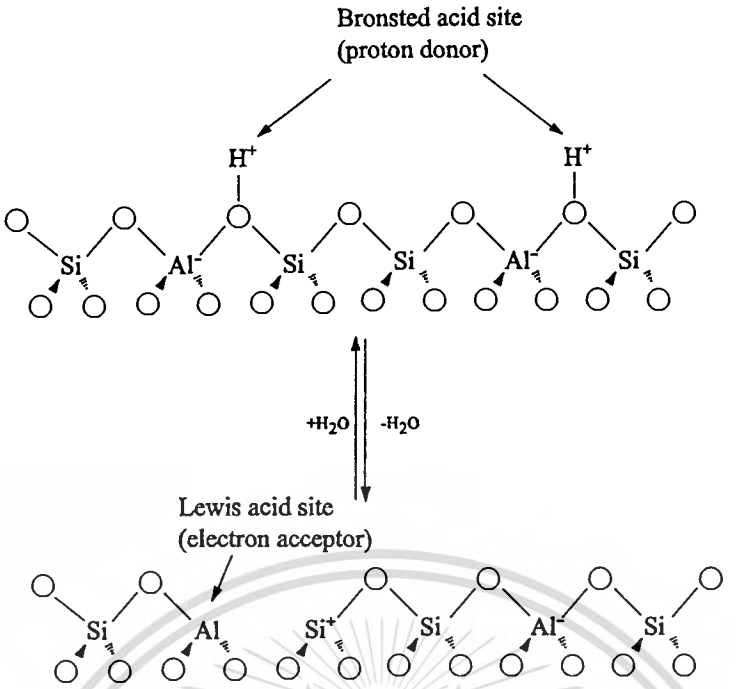

Figure 2.11 Bronsted acid and Lewis acid sites of zeolite.

According to the stoichiometry, one Lewis acid site is formed from two Bronsted acid sites; the result has been confirmed by measurement of the number of adsorbed pyridinium ions (indicating Bronsted acid sites) and Al^{3+} coordinated pyridine molecules (indicating Lewis acid sites) [5].

2.3.3 Metal doped zeolite

Zeolites are especially suitable as support materials for active components, such as metals and rare earths. Various methods, such as impregnation, ion-exchange, chemical vapor deposition, etc. are used to introduce metals into this support. With rare earths, the activity of the catalyst and its stability towards steam and heat can be increased. Suitable metals are effective catalysts, whereby the shape selectivity of the carrier is retained.

Catalysis by both metal and support, namely bifunctional catalysis is an advantageous phenomenon. It plays an important role, for example, in dehydrogenation and isomerization reactions occurring in the catalytic reforming of naphtha. One of the important reactions in the naphtha reforming is the dehydrocyclization of long chain paraffins, such as *n*-hexane [30]. A possible mechanism for this reaction is shown in Figure 2.12.

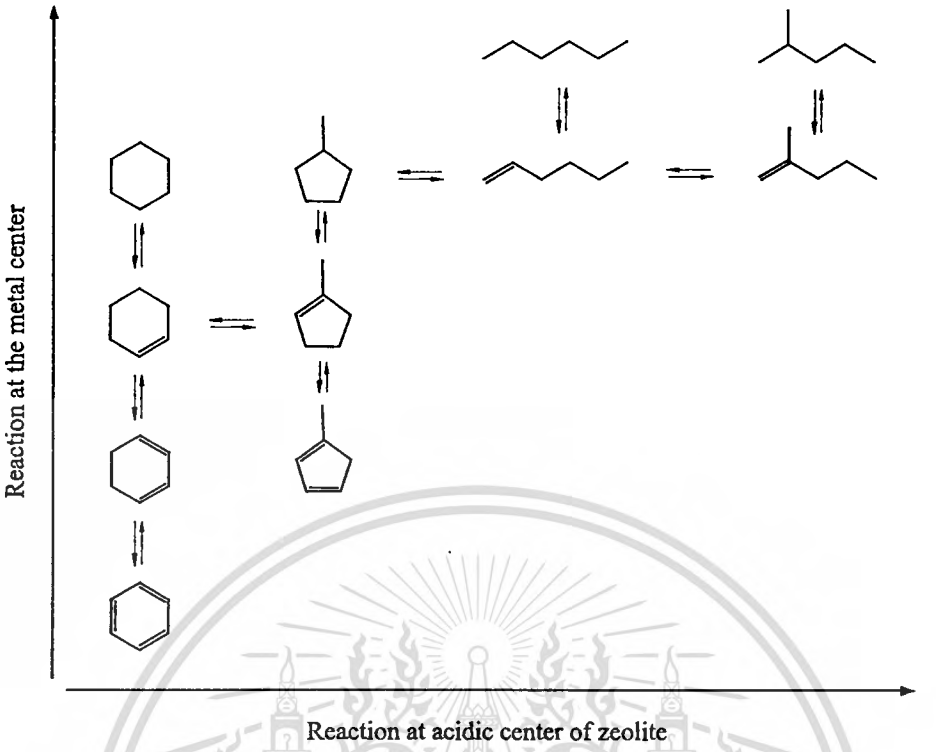

Figure 2.12 Bifunctionality of metal doped zeolite: dehydrocyclization of *n*-hexane.

In the first reaction in the pathway, the *n*-hexane is rapidly dehydrogenated on the metal surface; the resulting *n*-hexene is easily protonated by the acidic sites on the support to give a carbenium ion, which is converted into methylcyclopentane. This is dehydrogenated on the metal surface to give methylcyclopentene, which undergoes an acid catalyzed rearrangement to give cyclohexene, which is dehydrogenated on the metal surface, ultimately giving benzene.

It is noted that the important factors influencing the reactions of such bifunctional catalysts are the location of the metal, the particle size, and the metal-support interaction.

2.3.4 Reaction of carbocation

Acid catalyzed reactions of hydrocarbons are now generally accepted to involve carbocations, either as unstable species or as transient intermediates. This concept dates back to 1922 [31] and was later generalized by Whitmore [32] who found that structural rearrangements often occur during addition reactions of alkenes and dehydration of alcohols. Later this concept was successfully used to describe hydrocarbon reactions catalyzed by aluminum halides and

sulfuric acid in catalytic cracking [33]. However, because hydrocarbons are very weak bases, the equilibrium concentration of carbocations in regular acids is unobservably low and until the early sixties their existence was only hypothetical. Due to the development of superacids it became possible to generate long-lived carbocations in concentrations high enough to enable direct study by spectroscopic and other techniques. 1H and 13C NMR spectroscopy has been used to determine the structures of carbocations, their relative stabilities and the rates of rearrangements [34,35]. Besides NMR spectroscopy, calorimetry has been used to determine the heats of transformation of alkylcarbenium ions [36]. The results confirm the expected stability order of carbocations (tertiary >> secondary > primary).

Two types of carbocations are known, carbenium and carbonium ions. The difference between the two species is that in a carbenium ion the charged carbon atom is three-coordinated and in a carbonium ion five-coordinated. Contrary to carbenium ions, at least one of the substituents of the charged carbon atom of a carbonium ion is a hydrogen atom. Carbonium ions are formed by protonation of an alkane, as shown below:

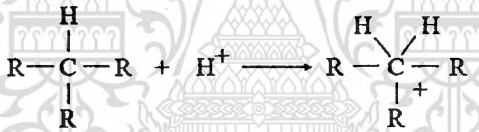

Carbonium ions are very unstable [37] and readily decompose into carbenium ions and hydrogen molecules or carbenium ions and alkanes:

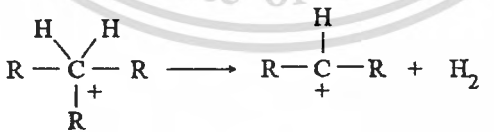

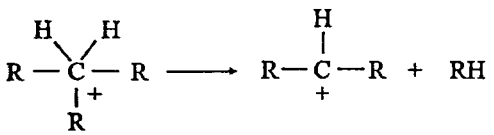

Carbenium ions can be formed in various ways: from carbonium ions by cracking or removal of hydrogen, from alkanes by hydride transfer toward a carbenium ion and from alkenes by protonation:

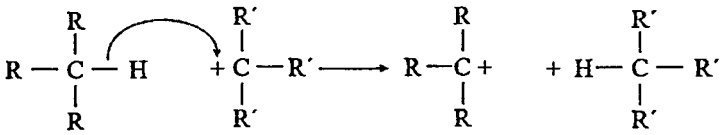

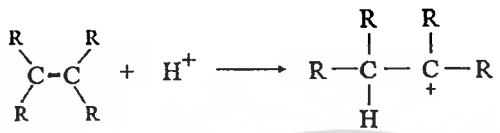

The important reactions of carbenium ions include isomerization proceeding by 1,2-hydride and 1,2-alkyl shifts, symbolized by H~ and CH_3~ [5], respectively:

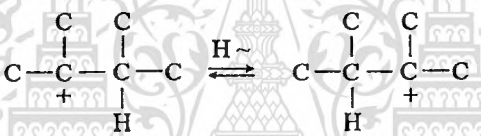

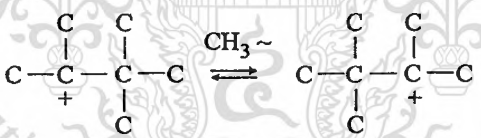

Another reaction of carbenium ions is β-scission of carbon-carbon bond [5]; this is the essential step in catalytic cracking process. The reaction generates an olefins and another carbenium ion. The rate depends on the relative stabilities of the reactant and product carbenium ions (tertiary >> secondary > primary):

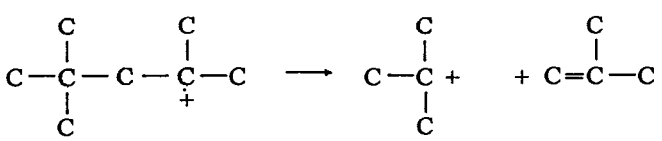

Another reaction of carbenium ions, which are strong Lewis acid, is hydride abstraction, another of the ion transfer reactions:

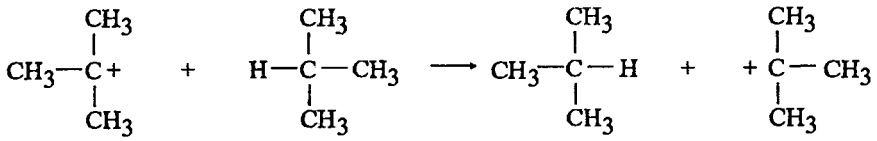

Another bimolecular reaction of the carbenium ions is alkylation, the reverse of β-scission [5]. The reactants are the carbenium ion (a Lewis acid) and an olefin (a Lewis base); the product is a larger carbenium ion.

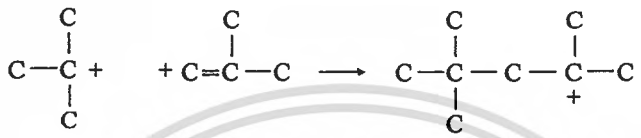

In alkylation process carried out on commercial scale, typically with isobutane and propylene as the reactants, C_7 (gasoline range) products are formed by this kind of carbon-carbon bond formation. Isomerization takes place rapidly leading to branch products.

2.3.5 Hydrocarbon activation on solid acid

The adsorbed carbocations are short-lived intermediates and that protonated alkenes are converted to alkoxides [38]. The generation of alkoxides has been confirmed experimentally by NMR spectroscopy [39,40,41] and infrared spectroscopy [42]. For example, the protonation of ethylene is depicted in Figure 2.13. Initially, the double bond of the alkene interacts with the Bronsted acidic hydrogen atom while one of the two carbon atoms interacts with a neighboring oxygen atom of the lattice that does not carry a hydrogen atom; this is called a π-complex (a). In the transition state (b), the acidic hydrogen attaches to one of the carbon atoms while the other carbon atom becomes more strongly bonded to the mentioned neighboring oxygen atom. This stronger interaction results from the fact that the proton transfer induces simultaneously a positive charge on the hydrocarbon fragment and a negative charge on the lattice oxygen atoms. In the final state (c), the hydrocarbon fragment becomes strongly and covalently bonded to the neighboring oxygen atom forming an alkoxide $-OC_2H_5$; this is called a σ-complex.

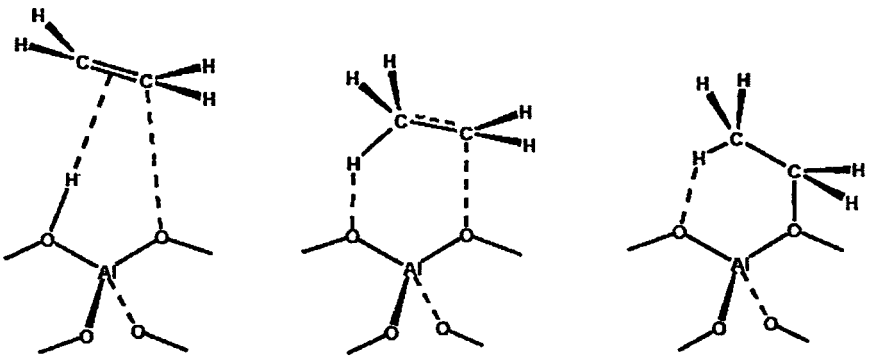

Figure 2.13 Interaction of ethylene with a solid Bronsted acid site. (a) π-complex, (b) transition state, and (c) σ-complex.

2.4 Metal surface catalysis

According to Boudart (1984) [43], catalytic reactions are divided into two types: (1) structure sensitive reaction and (2) structure insensitive reaction. In structure sensitive reactions, specific activity or turn over frequency (TOF) depends on surface structure, i.e., is a function of the geometric distribution of sites. In other word, structure sensitive reactions require special sites. The distribution of these special sites may vary with metal loading, crystallite size, dispersion (fraction exposed), and/or preparation method.

The variation in atomic coordination number Ci (i = number of nearest neighbors) for different atoms at the surface of the metal crystallite is illustrated in Figure 2.14, a ball model of a closed packed imperfect surface. Several different kinds of atomic coordination are evident:

(1) Planar (P) or face sites having coordination number 9 (C9; note that hexagonal close packing (hcp) bulk atom have C12 coordination (6 in the same plane, 3 above, and 3 below))

(2) Edge (E) atoms having C7 coordination

(3) Corner (C) sites having C6 coordination

(4) Edge atoms (A_E) with C5 coordination

(5) Terrace adatoms (A_T) having C3 coordination

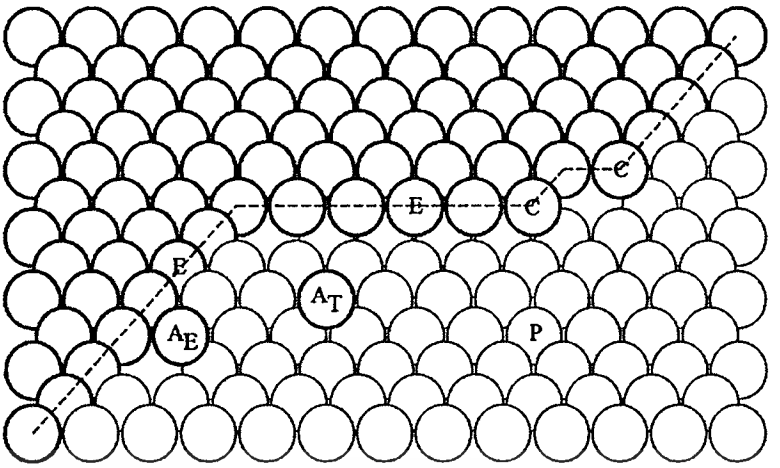

Figure 2.14 Model of closed-packed imperfect surface; atoms of differing coordination are designated as planar (P), edge (E), corner (C), edge adatom (A_E), and terrace adatom (A_T) [8].

It is logically anticipated that surface atoms of lower coordination (i.e., having a greater fraction of their bonding capacity unsatisfied) would adsorb atoms more strongly than surface atoms of higher coordination. Thus one might expect terrace and edge adatoms, corner atoms, and edge atoms to be the most active sites at least initially, and possibly the ones to be poisoned most rapidly by feed impurities or coke. If the fraction of low coordination sites at a crystallite surface is a function of crystallite diameter, a variation in activity with metal dispersion is predicted.

The structure insensitive reactions are listed in Table 2.3 [8]. A number of hydrogenation reactions (hydrogenation of ethylene, benzene and CO) have been shown to have the same TOF on both supported metal and single crystal surfaces. The hydrogenation of CO has been shown to be structure insensitive on Co, Fe, Ni, Rh, and Ru catalysts. While, the structure sensitive reaction (Table 2.4) includes neopentane isomerization, ammonia synthesis, and ethane hydrogenolysis [8].

Table 2.3 Structure insensitive reaction.

Metal	Reaction
Pt	n-C_3H_6 hydrogenation
Ni	C_2H_4 hydrogenation
	C_6H_6 hydrogenation
Co, Fe	CO hydrogenation
Ni, Ru	CO hydrogenation
Rh	CO hydrogenation
Pt	n-C_6H_{10} hydrogenation
Pd	CO oxidation

Table 2.4 Structure sensitive reaction.

Metal	Reaction
Pt	neopentane isomerization
Fe	NH_3 synthesis
Pt, Ni	ethane hydrogenolysis
Pt	H_2 oxidation
Pd, Rh	CO+NO

The ethane hydrogenolysis reaction on Ni(100) and Ni(111) surfaces shows clearly structure sensitive effect. It is found that methane formation rate is significantly higher at any temperature on the Ni(100) surface relative to the Ni(111). Upon the examining the arrangement of atoms on the two surfaces, it is evident that the distance between four-fold sites on the Ni(100) surface is larger than that between three-fold sites of the Ni(111) surface. This distance between four-fold sites in Ni(100) is possibly ideal for cleaving the C-C bond of ethane [8].

2.4.1 Adsorption on metal surface

A molecule enters to a reactive state. It must undergo adsorption on the catalyst surface [5]. Hence the catalyst must chemisorb at least one of the reaction steps. The strength of adsorption of the molecules is decisive for effective catalysis. Neither too strong nor too weak binding of the reactants can induce the required reactivity, a certain medium binding strength is optimum. The active centers on the catalyst surface are probably the result of free valences or electron defects, which weaken the bonds in the adsorbed molecules to such an extent that a reaction can readily occur.

The chemisorption of gases on metals has been the subject of particularly intensive investigations, and the available data allow the catalytic properties of metals to be explained well. Experimentally determined, qualitative orders of catalytic effectiveness are often found in the literatures. For example, for the adsorption of hydrocarbons [7]:

acetylenes > dienes > alkenes > alkanes

polar substances > nonpolar substances

The electronic structure of the metals is decisive for their catalytic activity. The transition metals, with their partially filled d orbitals, are particularly good catalysts. These orbitals are responsible for the covalent binding of gases on metal surfaces in chemisorption and catalysis. Whereas transition metals have one or more unpaired d electrons in the outer electron shell, the weakly chemisorbing main group elements have only s or p electrons. It is postulated that unpaired d electrons are necessary to hold the chemisorbed molecules in a weakly bound state, from which they can then be transferred into a strongly bound state [7].

Adsorption is an exothermic process in which strong binding forces arise between the adsorbed molecules and the surface atoms of the catalyst. At the same time the degree of freedom of the molecules decreases when they leave the gas phase and are adsorbed on the catalyst. Therefore, the entropy S is negative. For a thermodynamically feasible adsorption process, the Gibbs free energy should be negative [4]:

$$\Delta G = \Delta H - T\Delta S$$

The adsorption enthalpy ΔH will depend, as a first approximation, mainly on the strength of chemical bonding between the gas molecules and the catalyst. Two fundamental types of chemisorption processes can be distinguished [7]:

– Molecular or associative chemisorption, in which all bonds of the adsorbate molecule are retained.

– Dissociative chemisorption, in which the bonds of the adsorbate molecule are cleaved and molecular fragments are adsorbed on the catalyst surface.

Molecular chemisorption occurs with molecules having multiple bonds or free electron pairs. For example, on platinum surfaces (Figure 2.15), ethylene gives up two π electrons of its double bond and forms two σ bonds with Pt atoms. The resulting sp^3 hybridization results in a tetrahedral arrangement of bonds.

Figure 2.15 Molecular chemisorption of ethylene on a Pt surface.

Dissociative chemisorption occurs mainly with molecules containing single bonds. For example, the adsorption of H_2 on nickel surface, in which the hydrogen is adsorbed in atomic form on the surface. The total process can be described schematically, as shown in Figure 2.16.

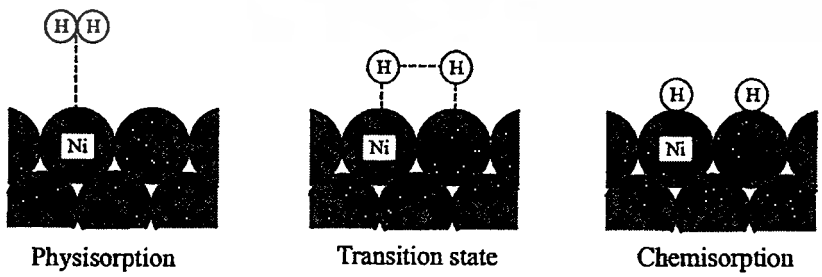

Figure 2.16 Dissociative adsorption of hydrogen on nickel surfaces.

Dissociative chemisorption occurs preferably with alkenes in which the allylic methyl group is highly activated (e.g., propene). Hydrogen abstraction gives an allyl radical, which can be bound as follows:

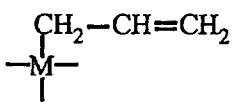

Chemisorbed
σ-allyl radical

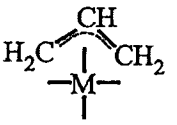

Chemisorbed
π-allyl radical

Other species can occur on certain metal oxides:

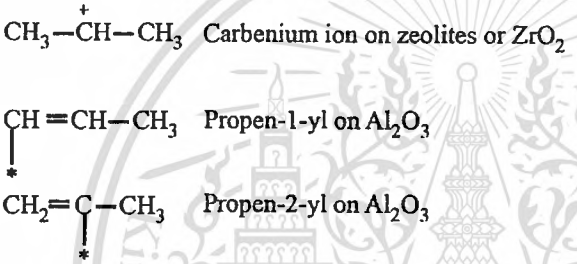

$CH_3-\overset{+}{C}H-CH_3$ Carbenium ion on zeolites or ZrO_2

$CH(*)=CH-CH_3$ Propen-1-yl on Al_2O_3

$CH_2=C(*)-CH_3$ Propen-2-yl on Al_2O_3

The molecular chemisorption of ethylene is observed below room temperature, but at higher temperatures (> 100°C) the adsorbed alkene ,i.e. ethylene can be cleaved with formation of ethylidyne complex:

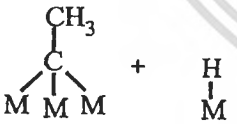

2.4.2 Inert supports: SiO_2 and TiO_2

Silica (SiO_2) is an amorphous solid that its internal surface area can be reach 500 m^2/g [5]. The silica surface is nearly inert. The most reactive groups are the –OH groups (called silanol groups) that terminate the primary particles; these are weakly acid, comparable to alcohols. The bulk may be terminated entirely by –OH groups, which can be removed by dehydroxylation. Two types of silanol groups are usually distinguished, isolated groups and neighboring (vicinal) groups that may be hydrogen bonded to each other. Fully, hydrated samples, heated in air (i.e., calcined) at temperatures < 200°C, also contain geminal groups,

$Si(OH)_2$. Complete removal of silanol groups requires temperature higher than 700°C and results in significant changes in surface morphology. The aprotic sites present after dehydroxylation at 600-800°C have been suggested to be primarily highly strained Si-O-Si linkages.

Titania (TiO_2) crystallizes in three major different structures; rutile (tetragonal), anatase (tetragonal) and brookite (rhombohedrical). Other structures exist as well, for example, cotunnite TiO_2 has been synthesized at high pressure and is one of the hardest polycrystalline materials known [44]. Commercial high surface area titanias (25-100 m^2/g) are formed by precipitation from titanate solutions or by the decomposition of organotitanates [8], although new preparations from the aerogel promise to provide materials of high surface area (200-400 m^2/g). In general, commercial titanias consist of anatase and rutile. Anatase is the most important catalytically, in that it has a surface area of about 50-80 m^2/g, while the rutile structure forms at about 550°C and has low surface area. Accordingly, the transformation of anatase to rutile generally results in the surface area loss, occlusions of the catalytic material, and thereby deactivation.

2.5 Literature review

The shape selective medium-pore zeolite, ZSM-5 was observed to exhibit excellent catalytic properties that were suitable for the conversion of a variety of hydrocarbon feeds starting from LPG containing propane and butane to light naptha (LN) containing *n*-pentane and *n*-hexane to aromatics compounds [45,46,47]. The Cyclar process of Universal Oil Products (UOP), aroforming of IFP, M-2 forming of Mobil were some of the commercial examples that were reported to be catalyzed by HZSM-5 alone or in combination with metal ions such as Ga, Zn, Re, Pt, and Mo [48,49,50,51].

In naphtha to gas and gasoline process (NTGG), HZSM-5 catalyzed the formation of the small molecules as propane and butane (LPG) along with gasoline and aromatics in considerable amount through cracking and hydrogen-transfer reaction over acid sites. The formation of aromatics was believed to be a cracking-based aromatization that mainly consisted of sequential steps such as cracking, oligomerization, cyclization, and hydrogen transfer.

With HZSM-5 catalysts, the first stage of alkane aromatization proceeded via two routes, as protolytic cracking route (cracking of C-C and C-H bounds in the alkane molecules) and hydrogen transfer route that involved the reaction between the alkane with the product alkenes adsorbed on the acid site of the zeolite [52,53,54,55,56]. The second stage, alkene formed from

cracking in the first step was oligomerized to be larger alkene [57]. In the third stage, the oligomerized alkene was cyclized to napthene, then because of hydrogen transfer [52,58,59,60,61] from naphthenes to smaller olefins, the formation of the hydrogen-deficient hydrocarbon such as aromatics was balanced by the formation of alkanes [58,59,60]. These product alkanes can undergo cracking into light alkenes until non-aromatizable as methane and ethane were formed. Unfortunately, the final step also produces the high molecular weight aromatics (coke) that were too large to diffuse out of the zeolite window; therefore, it clogged in the pore of zeolite leading to the blockage of active sites of the catalyst and causing to the catalyst deactivation [62,63,64].

Thus, unlike in classical reforming process, the nature of the aromatics compound was independent of the carbon number of the feed, i.e., the amount of benzene in the products was low even *n*-hexane was employed as the feedstock [65]. However, there were some drawbacks when the formation of aromatics was performed over HZSM-5 catalyst, i.e:

- Thermodynamics data revealed that alkane to aromatics conversion became difficult, as size of the alkane was decreased (by cracking) and that aromatics were not thermodynamically favored although using the corresponding alkane structure [66,67].
- On HZSM-5, the aromatization of alkanes was kinetically limited by the formation of olefinic compounds. This formation occurred through scission of carbonium ions into carbenium ions and hydrogen or alkenes [68].
- Formation of aromatics occurred by the hydrogen transfer from naphthenes to smaller olefins in the final step of the reaction. In this process three moles of smaller paraffins (mainly in the LPG range) formed simultaneously with the one mole of aromatics, which limited the aromatics to paraffins yield ratio [68].
- Steric constrainsts in the pore structure of ZSM-5 limited the hydrogen transfer from naphthenes to olefininc compounds [68].

Effective conversion of the paraffins can be achieved by the addition of a dehydrogenating metal to the HZSM-5 catalyst. The metal ion provided an alternative path for the formation of olefins and aromatics. Aromatization activity of metal-loaded zeolite depended on its dehydrogenation activity [69,70], which ultimately determined by the electronic properties of the metal [71,72]. The various researchers studied the aromatization of alkanes over various

transition metal-loaded ZSM-5 catalysts that underlined the superiority of gallium and zinc over the other metals studied [73,74].

The first step of alkane aromatization over GaZSM-5 catalysts was the alkane dehydrogenation to form the corresponding alkene. For example, propene was primarily produced in the propane aromatization which was kinetically limited by this dehydrogenation step [70]. In Figure 2.17, the propane aromatization involved the accompanying of acid sites and Ga ion (complex Ga ion species) which acted as dehydrogenating sites converting propane to propene (step 1). Then, propene was oligomerized by acid sites to C_6-C_{10} alkene (step 3) which was able to dehydrogenate to C_6-C_{10} dienes (step 5). After that, acid site would cyclize such C_6-C_{10} diene to C_6-C_{10} cyclo-olefins (step 7) which was dehydrogenated again to be aromatics (step 9-10). Step 2, 4, 6 and 8 corresponded to the migration of desorbed intermediates from dehydrogenation sites to protonic sites and *vice versa*. The participation of Ga species in step 1, 5, 9 and 10 was demonstrated through kinetic modeling of propane and propene aromatization over Ga/HZSM-5 catalysts [75,76] as well as by the use of model reactions [70]. The much higher activity of propene as compared to that of propane supported that the formation of aromatics from propene was favored and the kinetic limitation of propane aromatization was propane dehydrogenation (step 1).

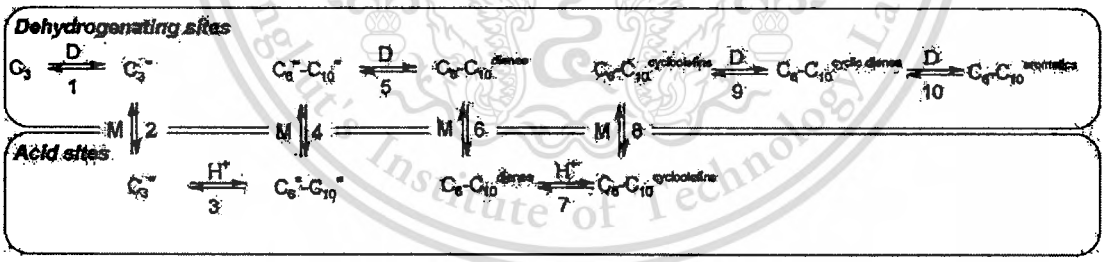

Figure 2.17 Propane aromatization over GaZSM-5 catalysts with bifunctional reaction scheme [69].

In the absent of Ga, the reaction would follow the cracking-based catalysis as mention previously. The zeolite protonic sites were able to catalyze step 1, 5, 9 and 10 of Figure 1. Step 1 occurred through protolysis cracking (C-H or C-C cracking) while step 5, 9 and 10 occurred essentially through hydrogen transfer from long chain, and cyclic olefins and dienes to light alkenes. In addition to propene, the protonated propene namely propyl cation can be cracked to

methane and ethene. Moreover because of the competitive adsorption over the protonic acid sites, the aromatics molecules affects significantly on the rate of the reaction of step 1, 5, 9 and 10 [75,76].

In addition, Ga species were shown to be able to catalyze not only the dehydrogenating step but also propane cracking into methane and ethene, the hydrogenation of olefins in particular of ethene, and the hydrogenolysis of methyl aromatics [75,76,77]. A recent study of propane transformation at 500°C over different polymorphous Ga_2O_3 confirmed the catalytic activity of this oxide for propane dehydrogenation and cracking [78]. β-Ga_2O_3 which had the largest amount of the acid sites was the most active and selective for propene formation. Gallium oxide being hardly reduced below 600°C and the reduced oxide being not restore after O_2 treatment, propane dehydrogenation was proposed to occur (like on ZnO) through a heterolytic dissociation pathway rather than through a redox mechanism. In agreement with this proposal, dihydrogen molecules were demonstrated to be dissociated over Ga_2O_3 to form gallium hydride species (Ga^{x+}-H) [79]. This result found were very similar to that found over ZnO [80].

Figure 2.18 shows the mechanism of dehydrogenation proposed by Meriaudeau and Naccache [81]. The first step was the heterolytic dissociation of propane with the formation of Ga hydride and Ga alkoxide species. Over pure gallium oxide, these alkoxides would decompose into propene and H^+ bonded to the surface oxygen (step 2); the last step would be the formation of hydrogen from H^+, H^- species with recovering of the Ga sites, the propyl carbenium ions formed in step 1 will easily exchange with zeolite proton through an alkyl surface migration (step 4). This new pathway allowed one to bypass the limiting step of propene formation over pure Ga oxide. A slightly different mechanism was proposed by Buckles and Hutchings [82] that propane would be activated at the interface between Ga oxide and protonic sites; initial process would be the polarization of the C-H bond by Ga oxide, the second one the cleavage of the polarized C-H bond by interaction with the protonic sites. Furthermore, from propane 2-^{13}C transformation followed by ^{13}C MAS NMR spectroscopy, Derouane et al. [83] concluded to the participation as first intermediate of a protonated pseudo-cyclopropane species formed by propane activation on a (Ga^{3+},O^{2-}) ion pair and its protonation by a nearby protonic acid site. Lastly, according to Ono [84], the role of the protonic sites would be to scavenge the Zn (or Ga) hydride species formed by heterolytic dissociation of propane, e.g. $[ZnH]^+ + H^+ \longrightarrow Zn^{2+} + H_2$.

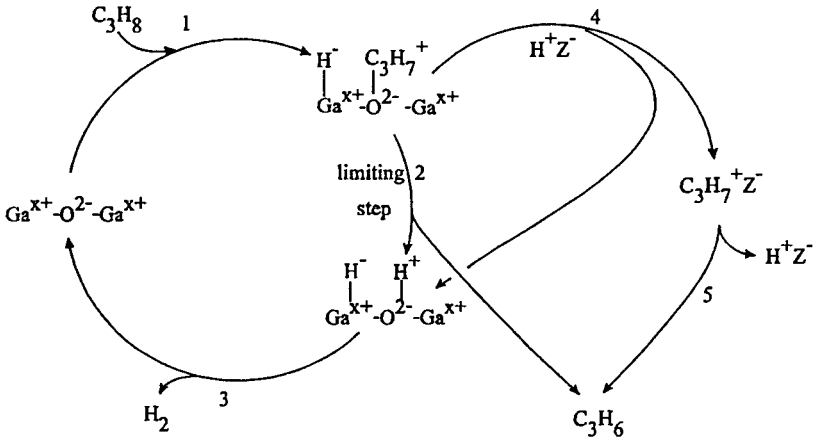

Figure 2.18 Ga-acid bifunctional mechanism of propane dehydrogenation over GaHZSM-5 catalyst.

In the mechanism proposed by Biscardi and Iglesia [85], the first step was the activation of the C-H bond over the protonic sites, the role of the Ga species being to act as efficient "portholes" for the removal of the H atom produced during the activation step. To demonstrate this mechanism, reaction of C_3H_8/C_3D_8 mixture were carried out over HZSM-5 and Ga/HZSM-5 catalysts [85]. Both the roles of propane transformation and C-H bond activation (cross exchange of D atom between deuterated and light propane molecules) can be determined from these experiments. Over HZSM-5, the activation of the C-H bond was found to be much faster (35 times) than propane conversion. This suggested that the protonic sites can activate C-H bonds very effectively but cannot dispose rapidly of the H atom formed in the C-H bond scission. Therefore, these H atoms were used to hydrogenate surface carbenium ions. Over Ga/HZSM-5, propane transformation was 3-times faster thane over HZSM-5, whereas the C-H bond activation occurred at similar rates over both catalysts. To explain that, it was proposed that H atom removal could be achieved not only through H transfer to carbenium ions, but also recombinative desorption involving Ga species. Over pure HZSM-5, hydride ions would be momentarily stabilized by adsorption on Al atom sites, these unstable hydride species would react with carbenium ions to form alkane species (Eq.(2.1)) [86].

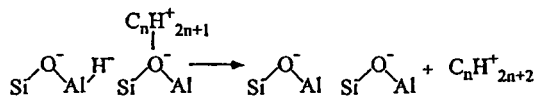

(2.1)

Over Ga/HZSM-5, the hydride species stabilized by Ga ions would combine with zeolite protons to form H_2 (Eq.(2.2)) [86]

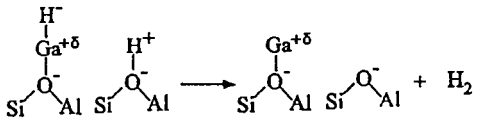

(2.2)

There are no definite arguments in favor of the a or of the b mechanisms. It is furthermore likely that both mechanisms could play a role in dehydrogenation steps over Ga/HZSM-5 catalysts. Whatever it will be, the bifunctional character of the sites of Ga/HZSM-5 catalysts which are active in dehydrogenation is generally admitted. For long chain paraffinic hydrocarbons (C_6-C_8), the dehydrogenation could be the first activation step. The adsorbed olefins were able to directly cyclize to aromatics. This pathway was defined by the highly observed benzene, toluene and xylene from the *n*-hexane, *n*-heptane, and *n*-octane, respectively, conversion over GaZSM-5 [114].

Ga/HZSM-5 samples with Ga under the form of Ga^+ in exchange cations and which contained practically no protons were shown to be active in alkane dehydrogenation. A mechanism was proposed for this dehydrogenation on the basis of the results of diffuse reflectance infrared spectroscopy (DRIFT) experiments with ethane [87]. After heating of Ga/HZSM-5 in ethane atmosphere at 250 ^{O}C, 4 weak stretching bands appeared at 2882, 2914, 2939 and 2962 cm^{-1} which were ascribed to ethyl species grafted to Ga^+. Another band appears at 2057 cm^{-1} with a shoulder at 2040 cm^{-1} which corresponded to gallium hydride species. The formation of these bands could be described by the following reaction (Eq. (2.3)):

$$ZO^-...Ga^+ + C_2H_6 \longrightarrow ZO^-...[Ga^{3+}(H^-)(C_2H_5^-)]^+ \quad (2.3)$$

Prolonged heating resulted in the decomposition of ethyl species with an appearance of new C-H stretching bands at 3024, 3055 and 3072 cm^{-1} typical of olefin or aromatic hydrocarbons and with a shift of the maximum of the Ga hydride band to 2040 cm^{-1} which indicated the formation of gallium dihydride species, as shown in Eq. (2.4) [87].

$$ZO^-...[Ga^{3+}(H^-)(C_2H_5^-)]^+ \longrightarrow ZO^-...[Ga^{3+}(H^-)_2]^+ + C_2H_4 \quad (2.4)$$

It should be remarked that in Eq. (4.3), there was an alkyl activation of ethane ($C_2H_5^-$) and not a carbenium activation ($C_2H_5^+$), as proposed in the mechanism advanced by Meriaudeau and Naccache [81]. Quantum chemical calculation were undertaken to discriminate between those two possibilities and also to specify the nature of the active Ga species: dihydride gallium ion $(GaH_2)^+Z^-$ or gallyl ion $(Ga{=}O)^+Z^-$ [88]. The conclusion were that $(GaH_2)^+Z^-$ was the likely active species and that alkane activation occurred via an alkyl mechanism involving three successive steps: scission of a C-H bond (1), formation of dihydrogen from the proton and the hydrogen bond to Ga (2) and the formation of ethene from the ethyl group bound to Ga [88]. Ethane dehydrogenation over dihydride gallium ions was recently reconsidered [89], the conclusion being that a one step concerted mechanism was more likely than the three steps mechanism proposed by Frash and van Santen [88].

These conclusions on the mode of ethane activation and on the active sites were recently disputed by Joshi and Thomson [90] from density functional theory (DFT) pathway analysis. Two types of sites were considered: the mono Al site of the form $Z^-[GaH_2]^{2+}$ (dihydride gallium ion) and a di-Al site: $Z^{2-}[GaH_2]^{2+}$. With the first type of sites, the calculated activation energies were too high compared to experimental values, which led the author to conclude that the sites were not likely responsible for alkane dehydrogenation. $[GaH]^{2+}$ species residing near di-Al sites were proposed to be the active sites. They can be reduced by hydrogen with formation of protonic acid sites (Eq. (2.5)).

$$[GaH]^{2+} + H_2 \longrightarrow [GaH_2]^+ + H^+ \qquad (2.5)$$

This reaction being endothermic reaction, $[GaH]^{2+}$ species were predominant at low temperature. However, both species could be presented under normal reaction condition. A carbenium activation mechanism consisting of three distinct steps: activation of the C-H bond with formation of an alkoxide like intermediate (1), desorption of ethene (2) and then of molecular hydrogen was proposed. There was an optimal Al-Al distance due to opposite effected on the activation barrier for C-H activation and for H_2 removal [90]. However, an argument against this proposal of a di-Al route was the low probability of finding Al pairs in the high Si/Al ZSM-5 zeolite which were generally used in aromatization.

Gallium can be introduced into Ga/HZSM-5 catalysts through different ways: impregnation with various salts, ion exchange, chemical vapor deposition, mechanical mixture of

Ga_2O_3 and HZSM-5, synthesis of MFI gallosilicate, etc. Ga can have a beneficial effect on the rate and selectivity of alkane aromatization. The impregnated and ion exchanged HZSM-5 led to the preferential deposition of mostly GaO(OH) species on the outer surface of zeolite crystallites [91], for hydrated Ga^{3+} cations were too bulky to enter the channels of HZSM-5 [92]; during calcination, these extra-crystalline Ga species were converted to Ga_2O_3 crystals [91,93,94,95]. Furthermore, the calcination of the gallosilicates at high temperature (>700°C) caused the degalliation of the framework and the formation of extra-framework Ga species which deposited on the outer surface of the crystals or within the mesopores under the form of Ga_2O_3 [96,97,98]. The extra-framework species were shown to be at least 150 times more active than the tetrahedral framework Ga species. However, a complete inactivity of the tetrahedral Ga species had been suggested [97].

After calcination, therefore; most of the synthesized GaZSM-5 catalysts can be considered as mixtures of Ga_2O_3 and HZSM-5. However, these mixtures were not the real aromatization catalysts for significant changes in the nature and location of the Ga species as well as in the zelite acidity were shown to occur during pretreatment with hydrogen or during propane aromatization (because of hydrogen production) at 500°C. These changes can have a significant beneficial effect on the aromatization activity and selectivity. However, the intimacy of Ga_2O_3 and HZSM-5 was of paramount importance. Thus, with catalysts prepared by gentle mixture of Ga_2O_3 and HZSM-5, the increase in activity was not substantial [82], whereas with highly intimate mixtures a significant increase can be observed [99].

The origin of this increase was firstly investigated by Kanizarev, Price and colleagues using gravimetric, DRX, and FTIR techniques [94,95,99 ,100, 101,102]. Reduction was shown to occur during hydrogen treatment at high temperature by a sequence of steps involving the formation of Ga_2O species which can migrate into the zeolite channels and undergo solid-state exchange with the zeolite protonic sites (Eq. (2.6) and (2.7)).

$$Ga_2O_3 + 2H_2 \longrightarrow Ga_2O + 2H_2O \qquad (2.6)$$

$$Ga_2O + 2H^+Z^- \longrightarrow 2Ga^+Z^- + H_2O \qquad (2.7)$$

This reduction was confirmed by the shift in Ga K-edge energy to lower values detected by in situ X-ray absorption measurement [93]. These measurements also shown that the reduced Ga species consisted of monometric Ga^0 or Ga^+ compound and that the re-oxidation of reduced

species to Ga^{3+} species occurred upon cooling to room temperature even in H_2 or propane [99]. Therefore, the active form of Ga species can be detected only at reaction conditions. Biscardi and Iglesia [85] suggested that the neutral [GaOH] species stabilized by interaction with basic oxygens within ZSM-5 channels were the steady state form of reduced Ga (Eq. (2.8)).

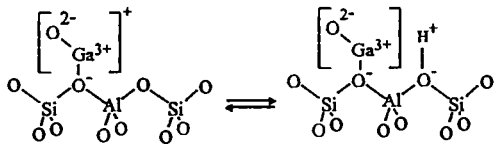

(2.8)

In agreement with Eq. (2.7), H_2 treatment at high temperature of Ga/HZSM-5 samples caused a very significant decrease in the intensity of the bridging OH band at 3610 cm^{-1} [103]. However, a more limited decrease in the activity for model acidic reaction was observed: decrease by 1.5 times of the activity for *m*-xylene isomerization, by 1.4-2 times of that for propane transformation into methane [70] and by 1.4-1.6 times of the activity for 2-methyl-2-pentene isomerization [85]. This discrepancy could be due to reoxidation of reduced Ga species upon cooling of the catalyst to room temperature for IR measurements.

However, this reoxidation cannot occur when all the protonic sites were exchanged by Ga^+ [104]. The corresponding GaZSM-5 catalyst which had no measurable protonic acidity had a low activity for propane aromatization. Contrary to what was often observed over Ga/HZSM-5 catalysts, aromatics were secondarily formed, which meant that aromatization was limited by propene transformation (and not by propane dehydrogenation). A monofunctional mechanism was proposed to explain this aromatization in the apparent absence of protonic sites [104]. It could be noted that an undetectable amount of protonic sites could be responsible for the very facile (at high reaction temperature) oligomerization and cyclization steps involved in bifunctional aromatization.

More recently, a DRIFT study of the nature of gallium species in GaZSM-5 samples prepared by incipient wetness impregnation or via anchoring of trimethylgallium was carried out [87]. Reduction of the samples in hydrogen and evacuation at high temperature resulted in quantitative replacement of the protonic sites by Ga^+ ions. Ga^+ ions were shown to be partially oxidized by water at 300°C with release of H_2. After evacuation at 300°C and cooling to room temperature, a partial regeneration of protonic sites was also observed (regeneration of the

bridging OH band at 3610 cm^{-1}). The following reactions (Eq. (2.9)-(2.11)) were proposed to explain these observations:

$$ZO^-Ga^+ + H_2O \longrightarrow ZO^-...[Ga^{3+}(OH^-)(H^-)]^+ \quad (2.9)$$

$$ZO^-...[Ga^{3+}(OH^-)(H^-)]^+ + H_2O \longrightarrow ZO^- ...[Ga^{3+}(OH^-)_2]^+ + H_2 \quad (2.10)$$

$$ZO^- ...[Ga^{3+}(OH^-)_2]^+ \longrightarrow ZO\text{-}...H^+ + GaOOH \quad (2.11)$$

Moreover, it was reported that $[Ga^{3+}(OH^-)_2]^+$ was also formed after calcination and was primarily exchanged into the negative framework of HZSM-5. Such specie can be dehydrated to form GaO^+ at high temperature [87,95] and dispersed over the exchangeable sites in the zeolite framework. However, in the hydrogen stream, GaO^+ was not stable, it can readily reduced to form Ga^+ species [105,106]. Oxidative addition of hydrogen to Ga^+ at 500 ^oC resulted in the formation of stable gallium dihydride species. All the steps described were shown in Eq. (2.12)-(2.14). However, the authors [87] concluded that under typical aromatization conditions monovalent Ga^+ species were predominant even if $(GaH_2)^+$ species were also present. These species would be the active species able through an oxidative process to dissociate ethane into $C_2H_5^-$ and H^- species as was the case of H_2.

$$[Ga^{3+}(OH^-)_2]^+ \longrightarrow GaO^+ + H_2O \quad (2.12)$$

$$GaO^+ + H_2 \longrightarrow Ga^+ + H_2O \quad (2.13)$$

$$Ga^+ + H_2 \longrightarrow [GaH_2]^+ \quad (2.14)$$

Depending on the authors and on the alkane reactants, Zn/HZSM-5 catalysts were found more or less active and selective in aromatization than Ga/HZSM-5 catalysts. However, under the severe conditions of alkane aromatization, Zn^0 can be formed by reduction with hydrogen or hydrocarbon and eluted from the catalyst, which constituted a serious drawback for the industrial use of ZnZSM-5 catalysts [107].

Like with Ga/HZSM-5 catalysts, it seemed clear that aromatization of small alkanes occurred through the bifunctional catalysis path way presented in Figure 2.17 which involved successively dehydrogenating steps (step 1, 5, 9, and 10) over Zn-containing species and oligomerization (step 3) and cyclization (step 7) steps over the protonic zeolite sizes. Also like

with Ga/HZSM-5 catalysts, despite significant advances, the nature of the dehydrogenating species and the dehydrogenation mechanism were not perfectly established.

Metal supported catalyst has been widely used to convert various alkane hydrocarbons to valuable products via dehydro-hydrogenation, isomerization, cyclization, and hydrogenolysis [5,7]. During H_2 reduction to create metal species, Tauster et al. suggested the strong-metal support interaction (SMSI) to be taken place [108]. Especially, the group VIII metals, i.e., Fe, Ni, Rh, Pt, Pd, and Ir, supported on reducible oxides (TiO_2, TaO_5, CeO_2, NbO, etc.) were reduced at high temperature (~500°C) [108]. The SMSI effect was observed as a severely negative effect on CO and H_2 adsorption [108,109]. It also has a negative effect on the reaction rate for reactions such as alkane hydrogenolysis [110,111].

In case of Pt/TiO_2, the SMSI was described by the migration of titanium suboxide (TiO_x) covering the platinum metal surface. Cairns et al. [112] used Rutherford (very high energy, e.g., several mega-electron volts) backscattering of He^+ from a rather thick (2000 Å) Pt film deposited on singlecrystal TiO_2 (rutile) reduced at very high temperature (1173 K) to demonstrate interdiffusion between the metal and the support. Kelley et al. [113] used low-energy (2 keV) ion scattering of $^4He^+$ and $^{20}Ne^+$, which gives much higher surface sensitivity than does Rutherford backscattering. Moreover, they used a highly dispersed, low-loading Pt on anatase powder to prepare a conventional catalyst. Their results show that Pt particles are less visible to ion scattering after 673 K reduction than after 473 K reduction, a result clearly consistent with covering of the Pt particles by a TiO_x, species.

The mechanism of TiO_x migration cover the metal was proposed by Vishwanathan et al. [114] using Rh/TiO_2 as modeled catalyst. The loss of –OH group of TiO_2 change co-ordinatively saturated Ti^{4+} species (Ti^{4+}_s) to co-ordinatively unsaturated Ti^{3+} species which finally is the TiO_x. The formed TiO_x is not stable requiring electron; therefore, they would migrate to the Pt metal which possesses higher electron density. As the TiO_x jumps to cover the Pt metal, the vacant site for generating the new comer TiO_x is automatically formed. Eventually, the Pt metal can be covered by TiO_x network, as shown in Figure 2.19.

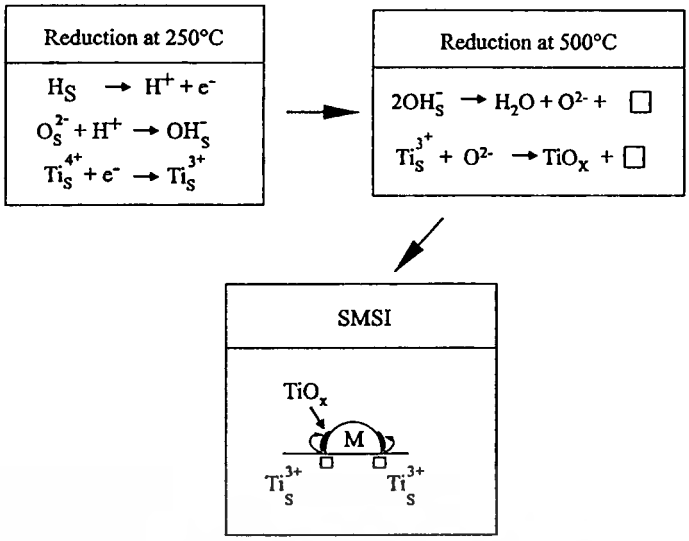

Figure 2.19 Proposed reaction pathway involved the formation of SMSI.

Moreover in the oxidative atmosphere, there has been reported that the SMSI effect seemed to be more likely [115,116]. Their XPS results indicated that in an oxidizing environment some of Pt species can diffused into the TiO_2 lattice to be oxidized to Pt^{2+}, which is substituted for Ti^{4+} or forms interstitial ions at a temperature as low as 473 K. In support with this view, Lin et al. [117] ascribed their TPR results that when the catalyst precursor (H_2PtCl_6/TiO_2(B) nanofiber) was calcined at a temperature that exceeded 773 K, the surface PtO_x was diffused into the TiO_2 (B) lattice.

Over metal sites, alkanes must be dissociatively adsorbed to cleavage C-H bond, i.e., dehydrogenation. Then, the reaction would proceed to cyclization, isomerization, and/or hydrogenolysis depending on the geometric/electronic of its intermediate which is feasible over such metal at that operating condition. Results for dehydrocyclization of *n*-octane show that as the metal loading on nonacidic alumina increased from 0.05 to 0.6 wt.% Pt, the ethyl benzene : *o*-xylene ratio changed from a 1.4:1 to 1:1 selectivity at the highest loading [118]. These results show that the selectivity changed with increasing metal loading from favoring one isomer to a nearly equal selectivity for all isomers allowed by direct C_6 ring closure. In addition, the hydrogenolysis-demethylation activity increased from a negligible level at the lowest loading to such a high level as to preclude selectivity studies at about 2 wt.% Pt or higher.

Many of the Pt catalyst are prepared by impregnation with chloroplatinic acid (H_2PtCl_6) so there is a concern whether the retained chloride influences the cyclization pathway. The conversion of 3-methylheptane at atmospheric pressure demonstrates that the chlorine containing

catalyst, even on non acidic alumina, yields an isomer distribution that differs from one without chlorine [119]. The amount of the isomerization of *m*-xylene, as well as for each of the other three aromatics products, when pass over the catalyst, with or without added hydrogen, is negligible in comparison to the amount of the alkane dehydrocyclization under the same reaction condition. Thus, secondary isomerization of the initially formed aromatics is not the source of *m*-xylene. *m*-Xylene is not allowed by direct C_6 cyclization of 3-methylheptane but is the only C_8 product from the cyclyzation of both 2- and 4-methylheptane. This suggests that the chlorine merely provides an isomerization pathway. Since 0.8 wt.% Cl, added to the Pt-Al_2O_3-K catalyst as NH_4Cl, did not significantly change isomer distribution, the chlorine added as chloroplainic acid is probably a specific type.

The dehydrocyclization of many alkanes, each contains eight or more carbons and at least one chain with six or more carbons, with a Pt-nonacidic alumina catalyst produced 90% or more of the aromatics predicted for the operation of only a six-carbon ring forming mechanism [120]. Fogelberg et al. [121,122] utilized a commercial Pt-alumina catalyst and a catalyst made nonacidic by calcining the alumina support at high temperature to produce a low surface area for the dehydrocyclization of *n*-octane as well as C_8-hexane and heptane isomers. With the commercial catalyst, they obtained a nearly equilibrium C_8 aromatics composition; however, with the nonacidic catalyst the aromatics were predominantly (> 90%) those expected for a direct six-carbon ring formation.

Some C_8 alkane isomers would form 1,1,3-trimethylcyclopentane (VI) by a C_5 ring closure, Figure 2.20. Of the four reactants, only 2,4-dimethylhexane (IV) provides a pathway that could lead to any cyclopentane isomer other than 1,1,3-trimethylcyclopentane. The experimental data from the cromia catalyst make it apparent that I, II, and III do not yield the same C_8 aromatics distribution. In addition, they do not resemble the C_8 aromatics distribution obtained from the conversion of 1,1,3-trimethylcyclopentane. The amount of ethylbenzene and *o*-xylene relative to *m*-xylene which Pines and Chen [123] obtained from 1-methyl-2-ethylcyclopentane eliminate this ring structure from making a major contribution to the reaction pathway. 1,2,3-trimethylcyclopentane can also be eliminated as a possible intermediate because only *o*-xylene and *p*-xylene can be formed from it by a simple ring expansion pathway. The only C_5 cyclization pathway leading to *m*-xylene is through 1,1,3-trimethylcyclopentane followed by ring expansion route (d) in compound VI. For 2,5-dimethylhexane, the trace amount of *m*-xylene excludes ring expansion (d) so that the ring expansion must follow path (a) in order to produce the *p*-xylene

product. Thus, cyclization of both 2,4 and 2,5-dimethylhexane through the common C_5 ring compound, 1,1,3-trimethylcyclopentane, would mutually exclude all of the ring expansions that lead to C_8 aromatics. A direct C_5 cyclization for 2,2,4-trimethylpentane followed by ring expansion to a six carbon ring requires expansion (a) but not (d) ; furthermore, (a) would have to be at least 5 times longer than (c)+(d) to yield the experimental aromatics distribution.

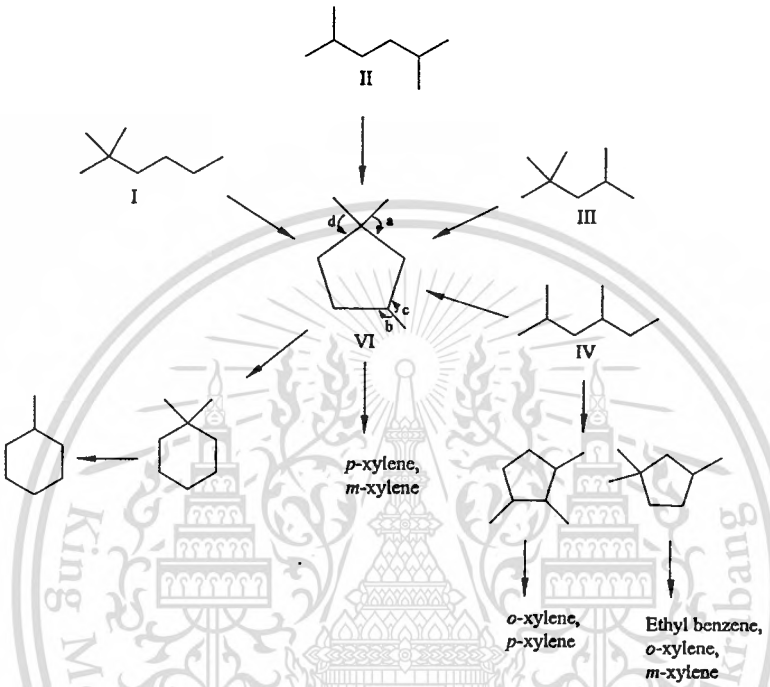

Figure 2.20 Dehydrocyclization of some C_8 alkanes.

Wheatcroft [124] used ^{14}C-isotope to study the dehydrocyclization of *n*-heptane, (*n*-heptane $\xrightarrow{k_1}$ heptene $\xrightarrow{k_2}$ toluene) where k_1 is the rate of dehydrogenation and k_2 is the rate of cyclization. A steady state was assumed for the heptene concentration. With a system of consecutive unimolecular reactions, as well as assuming that hydrogenation of heptene was of secondary importance. Wheatcroft solved the differential equations describing the system and obtained an expression relating the fraction of intermediate (heptene) in the product to the amount of heptane conversion. Wheatcroft used literature values from earlier studies [125,126,127,128] and found that a ratio of $k_2/k_1 = 5$ provided a good fit to the data. Wheatcroft concluded that his treatment showed that the alkene is a compulsory intermediate and that the rate of cyclization is five times faster than the rate of dehydrogenation to the olefin.

As similar to heptanes and octanes dehydrocyclization, *n*-pentane can be cyclized. However, with five carbons, *n*-pentane is not able to cyclize to aromatics. The reaction is proceeded to form C_5 ring and subsequently to cyclopentane [129] and cyclopentadiene [130]. Over the inert support as MFI type with high Si/Al ratio, the Group VIII metal (platinum, iridium, and palladium) are incorporated. The reaction conditions are at the temperature range from 450-600°C and at the pressure range from 0.1-1 atm. The reaction pathway for *n*-pentane dehydrocyclization proposed by Bent [131] is shown in Figure 2.21.

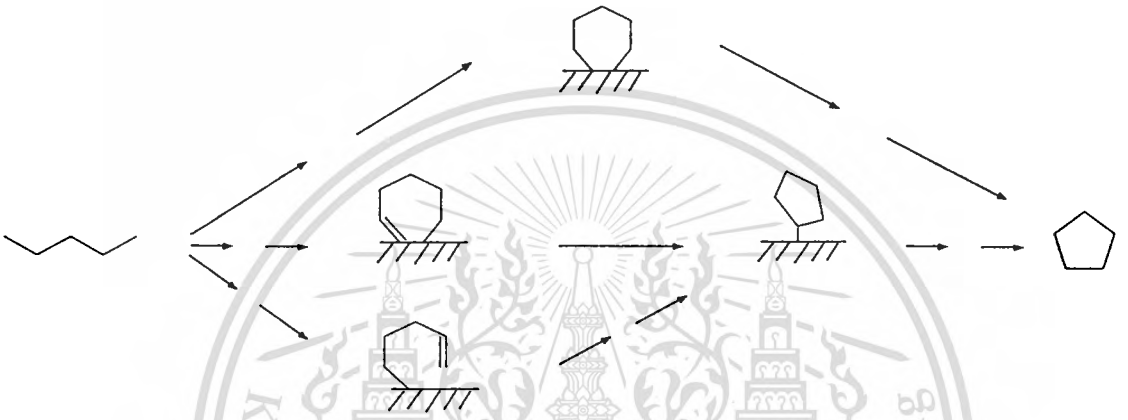

Figure 2.21 Dehydrocyclization of *n*-pentane.

One of the alkane reaction over metal surface is hydrogenolysis [132]. It was establish that the kinetics of hydrogenolysis of ethane was consistent with the occurrence of dehydrogenation to produce a surface specie with carbon having three bonds to the metal surface. This dehydrogenation and multiple bonding to the surface was sufficient to weaken the C-C bond, to allow it to rupture to produce C1 fragments, and the two fragments to be hydrogenated to produce methane [133, 134,135]. With higher carbon number alkanes, a selectivity is introduced there are multiple C-C bonds. For *n*-hexane three types of C-C bond positions are available. Davis et. al. [136] reported that the position selectivity for *n*-hexane hydrogenolysis showed a marked dependence on the surface structure of platinum. Surface with a high concentration of (1 0 0) microfacets [(1 0 0) and (13 1 1)] exhibit a high specificity for scission of internal C-C bonds. In contrast, the surface composed mostly of (1 1 1) microfacets [(1 1 1), (3 3 2), and (10 8 7)] showed a clear preference for central and terminal C-C bond scission. The results reported by Davis et. al. [136] differ from those who report a nearly statistical bond hydrogenolysis of *n*-hexane [137,138].

In agreement with the results of Myers and Munns [133], van Schaik [139], Cinneide and Gault [140], Anderson and Shimoyama [134] find a preference for the hydrogenolysis of the central C-C bond. Furthermore, for conversion at 273°C, 100 Torr, H_2/HC = 10/1 in a recirculating apparatus, the position of C-C bond attack did not appear to be dependent upon the Pt particle size, except perhaps for very large particles. For the largest particle, terminal C-C bond hydrogenolysis may be favored but the central C-C bond cleavage is favored for particle sizes in the range normally encountered in naphtha reforming catalyst. The data show a relative selectivity of C_1-C_2 : C_2-C_3 : C_3-C_4 = 1: 1.3 : 1.8.

Gault [141] identified two extremes for hydrogenolysis of methylcyclopentane as statistical and selective. With highly dispersed platinum catalyst, the data agree with the non-selective reaction pathway. Gault concludes that more than two ring opening pathway are needed to describe the data. Over Pt-alumina catalyst, Gault [142] converted methylcyclopentane with a series of Pt particle size controlled by varying the Pt content from 0.15-20 wt.%. The runs were made in a batch reactor at 315°C and 30 atm. The ratio of bond breakings ($R_{\beta/\gamma}$ and $R_{\gamma/\alpha}$) are plotted versus increasing platinum content (increasing platinum particle size). For the low loading (low Pt particle size) the ratio $R_{\beta/\gamma}$ is nearly constant at 2.5, slightly higher than the value of 2.0 for pure non-selective bond rupture. The other selectivity strongly depends on Pt particle size.

For the hydrogenolysis of *n*-alkane, the rate of C-C bond rupture normally has an inverse dependence on hydrogen pressure. However, the data of Brandenberger et al. [143] show that the rate of ring opening hydrogenolysis of methylcyclopentane has a positive, rather than negative, dependence on hydrogen partial pressure. These results imply that the rate limiting step does not involve dehydrogenation of methylcyclopentane to produce a carbon that is multiply bonded to a surface Pt atom. It is evident that hydrogenolysis is nonselective and that the selectivity for ring opening does not depend to a measurable extent upon hydrogen partial pressure. In contrast, Levitskii and Minachev [144] reported a selectivity that depends upon hydrogen partial pressure for a Pt/SiO_2 catalyst (*n*-hexane : 2-methylheptane : 3-methylheptane = 1.0 : 4.2 : 1.5 at 10 atm H_2 and 1.0 : 1.4 : 0.8 at 50 atm).

Yamada et al. [145] investigatedthe impact of the reaction temperature upon a series of Pt-Re-alumina catalysts that were used for the hydrogenolysis of methylcyclopentane at 300°C and 1 atm total pressure. For the catalyst that was reduced at low temperature, the three allowed hexane isomers are presented in a ratio that is similar to that of nonselective mechanism. In addition, slightly more than 10% of the products result from hydrogenolysis to produce methane

and cyclopentane. As the reduction temperature increases (and Pt particle size increases), the product distribution changes. The amount of *n*-hexane increases with increasing particle size.

For methylcyclopentane hydrogenolysis, it appears the conversion is essentially nonselective for platinum that is highly dispersed on non-zeolitic supports. For the non-zeolite catalysts that are effective as dehydrocyclization catalysts, it is concluded that any contribution of C_5-ring formation will lead to isomerization through a nonselective mechanism for hydrogenolysis of cyclopentane isomers. It is puzzling that only a few authors report hydrogenolysis of methylcyclopentane to produce methane plus cyclopentane. For Pt-zeolite catalysts hydrogeneolysis of methylcyclopentane is selective but for *n*-propyl cyclopentane it is nonselective. There is insufficient data to define the overall selectivity character of Pt-zeolite catalysts.

The hydrogenolysis of cyclohexane or alkylcyclohexane does not make a significant contribution during their conversion under normal reforming processes. The results obtained for the conversion of ^{14}C-labeled methylcyclohexane showed that more than 95% of the methylcyclohexane was converted to toluene with either Pt-nonacidic alumina or Pt-acidic alumina at 482°C and 400 psig [146]. Demethylation by hydrogenolysis and/or dealkylation/transalkylation was the most prominent side reaction, even with the Pt-acidic alumina catalyst. Cracking to C_6- products made a small contribution to the minor amounts of side reactions.

2.6 References

[1] http://en.wikipedia.org/wiki/*n*-pentane

[2] http://en.wikipedia.org/wiki/isopentane

[3] http://en.wikipedia.org/wiki/cyclopentane

[4] Laidler, K.J. and Meiser, J.H. 1999. **Physical chemistry.** 3rd ed. Berkeley: Houghton Mifflin.

[5] Gates, B.C. 1992. **Catalytic chemistry.** New York: John Wiley & Sons.

[6] Levenspiel, O. 1999. **Chemical reaction engineering.** 3rd ed. New York: John Wiley & Sons.

[7] Hagen, J. 2006. **Industrial catalysis.** Weinheim: WILEY-VCH.

[8] Bartholomew, C.H. and Farrauto, R.J. 2006. **Fundamentals of industrial catalytic processes.** 2nd ed. New Jersey: John Wiley & Sons.

[9] Csicsery, S.M. 1986. "Catalysis by shape selective zeolites-science and technology." **Pure & Applied chemistry.** 58: 841-856.

[10] Csicsery, S.M. 1984. "Shape selective catalysis in zeolite." **Zeolites.** 4: 202-213.

[11] Koningsveld, H.V. 2007. **Compendium of zeolite framework types: building schemes and type characteristics.** Amsterdam: Elsevier.

[12] http://www.iza-online.org

[13] Kokotailo, G.T., Lawton, S.L. and Olson, D.H. 1978. "Structure of synthetic zeolite ZSM-5." **Nature.** 272: 437-438.

[14] Olson, D.H., Haag, W.O. and Lago, R.M. 1980. "Chemical and physical properties of ZSM-5 substitutional series. " **Journal of Catalysis.** 61: 390-396.

[15] Thomas, J.M., Ramdas, S., and Millward, B. 1982. "Zeolite shape up to modern catalysis." **New Scientist**, 96: 435-439.

[16] Thomas, J.M., Millward, G.R., Ramdas, S., Bursill, L.A., and Audier, M. 1981. in "Faraday discussions of the chemical society." 72: 345.

[17] Thomas, J.M. and Millward, G.R. 1982. "Direct, real-spece determination of intergrowths ZSM-5/ZSM-11 catalysts." **Journal of chemical society, chemical communications.** 24: 1380-1383.

[18] Dominguez E., J.M., Acosta N., D.R., and Schifter S., I. 1983. "On the crystallography of twinned ZSM-5 type zeolites." **Journal of catalysis.** 83: 480-486.

[19] Meier, W.M. and Olson, D.H. 1978. **Atlas of Zeolite Structure Types, Structure Comission of IZA**. Pennsylvania: Polycrystal Book Service.

[20] Flanigen, E.M., Bennett, J.M., Grose, R.W., Cohen, J.P., Patton, R.L., Kirchner, R.M., and Smith, J.V. 1978. "Silicalite, a new hydrophobic crystalline silica molecular sieve." **Nature.** 271: 512-516.

[21] Dejaifve, P., Auroux, A., Gravelle, P.C., Vedrine, J.C., Gabelica, Z., and Derouane, E.G. 1981. "Methanol conversion on acidicZSM-5, offretite, and mordenite zeolite: a comparative study of the formation and stability of coke deposits." **Journal of Catalysis.** 70: 123-136.

[22] Rollmann, L.D. 1977. "Systematics of shape selectivity in common zeolites." **Journal of Catalysis.** 47: 113-121.

[23] Walsh, D.E. and Rollmann, L.D. 1977. "Radiotracer experiments on carbon formation in zeolites." **Journal of Catalysis.** 4: 369-375.

[24] Rollmann, L.D. and Walsh, D.E. 1979. "Shape selectivity and carbon formation in zeolites." **Journal of Catalysis.** 56: 139-140.

[25] Walsh, D.E. and Rollmann, L.D. 1979. "Radiotracer experiments on carbon formation in zeolites. II." **Journal of Catalysis.** 56: 195-197.

[26] van Santen, R.A., Kramer, G.J. 1995. "Reactivity theory of zeolitic Bronsted acid sites." **Chemical Reviews.** 95: 637-660.

[27] Gillespie, R.J., Peel, T.E., and Robinson, E.A. 1971. "Hammett acidity function for some super acid systems. I. Systems H_2SO_4-SO_4, H_2SO_4-HSO_3F, H_2SO_4-HSO_3Cl, and H_2SO_4-$HB(HSO_4)_4$." **Journal of the American Chemical Society.** 93: 5083-5087.

[28] Walling, C. 1950. "The acid strength of surfaces." **Journal of the American Chemical Society.** 72: 1164-1168.

[29] Umansky, B. and Hall, W.K. 1990. "A spectrophotometric study of the acidity of some acid acids." **Journal of Catalysis.** 124: 97-108.

[30] Parera, J.M. and Figoli, N.S. 1995. **Catalytic naphtha reforming**, New York: Marcel Dekker.

[31] Meerwein, H. and van Emster, K. 1922. "Über die Gleichgewichts-Isomerie zwischen Bornylchlorid, Isobornylchlorid und Camphen-chlorhydrat." **Berichte der Deutschen Chemischen Gesellschaft.** 53: 2500-2528.

[32] Whitmore, F.C. 1932. "The common basis of intramolecular rearrangements." **Journal of the American Chemical Society.** 54: 3274-3283.

[33] Greensfelder, B.S., Voge, H.H., and Good, G.M. 1949. "Catalytic and thermal cracking of pure hydrocarbons: mechanism of reaction." **Industrial and Engineering Chemistry.** 41: 2573-2584.

[34] Fraenkel, G., and Farnum, D.G. 1968. **Carbonium ions.** New York: Wiley.

[35] Brouwer, D.M. 1968. "PMR spectroscopic investigation of structures, stabilities, and rearrangement reactions of C_4-C_7*tertiary* carbonium ions in HF-SbF_5." **Recueil des Travaux Chimiques des Pays-Bas.** 87: 210-224.

[36] Bittner, E.W., Arnett, E.M., and Saunders, M. 1976. "Quantitative preparation and enthalpy of rearrangement of the sec-butyl cation." **Journal of the American Chemical Society.** 98: 3734-3735.

[37] Hiraoka, K. and Kebarle, P. 1976. "Stabilities and energetics of pentacoordinated carbonium ions. The isomeric protonated ethane ions and some higher analogs: protonated propane and protonated butane." **Journal of the American Chemical Society.** 98: 6119-6125.

[38] Kazansky, V.B. and Senchenya, I.N. 1989. "Quantum chemical study of the electronic structure and geometry of surface alkoxy groups as probable active intermediates of heterogeneous acidic catalysts: What are the adsorbed carbenium ions?" **Journal of Catalysis.** 119: 108-120.

[39] Haw, J.F., Nicholas, J.B., Xu, T., Beck, L.W., and Ferguson, D.B. 1996. "Physical Organic Chemistry of Solid Acids: Lessons from in Situ NMR and Theoretical Chemistry." **Accounts of Chemical Research.** 29: 259-267.

[40] Haw, J.F., Richardson, B.R., Oshiro, I.S., Lazo, N.D. and Speed, J.A. 1989. "Reactions of propene on zeolite HY catalyst studied by in situ variable temperature solid-state nuclear magnetic resonance spectroscopy." **Journal of the American Chemical Society.** 111: 2052-2058.

[41] Xu, T. and Haw, J.F. 1994. "Cyclopentenyl carbenium ion formation in acidic zeolites: An in situ NMR Study of cyclic precursors." **Journal of the American Chemical Society.** 116: 7753-7759.

[42] Forester, T.R., and Howe, R.F. 1987. " In situ FTIR studies of methanol and dimethyl ether in ZSM-5." **Journal of the American Chemical Society.** 109: 5076-5082.

[43] Boudart, M., and Djega-Mariadassou, G. 1984. **Kinetics of Heterogeneous Catalytic reactions.** New Jersey: Princeton University Press.

[44] Diebold, U. 2003. "The surface science of titanium dioxide." **Surface Science Reports.** 48: 53-229.

[45] Guisnet, M., Gep, N.S., and Alario, F. 1992. "Aromatization of short chain alkane on zeolite catalysts." **Applied Catalysis A: General.** 89: 1-30.

[46] Sherman, J.D. 1999. "Synthetic zeolite and other microporous oxide molecular sieves." **Proceedings of the National Academy of Sciences colloquium.** U.S.A. 96: 3471-3478.

[47] Sanati, M., Hornell, C., and Jaras, S.G. 1999. "The oligomerization of alkenes by heterogeneous catalysts." **Catalysis.** 14: 236-287.

[48] Morrison, R.A., and Deptford, W. "Aromatization process using zinc and rhenium modified ZSM-5 catalyst." U.S. Patent no. 3855115, December 1974.

[49] Le Van Mao, R., and Yao, J. "Catalysts for the aromatization of light paraffins and olefins." U.S. Patent no. 5135898, April 1992.

[50] Allison, J.D., Basso, S., LeDoux, M., Pham-Huu, C., and Wright, H.A. "Catalyst and process for aromatic hydrocarbons production from methane." U.S. Patent no. 6552243, April 2003.

[51] Mitchell, S.F., Jutta, G.G., and Smith, R.S. "Process for alkane aromatization using platinum-zeolite catalyst." U.S. Patent no. 7186871, March 2007.

[52] Gnep, N.S., Doyemet, J.Y., Seco, A.M., Ramoa Ribeiro, F., and Guisnet, M. 1987. "Conversion of light alkanes to aromatic hydrocarbons. 1-Dehydrocyclodimerization of propane on PtHZSM-5 catalysts." **Applied Catalysis A: General.** 35: 93-99.

[53] Haag, W.O., and Dessau, R.M. 1984. "Duality of mechanism for acid catalyzed paraffins cracking." **Proceedings of the 8th International Congress on Catalysis.** Frankfurt-am-Main. 2: 305-316.

[54] Kitagawa, H., Sendoda, Y., and Ono, Y. 1986. "Transformation of propane into aromatic hydrocarbon over ZSM-5 zeolites." **Journal of Catalysis.** 101: 12-18.

[55] Krannila, H., Haag, W.O., and Gates, B.C. 1992. "Monomolecular and bimolecular mechanism of paraffins cracking catalyzed by ZSM-5." **Journal of Catalysis.** 135: 115-124.

[56] Lukyanov, D.B., Gnep, N.S., and Guisnet, M.R. 1995. "Kinetic modeling of propane aromatization reaction over HZSM-5 and GaZSM-5." **Industrial and Engineering Chemistry Research.** 34: 516-523.

[57] Garwood, W.E. 1983. "Conversion of C_2-C_{10} to higher olefins over synthetic zeolite ZSM-5." **ACS Symposium series.** 218: 383-396.

[58] Pines, H. 1981. **Chemistry of Catalytic Hydrocarbon Conversion.** New York: Academic Press.

[59] Poutsma, M.L. 1976. "Mechanistic consideration of hydrocarbon transformations catalyzed by zeolites." **Zeolite Chemistry and Catalysis.** 171: 437-528.

[60] Quann, R.J., Green, L.A., Tabak, S.A., and Krambeck, F.J. 1988. "Chemistry of olefin oligomerization over ZSM-5 catalyst." **Industrial and Engineering Chemistry Research.** 27: 565-570.

[61] Vedrine, J.C., Dejaifve, P., Garbowski, E.D., and Derouane, E.G. 1980. "Aromatics formation from methanol and light olefins conversions on HZSM-5zeolite: mechanism and intermediate species." **Studies in Surface Science and Catalysis.** 5: 29-38.

[62] Suarez, W., Cheng, W-C., Rajagopalan, K., and Peters, A.W. 1990. "Estimate of hydrogen transfer rates over zeolite catalysts." **Chemical Engineering Science.** 45: 2581-2588.

[63] Guisnet, M., and Magnoux, P. 2001. "Organic chemistry of coke formation." **Applied Catalysis A: General.** 212: 83-96.

[64] Reyniers, M.F., Beirnaert, H., and Marin, G.B. 2000. "Influence of coke formation on the conversion of hydrocarbons I. Alkanes on a USY-zeolits." **Applied Catalysis A: General.** 202: 49-63.

[65] Viswanadham, N., Gupta, J.K., Murali Dhar, G., and Garg, M.O. 2006. "Effect of synthesis Methods and modification treatments of ZSM-5 on light alkanes aromatization." **Energy and Fuels.** 20: 1806-1814.

[66] Sirokman, G., Sendoda, Y., and Ono, Y. 1986. "Conversion of pentane into aromatics over ZSM-5 zeolite." **Zeolite.** 6: 299-303.

[67] Stull, D.R., Westrum, E.F., and Snike, G.C. 1991.**The Chemical Thermodynamics of Organic Compounds.** New York: Wiley/Interscience.

[68] Guisnet, M.R., Aillaleb, D., Doyemet, J.Y., and Gnep, N.S. 1991. **Conversion of light alkanes to aromatics.** New York: ACS.

[69] Caeiro, G., Carvalho, R.H., Wang, X., Lemos, M.A.N.D.A., Lemos, F., Guisnet, M., and Ramoa Ribeiro, F. 2006. "Activation of C_2-C_4 alkanes over acid and bifunctional zeolite catalysts." **Journal of Molecular Catalysis A: Chemical.** 255: 131-158.

[70] Guisnet, M., and Gnep, N.S. 1996. "Aromatization of propane over GaHMFI catalysts. Reaction scheme, nature of the dehydrogenating species and mode of coke formation." **Catalysis Today.** 31: 275-292.

[71] Halgeri, A.B., and Prasada Rao, T.S.R. 1988. in **Proceedings of the International Symposium on Acid Base Catalysis.** Japan.

[72] Jana, A.K., and Rao, M.S. 1993. "Selective aromatization of C_3 and C_4 paraffins over modified encilite catalysts. 1. Quantitative study." **Industrial and Engineering Chemistry Research.** 32: 1046-1052.

[73] Park, Y.K., Kim, D.H., and Woo, S.I. 1997. "Aromatization of pentane catalyzed over various metallosilicates." **Korean Journal of Chemical Engineering.** 14: 249-256.

[74] Guo, J., Lou, H., Zhao, H., Zheng, L., and Zheng, X. 2005. "Dehydrogenation and aromatization of propane over rhenium-modified HZSM-5 catalyst." **Journal of Molecular Catalysis A: Chemical.** 239: 222-227.

[75] Lukyanov, D.B., Gnep, N.S., and Guisnet, M. 1994. "Kinetic modeling of ethene and propene aromatization over HZSM-5 and GaHZSM-5." **Industrial and Engineering Chemistry Research.** 33: 223-234.

[76] Lukyanov, D.B., Gnep, N.S., and Guisnet, M. 1995. "Kinetic modeling of propane aromatization reaction over HZSM-5 and GaHZSM-5." **Industrial and Engineering Chemistry Research.** 34: 516-523.

[77] Gnep, N.S, Doyemet, J.Y., and Guisnet, M. 1988. "Role of gallium species on the dehydrocyclodimerization of propane on ZSM-5 catalysts." **Journal of Molecular Catalysis.** 45: 281-284.

[78] Zheng, B., Hua, W., Yue, Y., and Gao, Z. 2005. "Dehydrogenation of propane over different polymorphs of gallium oxide." **Journal of Catalysis.** 232: 143-151.

[79] Meriaudeau, P., and Primet, M. 1990. "FTIR of hydrogen adsorption on α-Ga2O3." **Journal of Molecular Catalysis.** 61: 227-234.

[80] Kokes, R.J., and Dent, A.L. 1972. **Advance in Catalysis.** 22:1.

[81] Meriaudeau, P. and Naccache, C. 1990. "The role of Ga_2O_3 and proton acidity on the dehydrogenation activity of Ga_2O_3-HZSM-5 catalysts: evidence of a bifunctional mechanism." **Journal of Molecular Catalysis A: Chemical.** 59: L31-L36.

[82] Buckles, G.J. and Hutchings, G.J. 1996. "Aromatization of propane over Ga/HZSM-5: comments on the activation of propane." **Catalysis Today.** 31: 233-246.

[83] Dorouane, E.G., Abdul Hamid, S.B., Ivanova, I.I., Blom, N., and Hojiund-Nielsen, P.E. 1994. "Thermodynamics and mechanistic studies of initial stage in propane aromatization over Ga-modified HZSM-5 catalysts."**Journal of Molecular Catalysis** 86: 371-400.

[84] Ono, Y. 1992. "Transformation of lower alkanes into aromatics hydrocarbons over ZSM-5 zeolites." **Catalysis Review: Science and Engineering.** 34: 179-226.

[85] Biscardi, J.A. and Iglesia, E. 1996. "Structure and function of metal cations in light alkane reactions catalyzed by modified HZSM-5." **Catalysis Today.** 31: 207-231.

[86] Iglesia, E. and Baumgartner, J.E. 1992. "Kinetic coupling and hydrogen surface fugacities in heterogeneous catalysis: I. Alkane reaction on Te/NaX, HZSM-5, and Ga/HZSM-5." **Journal of Catalysis.** 134: 549-571.

[87] Kazansky, V.B., Sobbotina, I.R., van Santen, R.A., and Hensen, E.J.M. 2005. "DRIFTS study of the nature and chemical reactivity of gallium ions in Ga/ZSM-5: II. Oxidation of reduced Ga species in ZSM-5 by nitrous oxide or water." **Journal of Catalysis.** 233: 351-358.

[88] Frash, M.V. and van Santen, R.A. 2000. "Activation of small alkanes in Ga-exchanged zeolites: a quantum chemical study of ethane dehydrogenation." **Journal of Physical Chemistry A.** 104: 2468-2475.

[89] Pereira, M.S. and Nascimento, M.A.C. 2005. "Theoretical study of the dehydrogenation reaction of ethane catalyzed by zeolites containing non-framework gallium species: The 3-step mechanism x the 1 step concerted mechanism." **Chemical Physics Letters.** 406: 446-451.

[90] Joshi, Y.V. and Thomson, K.T. 2005. "The roles of gallium hydride and Bronsted acidity in light alkane dehydrogenation mechanism using Ga-exchanged HZSM-5 catalysts: A DFT pathway analysis." **Catalysis Today.** 105: 106-121.

[91] Nowak, I., Quartararo, J., Derouane, E.G., and Vedrine, J.C. 2003. "Effect of H_2-O_2 pre-treatments on the state of gallium in Ga/H-ZSM-5 propane aromatization catalysts." **Applied Catalysis A: General.** 251: 107-120.

[92] Kaliaguine, S., Lemay, G., Adnot, A., Burelle, S., Audet, R., Jean, G., and Sawicvki, J.A. 1990. "Ion exchange of Fe^{3+} in ZSM-5" **Zeolites.** 10: 559-564.

[93] Meitzner, G.D., Iglesia, E., Baumgartner, J.E., and Huang, E.S. 1993. "The chemical state of gallium in working alkane dehydrocyclodimerization catalysts. in situ gallium K-edge X-ray absorption spectroscopy." **Journal of Catalysis.** 140: 209-225.

[94] Price, G.L. and Kanazirev, V. J. 1990. "Ga_2O_3/HZSM-5 propane aromatization catalysts: Formation of active centers via solid state reaction." **Journal of Catalysis.** 126: 267-278.

[95] Dooley, K.M., Chang, C., and Price, G.L. 1992. "Effects of pretreatments on state of gallium and aromatization activity of gallium/ZSM-5 catalysts." **Applied Catalysis A: General** 84: 1730.

[96] Giannetto, G., Monque, R. and Galiasso, R. 1994. "Transformation of LPG into aromatics hydrocarbons and hydrogen over zeolite catalysts." **Catalysis Review: Science and Engineering.** 36: 271-304.

[97] Giannetto, G., Montes, A. Gnep, N.S., Florentino, A., Cartraud, P. and Guisnet, M. 1994. "Conversion of light alkanes into aromatic hydrocarbons. VII. Aromatization of propane on gallosilicates: Effect of calcination in dry air." **Journal of Catalysis.** 145: 86-95.

[98] Giannetto, G., Leon, G., Papa, J., Monque, R., Galiasso, R. and Gabelica, Z. 1993. "Preparation of acidic or bifunctional catalysts by means of straightforward calcination of as-synthesized [Ga]-ZSM-5 zeolites obtained from alkali-free media. Propane aromatization." **Catalysis Letter.** 22: 381-386.

[99] Dooley, K.M., Price, G.L., Kanazirev, V.I. and Hart, V.I. 1996. "Gallium loaded zeolites for light paraffin aromatization: evidence for exchanged gallium cation active centers." **Catalysis Today.** 31: 305-315.

[100] Kanazirev, V., Piffer, R., and Forster, H. 1991. "FTIR spectroscopic evidence for a key role of hydrogen in creating an active state of Ga_2O_3/HZSM-5 mixed catalysts." **Journal of Molecular Catalysis.** 69: L15-L18.

[101] Kanazirev, V., Price, G.L. and Dooley, K.M. 1990. "Enhancement in propane aromatization with Ga_2O_3/HZSM-5 catalysts." **Journal of the Chemical Society, Chemical Communications.** 9: 712-713.

[102] Price, G.L. and Kanazirev, V. 1991. "The oxidation state of Ga in Ga/ZSM-5 light paraffin aromatization catalysts." **Journal of Molecular Catalysis.** 66: 115-120.

[103] Meriaudeau, P., Sapaly, G., Wicker, G., and Naccache, C. 1994. "Revisiting Ga_2O_3/HZSM-5 propane aromatization catalysts." **Catalysis Letter.** 27: 143-148.

[104] Price, G.L., Kanazirev, V., Dooley, K.M., and Hart, V.I. 1998. "On the mechanism of propane dehydeocyclization over cation-containing, proton poor MFI zeolite." **Journal of Catalysis.** 173: 17-27.

[105] Gonzales, N.O., Chakraborty, A.K., and Bell, A.T. 1999. "A density functional theory study of hydrogen recombination and hydrogen-deuterium exchange on Ga/HZSM-5." **Topic in Catalysis.** 9: 207-213.

[106] Rane, N., Overweg, A.R., Kazansky, V.B., van Santen, R.A., and Hensen, E.J.M. 2006. "Characterization and reactivity of Ga^+ and GaO^+ cations in zeolite ZSM-5." **Journal of Catalysis.** 239: 478-485.

[107] Seddon, D. 1990. "Paraffin oligomerization to aromatics" **Catalysis Today.** 6: 351-372.

[108] Tauster, S.J., Fung, S.C., and Garten R.L. 1978. "Strong metal-support interactions. Group 8 noble metals supported on titanium dioxide." **Journal of the Americal Chemical Society.** 100: 170-175.

[109] Tauster, S.J., and Fung, S.C. 1978. "Strong metal-support interactions: Occurrence among the binary oxides of groups IIA–VB." **Journal of Catalysis.** 55: 29-35.

[110] Ko, E.I., Garten, J. 1981. "Ethane hydrogenolysis studies of TiO_2-supported group VIII metal catalysts." **Journal of Catalysis.** 68: 233-236.

[111] Resasco, D.E., and Haller, G.L. 1982. "Dispersion Effects on Alkane Hydrogenolysis over Rhodium Supported on Titanium Oxide." **Study of Surface Science and Catalysis.** 11: 105-112.

[112] Cairns, J. A., Baglin, J. E. E., Clark, G.J. , and Ziegler, J.F. 1983. "Strong metal-support interactions for Pt and Rh on Al_2O_3 and TiO_2: Application of nuclear backscattering spectrometry." **Journal of Catalysis.** 83: 301-314.

[113] Kelley, M. J., Short, D. R., and Swartzfager, D. G. 1983. "*In situ* tem and iss studies of supported metal 'SMSI' catalysts." **Journal of Molecular Catalysis.** 20: 235-249.

[114] Vishwanathan, V. and Narayanan, S. 1993. "Evidence for strong metal support interaction (SMSI) in Rh/TiO_2 system." **Catalysis Letter.** 21: 183-189.

[115] Li, Q., Wang, K., Zhang, M., Yang, J., and Jin, Z. 2006. "Effect of photo catalytic activity of CO oxidation on Pt/TiO_2 by strong interaction between Pt and TiO_2 under oxidizing atmosphere." **Journal of Molecular Catalysis A: Chemical.** 258: 83-88.

[116] Zhang, M., Jin, Z., Zhang, Z., and Dang, H. 2005. "Study of strong interaction between Pt and TiO_2 under oxidizing atmosphere." **Applied Surface Science.** 250: 29-34.

[117] Lin, C., Chao, J., Liu, C., Chang, J., and Wang, F. 2008. "Effect of calcination temperature on the structure of a Pt/TiO_2 (B) nanofiber and its photocatalytic activity in generating H_2." Langmuir. 24: 9907-9915.

[118] Davis, B.H. 1976. "Paraffin dehydrocyclization : V. The influence of Pt loading on the aromatic selectivity." **Journal of Catalysis.** 42: 238-246.

[119] Davis, B.H. 1971. "Dehydrocyclization of paraffins. Influence of chlorine on cyclization pathway over $Pt\text{-}Al_2O_3$catalysts." **Journal of Catalysis.** 23: 355-357.

[120] Davis, B.H., and Venuto, P.B. 1969. "Paraffin dehydrocyclization : Distribution of aromatic products obtained with "nonacidic" supported Pt catalysts ." **Journal of Catalysis.** 15: 363-372.

[121] Fogelberg, L.G., Gore, R., and Rånby, B. 1967. "Aromatization of paraffin hydrocarbons." **Acta Chemica Scandinavica.** 21: 2041-2049

[122] Fogelberg, L.G., Gore, R., and Rånby, B. 1967. "Aromatization of paraffin hydrocarbons. II. Aromatization of C_8 heptanes and hexanes over platinum/alumina catalysts." **Acta Chemica Scandinavica.** 21: 2050-2060.

[123] Pines, H., and Chen, C.T. 1961. "Alumina: Catalyst and support: XXXI. Dehydrogenation of 2-phenylbutane-2-C^{14}." **Journal of Catalysis.** 6: 380-384.

[124] Wheatcroft, R.W. 1949. Ph.D. Thesis, University of California.

[125] Taylor, H.S. and Turkevich, J. 1939. "Fundamentals in the catalytic ring closure of open chain hydrocarbons" **Transactions of the Faraday Society.** 35: 921-934.

[126] Hoog, H., Verheus, J., and Zuiderweg, F. 1939. "Investigations into the cyclisation (aromatization) of aliphatic hydrocarbons." **Transactions of the Faraday Society.** 35: 993-1006.

[127] Mattox, W. 1944. "Effects of Temperature, contact time, and water vapor on the olefin-aromatic ratio in the dehydrogenation of *n*-heptane with chromia-alumina." **Journal of the American Chemical Society.** 66: 2059-2063.

[128] Taylor, H.S. and Fehrer, H. 1941. "The Mechanism of Reaction and of Poisoning in the Dehydroaromatization of *n*-Heptan." **Journal of the American Chemical Society.** 63: 1387-1392.

[129] Dessau, R.M. "Upgrading of normal pentane to cyclopentane." U.S. Patent no. 5283385, February 1994.

[130] Dessau, R.M. "Upgrading of normal pentane to cyclopentene." U.S. Patent no. 5284986, February 1994.

[131] Bent, B.E. 1996. "Mimicking aspects of heterogeneous catalysis: generating, isolating, and reacting proposed surface intermediates on on single crystals in vacuum." **Chemical Review.** 96: 1361-1390.

[132] Cimino, A., Boudart, M., and Taylor, H.S. 1954. "Ethane hydrogenation-cracking on iron catalysts with and without alkali." **Journal of Physical Chemistry.** 58: 796-800.

[133] Myers, C.G. and Munns Jr., G.W. 1958. "Platinum hydrocracking of pentanes, hexanes, and heptanes" **Industrial and Engineering Chemistry.** 50: 1727-1732.

[134] Anderson, J.R., Shimoyama, Y. 1973. in: W. Hightower (Ed.), 5th Int. Congr. Catal. J., Miami Beach, FL, 20–26 August 1972, North-Holland, Amsterdam, 695–715.

[135] Chow, M. and McVicker, G.B. 1988. "Conversion of methylcyclopentane and acyclic hexanes over supported platinum catalysts : I. Isomerization kinetics and hydrogenolysis selectivities." **Journal of Catalysis.** 112: 290-302.

[136] Davis, S.M., Zaera, F. and Somorjai, G. 1984. "Surface structure and temperature dependence of *n*-hexane skeletal rearrangement reactions catalyzed over platinum single crystal surfaces: Marked structure sensitivity of aromatization." **Journal of Catalysis.** 85: 206-223.

[137] Santacessaria, E., Gelosa, D., Carra, S., and Adami, I. 1978. "Influence of Metal Dispersion on n-Hexane Reactions over Platinum-Alumina Catalysts." **Industrial and Engineering Chemistry Product Research and Development.** 17: 68-71.

[138] Karpinski, Z. and Koscielski, T. 1980. "Catalytic reactions of hydrocarbons over Pt---Pd alloys : III. Skeletal reactions of *n*-pentane and *n*-hexane over Pt---Pd/SiO_2 catalysts." **Journal of Catalysis.** 63: 313-323.

[139] van Schaik, J.R.H., Dessing, R.P., and Ponec, V. 1975. "Reactions of alkanes on supported Pt-Au alloys." **Journal of Catalysis.** 38: 273-282.

[140] Cinneide, A.D. and Gault, F.G. 1975. "Reactions of hexanes, unlabeled and Labeled with ^{13}C, on alumina-supported palladium-gold and platinum-gold alloys." **Journal of Catalysis.** 37: 311-323.

[141] Gault, F.G. 1981. "Mechanisms of skeletal isomerization of hydrocarbons on metals." **Advance in Catalysis.** 30: 1-95.

[142] Gault, F.G. 1957. **Compt Rendu** 245: 1620.

[143] Brandenberger, S.G. Callender, W.L., and Meerbott, W.K. 1976. "Mechanisms of methylcyclopentane ring opening over platinum-alumina catalysts." **Journal of Catalysis.** 42: 282-287.

[144] Levitskii, I.I. and Minachev, K.M. 1975. in: F. Márta, D. Kalló (Eds.), Mechanisms of Hydrocarbon Reactions: a Symposium,Elsevier, Amsterdam, 81–95.

[145] Yamada, M., Yamamoto, E., and Amano, A. 1982. "Hydrogenolysis of methylcyclopentane by supported Pt-Re catalyst." **Journal of the Japan Petroleum Institute.** 25: 112-117.

[146] Davis, B.H. 1973. "^{14}C tracer study of the fate of methylcyclohexane during naphtha conversion over Pt---Al_2O_3 catalysts." **Journal of Catalysis.** 29: 395-397.

CHAPTER 3

MATERIALS AND METHOD

3.1 Materials and apparatuses

3.1.1 Materials

-*n*-Pentane (C_5H_{12}, Aldrich)

- Isopentane (C_5H_{12}, Aldrich)

- Cyclopentane (C_5H_{10}, Aldrich)

- Gallium (III) nitrate ($Ga(NO_3)_3 \cdot xH_2O$, Aldrich)

- Zinc (II) nitrate ($Zn(NO_3)_2 \cdot 6H_2O$, Carlo Erba)

- Copper Oxide (CuO)

- Potassium bromide (KBr, Jasco, spectroscopy grade)

- Ethylene glycol (commercial)

- di-Hydrogen, hexa-chloro platinate (Fluka, H_2Cl_6Pt)

- HZSM-5 zeolite (Si/Al = 28, 45, 180 and 500, Zeolyst)

- H-Beta (Si/Al = 11, Zeolyst)

- Commercial amorphous silica (SiO_2, Carlo Erba)

- Titania (TiO_2)

- Quartz wool (SiO_2, Grace)

- Distilled water

- De-ionized water

- Hydrogen gas (H_2, Praxair)

- Helium gas (He, Praxair)

- Air zero (79%N_2 and 21%O_2, Praxair)

- Nitrogen gas (N_2, Praxair)

- Liquid nitrogen (TIG)

- Standard methane, ethane, ethylene, LPG, benzene, toluene, and xylene

- Methanol (CH_3OH, Lab-Scan)

- Hydrofluoric acid solution (HF 40 wt. % in water, Panreac)

- Methylene chloride (CH_2Cl_2)

- Ice and ice bath

3.1.2 Apparatuses

- Packed bed reactor and catalytic testing unit
- Saturator
- Water circulating cooling bath
- Bubble flow meter
- Digital flow meter
- Vertical tube furnace
- Horizontal tube furnace and alumina boat
- Mass flow controller sets
- Temperature programmed reduction (TPR)/temperature program desorption (TPD) apparatus
- Flame-ionization detector gas chromatograph (910, BUCK)
- Gas chromatograph-mass spectrometer apparatus (6890N, Agilent technologies-5973N, Agilent Technologies)
- Mass spectrometer (Omnistar-Pfiffer)
- Scanning electron microscope (LEO 1455VP, LEO Electron Microscopy)
- Transmission electron microscope (JEM-2100, Jeol)
- X-ray powder diffractometer (D8 Advance, Bruker AG)
- X-ray fluorescence spectrometer (SRS 3400, Bruker AG)
- Fourier transforms infrared spectrometer (Spectrum 1, Perkin Elmer)
- Inductively coupled plasma spectrometer (ICP-Plasma-1000, Perkin Elmer)
- Thermogravimetric analyzer (Pyris 1 TGA, Perkin Elmer)
- Gas adsorption analyzer (Autosorb-1, Quantachrome)
- Ultrasonic bath
- Sieve kit (20 and 30 mesh)
- Agate mortar and pestle sets
- Power regulator and heating tape
- Refrigerator
- Balance
- Oven, vials, and laboratory glassware
- Tube cutter (1/4 and 1/8 inch O.D.), wrench, spanner and hand tools

3.2 Experimental method

3.2.1 Preparation of GaZSM-5 and ZnZSM-5

Gallium and Zinc are introduced into the zeolite by incipient wetness impregnation using aqueous solution of $Ga(NO_3)_3$ and $Zn(NO_3)_2$. First, HZSM-5 samples are weighted to a desired amount as detailed in Table 3.1, and then gradually drop the prepared metal solution into such supports. After the samples appeared to be wetted, the wet samples are left to dry at room temperature. The process is repeated until the desired metal loading (~0.7 wt.%) is achieved. Finally, the impregnated GaZSM-5 and ZnZSM-5 catalysts are calcined in air stream with a flow rate of 60 ml/min at 500°C for 5 hours at a heating rate of 3°C/min in a horizontal tube furnace.

Table 3.1 Details of impregnation synthesis reagent.

Catalyst designations	HZSM-5 weight (g)	Si/Al ratio	Concentration of metal salt solution (g/l)	Desired volume (ml)
GaZSM-5 (28)	10	28	3.125	32.3
GaZSM-5 (45)	10	45	3.125	32.3
GaZSM-5 (180)	10	180	3.125	32.3
GaZSM-5 (500)	10	500	3.125	32.3
ZnZSM-5 (180)	10	180	5.23	19.3

3.2.2 Preparation of Pt/SiO_2 and Pt/TiO_2

Platinum is introduced into the SiO_2 and TiO_2 by incipient wetness impregnation using aqueous solution of H_2Cl_6Pt. First, SiO_2 and TiO_2 samples are weighted to a desired amount as 10 gram, and then gradually drop the prepared metal solution with a concentration of 2.038 g/l into such supports. After the samples appear to be wetted, the wet samples are left to dry at room temperature. The process is repeated until the desired volume is achieved (49.6 ml) to get the desired metal loading (~1wt.%). Finally, the impregnated Pt/SiO_2 and Pt/TiO_2 catalysts are calcined in air stream with a flow rate of 60 ml/min at 500°C for 5 hours at a heating rate of 3°C/min in a horizontal tube furnace.

3.2.3 Characterization of catalysts

3.2.3.1 Morphology

A scanning electron microscope (SEM, LEO model 1450 VP) is used to determined the catalyst morphology. The sample is prepared by thoroughly placing catalyst onto the sample holder. It is then coated with gold thin film by ion sputtering. The sample is placed in the sample chamber of scanning electron microscope and evacuated from ambient pressure to 10^{-4} torr. The scanning electron micrographs are taken at the magnification of 500, 1000, 2000 and 3000 times.

A transmission electron microscope (TEM, JEOL model JEM-2010) is also employed. For characterization of active metal clusters by transmission electron microscopy, the wet sample is crushed in a mortar, and the suspended powder is subjected to be dispersed on a carbon-coated copper TEM grid. Electron micrographs are acquired in the magnification range of 3000-1500000 times.

3.2.3.2 Surface area

Gas adsorption analyzer (Autosorb-1) is employed for surface area determination. The sample is weighed about 50 mg and transferred to a clean, dry empty sample cell. This sample cell is loaded to the outgassing station. Then, heating mantle is installed with the sample cell and temperature is raised to 350°C under vacuum. The sample is out-gassed about 18 hours. The sample cell is then removed from the out gassing station after the nitrogen is filled, and loaded to the analysis station. The equilibration time is set to 3 minutes and the nitrogen adsorption is measured at the partial pressure (P/P_0) ranged from 10^{-6} to 1.0 at -195.6°C. When adsorption is complete, the sample cell is removed from the sample station and reweighed. The total surface area of the catalysts is calculated by using Brunauer, Emmett, and Teller (BET) equation.

3.2.3.3 Structure and crystallinity

The catalyst structure and crystallinity are determined by X-ray diffractometer (Siemens model D8). The sample is prepared by packing the catalyst in the sample holder. CuKα X-ray beam is used for analysis at 40 kV, 40 mA. The sample is scanned from 2θ angle of 5° to 60° for zeolite and 5° to 80° for SiO_2 and TiO_2 with 1 second/step time and 0.04 2θ/step increment. X-ray diffraction pattern of sample is compared with standard X-ray diffraction pattern for determining the structure.

3.2.3.4 Elemental analysis

Elemental analysis of the metal-modified catalyst is performed by inductively coupled plasma/atomic emission spectroscopy (ICP/AES, Perkin Elmer model PLASMA-1000). An accurate 25 mg of catalyst is weighed and then digested with hydrofluoric acid. This solution is diluted to 50 mL in a plastic volumetric flask. Then, the diluted sample solution is measured against a blank. Finally, the metal content is calculated using calibration curves.

The chemical composition of catalysts can be also determined by an X-ray fluorescence spectrometer (Siemens model SRS3400). The sample is prepared by mixing 4.5 grams of boric acid and 0.5 grams of catalyst and send to a grinder. The mixture is packed onto sample holder and then compressed at 150 kN. The sample is placed in the sample chamber. Rhodium is employed as a source for measure at 50 kV, 60 mA.

3.2.3.5 Reducible metal oxide species in the catalyst

The temperature programmed reduction (TPR) experiment is done by treating 200 mg of the catalyst in air at 500°C for 3 hours, followed by N_2 purge until the temperature is reduced to 50°C. A 10% H_2/Ar gas mixture with a total flow rate of 38 ml/min is fed through the catalyst bed with a linear heating rate of 10°C /min. The water produced during reduction is trapped at -50°C and the hydrogen consumption is recorded by an on-line TCD detector (VICI model TCD2-NIFED).

3.2.3.6 Acid sites of catalyst

The temperature programmed desorption of NH_3 and/or pyridine are employed to determine the acidity and acid strength of the catalyst. A 150 mg of the catalyst is treated in air at its calcined temperature for 1 hour, followed by He purge until the temperature is reduced to 30°C. A 1% NH_3/He or saturated pyridine (at 15°C) with a total flow rate of 20 ml/min is continually fed through the catalyst bed at this temperature for 3 hours, followed by He purge for 1 hour. He gas with a total flow rate of 80 ml/min is then fed through the catalyst bed and the catalyst is heated with a linear heating rate of 10°C /min, the desorbed ammonia/pyridine is monitored by an on-line TCD detector (VICI model TCD2-NIFED).

3.2.3.7 Gas desorption

Temperature programmed hydrogen evolution (TPHE) is performed as followed. A 200 mg of catalyst is treated in a continuous flow of air (~20 ml/min) at 500°C for 1 hour. Then, the calcined catalyst is purged by helium gas at 500°C for 15 minutes. A H_2 (~15 ml/min) is fed through the catalyst bed together with an increase in temperature to 550°C. The catalyst is kept at this temperature for 2 hours, after that it is cooled down to 50°C in a hydrogen stream. The reduced catalyst is purged by He (~21 ml/min) for 30 minutes, after that the temperature is increased from 50°C to 800°C with a heating rate of 10°C/min. The desorbed hydrogen (m/z = 2) is detected by an-online mass spectrometer (Omnistar-Pfiffer).

Temperature programmed chlorine desorption (Cl_2-TPD) is performed as followed. A 100 mg of catalyst is fed by air or 2%H_2 in Ar (~ 20 ml/min) as carrier for 30 minutes. After that, it is heated from 50°C to 700°C with heating rate of 10 ml/min. The desorbed Cl_2 (m/z = 70) is detected by an on-line mass spectrometer (Omnistar-Pfiffer).

3.2.3.8 Oxidation state of elements

Electron spin resonance spectrometry (ESR) is performed using an X-band JEOL, model JES-RE2X spectrometer (frequency of 8.8-9.6 GHz) equipped with a TE011 sample cavity. The sample temperature is kept constant at about 77 K with a cold, dry liquid N_2 flow cryostat. The line position is calibrated with DPPH (1,1-diphenyl-2-picrylhydrazyl), g = 2.0036.

The X-ray absorption near edge structure (XANES) measurement is carried out at the beam line BL8 of the Siam Photon Laboratory. The samples are crushed in an agate mortar, spattered over the Kapton tape attached with a transparent frame and loaded into the sample chamber. Fluorescence mode XAS is performed to obtain Chlorine K-edge spectra and Platinum M-edge spectra which are calibrated with potassium chloride (edge energy at 2822 eV) and platinum foil (edge energy at 2122 eV), respectively.

3.2.3.9 Coke analysis

A fourier transforms infrared spectrometer (FTIR, Perkin Elmer model Sepectrum 1) is used to determine the structure of coke. FTIR spectra are recorded in the framework region (400 to 4000 cm^{-1}) in transmittance mode. The used ZSM-5 catalysts are collected. A destruction of used ZSM-5 (300 mg) framework by hydrofluoric acid solution (1 mL), followed by CH_2Cl_2 (3 mL) extraction is preparation procedure to get the high molecular

weight liquid samples. The IR Spectrums of such liquid samples are recorded with an Elmer-Perkins FTIR spectrometer with 1 cm^{-1} resolution and averaged over 500 scans.

Temperature programmed desorption-mass spectrometer (TPD-MS) is performed as followed. A 100 mg of used catalyst is purged by He with a flow rate of 20 ml/min at room temperature. After that, it is heated with a linear heating rate of 10°C/min, the desorbed hydrocarbons are monitored by an on-line mass spectrometer (Omnistar-Pfiffer).

A thermogravimetric analyzer (TGA, Perkin Elmer model TGA Pryis 1) is used to determine coke content. Approximately 10 mg of the used catalyst is placed in a platinum pan hanging from a microbalance and nitrogen is introduced as a carrier gas. The sample is then heated under air or nitrogen (50 ml/min) for %weight loss from 50°C to 800°C at a heating rate of 10°C/min

The characterization methods of the catalysts for the reaction over metal loaded zeolites and metal loaded inert supports are summarized in Table 3.2.

Table 3.2 Catalyst characterization for the reaction over metal loaded zeolites and metal loaded inert supports.

Characterization method	Metal loaded zeolites (GaZSM-5, ZnZSM-5)	Metal loaded inert supports (Pt/SiO_2, Pt/TiO_2)
SEM	✓	-
TEM	-	✓
BET	✓	✓
XRD	✓	✓
ICP	✓	-
XRF	-	✓
H_2-TPR	✓	✓
NH_3-TPD	✓	✓
Pyridine-TPD	-	✓
TPHE	✓	-
Cl_2-TPD	-	✓
ESR	-	✓
XANES	-	✓
FTIR	✓	-
TPD-MS	✓	✓
TGA	✓	✓

3.2.4 Catalytic activity testing

The catalyst is compressed (pressure ~ 3 ton) to be a pellet and it is sieved through 20-30 mesh before packing in the middle of reactor made with a quartz tube. To minimize the channeling, the quartz tube diameter (7 mm) is typically greater than 8 times of the diameter of the sieved catalyst (~0.7 mm) [1]. The catalytic activity testing of the prepared catalysts is carried out in a downward flow direction, as depicted in Figure 3.1. Before the reaction, the catalyst is activated in air (20 ml/min) at its calcine temperature (300-500°C) for 1 hour at a heating rate of 3°C/min. After that, the catalysts are typically reduced (at 550°C for GaZSM-5 and ZnZSM-5

and at 300-500°C for Pt/SiO_2 and Pt/TiO_2) for 2 hours in a flow of H_2 (13 ml/min). The temperature is kept at the reaction temperature (typically at 500°C), and a saturated vapor of a C_5 hydrocarbon (isopentane at -5°C, *n*-pentane at -5°C and cyclopentane at 3.5°C) is carried by hydrogen/helium (with a total flow of 15-22 ml/min) through a fixed bed reactor made with a quartz tube. The products of the reaction are quantitatively analyzed by an on-line gas chromatograph (BUCK Scientific Model 910) with a flame-ionization detector (FID) using HP1 column (for reaction over GaZSM-5 and ZnZSM-5) and HP-PLOT column (for reaction over Pt/SiO_2 and Pt/TiO_2). The details of GC conditions of both columns and the reactor characteristics are summarized in Table 3.3 and 3.4. The peak area from the chromatogram is measured and calculated as the peak area percent value. Then the unknown peak can be identified by GC-MS technique. The composition of the hydrocarbon samples are determined by the normalization method.

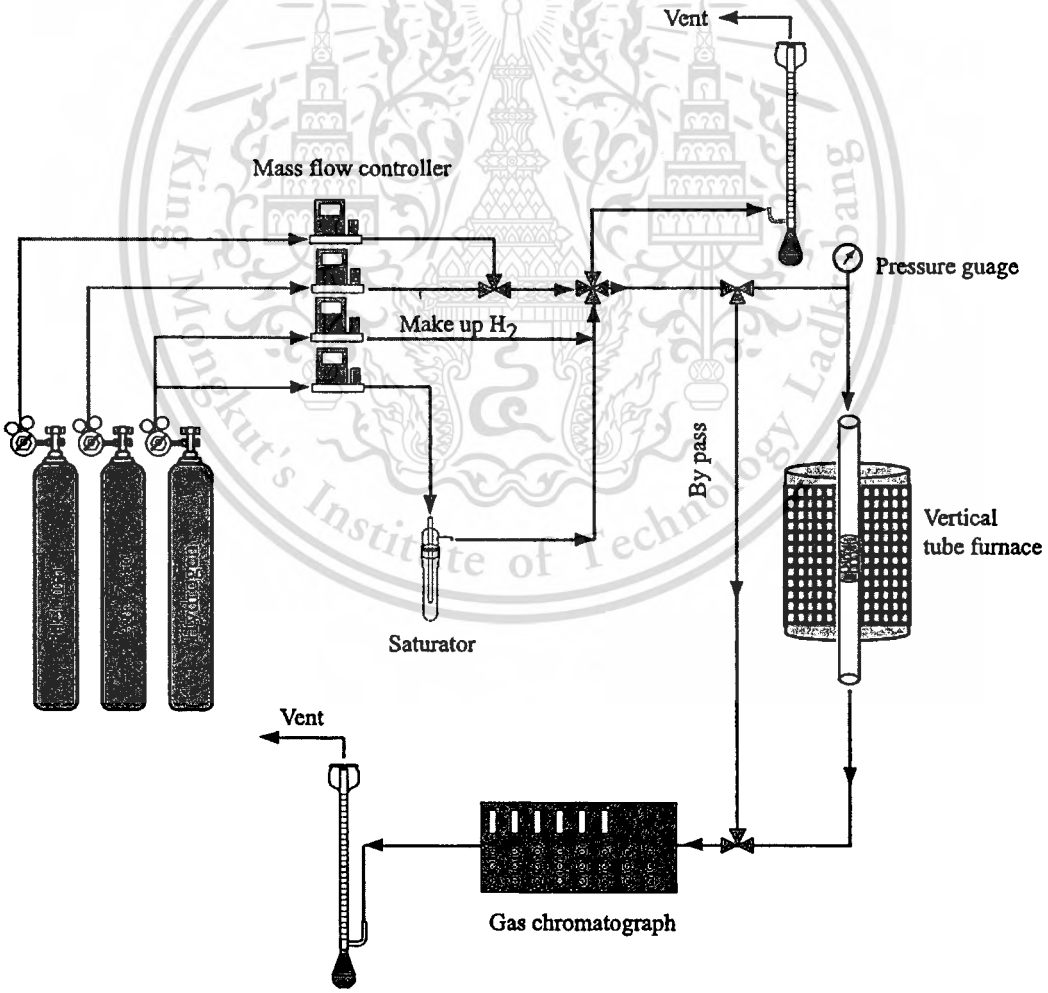

Figure 3.1 Experimental set up of the test unit.

Table 3.3 GC conditions.

Column	HP1	HP-PLOT
Diameter (mm)	0.25	0.53
Length (m)	100	30
Carrier gas	N_2	N_2
Detector	FID	FID
Detector temperature (^{o}C)	250	250
Detector gases		
H_2 (ml/min)	25	25
Air (ml/min)	250	250
Sample loop (µl)	25	25
Column head pressure (psi)	24	3
Linear velocity (cm/s)	36	32
Oven temperature		
Initial temperature (^{o}C)	40	80
Initial time (min)	16	20
Rate (^{o}C/min)	25	-
Final temperature (^{o}C)	250	-
Final time (min)	26	-
Total time (min)	50	20

Table 3.4 Description of the reactor set up and the operating condition.

Parameters	Value
Reactor inside diameter (mm)	6
Reactor outside diameter (mm)	8
Total Flow (ml/min)	~15
Bed length (mm)	3-25
Catalyst weight (g_{cat})	0.03-0.3
Contact time (g_{cat} h/mol C_5)	~5-30
WHSV (g_{C5}/ g_{cat} h)	2-14
Catalyst size (mesh)	20-30
Catalyst activation (before running reaction)	in air at 500°C and reduce by H_2 typically at 300-500°C
H_2/C_5	~ 3-4
Reaction temperature	Typically at 500°C
Reaction pressure	Ambient (~1atm)

3.3 References

[1] Pereira, C.J. and Leib, T.M. 2008. "Perry's Chemical Engineers' Handbook." McGraw-Hill.

CHAPTER 4

CONVERSION OF C_5 HYDROCARBONS TO AROMATICS

4.1 Introduction

At the beginning of the 20th century, the demand for aromatics and its derivatives were increased to support many petrochemical industries. For example, ethylbenzene synthesized by alkylation of benzene with ethylene was required to produce styrene monomer, the basic chemical for all polystyrene products [1]. Cumene produced by alkylation of benzene with propylene was used worldwide as the principal chemical for production of phenol and acetone. The phenol yielded phenolic resins, bisphenol-A, caprolactam, and other products. Phenolic resins were used extensively to bond wood and composition board. Both phenol and acetone are used increasingly in the production of polymer, such as epoxy, polycarbonate resins, and nylon-6 [2]. *p*-Xylene was used to produce purified terephthalic acid which was reacted with ethylene glycol to make the poly-(ethylene terephthalate), the basis of polyester fibers [2]. Polyester fibers have revolutionized clothing with proportion for any climate, as well as low cost, excellent durability, and ease of washing with little of water and detergent. From the recent strong demand of *p*-xylene, isomerization of any xylene isomers and disproportionation of toluene were performed to produce such aromatics additionally [1]. Moreover, aromatic hydrocarbons especially benzene used to be a blending component in gasoline to increase the octane quality [1] but nowadays world-wide public concerns about the earth's environment and health consideration, aromatics in gasoline is decreased due to new regulations requiring the reduction of aromatic compound [2]. However, aromatics are still significant as raw materials especially for petrochemical processes, as mentioned above.

From the important of these aromatics, the conventional heterogeneous catalytic process well known as aromatization was established to convert low-value liquidfied petroleum gas (LPG; C_3-C_4) or light feed stock (C_5-C_6) containing olefins and paraffins to high-value, petrochemical grade liquid aromatics products, particularly benzene, toluene, and xylene (BTX). In addition, there are futile hydrocarbons from the fractionation of naphtha cracking unit including saturated

C_5 hydrocarbons such as *n*-pentane, isopentane and cyclopentane. Therefore, aromatization of these C_5 hydrocarbons to the valuable aromatics is attractive.

Both mono-functional and bi-functional catalysts are available for aromatization process. In mono-functional catalyst, only the metallic function takes part in the reaction mainly for the dehydrocyclization of C_6-C_8 *n*-alkanes [3,4]. In bi-functional catalyst, acid sites and metal sites are incorporated and together work to transform alkanes to aromatics. Acid sites normally catalyze isomerization, oligomerization, and cyclization while metal sites mainly catalyze dehydrogenation [5,6].

It has been reported that GaZSM-5 and ZnZSM-5 possess high activity and selectively to convert various saturated hydrocarbons to aromatics. The essential role of metal active sites is to promote the formation of the dehydrogenated products which can further oligomerized and cyclized to aromatics over the acid sites. However, this mechanism seems to be existed especially for small paraffinic hydrocarbons (C_2-C_4) [7]. The long chain hydrocarbons (C_6-C_8) can directly convert to aromatics via dehydrocyclization [4], whereas the formation of aromatics from C_5 hydrocarbons is still not clearly defined.

It is expected that the conversion of five-carbon hydrocarbon reactants to aromatic ring is a certain complex reaction. With the different saturated C_5 structures, i.e., linear hydrocarbon of *n*-pentane, branch hydrocarbon of isopentane, and cyclic hydrocarbon of cyclopentane, this may affect to the formation of aromatics. This chapter are intentionally studied the formation of aromatics from such C_5 hydrocarbons. The reaction pathway are proposed and discussed together with the effect of contact time, Si/Al ratio of catalyst, reaction and reduction temperature, and H_2 partial pressure.

4.2 Experimental

HZSM-5 with Si/Al = 28, 45, 180 and 500 were calcined at 500°C and used as catalysts. The GaZSM-5 and ZnZSM-5 were prepared by incipient wetness impregnation of the parent HZSM-5 with aqueous solution of $Ga(NO_3)_3$ (Aldrich) and and $Zn(NO_3)_2$ (Carlo Erba), as previously shown in Chapter 3. The samples were subsequently dried and calcined in air at 500°C for 5 h.

The metal loading was determined by ICP atomic emission spectrometer (Perkin Elmer model PLASMA-1000). The surface areas (BET) of catalysts were determined by N_2 adsorption (Autosorb-1). The catalyst structure and crystallinity are determined by X-ray diffractometer (Siemens model D8). The morphology and surface composition was quantified by SEM-EDX (LEO model 1450 VP). Temperature programmed reduction (TPR) and temperature programmed NH_3 desorption (TPD) experiments were performed in a quartz micro-reactor. The H_2 consumption and NH_3 desorption were recorded by an on-line TCD detector (VICI model TCD2-NIFED).

The reaction was carried out at 500-600°C and ambient pressure. Before the reaction, the catalyst was activated in air (20 ml/min) at 500°C for 3 h. After that, the catalysts were typically reduced at 550°C for 2 h in a flow of H_2 (13 ml/min). At the reaction temperature (typically at 500°C), saturated vapor of isopentane (at -5°C) or *n*-pentane (at -5°C) or cyclopentane (at 3.5°C) was carried by hydrogen/helium (a total flow of 15-22 ml/min) through a fixed bed reactor made with a quartz tube (O.D. = 8 mm). The products of the reaction were analyzed by an on-line gas chromatograph (BUCK Scientific Model 910) with an FID detector using HP1 column (ϕ = 0.25 mm, L = 100 m).

For coke characterization, the carbonaceous compounds were liberated from the zeolite channel by dissolution of the aluminosilicate matrix in a hydrofluoric solution (40%) at room temperature, then it was extracted by CH_2Cl_2 to analyze using an FTIR (Perkin Elmer model Sepectrum 1). TPD-MS of the coked catalysts was performed in a quartz reactor and the coke content was analyzed by TGA (Perkin Elmer model TGA Pryis 1). The details of each experimental procedure are mentioned thoroughly in Chapter 3.

4.3 Results and discussion

4.3.1 Catalysts characterization

4.3.1.1 Metal loading

The gallium and zinc content in the impregnated zeolite catalysts are determined by inductively coupled plasma/atomic emission spectroscopy (ICP/AES). The metal loading is approximately 0.7wt.% for all GaZSM-5 and ZnZSM-5 catalysts. The results are shown in Table 4.1.

Table 4.1 The elemental analysis and surface area of ZSM-5 zeolite used in this study.

Catalyst	Si/Al ratio	Metal loading (wt.%)	BET surface area (m^2/g)
HZSM-5	28	-	382
HZSM-5	45	-	371
HZSM-5	180	-	365
HZSM-5	500	-	377
GaZSM-5	28	0.74	386
GaZSM-5	45	0.75	367
GaZSM-5	180	0.74	352
GaZSM-5	500	0.72	346
ZnZSM-5	180	0.79	330

4.3.1.2 Surface area

Surface area of all zeolite catalysts is determined by nitrogen adsorption technique using Brunauer-Emmet-Teller (BET) as model equation. The calculated surface area for each sample is summarized in Table 4.1. All zeolite catalysts possess high surface area (> 300 m^2/g); therefore, the high dispersion of metals (Ga and Zn) would be obtained.

4.3.1.3 Crystal structure

The diffraction pattern of zeolite catalyst is obtained by X-ray powder diffraction technique (XRD). The XRD patterns are shown in Figure 4.1. It reveals characteristic peaks at 2θ of 7.972, 8.818, 8.917, 23.080, 23.320, and 23.95. These indicate that all ZSM-5 catalysts have the pentasil pore opening structure of MFI, as compared to their reference diffraction pattern (APPENDIX B).The peak intensities are relatively high, suggesting that all catalysts are well-define crystalline micro-porous materials.

4.3.1.4 Catalyst morphology

The catalyst morphology from scanning electron micrograph in Figure 4.2 exhibits that the crystals of zeolites are in spherical shape. The crystal size of HZSM-5 with Si/Al of 28 and 45 are smaller than 1 micron. Moreover, an agglomeration of HZSM-5 with Si/Al of 45 is particularly observed. This is because it possesses a very small crystal size which is consistent with the observed peak broadening in XRD pattern (Figure 4.1). In addition, relatively large crystalline are observed for HZSM-5 with Si/Al of 180 and 500. Although the particle size of these zeolites is different, no significantly difference in their surface area is observed suggesting that such surface area is mainly contributed from the inner surface area of the pore system.

After gallium and zinc loading and calcination, the same XRD pattern (Figure 4.1) and catalyst morphology (Figure 4.2) are observed. It is suggesting that a well-dispersed and very small metal oxide (Ga_2O_3 and ZnO) cluster would be obtained.

4.3.1.5 Surface composition of GaZSM-5

The energy dispersive analysis of GaZSM-5 catalysts is shown in Figure 4.3. The gallium, aluminium, and silicon represent as yellow, green, and pink points, respectively. It can be seen that the gallium with 0.7 wt.% is almost uniformly dispersed on ZSM-5 surface. This indicates that the interaction between gallium and zeolite are relatively high. It is likely that the electrostatic charge of the gallium and the zeolite framework constrains the gallium species to position mostly at the exchangeable sites. However at Si/Al ratio of 500, gallium may be in excess to the exchangeable sites and some gallium species may be dispersed on other locations, i.e., silanol or siloxane.

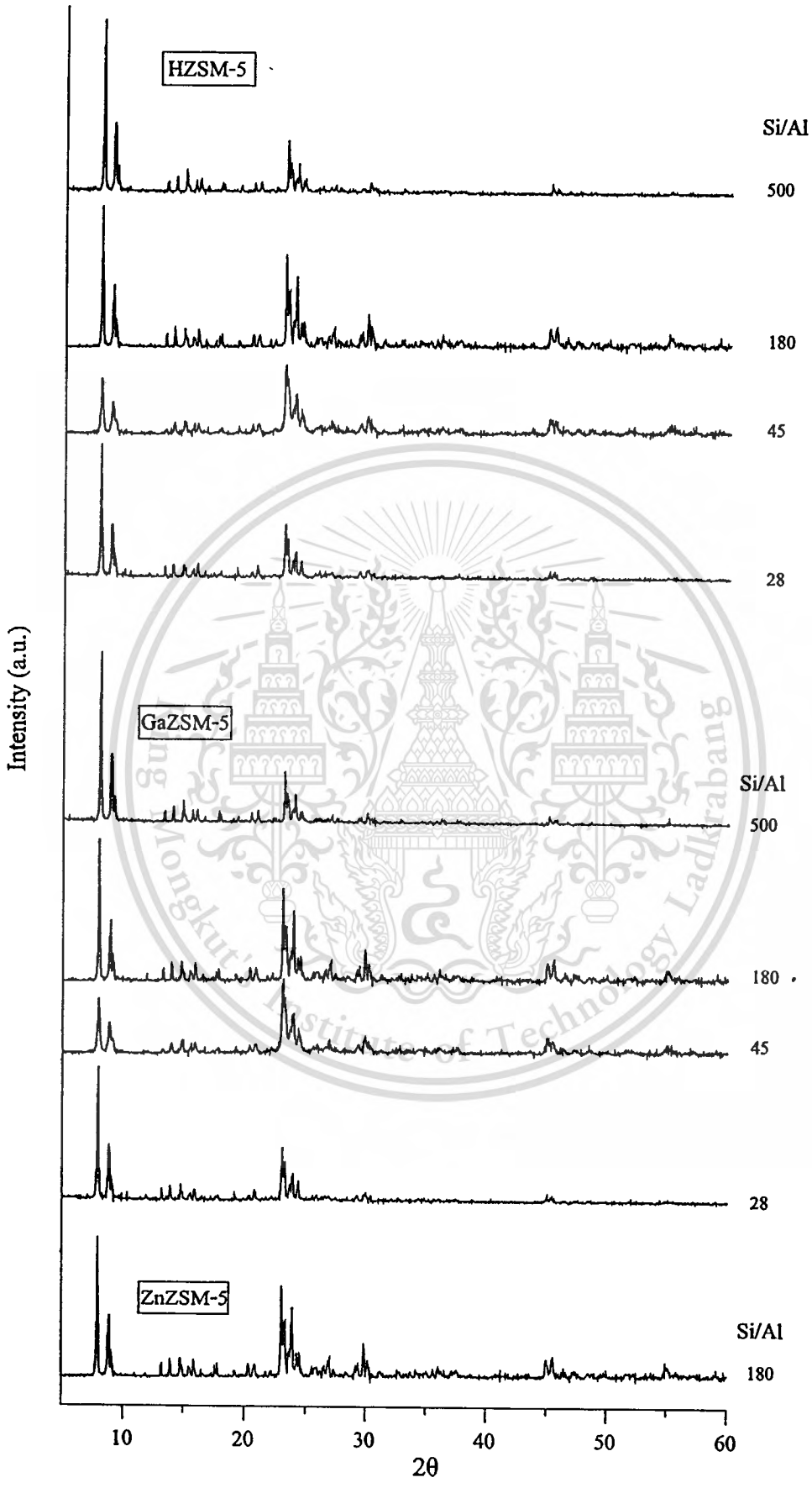

Figure 4.1 X-ray diffraction patterns of HZSM-5, GaZSM-5 (0.7 wt.%), and ZnZSM-5 (0.7 wt.%)

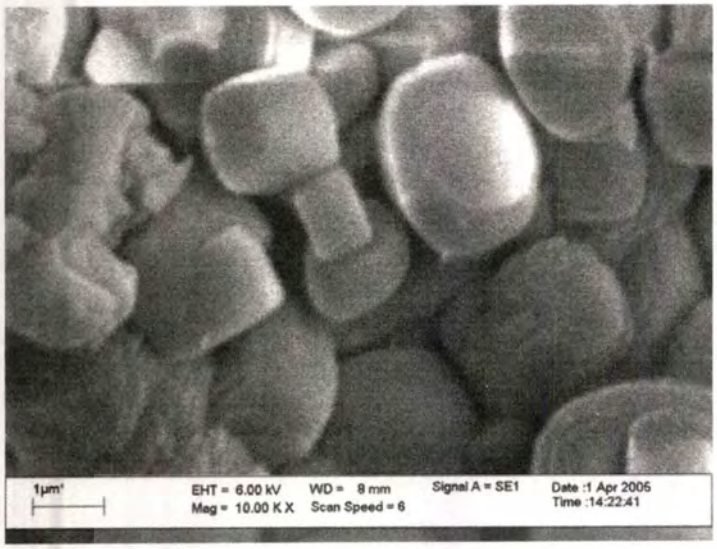

HZSM-5, Si/Al = 500

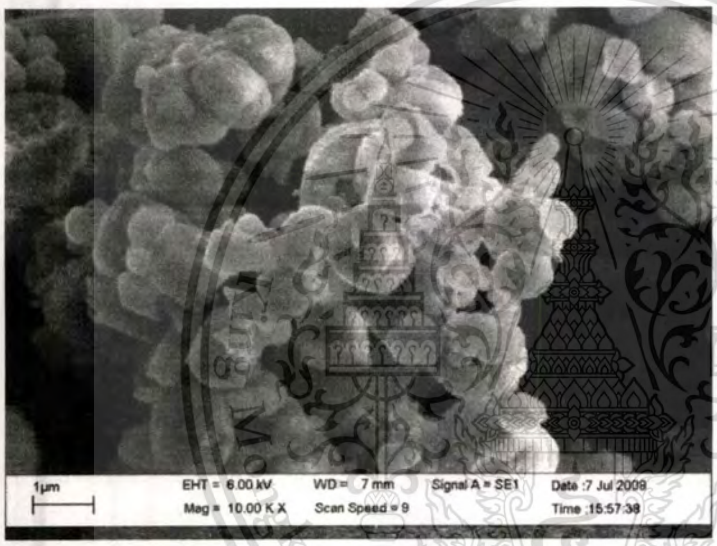

HZSM-5, Si/Al = 180

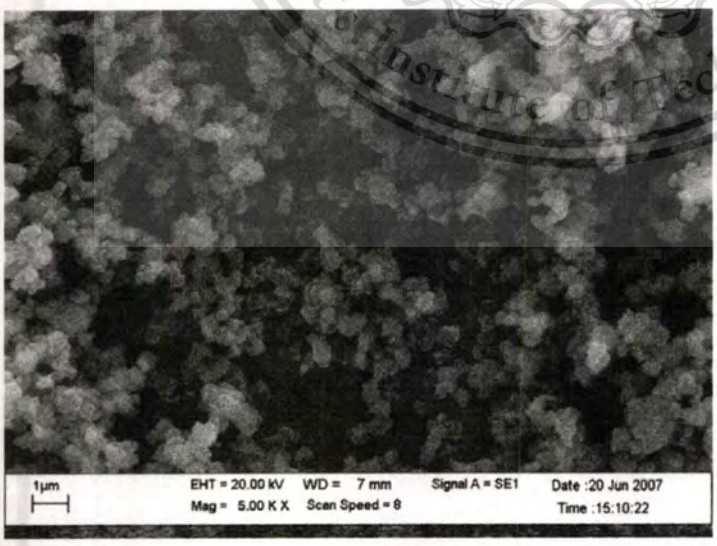

HZSM-5, Si/Al = 45

Figure 4.2 SEM images of HZSM-5, GaZSM-5, and ZnZSM-5.

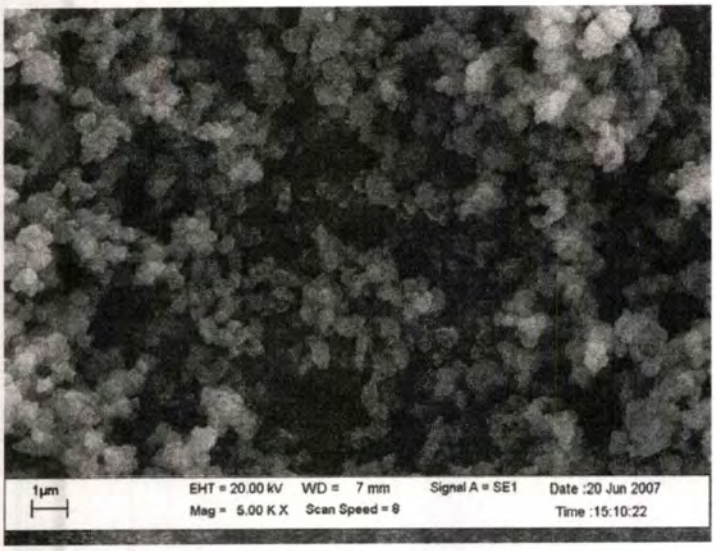

HZSM-5, Si/Al = 28

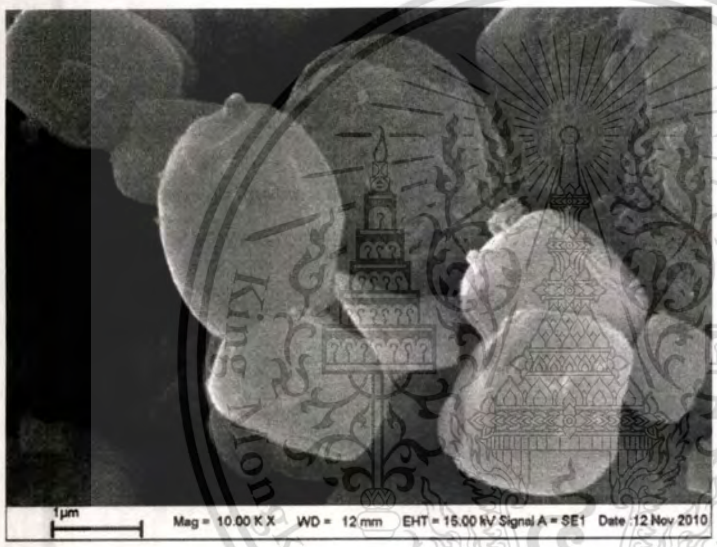

GaZSM-5, Si/Al = 500

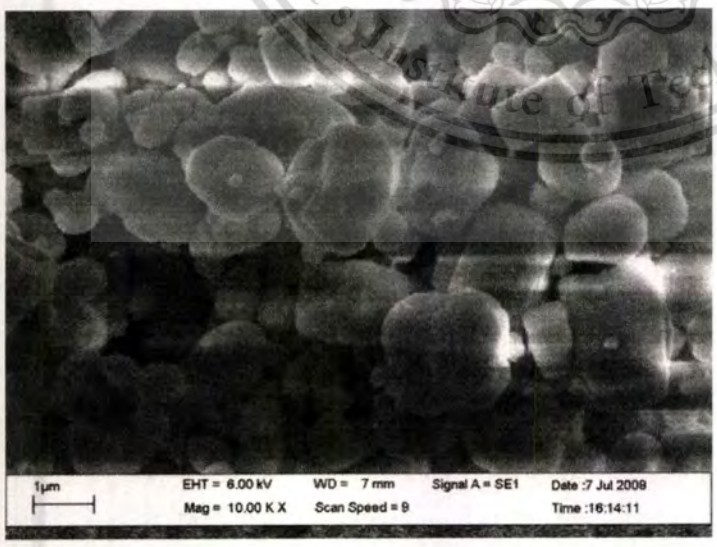

GaZSM-5, Si/Al = 180

Figure 4.2 SEM images of HZSM-5, GaZSM-5, and ZnZSM-5 (continued).

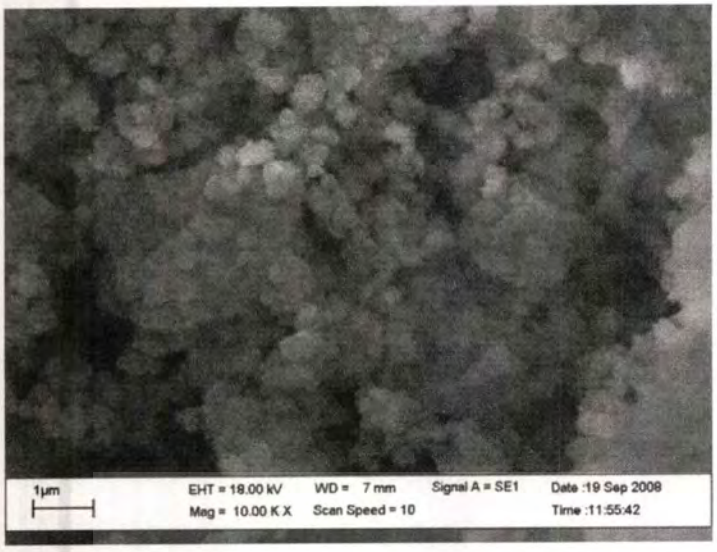

GaZSM-5, Si/Al = 45

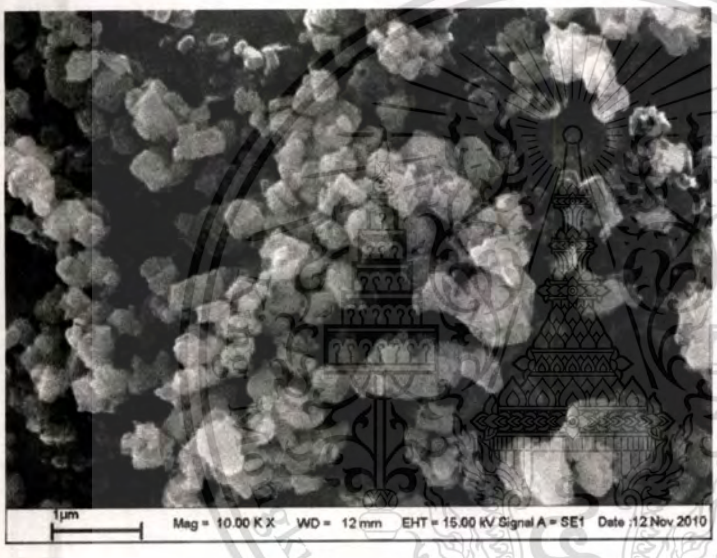

GaZSM-5, Si/Al = 28

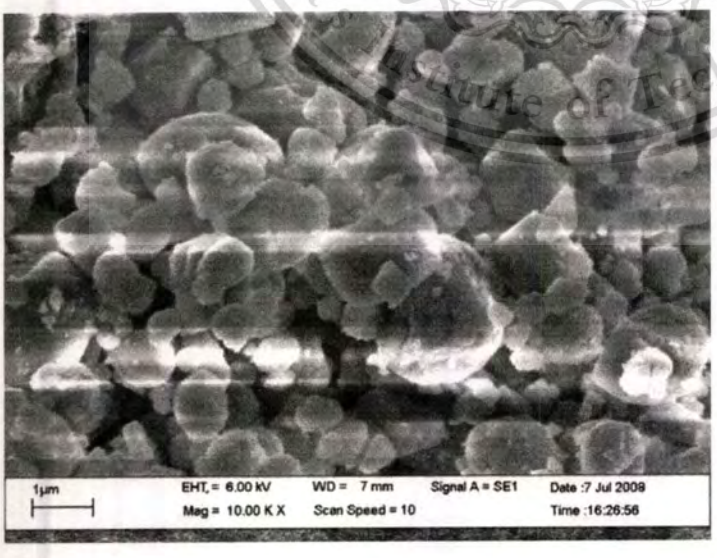

ZnZSM-5, Si/Al = 180

Figure 4.2 SEM images of HZSM-5, GaZSM-5, and ZnZSM-5 (continued).

GaZSM-5, Si/Al = 500

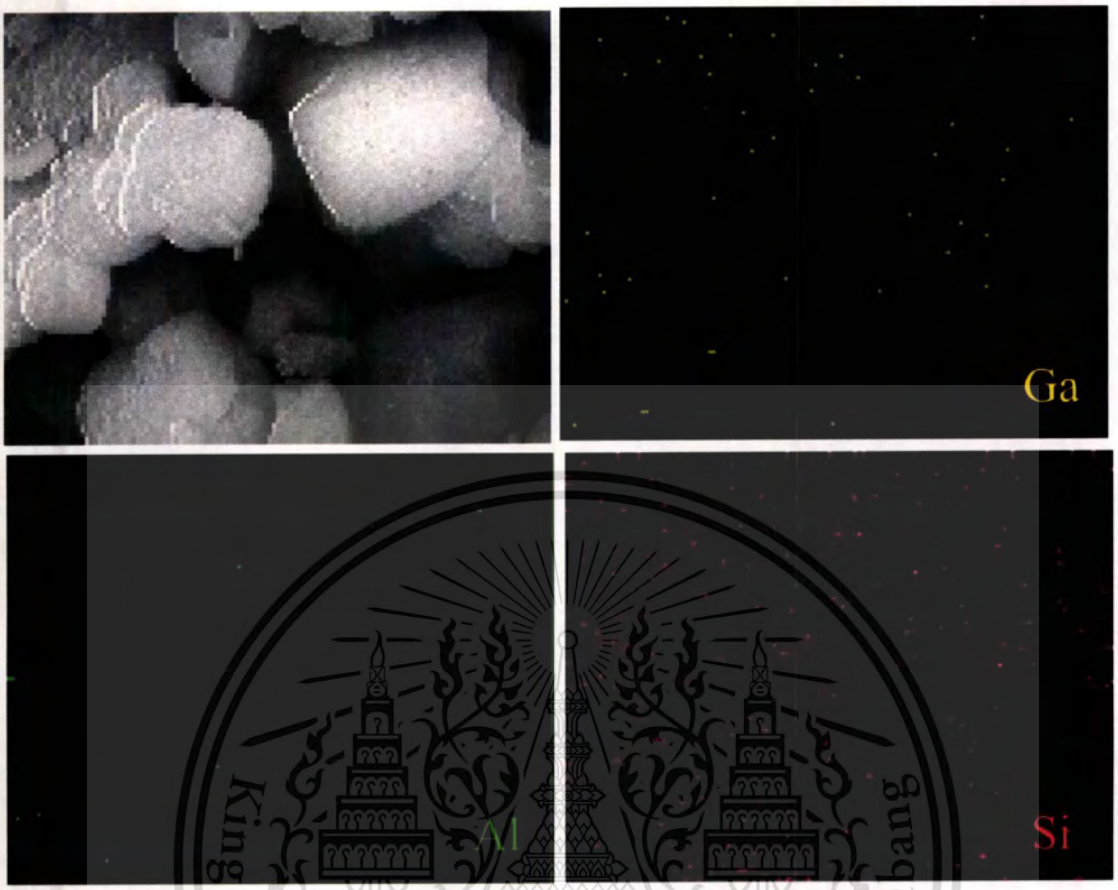

Figure 4.3 SEM-EDX of GaZSM-5 (0.7 wt.%) catalysts.

GaZSM-5, Si/Al = 180

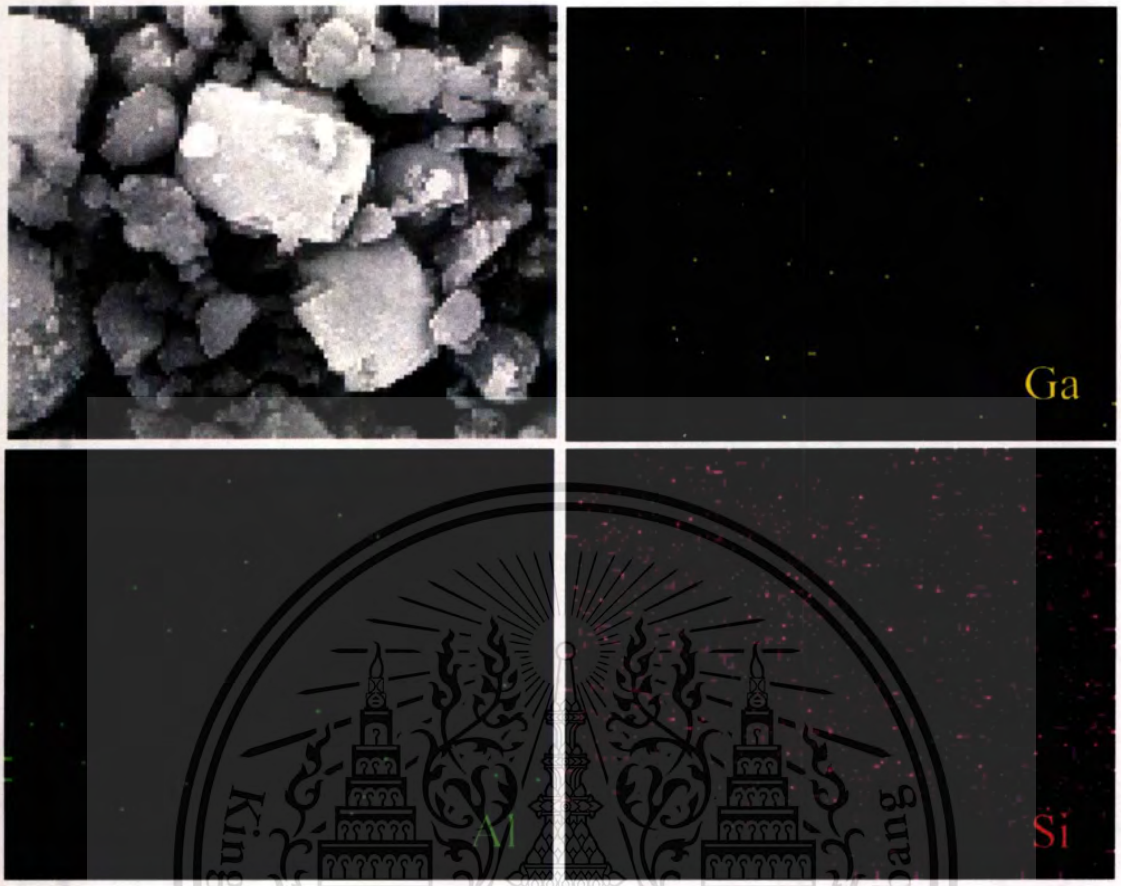

Figure 4.3 SEM-EDX of GaZSM-5 (0.7 wt.%) catalysts (continued).

GaZSM-5, Si/Al = 45

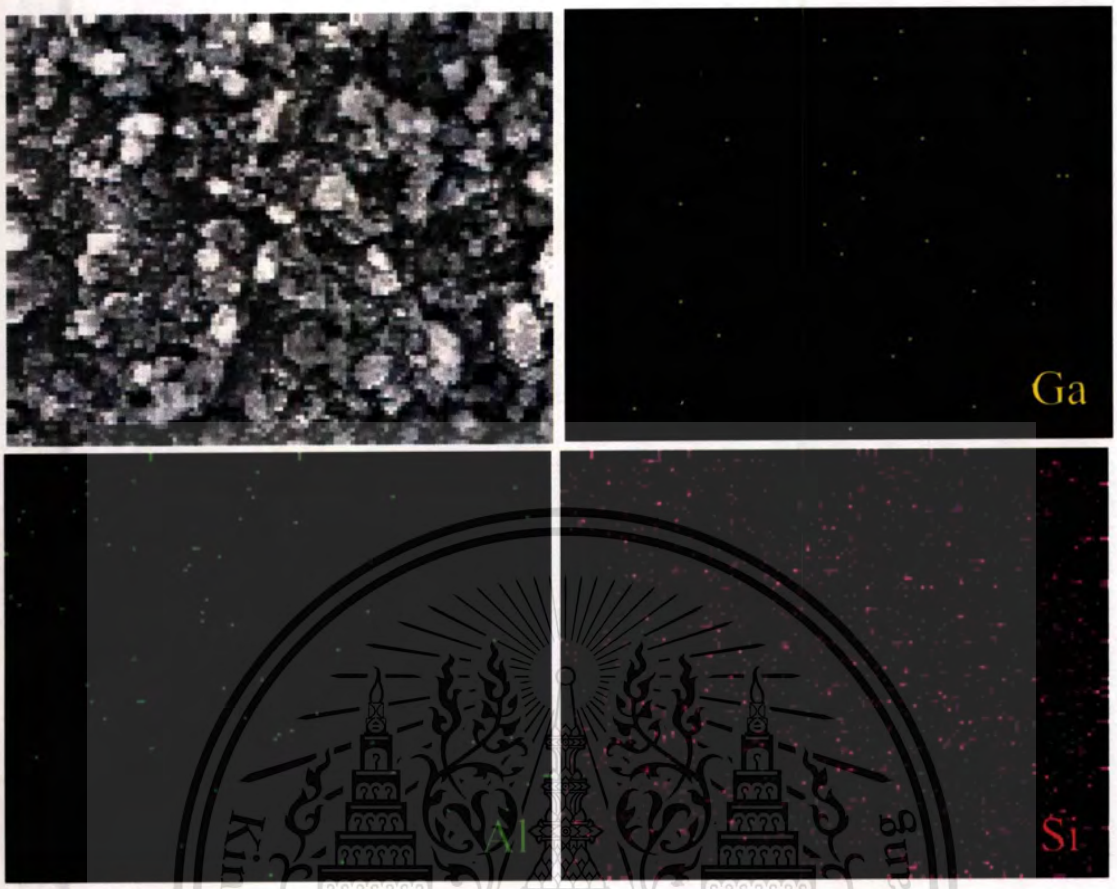

Figure 4.3 SEM-EDX of GaZSM-5 (0.7 wt.%) catalysts (continued).

GaZSM-5, Si/Al = 28

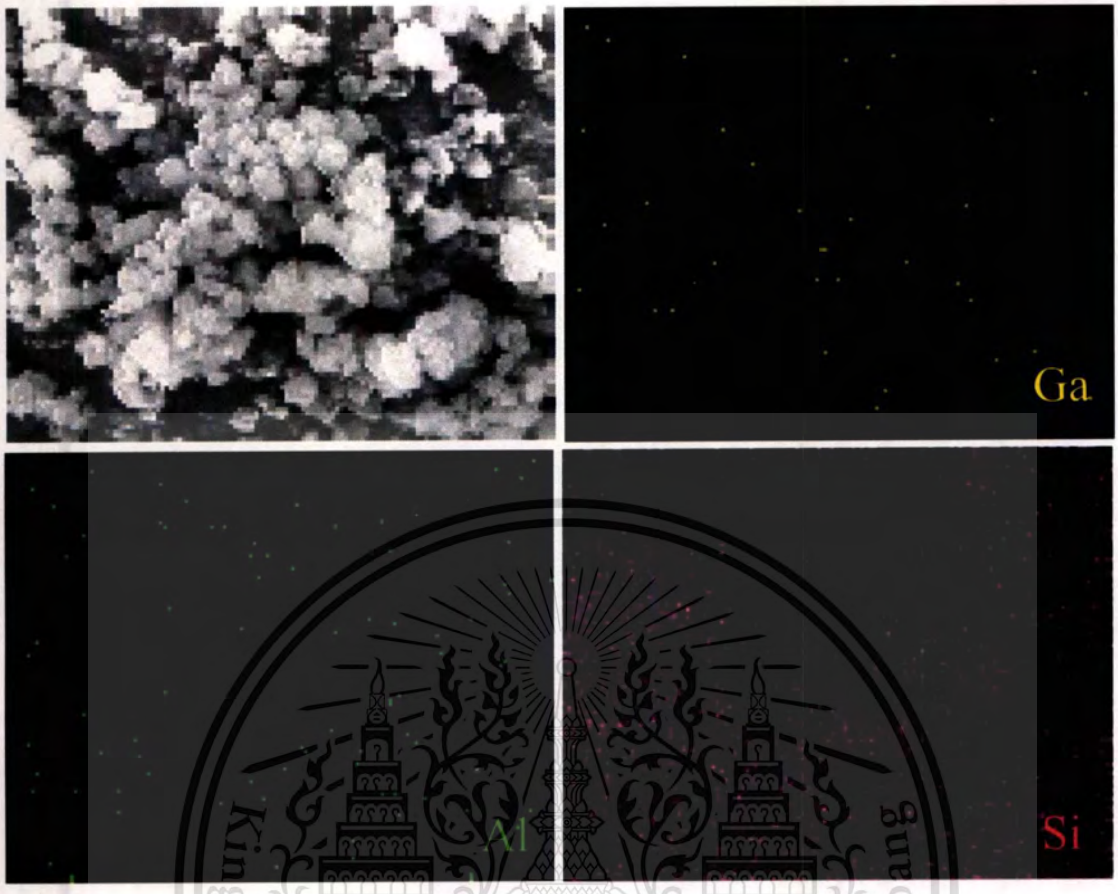

Figure 4.3 SEM-EDX of GaZSM-5 (0.7 wt.%) catalysts (continued).

4.3.1.6 Temperature programmed H_2 reduction

TPR of GaZSM-5 shows two broad reduction peaks at about 500, 600°of the catalysts suggesting that various Ga species are formed after calcining at 500°C (Figure 4.4). These two peaks are previously observed [7] and assigned to the reduction of finely dispersed Ga_2O_3 (~500°C) and GaO^+ ion (~600°C) to Ga^+ [8,9,10,11]. It can be seen in Figure 4.4 that the intensity of reduction peak at 600°C increased with a decrease in Si/Al ratio (from 500 to 45). This suggests that formation of GaO^+ specie is facilitated when acidity of the catalyst is increased. Therefore, it is likely that GaO^+ is formed by reaction of Ga_2O_3 and Bronsted protons of the zeolite as shown in Eq. (4.18) [12],

$$Ga_2O_3 + 2H^+ \longrightarrow 2GaO^+ + H_2O \qquad (4.18)$$

As the number of the Bronsted protons increases (low Si/Al), the formation of GaO^+ would be largely promoted. However, no reduction peak at 600°C is observed for GaZSM-5 with Si/Al ratio of 28 despite the same Ga contents is incorporated (0.7 wt%). It is suggested that GaO^+ might not be present in GaZSM-5 with such high acidity (Si/Al of 28). This is because the incorporated Ga species may well be inserted into the framework either by (i) reacting with defect silanol groups or (ii) replacing the dislodged Al^{3+} framework after calcination. The framework Ga species formed would not be easily reduced. Only the finely dispersed Ga_2O_3 retained from the insertion can be reduced and that could be observed in a small extent, as compared to that in other GaZSM-5 samples with high Si/Al ratio. For ZnZSM-5, only single peak for reduction of Zn^{2+} specie to Zn^0 metal is expectedly observed at 550°C [13].

As mentioned previously that finely dispersed Ga_2O_3 is reduced to be Ga^+ [8,9,10], and such specie would chemisorb H_2 to form GaH_2^+ [14,15] in the presence of continuous flow of H_2. As the catalysts are subjected to H_2 reduction at 550°C, it is likely that the reduced formed of finely dispersed Ga_2O_3 (Ga^+ and subsequently changed to GaH_2^+) and GaO^+ (retained from reduction at lower temperature than 600°C) are available active sites in the GaZSM-5 catalysts.

In case of ZnZM-5, the possible active sites are Zn^0 formed after H_2 reduction at 550°C and the retained Zn^{2+}, as reported in the literature [14,16].

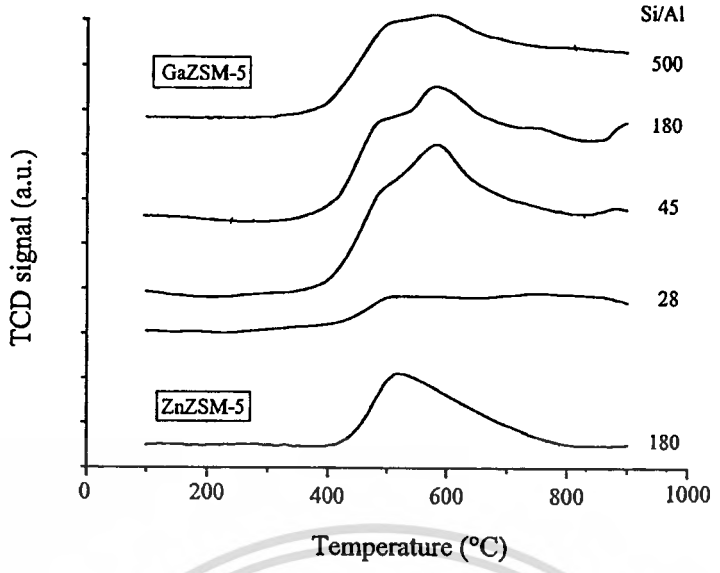

Figure 4.4 TPR of GaZSM-5 (0.7 wt.%) and ZnZSM-5 (0.7 wt.%).

4.3.1.7 Temperature programmed NH_3 desorption

The acidity and acid strength of HZSM-5 with Si/Al = 28, 45, 180 and 500 are shown in Figure 4.5. It is found that strong acid sites (Bronsted acid sites) of HZSM-5 is observed by ammonia desorption peak at 350°C. A decrease of ammonia intensity is obtained when the Si/Al ratio of the HZSM-5 is increased. This suggests that lower acid sites can be achieved when using HZSM-5 with high Si/Al ratio. Moreover, a decrease in acid strength is observed from HZSM-5 with Si/Al = 500. This may be due to the weak interaction between the proton and high silica framework.

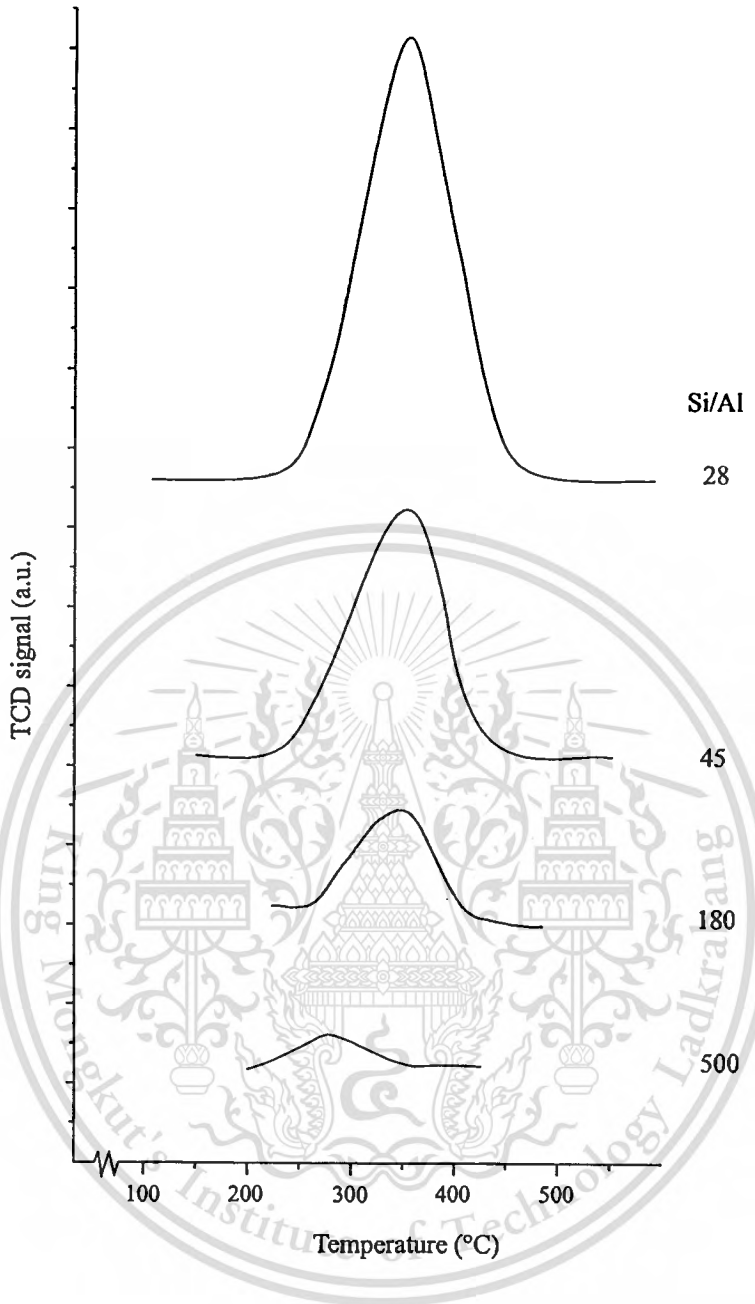

Figure 4.5 NH_3-TPD of HZSM-5 with Si/Al ratio of 28, 45, 180 and 500.

In Figure 4.6, the acidity and acid strength of HZSM-5 and GaZSM-5 with Si/Al = 180 are presented. From the previous results, the strong acid sites (Bronsted acid sites) of HZSM-5 is observed by ammonia desorption peak at 350°C. The calcined GaZSM-5 (at 500°C) shows a smaller desorption peak at 290°C. This is because H^+ is partly replaced by GaO^+ [17,18], as Ga is loaded in non-excessively stoichiomatric ratio with the Al in the framework. Therefore, the acidity of the calcined GaZSM-5 is smaller than that of HZSM-5. However, a significant decrease in Bronsted acid site is observed when the GaZSM-5 is treated with H_2. This is due to the additional formation of GaH_2^+ formed from reduction of finely dispersed Ga_2O_3 to Ga^+ which subsequently chemisorb H_2 [19]. The GaH_2^+ can exchange with remaining Bronsted protons. A decrease in acid strength after incorporating Ga of HZSM-5 is likely due to the interaction between Bronsted acid site and Ga species.

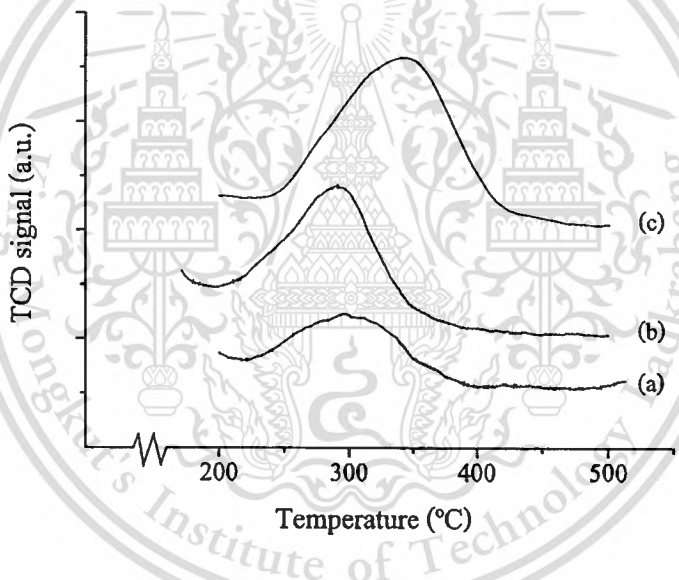

Figure 4.6 NH_3-TPD of GaZSM-5 (0.7 wt.%, Si/Al=180) (a) calcined at 500°C then reduced at 550°C, (b) calcined at 500°C and (c) HZSM-5 (Si/Al = 180).

4.3.2 Activity testing

4.3.2.1 Conversion of pentanes over HZSM-5

The conversions of *n*-pentane, isopentane, and cyclopentane over HZSM-5 with Si/Al ratio of 180 are shown in Figure 4.7. It is expected that isopentane should be the most active over Bronsted acid sites because branch structure of isopentane would form a relatively more stable tertiary carbocation, as compared to the secondary carbocation formed from *n*-pentane and cyclopentane. Moreover, cyclopentane should be less active than *n*-pentane, because of its cyclic structure. However, cyclopentane shows higher conversion (26.5%) than that of isopentane (12.9%) and *n*-pentane (10.1%). This is possibly due to restricted pore size of HZSM-5 (5-6 Å) which may exclude isopentane (~6 Å) and *n*-pentane (~6-7 Å) to diffuse to the internal Bronsted acid sites. On the other hand, cyclopentane with a smaller kinetic diameter (~4 Å) can readily diffuse and be activated in the pore of HZSM-5.

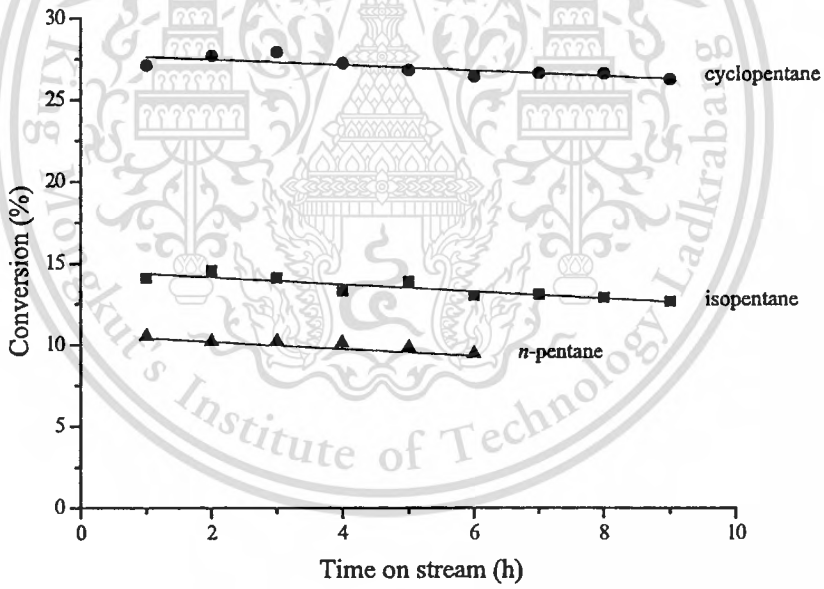

Figure 4.7 Conversion of *n*-pentane, isopentane, and cyclopentane over HZSM-5 (Si/Al = 180, W/F = 9.52 g h/mol, reaction temperature 500 ^{o}C).

To demonstrate the shape selectivity of catalyst, reaction of *n*-pentane, isopentane, and cyclopentane over the larger channel, H-Beta zeolite (6-7 Å) is tested as shown in Figure 4.8. It can be seen that, over H-Beta zeolite, isopentane shows higher conversion than that of *n*-pentane and cyclopentane, as expected. This reveals that the observed activity of HZSM-5 was governed by diffusion of reactant through restricted windows of the catalysts.

It is noted that a relatively high stability is also obtained over HZSM-5 (Si/Al = 180), as shown in Figure 4.7. Small deactivation is observed only at higher time on stream, presumably due to coke formation on parts of the active sites. In contrast, a rapid deactivation is obtained over H-Beta zeolite (Figure 4.8). This is because a higher acidity of H-Beta (Si/Al = 11) can readily promote oligomerization of the products which leads to higher coke deposit.

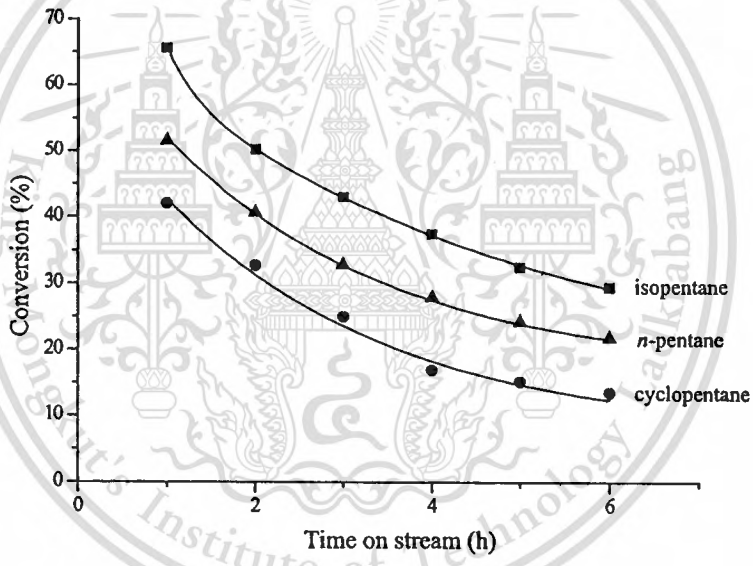

Figure 4.8 Conversion of *n*-pentane, isopentane, and cyclopentane over H-Beta (Si/Al = 11, W/F = 9.52 g h/mol, reaction temperature 500°C).

Over HZSM-5, the products distribution from *n*-pentane, isopentane, and cyclopentane conversion are shown in Table 4.2. These products could be categorized into three groups, i.e., C_1-C_4, BTX and C_{9+} aromatics. It can be seen that the most of products formed over HZSM-5 are C_1-C_4, i.e., methane (C_1), ethane (C_2), ethene ($C_2^=$), propane (C_3), propene ($C_3^=$), butane (C_4) and butene ($C_4^=$). It is suggested that cracking is a major reaction over HZSM-5 catalyst (Figure 4.9). Higher C_4 is observed when branch and cyclic structures are employed as

feed. This is probably due to the isomerization of the feed before undergo cracking. This reveals that Bronsted acid site of HZSM-5 promotes cracking of C_5 irrespective to the feed structure [20,21]. It can be noticed in Figure 4.9 that, with the same C_5 reactant, the selectivities of C_1-C_4 remains unchanged although the catalyst is deactivated by coke formation (different conversion at different time on stream). This suggests that the remaining active sites (Bronsted acid site) promote the similar reaction pathway in all pentanes reaction.

Table 4.2 Performance of ZSM-5 catalysts (Si/Al=180) for *n*-pentane, isopentane and cyclopentane transformation at 500°C.

Catalyst	HZSM-5			GaZSM-5 (0.7 wt.%)		
Reactant	*n*-pentane	isopentane	cyclopentane	*n*-pentane	isopentane	cyclopentane
Contact time (g h/mol)	9.52	9.52	9.52	9.52	9.52	9.52
Conversion (%)	10.1	12.9	26.5	29.0	46.8	36.9
Selectivity (mol%)						
C_1-$C_3^=$	36.7	33.3	21.1	29.5	21.7	8.70
C_3	56.3	39.8	47.3	42.6	26.9	11.2
$C_4^=$	0.00	4.48	0.44	18.7	12.5	1.60
C_4	4.28	19.0	21.7	5.19	10.5	5.32
C_5	2.79	3.47	4.63	2.36	3.65	4.86
C_6	-	-	-	-	0.57	-
B	-	-	0.86	0.72	1.61	2.82
C_7	-	-	-	-	0.09	-
T	-	-	1.28	0.95	6.45	6.78
C_8	-	-	-	-	-	-
X	-	-	1.77	-	10.2	18.1
C_{9+} aromatics	-	-	0.96	-	5.83	40.6

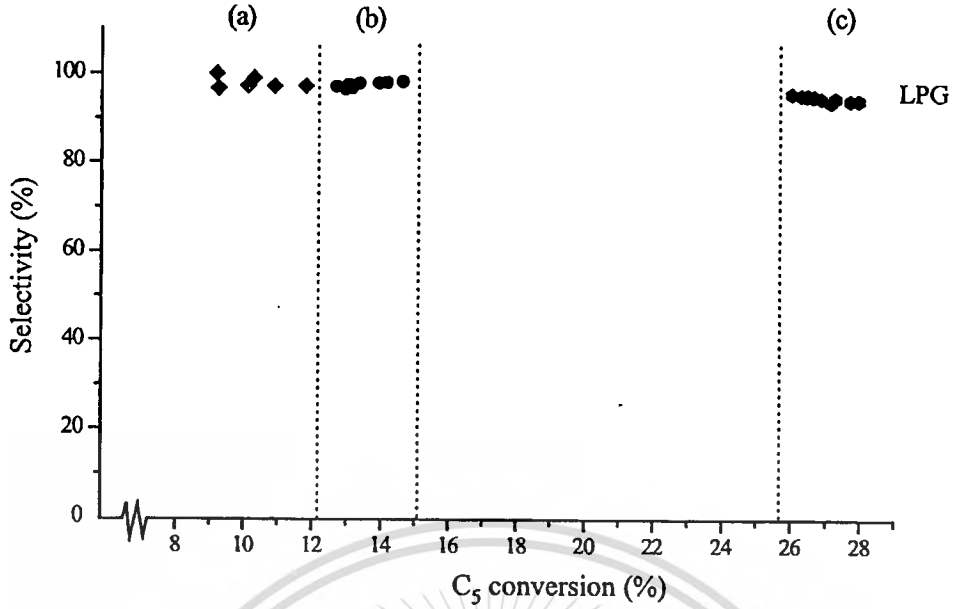

Figure 4.9 The selectivities of C_1-C_4 as a function of (a) *n*-pentane, (b) isopentane and (c) cyclopentane conversion over HZSM-5 (Si/Al = 180), W/F = 9.52 g h/mol, reaction temperature 500°C.

For all C_5 reactants, it can be seen in Figure 4.10 that only C_1-C_4 was observed at low contact time. As the contact time was increased, yield of C_1-C_4 increased almost linearly with an increase in conversion. Yields of BTX and C_{9+} aromatics were pronounced at higher contact time, and were gradually increased with the conversion. This suggested that C_1-C_4 was firstly produced followed by the formation of BTX and C_{9+} aromatics.

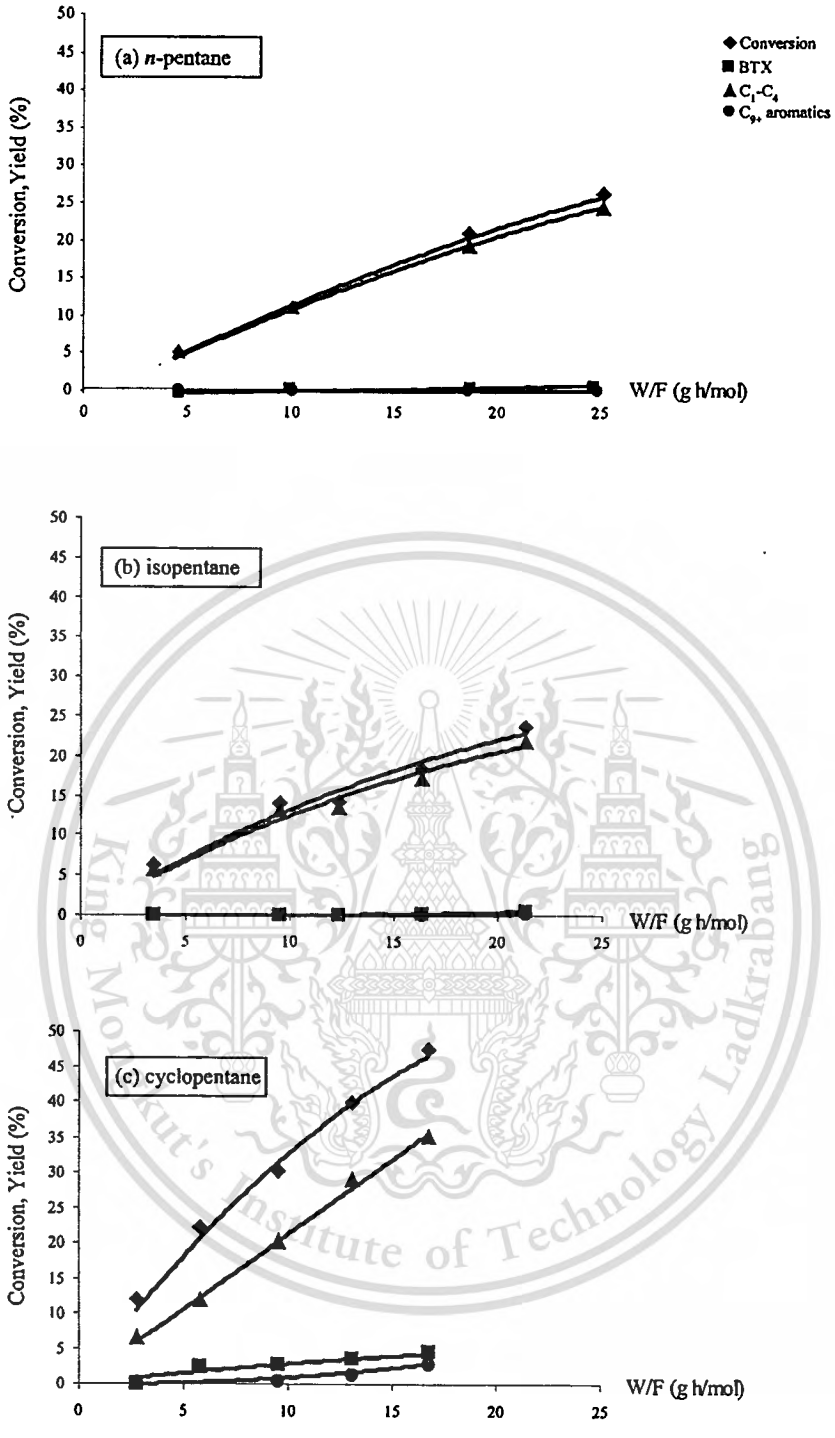

Figure 4.10 Effect of contact time for (a) *n*-pentane, (b) isopentane and (c) cyclopentane conversion over HZSM-5 (Si/Al = 180), reaction temperature 500°C.

In the mechanistic point of view, *n*-pentane should be primarily protonated into two forms of carbonium cations, as shown in Figure 4.11(a). Both intermediate I and II can be cracked to form $C_3+C_2^-$, $C_3^-+C_2$ and $C_1+C_4^-$. However, due to the higher stability of the intermediate I (from the higher electron density), C_3 and C_2^- is more pronounced, as compared to $C_3^-+C_2$ and $C_1+C_4^-$ from the intermediate II (Table 4.2). In case of isopentane, it can be protonated in different three positions, as shown in Figure 4.11(b). Due to the high stability of the intermediates IV, the C_3 and C_2^- are predominantly found in the cracked products (Table 4.2). However, C_4 are also observed likely from the hydrogen transfer reaction from the hydrocarbon lumps. Cyclopentane can be protonated and readily cracked to 1-pentene carbocation and cracked in a similar manner to *n*-pentane and/or isopentane (Figure 4.11(c)).

For all C_5 feeds, the produced C_1-C_4 may well oligomerize to larger intermediates, so called "aromatics pool" that would be the olefinic mixed with aromatics hydrocarbons and give BTX and C_{9+} aromatics (methyl substitute benzene) in a manner similar to that observed in small olefin aromatization [22, 23, 24].

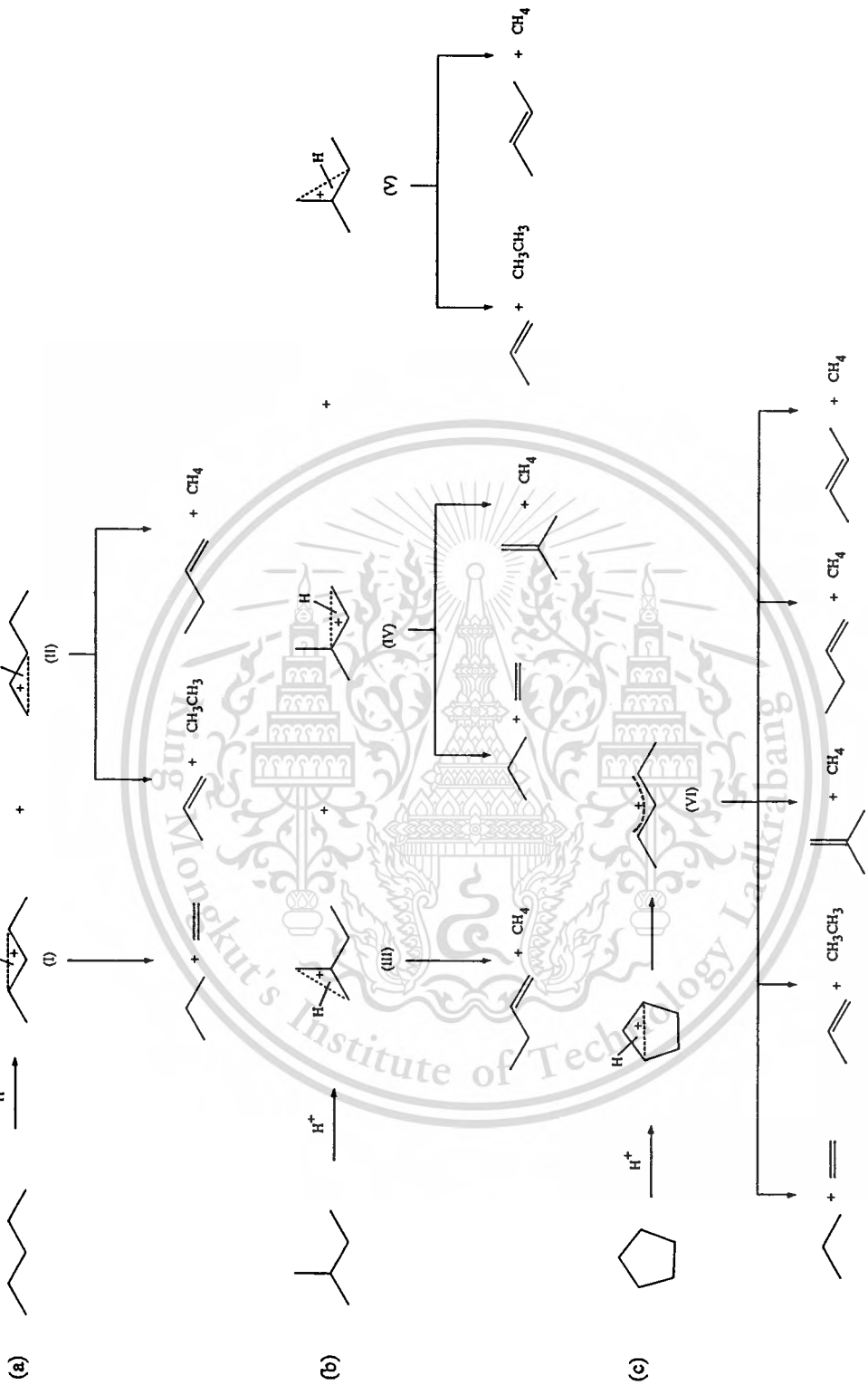

Figure 4.10 Proposed reaction pathway for (a) *n*-pentane, (b) isopentane and (c) cyclopentane cracking over HZSM-5 catalyst.

4.3.2.2 Effect of incorporated gallium species

A higher catalytic activity is obtained when gallium is incorporated as compared to that of HZSM-5 for all C_5 reactants (Table 4.2). However, over GaZSM-5, conversion of isopentane (46.85%) is significantly improved as compared to that of cyclopentane (36.94%) and *n*-pentane (28.96%) (Figure 4.12) suggesting that there are additional active sites presumably at the outer pore of zeolite when gallium is incorporated. Isopentane shows the highest activity because it can be easily activated. Over GaZSM-5, the conversion of cyclopentane is higher than *n*-pentane, as observed in the same series as the reaction over HZSM-5. This suggests that the shape selectivity of ZSM-5 still plays role on the observed activity.

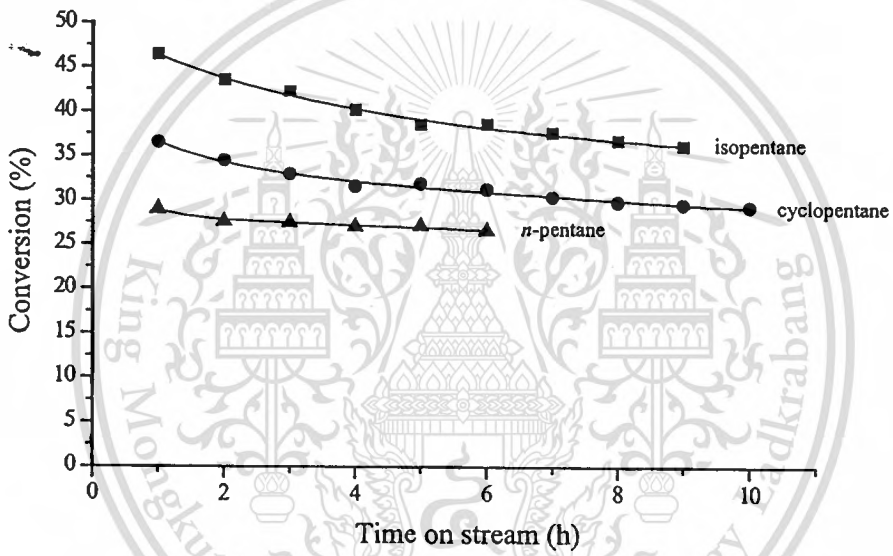

Figure 4.12 Conversion of *n*-pentane, isopentane, and cyclopentane over GaZSM-5 0.7 wt.% (Si/Al = 180, W/F = 9.52 g h/mol, reaction temperature 500°C).

For all C_5 feeds, BTX and C_{9+} aromatics are increasingly promoted, as compared to that over HZSM-5 (Table 4.2). Moreover, different BTX and C_{9+} aromatics selectivities are observed when different C_5 structures are employed. In Figure 4.13, it is found that the major C_{9+} products from *n*-pentane and isopentane are mostly methyl substituted benzene (i.e., 1-methyl-3-ethylbenzene, 1,2,3-trimethylbenzene, 1,3-dimethyl-2-ethylbenzene, etc.) While, the major C_{9+} aromatics obtained from cyclopentane conversion are indane derivatives (cyclic C_5 combined with benzene ring). These suggest that aromatics from different feed are obtained from different

reaction pathway. It is noted that all aromatics products would be mainly formed inside the pore of ZSM-5. The molecular diameter of these products is summarized in APPENDIX C.

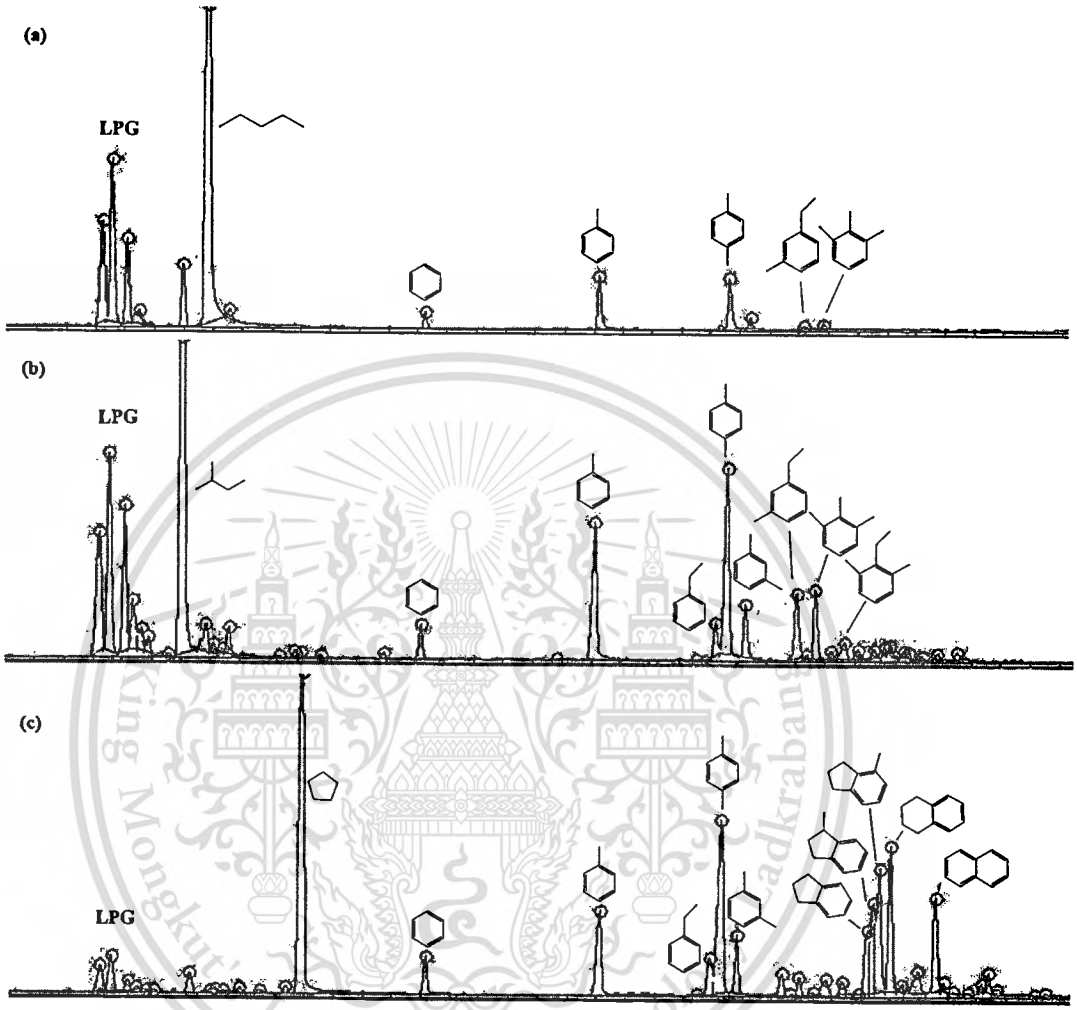

Figure 4.13 FID chromatograms of the products found from (a) *n*-pentane, (b) isopentane, and (c) cyclopentane conversion over GaZSM-5 0.7 wt.% (Si/Al = 180), reaction temperature 500°C.

In order to validate the reaction pathway, conversion of pentanes over GaZSM-5 with different contact time (W/F) is performed. It can be seen in Figure 4.14(a)-(b) that *n*-pentane and isopentane are converted to C_1-C_4 as primary products whereas cyclopentane conversion gives C_{9+} indane like aromatics at very low contact time (Figure 4.14(c)). As the contact time increases, BTX and C_{9+} alkyl aromatics are pronounced in case of *n*-pentane and isopentane feeds whereas C_1-C_4 and BTX are highly promoted in case of cyclopentane feed.

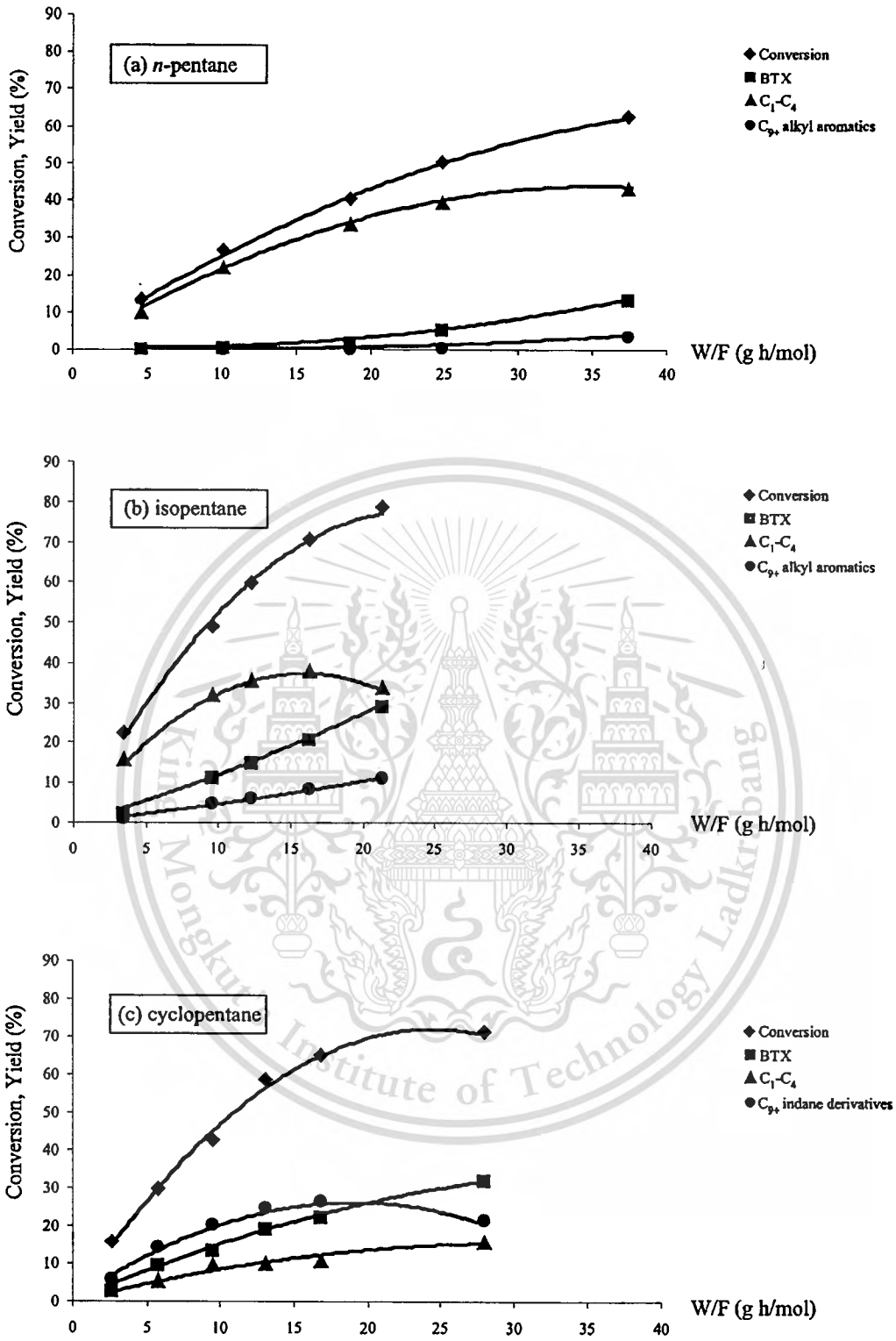

Figure 4.14 Effect of contact time for (a) *n*-pentane, (b) isopentane and (c) cyclopentane conversion over GaZSM-5 0.7 wt.% (Si/Al = 180), reaction temperature 500 °C.

In the mechanistic point of view, it suggests that *n*-pentane and isopentane would be primarily cracked to C_1-C_4 over GaZSM-5. Then, the produced C_1-C_4 would oligomerize and aromatized to BTX and C_{9+} alkyl aromatics. This seems to be a similar pathway as observed over HZSM-5, but with a higher activity. The fact that Ga active site (GaH_2^+ and GaO^+) possessed dehydrogenation activity [8,9,10,11,12], linear or branch olefins can be readily promoted and evolved/oligomerized to larger intermediates. Such C_5 olefinic mixture (hydrocarbon pool) would possess high extent of branching that further crack to C_1-C_4. As C_1-C_4 is largely produced from the branch hydrocarbon pool, the aromatics pool is proportionally formed and decomposed to BTX and C_{9+} alkyl aromatics, as observed at higher contact time.

Over GaZSM-5, cyclopentane would be primarily dehydrogenated to cyclopentene that subsequently oligomerizes to larger intermediate. This hydrocarbon pool would compose mainly condensed ring so call of cyclic hydrocarbon pool that could be further decomposed/hydrogenolyzed to C_{9+} aromatics with indane derivatives, as observed in Figure 4.13. As the contact time increases, the retained C_{9+} indane derivatives could be dealkylated/cracked into C_1-C_4 and BTX. However, at very high contact time, the C_1-C_4 can be oligomerized to additionally form aromatics, as mentioned previously.

It is noted that both branch hydrocarbon pool and cyclic hydrocarbon pool can lead to the coke formation [25] which causes the catalyst deactivation, as observed in Figure 4.12. From the observed results, the reaction pathway of *n*-pentane, isopentane, and cyclopentane conversion over ZSM-5 catalysts can be proposed in Figure 4.15.

The different reaction pathway for aromatics formation over GaZSM-5 catalyst reveals the effect of feed structure for the hydrocarbon pools and aromatics formation. The cyclic hydrocarbon pool is easily formed from the cyclic structure of cyclopentane. Whereas, the branch hydrocarbon pool is relatively difficult to form, as the aromatics are observed as secondary products.

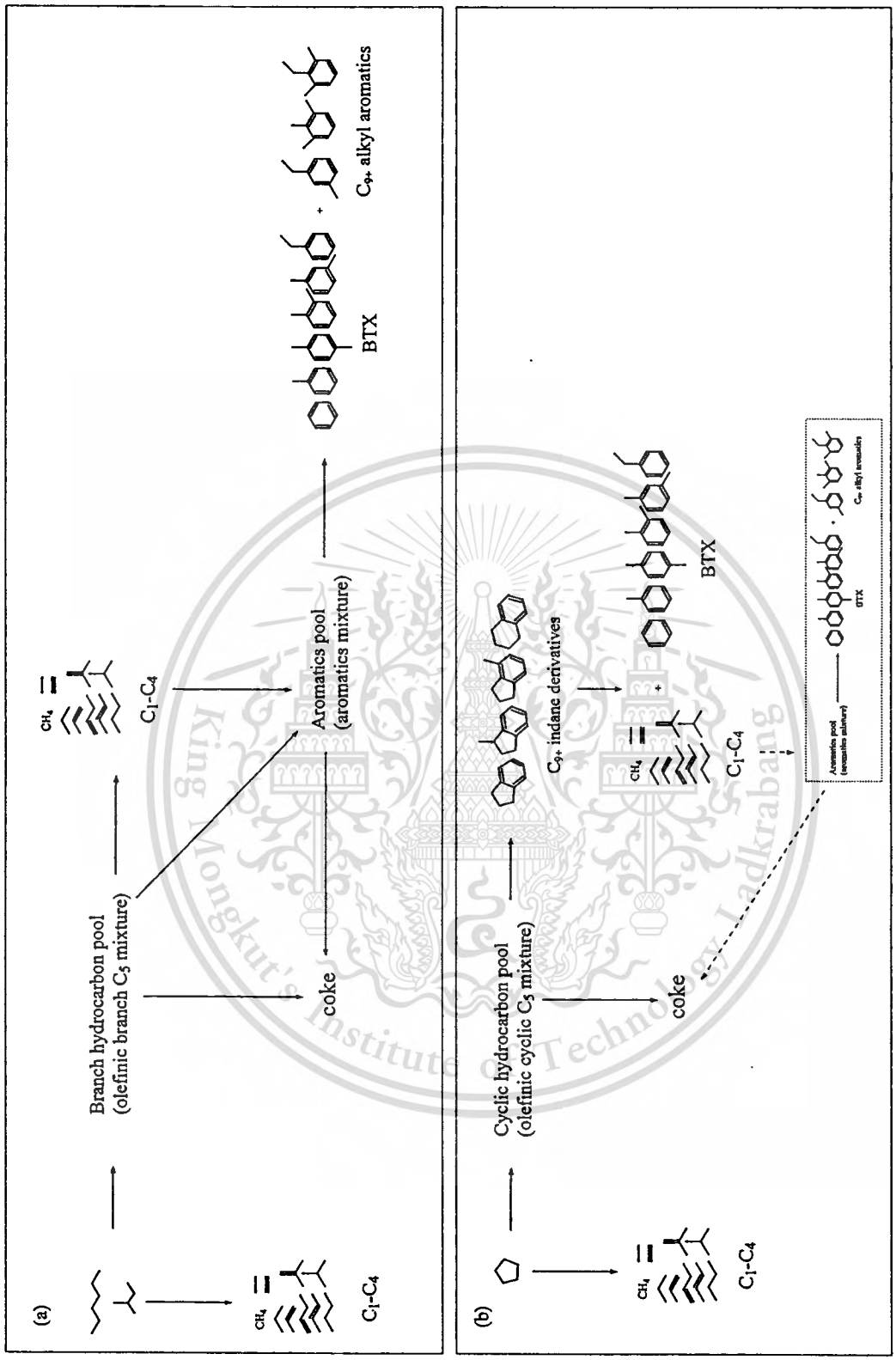

Figure 4.14 Proposed reaction pathways for (a) *n*-pentane and isopentane and (b) cyclopentane conversion over ZSM-5 catalysts.

In order to verify the different nature of hydrocarbon pool obtained from different feed, the extract from the used GaZSM-5 is determined by FTIR, as shown in Figure 4.16. The extracts from the catalyst for *n*-pentane and isopentane conversion show the existence of C-H bending of two adjacent CH_3 at 1,362 and 1,377 cm^{-1}. This suggests a high degree of branching for the hydrocarbon species left in the catalysts. In consistent with the product selectivity, it is likely that the branch hydrocarbon pool is formed for the *n*-pentane and isopentane conversion. Whereas, the extract from the catalyst for cyclopentane conversion shows only individual C-H bending of CH_3 at 1,377 cm^{-1}. This is likely to be a methyl group that locates at the terminal chain.

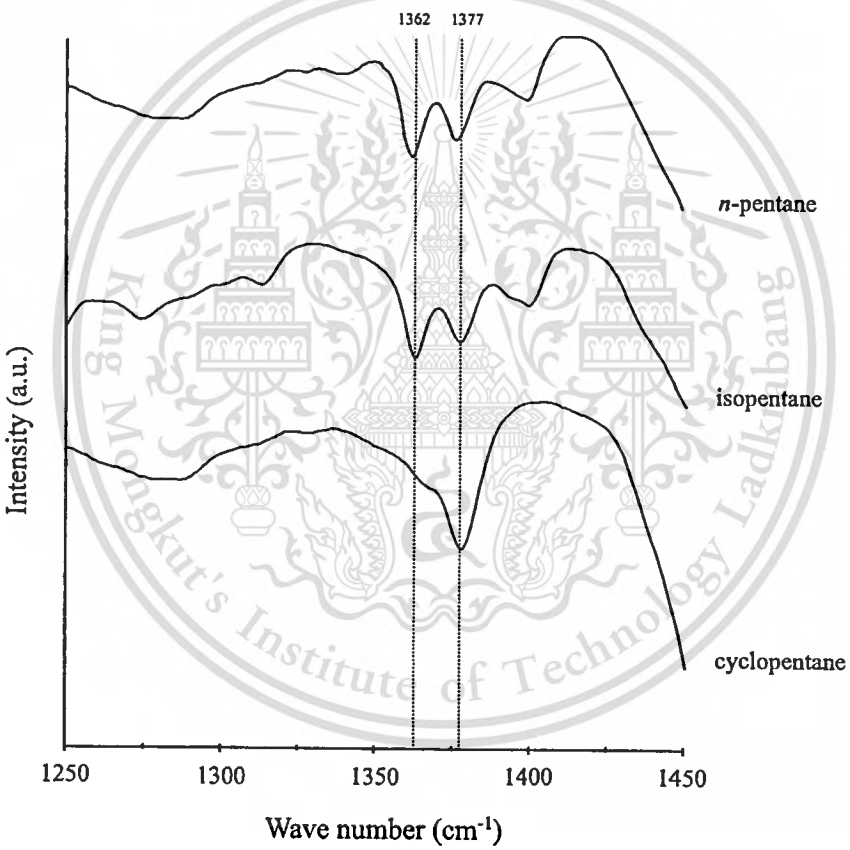

Figure 4.16 FTIR spectrums of the extracted high molecular weight formed from *n*-pentane, isopentane and cyclopentane conversion over GaZSM-5 at 500°C.

The results of the TPD-MS experiment of the used GaZSM-5 catalyst are also support the existence of different hydrocarbon pools, as shown in Figure 4.17. It can be seen that mass number of 27 and 42 atomic unit are observed as major products for all used catalyst. As the branch hydrocarbon pool can be cracked only to small products because it possesses a high degree of branching, no high molecular weight products are observed from *n*-pentane and isopentane catalysts. However, the high molecular weights presumably are the aromatics fragments (mass number of 75 and 87 atomic unit), are only observed in the used catalyst for cyclopentane conversion. This suggests a relatively unsaturated structure in the cyclic hydrocarbon pool that can be cracked to both aromatics and small products (C_2-C_3). Therefore, it is likely that the hydrocarbon pool from the cyclopentane conversion is mainly condensed rings, as suggested earlier.

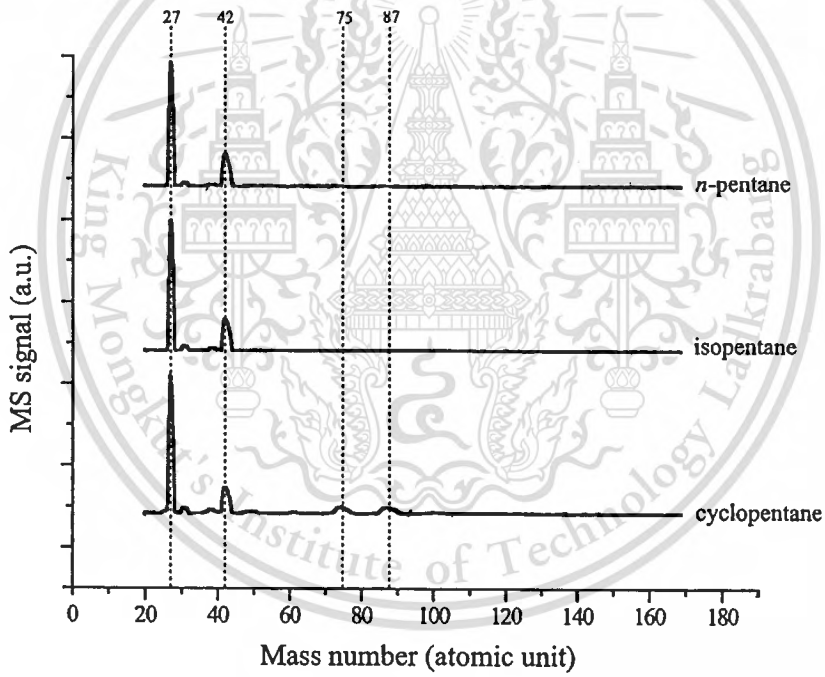

Figure 4.17 TPD-MS signals of the high molecular weight formed from *n*-pentane, isopentane and cyclopentane conversion over GaZSM-5 at 500°C (desorption temperature at 500°C).

4.3.2.3 Effect of incorporated zinc species

A higher catalytic activity (51.57%) in cyclopentane conversion is also obtained when zinc is incorporated, as compared to that of HZSM-5 (26.45%) and GaZSM-5 (36.94%). This may be due to the highly dehydrogenation activity of Zn active sites (Zn^0 and Zn^{2+}).

In Figure 4.18, it is observed that, for cyclopentane conversion over ZnZSM-5 C_{9+} indane like aromatics is primarily produced at low contact time. As the contact time is increased, yield of such C_{9+} aromatics is increased and reach a maximum (17 g h/mol). After that it is gradually reduced together with an increase in C_1-C_4 and BTX yields. These are similar to that observed over GaZSM-5. Cyclopentane is a precursor for cyclic hydrocarbon pool that can be decomposed/hydrogenolyzed to C_{9+} indane like aromatics and further dealkylated/cracked into C_1-C_4 and BTX, as proposed in Figure 4.15(b).

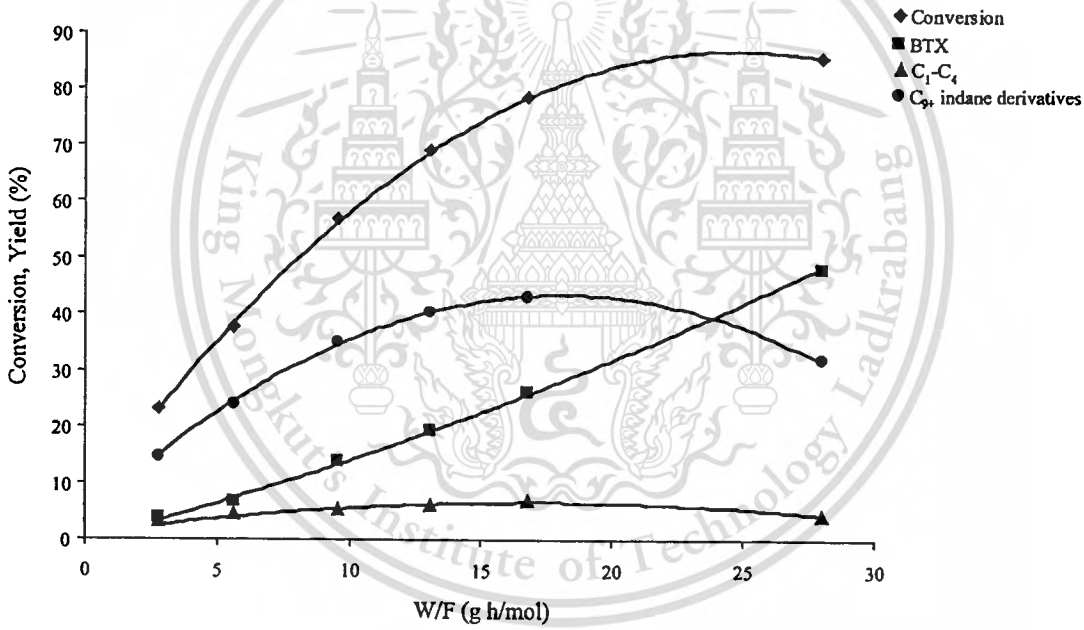

Figure 4.18 Effect of contact time for cyclopentane conversion over ZnZSM-5 0.7 wt.% (Si/Al = 180), reaction temperature 500°C.

However, a rapid deactivation is obtained from the cyclopentane conversion over ZnZSM-5, as shown in Figure 4.19. This may be due to either coke formation or the loss of Zn species during the reaction. The major deactivation presumably comes mainly from the latter case. The Zn^0 formed after H_2 reduction can be readily evaporized from the zeolite framework [13,26] in the continuous flow of H_2 at 500°C (reaction condition). In support manner, XRF

detects a decrease in zinc content of the catalyst from 0.7 wt.% to 0.2 wt.% after the reaction. This leads to an unrecoverable loss of activity of this catalyst. Hence, no further investigation is performed for ZnZSM-5.

It can be noted in Figure 4.19 that the selectivities of C_1-C_4, BTX, and C_{9+} aromatics remain unchanged although the catalyst is deactivated. This suggests that the remaining active sites (Zn^0 and Zn^{2+}) still promote the cyclopentane conversion with the same reaction pathway.

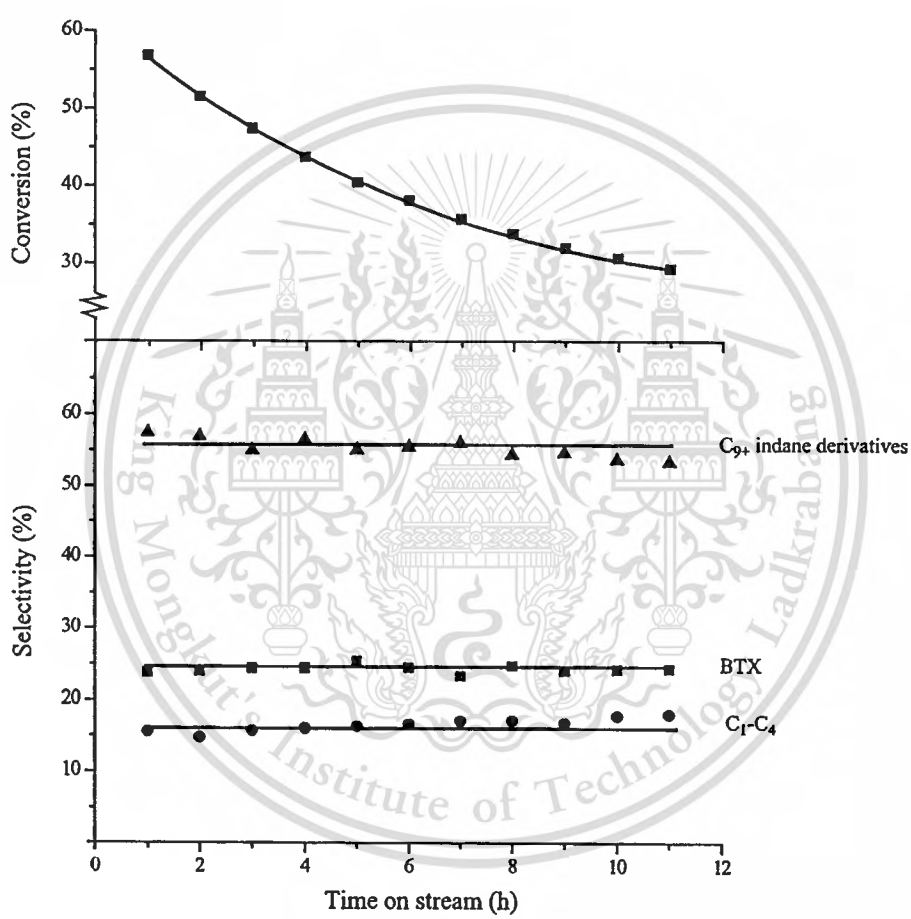

Figure 4.19 Cyclopentane transformation performance of ZnZSM-5 0.7 wt.% (Si/Al = 180) with time on stream, W/F = 9.52 g h/mol, reaction temperature 500°C.

From the similar behaviors of *n*-pentane and isopentane over HZSM-5 and GaZSM-5, isopentane is selected as model feed together with cyclopentane to comparatively study the effect of Si/Al ratio of catalyst, reaction and reduction temperature, and H_2 partial pressure, as discussed below.

4.3.2.4 Effect of Si/Al ratio of the catalyst

Effect of Si/Al ratio of HZSM-5 zeolite is shown in Figure 4.20. Conversion of isopentane over HZSM-5 (Figure 4.20(a)) give mainly C_1-C_4 that is increased with the aluminium content. No BTX and C_{9+} alkly aromatics are formed over the catalyst with low aluminium content. However, these aromatics are pronounced when the aluminium content reach 2.2 mol% (Si/Al = 45). This observation reveals that isopentane prefers to crack to C_1-C_4 over the acid sites of HZSM-5. As the acidity is high enough (at Si/Al = 45), the branch hydrocarbon pool can be additionally formed and further converted to BTX and C_{9+} alkyl aromatics.

In case of cyclopentane (Figure 4.20(b)), C_1-C_4 is a mainly product that is also increased with the aluminium content. BTX and C_{9+} indane derivatives can be observed despite the reaction takes place over the low aluminium catalyst. This suggests that the cyclic hydrocarbon pool which is a source of BTX and C_{9+} indane derivatives can be generated over relatively low acid sites catalyst. In other word, cyclopentane can be cracked to C_1-C_4 and in parallel, oligomerized to cyclic hydrocarbon pool over high Si/Al ratio catalyst. As the acid sites are increased, C_1-C_4 and aromatics are proportionally enhanced. However, at very high acid sites, cyclic hydrocarbon pool is increasingly formed while cracking of cyclopentane to C_1-C_4 starts to decline. It seems that site proximity of acid sites plays important role for oligomerization/cracking selectivities. As high aluminium catalyst is employed, the site proximity is expected; therefore, the protonated cyclopentane is closely adsorbed and easily oligomerized to the cyclic hydrocarbon pool. Whereas, over low aluminium catalyst, the protonated cyclopentane is far away from each other. They would be cracked to C_1-C_4 instead.

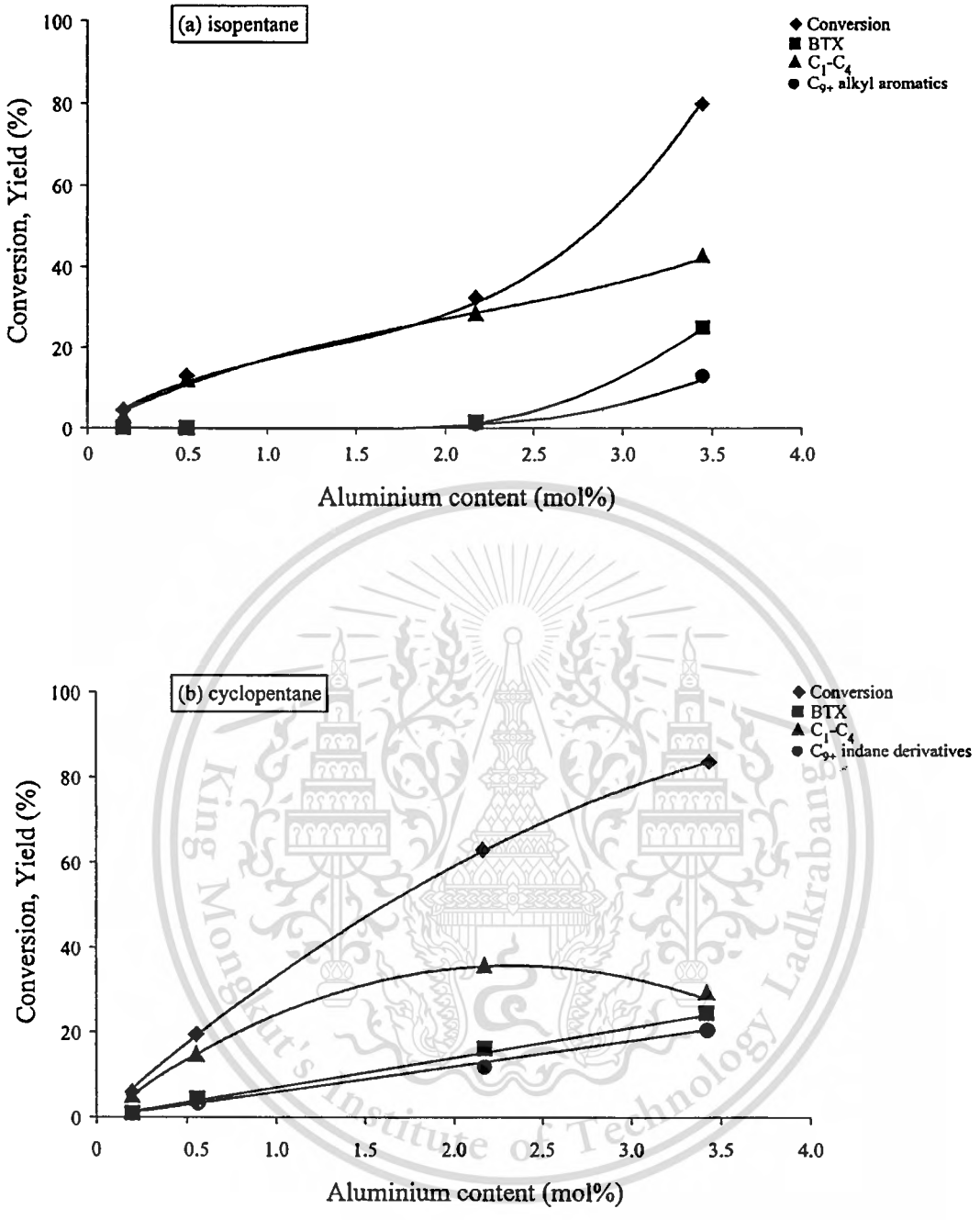

Figure 4.20 Effect of Si/Al ratio of the HZSM-5 on (a) isopentane and (b) cyclopentane conversion at 500°C, W/F=9.52 g h/mol.

Effect of Si/Al ratio on selectivity of oligomerization/cracking is more pronounced over GaZSM-5, as shown in Figure 4.21. The high activity of the catalyst could be observed when low Si/Al catalyst is employed. This is the effect of Ga active site to promote dehydrogenation activity. As the olefins are highly formed, the oligomerization to hydrocarbon pool and aromatics would be facilitated.

As expected, in the case of isopentane conversion (Figure 4.21(a)), cracking of isopentane to C_1-C_4 takes place as well as the formation of the branch hydrocarbon pool (as seen by BTX and C_{9+} alkyl aromatics yield) despite the reaction is performed over the low aluminium catalyst. This is because the incorporated Ga can produce olefins which are easily to oligomerize to the hydrocarbon pool, as mentioned above. Therefore, the aromatics are increasingly observed. Over high aluminium catalyst, a large number of appropriate Bronsted proton and Ga site proximity can be proportionally produced. Hence, the branch hydrocarbon pool formation could be enhanced, while cracking of isopentane to C_1-C_4 is suppressed.

This is more obvious for cyclopentane conversion (Figure 4.21(b)). The cyclic hydrocarbon pool is largely promoted over GaZSM-5, as the C_{9+} indane derivatives are mainly formed. This is due to the effect of Ga and site proximity promotes the cyclic hydrocarbon pool formation, whereas cracking of cyclopentane to C_1-C_4 is also decreased.

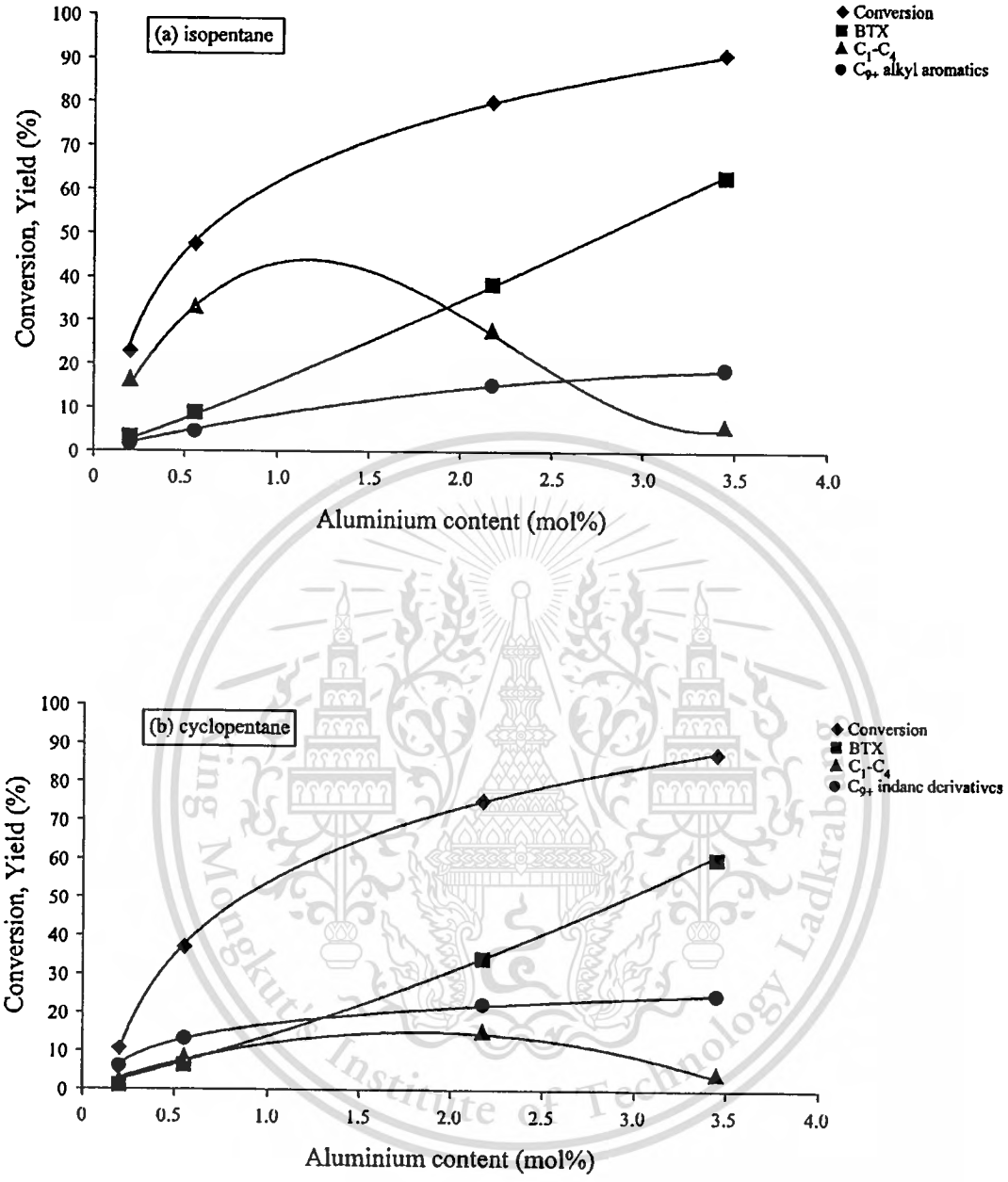

Figure 4.21 Effect of Si/Al ratio of the GaZSM-5 (0.7 wt.%) on (a) isopentane and (b) cyclopentane conversion at 500°C, W/F=9.52 g h/mol.

The catalytic activity of isopentane and cyclopentane over HZSM-5 and GaZSM-5 relatively to the aluminium content are summarized in Figure 4.22. It can be seen that the high aluminium catalyst (which promote site proximity) can enhance the hydrocarbon pool formation, while cracking activity is decreased. This is evidently observed when the Ga is incorporated, i.e., the hydrocarbon pool is largely promoted as well as the cracking of pentanes to C_1-C_4 is almost limited.

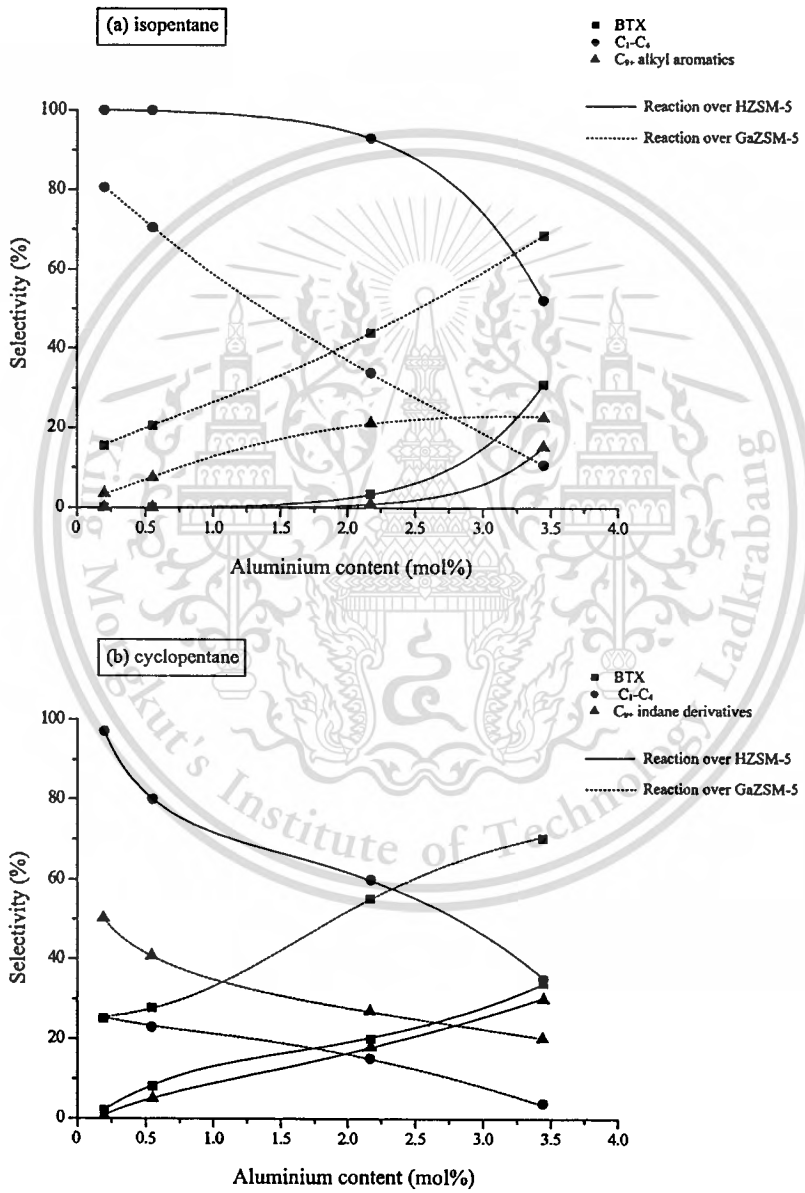

Figure 4.22 Summarized the catalytic activity of isopentane and cyclopentane conversion over HZSM-5 and GaZSM-5 (0.7 wt.%) as function of the aluminium content of zeolite.

4.3.2.5 Effect of reaction temperature

An effect of reaction temperature on the isopentane and cyclopentane conversion over GaZSM-5 is shown in Figure 4.23. The isopentane can be cracked or converted to the branch hydrocarbon pool over GaZSM-5 catalyst. As the temperature is increased (500-600°C), higher conversion of isopentane is found with an increase in C_1-C_4 and a decrease in BTX and C_{9+} alkyl aromatics selectivities (Figure 4.23(a)). As mentioned previously, C_1-C_4 may be produced by cracking from isopentane and/or cracking from the branch hydrocarbon pool. Both can be typically enhanced when the temperature is increased.

Over GaZSM-5, cyclopentane prefers to oligomerize to cyclic hydrocarbon pool rather than cracking to C_1-C_4. As the temperature is increased, (500-550°C), higher cyclopentane conversion is found (Figure 4.23(b)) with a similar product selectivity. This reveals that all steps of the reaction are proportionally promoted by increasing temperature. However, a decrease of C_{9+} indane derivatives with an increase of C_1-C_4 selectivity is observed at 600°C. This is because the cracking of C_{9+} indane derivatives to C_1-C_4 and BTX is enhanced at this temperature. Therefore, C_1-C_4 and BTX selectivities are increased but C_{9+} indane derivatives selectivity is dropped.

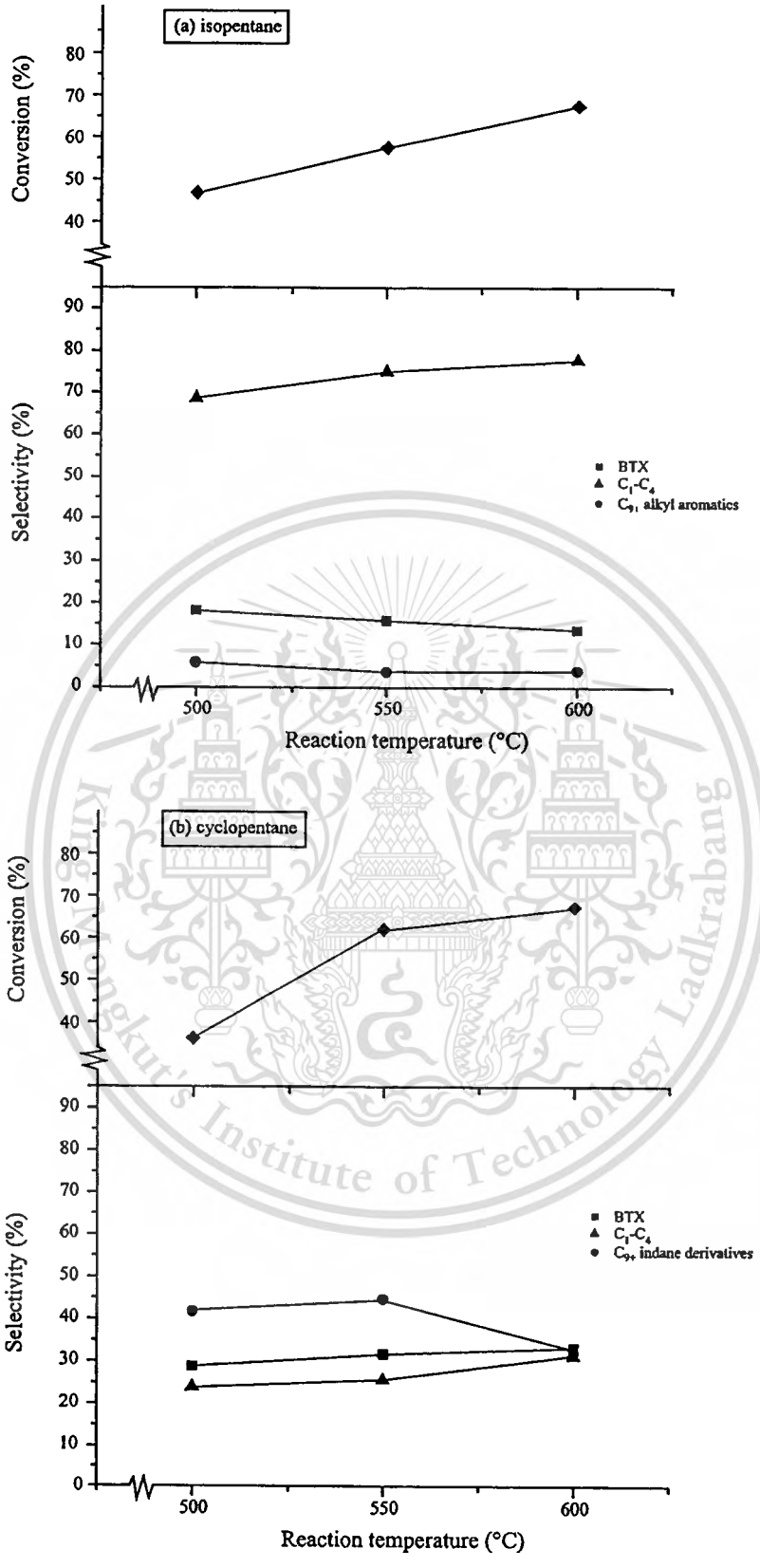

Figure 4.23 Effect of reaction temperature on (a) isopentane and (b) cyclopentane conversion over GaZSM-5 0.7 wt.% (Si/Al = 180), W/F = 9.52 g h/mol.

4.3.2.6 Effect of reduction temperature

Figure 4.24 shows the effect of reduction temperature on the catalytic activity of isopentane and cyclopentane conversion at 500°C. It is found that reduction at 550°C gives the highest activity as compared to that of the reduction at other temperatures. From TPR (Figure 4.4), Ga_2O_3 would be partially reduced to GaH_2^+, while GaO^+ cannot be reduced at 500°C. Hence, some of Ga^{3+} (Ga_2O_3 left after reduction), GaH_2^+ and GaO^+ may well be the available active species after reduction at 500°C. Whereas, the gallium species presented after reduction at 550°C are only GaH_2^+ (that formed after completely reduction of Ga_2O_3) and GaO^+. As the catalytic activity after reduction at 550°C is higher than that of the reduction at 500°C (Figure 4.24), this reveals that Ga^{3+} from Ga_2O_3 possesses lower activity for pentanes conversion, as compared to GaH_2^+ and GaO^+ species. After reduction at temperature higher than 600°C, the only active specie would be GaH_2^+ obtained from the completely reduction of Ga_2O_3 and GaO^+. The significant drop in activity would result from lost of GaO^+ specie after complete reduction.

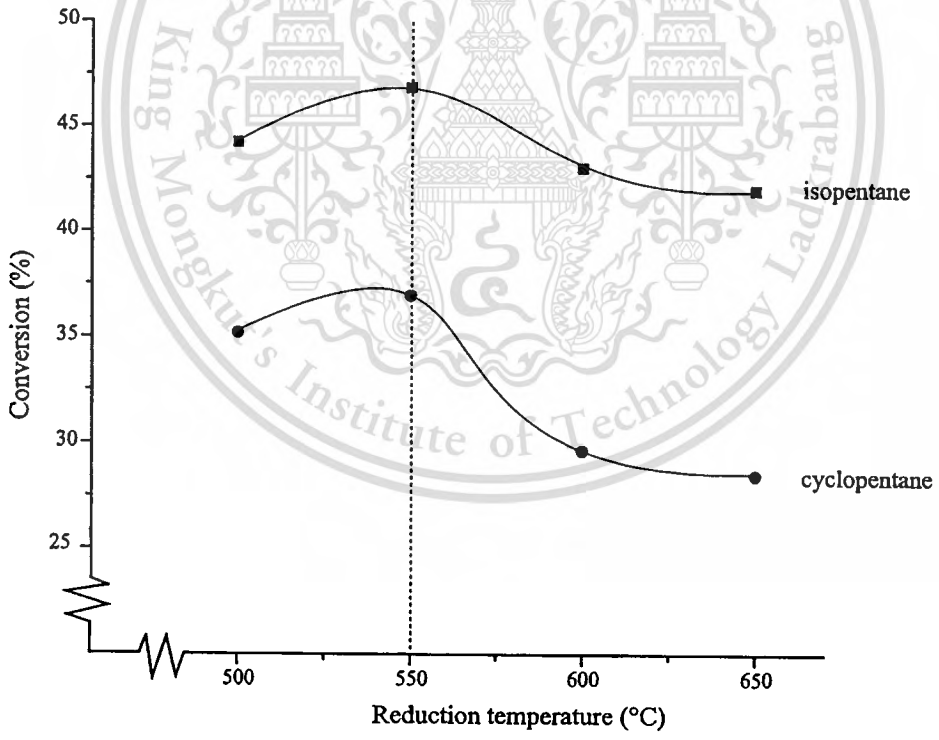

Figure 4.24 Effect of reduction temperature on isopentane and cyclopentane conversion over GaZSM-5 0.7 wt.% (Si/Al = 180), W/F = 9.52 g h/mol, reaction temperature 500°C.

However, one may expect that the sudden drop in activity may be arised from the loss of surface area and crystallinity structure when reduction at high temperature. To validate this speculation, XRD of GaZSM-5 after reduction at various temperatures is measured, as seen in Figure 4.25. It is shown that the crystallinity of GaZSM-5 does not markedly change when the catalyst is reduced at high temperature (600-650^{o}C). This reveals that the zeolite structure is remained. A decrease of catalytic activity obtained after reduction at temperature higher than 550^{o}C is not noticeably attributed from the destruction of zeolite framework, but likely due to the loss of GaO^{+} specie as discussed earlier. Accordingly, it is suggests that the catalytic activity of $GaO^{+} > GaH_2^{+} > Ga_2O_3$.

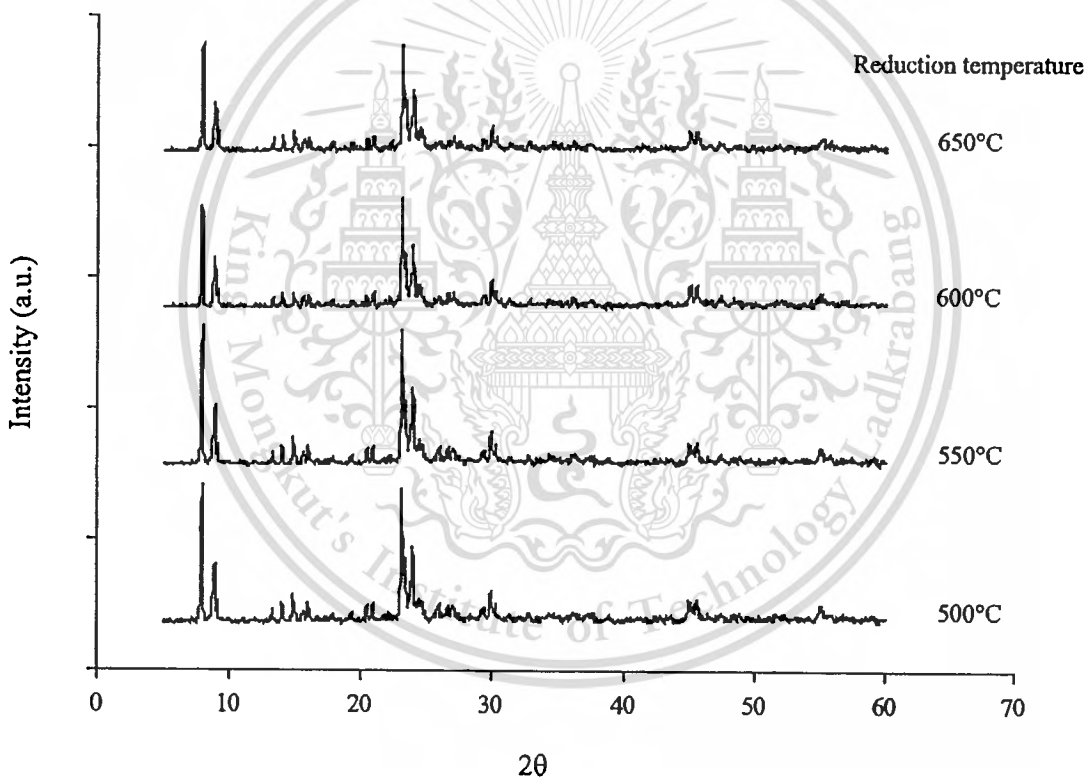

Figure 4.25 XRD patterns of the reduced GaZSM-5 0.7 wt.%, Si/Al = 180.

However, a similar selectivity is obtained despite the GaZSM-5 is reduced at different temperature (500-550^{o}C). Although the different gallium active sites are employed, isopentane still prefers to crack to C_1-C_4 (Figure 4.26(a)) whereas cyclopentane still prefers to oligomerize to the cyclic hydrocarbon pool (Figure 4.26(b)), as discussed previously. This reveals

that the reaction pathway for pentanes conversion over GaZSM-5 depends on the structure of feed, irrespective to the available gallium active species.

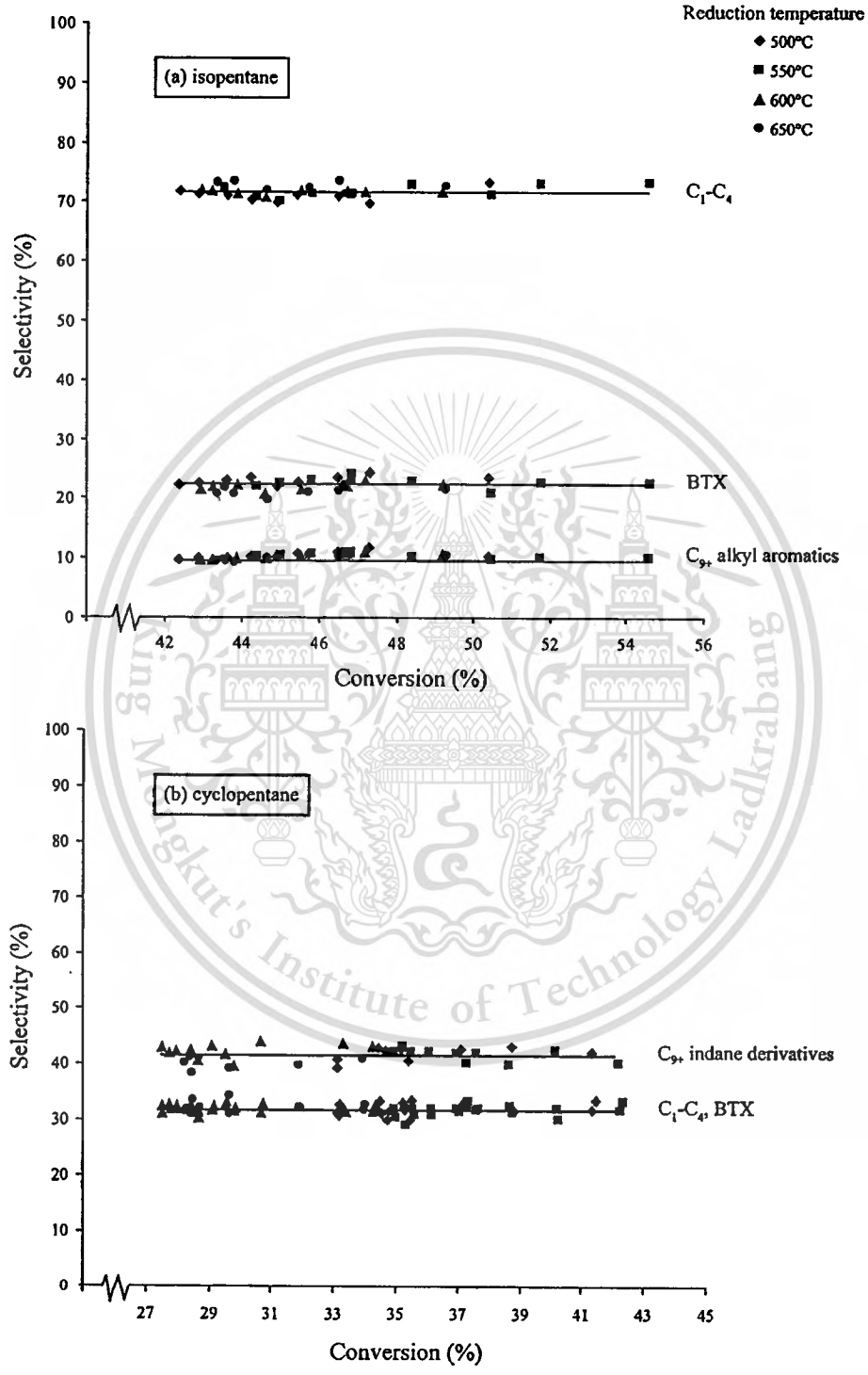

Figure 4.26 Product selectivities from (a) isopentane and (b) cyclopentane conversion over GaZSM-5 0.7 wt.% (Si/Al = 180), W/F = 9.52 g h/mol, reaction temperature 500°C.

4.3.2.7 Effect of H_2 partial pressure

In Figure 4.27, the different activity is markedly observed when a carrier gas is changed from H_2 into He. The higher catalytic activity (37%-48% for isopentane and 32%-48% for cyclopentane) is observed, with an increase in BTX and C_{9+} aromatics selectivities and a decrease in C_1-C_4 selectivity, after switching to He stream. The different in catalytic activity and selectivity suggests the different active sites may be formed in the absence of H_2. As mentioned previously, GaH_2^+ together with GaO^+ are available active sites for pentanes transformation under stream of H_2. After switching to He, GaH_2^+ would be decomposed to Ga^+, only GaO^+ is remained. Therefore, Ga^+ and GaO^+ are the active sites for pentanes conversion in the absence of H_2 stream.

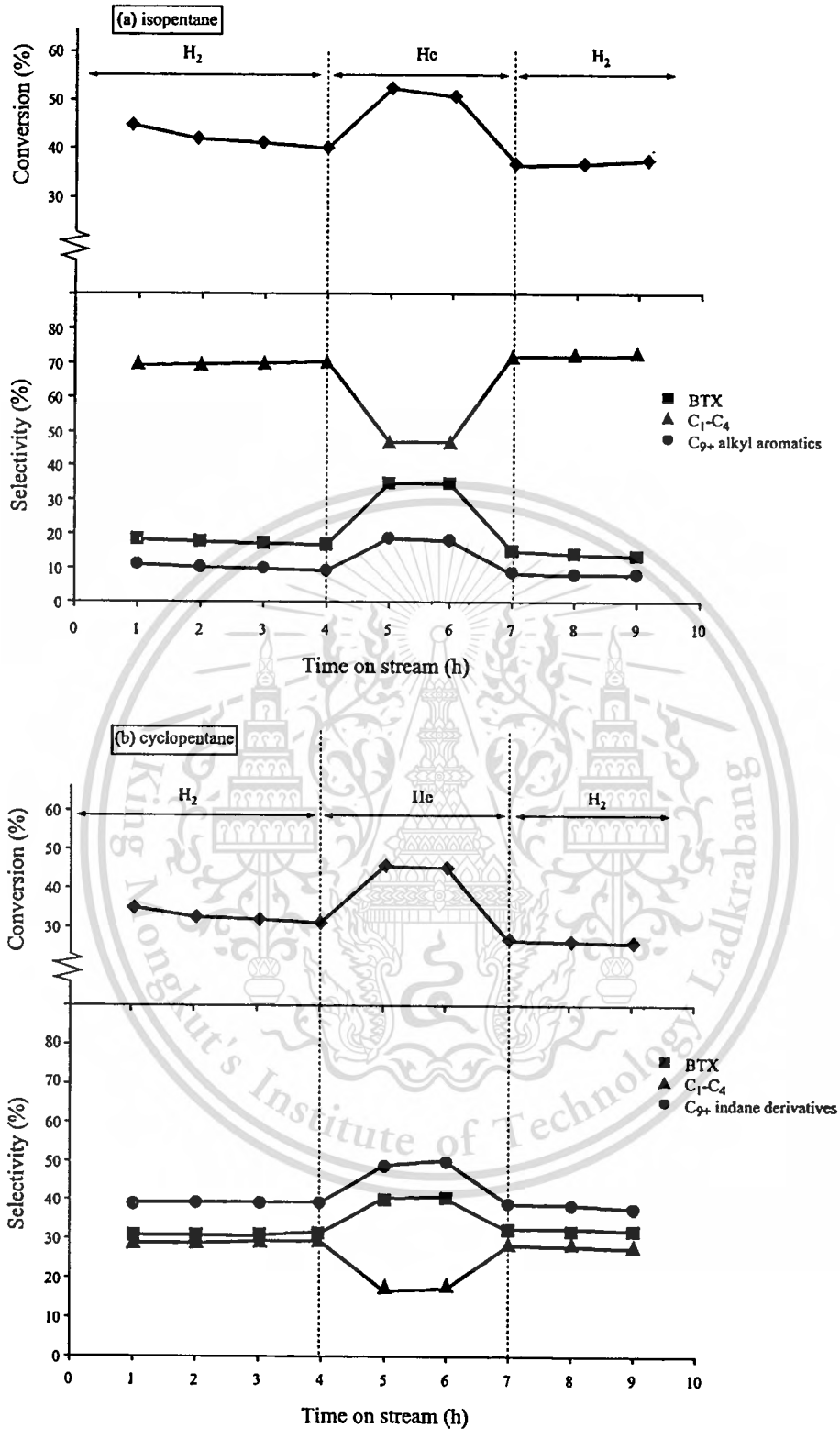

Figure 4.27 Catalytic activity of Ga active sites in GaZSM-5 0.7 wt.% (Si/Al = 180) for (a) isopentane and (b) cyclopentane conversion at 500°C, W/F = 9.52 g h/mol.

The fact that GaH_2^+ can be decomposed to Ga^+ is defined by the temperature programmed hydrogen evolution (TPHE) of the reduced GaZSM-5, as shown in Figure 4.28. It is found that H_2 is desorbed from the catalyst at 100 and 175°C. The observed H_2 desorption peaks at low and high temperature may be attributed form the two types of GaH_2^+ sites which located at the silanol and at the exchangeable site of the zeolite, respectively.

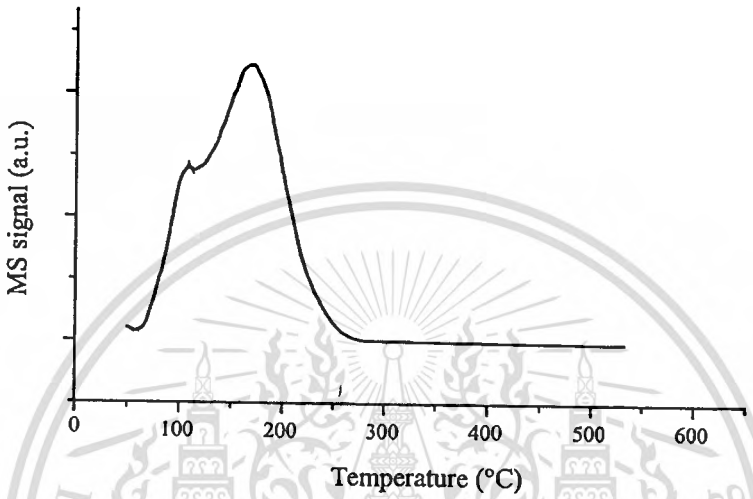

Figure 4.28 TPHE of GaZSM-5 0.7 wt.% (Si/Al = 180) reduced at 550°C.

It is likely that Ga^+ (in He) species would possess higher dehydrogenation activity, as compared to that of GaH_2^+ (in H_2) species. With high dehydrogenation activity of Ga^+, the branch and cyclic hydrocarbon pools are enhanced. Therefore, aromatics are largely formed in the absence of H_2 stream (Figure 4.27). The Ga^+ species can be reversibly recovered to GaH_2^+ in the presence of H_2. This is seen by switching the carrier gas back to H_2 and the catalytic activity become originally as it originates.

The presence of H_2 in the reaction would not only regulate the available active Ga species, but also promote the H-transfer to the forming pool leading to a decrease in aromatics fraction. This proportionally reduces the coke formation and increases catalyst stability.
In supported with this view, TGA (Table 4.3) shows that the coke deposit on the surface is decreased with H_2. When the H_2 is in excess (100%H_2 in carrier gas), the lowest coke content is observed (0.18 and 0.49 wt.% for isopentane and cyclopentane conversion, respectively). At the same H_2 partial pressure, it is noted that higher coke formation is observed for the cyclopentane conversion (0.49 wt.% > 0.18 wt.% and 1.37 wt.% > 0.48 wt.%). This may be due to cyclic

hydrocarbon pool is hardly cracked/decomposed to smaller products, as compared to the branch hydrocarbon pool.

Table 4.3 TGA results of GaZSM-5 0.7 wt.% (Si/Al = 180) catalyst left after isopentane and cyclopentane conversion at 500°C, W/F = 9.52 g h/mol.

Reactant	%H_2 in carrier gas	Conversion (%)	Carbon deposit (wt.%)
isopentane	0	57.4	0.48
	100	46.8	0.18
cyclopentane	0	46.3	1.37
	16	40.1	0.83
	35	38.4	0.7
	100	37.0	0.49

4.4 Conclusion

The aromatics can be obtained from conversion of *n*-pentane, isopentane, and cyclopentane over the shape selective GaZSM-5 and ZnZSM-5 catalysts at 500°C. With the pore restriction of HZSM-5, the activities are in the order of cyclopentane (26.5%) > isopentane (12.9%) > *n*-pentane (10.1%). However, after Ga loading the higher activities are mainly attributed from the Ga active sites located both outside and inside the pore leading to isopentane (46.8%) > cyclopentane (36.9%) > *n*-pentane (29.0%). TPR suggests that, over GaZSM-5, GaO^+ and Ga^+ (subsequently converts by H_2 adsorption to GaH_2^+) would be the active sites when the catalyst is reduced at 550°C. With the dehydrogenation activity of GaO^+ and GaH_2^+, *n*-pentane and isopentane are firstly converted to branch hydrocarbon pool that further cracks to C_1-C_4. The produced C_1-C_4 can be oligomerized to aromatics pool that further cracks to BTX and C_{9+} alkyl aromatics. Whereas, cyclopentane is primarily converted to cyclic hydrocarbon pool that further cracks to C_{9+} indane derivatives. The produced C_{9+} indane derivatives are later dealkelated/ cracked to C_1-C_4 and BTX. In support the existence of the different hydrocarbon pools, FTIR shows high degree of branching in the extracted product from the used GaZSM-5 for *n*-pentane and isopentane conversion. In addition, TPD-MS shows aromatics fragment from the used GaZSM-5 for cyclopentane conversion.

Over ZnZSM-5, Zn^0 and Zn^{2+} would be the active sites for pentanes transformation. Such catalyst can convert pentanes with the similar pathway, as observed over GaZSM-5. However, the Zn^0 is readily evaporated from the zeolite framework leading to an unrecoverable activity of this catalyst.

The aromatics formation can be improved by lowering the Si/Al ratio of the GaZSM-5 catalyst. This is because the increase in aluminium content would proportion increase an appropriate Bronsted proton and gallium site proximity. This site proximity can promote dehydrogenation and oligomerization of pentanes to the designate hydrocarbon pools. As the hydrocarbon pool formation is facilitated, the aromatics fraction would be proportionally enhanced.

The higher reaction temperature increases cracking activity. The higher conversion with an increase of C_1-C_4 selectivity and a decrease of aromatics selectivity is observed when the reaction is operated at high temperature.

The reduction of GaZSM-5 at 550°C prior activity testing can generate the most active gallium species, i.e., GaO^+ and GaH_2^+. The catalytic activity is in the series of $GaO^+ > GaH_2^+ > Ga_2O_3$. The product selectivity remains unchanged although the different gallium active sites are employed. This reveals that the reaction pathway for pentanes conversion over GaZSM-5 depends on the structure of feed, irrespective to the type of gallium active species.

The lower pentanes conversion is observed in H_2 stream. The GaO^+ and GaH_2^+ are acted as the active site in the presence of H_2, but GaO^+ and Ga^+ are the active sites in He. This suggests that the Ga^+ species possesses higher dehydrogenation activity, as compared to that of GaH_2^+. Therefore, the lower stability from the higher coke formation is obtained in the reaction with low H_2 concentration.

4.5 References

[1] Csicsery, S.M. 1986. "Catalysis by shape selective zeolites-science and technology." **Pure and Applied Chemistry.** 58(6): 841-856.

[2] Csicsery, S.M. "Acid or base catalyzed processes." **Encyclopedia of Hydrocarbons.** 2: 701-721.

[3] Davis, B.H. 1999. "Alkane dehydrocycliztion mechanism." **Catalysis Today.** 53: 443-516.

[4] Bhasin, M.M., McCain, J.H., Vora, B.V., Imai, T., and Pujado, P.R. 2001. "Dehydrogenation and oxydehydrogenation of paraffins to olefins." **Applied Catalysis A: General.** 221: 397-419.

[5] Caeiro, G., Carvalho, R.H., Wang, X., Lemos, M.A.N.D.A., Lemos, F., Guisnet, M., and Ramoa Ribeiro, F. 2006. "Activation of C_2-C_4 alkanes over acid and bifunctional zeolite catalysts." **Journal of Molecular Catalysis A: Chemical.** 255: 131-158.

[6] Guisnet, M., and Gnep, N.S. 1996. "Mechanism of short-chain alkane transformation over protonic zeolites. Alkylation disproportionation and aromatization." **Applied Catalysis A: General.** 146: 33-64.

[7] Kwak, B.S., and Sachtler, W.M.H. 1994. "Effect of Ga/proton balance in Ga/HZSM-5 catalyst on C_3 conversion to aromatics." **Journal of Catalysis.** 145: 456-463.

[8] Meitzner, G.D., Iglesia, E., Baumgartner, J.E., and Huang, E.S. 1993. "The chemical state of gallium in working alkane dehydrocyclodimerization catalysts. in situ gallium K-edge X-ray absorption spectroscopy." **Journal of Catalysis.** 140: 209-225.

[9] Price, G.L. and Kanazirev, V. J. 1990. "Ga_2O_3/HZSM-5 propane aromatization catalysts: Formation of active centers via solid state reaction." **Journal of Catalysis.** 126: 267-278.

[10] Dooley, K.M., Chang, C., and Price, G.L. 1992. "Effects of pretreatments on state of gallium and aromatization activity of gallium/ZSM-5 catalysts." **Applied Catalysis A: General** 84: 1730.

[11] Rane, N., Kersbulck, M., van Santen, R.A., and Hensen, E.J.M. 2008. "Cracking of *n*-heptane over Bronsted acid sites and Lewis acid Ga sites in ZSM-5 zeolite." **Microporous and Mosoporous Materials.** 110: 279-281.

[12] Ausavasukhi, A. 2009. "Study of properties and activities of gallium and silver species in ZSM-5 for light hydrocarbon conversion." Ph.D. Thesis of King Mongkut's Institute of technology Ladkrabang.

[13] Biscardi, J.A, Meitzner, G.D., and Iglesia, E. 1998. "Structure and density of active Zn species in Zn/H-ZSM5 propane aromatization catalysts." **Journal of Catalysis.** 179: 192-202.

[14] Kazansky, V.B., Subbotina, I.R., Rane, N., van Santen, R.A., and Hensen, E.J.M. 2005. "On two alternative mechanisms of ethane activation over ZSM-5 zeolite modified by Zn^{2+} and Ga^{+} cations." **Physical Chemistry Chemical Physics.** 7: 3088-3092.

[15] Kazansky, V.B., Subbotina, I.R., van Santen, R.A., and Hensen, E.J.M. 2004. "DRIFT study of the chemical state of modifying gallium ions in reduced Ga/ZSM-5 prepared by impregnation: I. observation of gallium hydrides and application of CO adsorption as a molecular probe for reduced gallium ions."**Journal of Catalysis.** 227: 263-269.

[16] Kolyagin, Y.G., Ordomsky, V.V., Klimyak, Y.Z., Rebrov, A.I., Fajula, F., and Ivanova, I.I. 2006. "Initial stages of propane activation over Zn/MFI catalyst studied by in situ NMR and IR spectroscopic techniques." **Journal of Catalysis.** 238: 122-133.

[17] Gonzales, N.O., Chakraborty, A.K., and Bell, A.T. 1999. "A density functional theory study of hydrogen recombination and hydrogen-deuterium exchange on Ga/HZSM-5." **Topic in Catalysis.** 9: 207-213.

[18] Rane, N., Overweg, A.R., Kazansky, V.B., van Santen, R.A., and Hensen, E.J.M. 2006. "Characterization and reactivity of Ga^{+} and GaO^{+} cations in zeolite ZSM-5." **Journal of Catalysis.** 239: 478-485.

[19] Kazansky, V.B., Sobbotina, I.R., van Santen, R.A., and Hensen, E.J.M. 2005. "DRIFTS study of the nature and chemical reactivity of gallium ions in Ga/ZSM-5: II. Oxidation of reduced Ga species in ZSM-5 by nitrous oxide or water." **Journal of Catalysis.** 233: 351-358.

[20] Viswanadham, N., Gupta, J.K., Murali Dhar, G., and Garg, M.O. 2006. "Effect of synthesis Methods and modification treatments of ZSM-5 on light alkanes aromatization." **Energy and Fuels.** 20: 1806-1814.

[21] Viswanadham, N., Muralidhar, G., and Prasada Rao, T.S.R. 2004. "Cracking and aromatization properties of some metal modified ZSM-5 catalysts for light alkane conversion." **Journal of Molecular Catalysis A: Chemical.** 223: 269-274.

[22] Choudhary, V.R., Banerjee, S., and Panjala, D. 2002. "Product distribution in the aromatization of dilute ethene over H-GaAlMFI zeolite: effect of space velocity." **Microporous and Mesoporous Materials.** 51: 203-210.

[23] Choudhary, V.R., Panjala, D., and Banerjee, S. 2002. "Aromatization of propene and *n*-butene over H-galloaluminosilicate (ZSM-5 type) zeolite." **Applied Catalysis A: General.** 231: 243-251.

[24] Solymosi, F., and Szechenyi, A. 2004. "Aromatization of isobutane and isobutene over Mo_2C/ZSM-5 catalyst." **Applied Catalysis A: General.** 278: 111-121.

[25] Guisnet, M., and Magnoux, P. 2001. "Organic chemistry of coke formation." **Applied Catalysis A: General.** 212: 83-96.

[26] Yu, T., and Qian, J. 2006. "The deactivation factor of a ZnNi/HZSM-5 catalyst during aromatization." **Petroleum Science and Technology.** 24: 1001-1008.

CHAPTER 5

CONVERSION OF C_5 HYDROCARBONS TO CYCLIC OLEFINS

5.1 Introduction

Cyclopentene (C_5H_8) and cyclopentadiene (C_5H_6) are versatile synthetic intermediate for many petrochemical industries. Metathesis of cyclopentene can produce polypentenamer, which has been used extensively as an elastomer [1]. A selective oxidation of cyclopentene gives the various products, such as maleic anhydride, phthalic anhydride and valerolactone [2,3]. These chemicals are widely used to produced polymer and plasticizer. With the acid catalysts, the reaction of cyclopentene with substituted benzene leads to produce alkylcyclopentylbenzene which possesses low pour point and high flash point [4]. These properties are of advantage for using as working fluid in hydraulic system. Over acid catalysts, cyclopenthylphenol can be produced and extensively tested as disinfectants, antioxidants and light stabilizers for polymers [5]. In fact, cyclopentadiene can be a source of cyclopentene and *vice versa* via selective hydrogenation/dehydrogenation process. Cyclopentadiene can be used as a precursor of some homogeneous catalysts, i.e. metallocene which are widely used in many pharmaceutical industries [6]. Chlorination of cyclopentadiene can produce hexachlorocyclopentadiene which is a precursor of several pesticides, such as aldrin, chlordane, endrin, heptachlor, and endoselfan [7]. These pesticides are inexpensive; however, the usage is nowadays limited because of the environmental awareness. In addition to regulatory pressures, these pesticides become less effective owing to genetic mutations of the targeted insects [8]. Alternatively, Diels-Alder addition reaction has been employed to convert cyclopentadiene to many valuable products, such as addition of cyclopentadiene with 1,3-butadiene to produce an adduct that are served as a termonomer in the production of ethylene-propylene terpolymer elastomers [4]. The Diels-Alder adduct of cyclopentadiene and maleic anhydride is used for the production of modified polyester resins [9]. Homopolymer of cyclopentadiene have been reported to be used as modifiers for high molecular polymers as base materials for coatings, adhesives, paper-sizing agents, and printing inks [4]. Dimerization of cyclopentadiene produces dicyclopentadiene which is served as a building block

for the production of modified hydrocarbon resins. These resins are mixed in the paint to improve drying rate, gloss, and hardness [4].

Cyclopentene and cyclopentadiene are available from coal tar. Moreover, both cyclic olefins can be achieved from steam cracking of naphtha and presented in the C_5 fraction of pyrolysis gasoline [4]. However, low content of such cyclic olefins is obtained and is insufficient for industrial demand.

Accordingly, the production of the cyclic olefins from the abundance C_5 such as *n*-pentane, isopentane and cyclopentane becomes attractive. The process including dehydrogenation and cyclization of acyclic hydrocarbons can be achieved using metal surface catalyst. Among the metal surface catalyst, the platinum has been reported to possess high dehydrogenation and cyclization activity for converting varouis paraffinic hydrocarbons to cyclic molecules, such as *n*-hexane and cyclohexane to benzene [10], *n*-heptane to toluene [10], *n*-octane to xylene [10]. The platinum surface is able to adsorb hydrogen not only the gas phase hydrogen but also the hydrogen atom from the hydrocarbon molecules [11]. The C-H dissociative adsorption of hydrocarbons leads to the formation of the akylidyne intermediates (carbon bond to metal atom) over the platinum surface [12]. In addition, this specie can be dehydrogenated and concerted with the enclosure of the hydrocarbon molecule, namely dehydrocyclization. The hydrocarbon feed with carbon number higher than C_6 can be readily converted to naphthenic or aromatics structure, as mentioned earlier. Accordingly, *n*-pentane, isopentane and cyclopentane are possibly activated and converted to cyclic olefins.

To obtain higher Pt metal surface, a high surface area support is generally employed. However, not all the support can be used without exception. To avoid the acidity that can promote other undesired reactions, i.e., isomerization, oligomerization, aromatization, etc., the inert support silica (SiO_2) is selected. It is expected that, with the lower acidity, platinum metal surface would only be the actives site for promoting only dehydrocyclization of such pentanes to cyclic olefins.

In this chapter, the conversion of *n*-pentane, isopentane and cyclopentane over Pt/SiO_2 to cyclopentene and cyclopentadiene is studied. The mechanism of such pentanes reactions is proposed. The nature of Pt active species responsible to the observed activity is discussed together with the effect of calcination temperature, contact time, reaction and reduction temperature, and H_2 partial pressure.

5.2 Experimental

The commercial amorphous SiO_2 obtained from Carlo Erba was calcined at 500°C and used as a support. The Pt/SiO_2 catalyst was prepared by incipient wetness impregnation of SiO_2 with an aqueous solution of H_2Cl_6Pt, as previously describe in Chapter 3. The sample was subsequently dried at room temperature, and then calcined at 300°C, or 500°C for 5 h.

The metal loading was determined by XRF spectrometer (Siemens model SRS3400). The surface areas (BET) of catalysts were determined by N_2 adsorption (Autosorb-1). The catalyst structure and crystallinity are determined by X-ray diffractometer (Siemens model D8). The morphology was observed by TEM (JEOL model JEM-2010). Temperature programmed reduction (TPR) and temperature programmed NH_3/pyridine desorption experiments were performed in a quartz micro-reactor. The H_2 consumption and NH_3/pyridine desorption were recorded by an on-line TCD detector (VICI model TCD2-NIFED). The electronic state of the Pt and Cl were determined by X-ray absorption near edge structure (XANES) and electron spin resonance (ESR) spectrometer. XANES measurement was carried out at the beamline BL8 of the Siam Photon Laboratory. Fluorescence mode XAS was performed to obtain Chlorine K-edge spectra and Platinum M-edge spectra which were calibrated with potassium chloride (edge energy at 2822 eV) and platinum foil (edge energy at 2122 eV), respectively. ESR was performed using an X-band JEOL, model JES-RE2X spectrometer (frequency of 8.8-9.6 GHz). The sample temperature was kept constant at about 77 K. The line position is calibrated with DPPH.

The *n*-pentane transformation was carried out at 500°C and ambient pressure. Before the reaction, the catalysts were activated in air (13 ml/min) at corresponding calcination temperature (300°C and 500°C). After that, the catalysts were reduced by H_2 (15 ml/min) at 500°C for 2 h. The temperature was set at 300-650°C, and a saturated vapor of *n*-pentane (at -5°C), isopentane (at -5°C) or cyclopentane (at 3.5°C) was carried by hydrogen/helium (a total flow of 15 ml/min) through a fixed bed reactor made with a quartz tube (O.D. = 8 mm). The products from the reaction were analyzed by an on-line gas chromatograph (BUCK Scientific, Model 910) with FID detector using HP-PLOT column (ϕ = 0.53 mm, L = 30 m).

For coke characterization, TPD-MS of the coked catalysts was performed in a quartz reactor and the coke content was analyzed by TGA (Perkin Elmer model TGA Pryis 1). The details of each experimental procedure are mentioned thoroughly in Chapter 3.

5.3 Results and discussion

5.3.1 Catalyst characterization

5.3.1.1 Elemental analysis

The platinum content in the impregnated Pt/SiO_2 are determined by an XRF spectrometer. It is found that the platinum loading is approximately 1 wt.%. Moreover, chlorine is retained in the catalyst, as observed in Table 5.1. The chlorine content is decreased with an increase in calcination temperature.

Table 5.1 The elemental analysis and surface area of Pt/SiO_2 used in this study.

Catalyst	Calcination temperature (°C)	Pt (wt.%)	Cl (wt.%)	BET surface area (m^2/g)
SiO_2 (used as support)	500	-	-	363
Pt/SiO_2	300*	1.03	0.53	351
Pt/SiO_2	500*	1.03	0.20	348

* calcination after Pt loading into the SiO_2 which is preliminary calcined at 500°C.

5.3.1.2 Surface area

Surface area of SiO_2 and Pt/SiO_2 catalysts are determined by nitrogen adsorption technique using Brunauer-Emmet-Teller (BET) as model equation. The calculated surface area for the Pt/SiO_2 calcined at 300°C and 500°C is summarized in Table 5.1. All Pt/SiO_2 catalysts possess relatively high surface area (> 300 m^2/g).

5.3.1.3 Structure

The diffraction patterns of Pt/SiO_2 catalysts are determined by XRD technique. The XRD patterns of SiO_2 and Pt/SiO_2 calcined at 300°C and 500°C are shown in Figure 5.1. The only broad peak is observed at 2θ of 15 to 30 for SiO_2 suggesting the amorphous structure. After Pt loading and calcination, the 2θ at 39.94 and 46.72 are observed and can be assigned to (111) and (200) planes of PtO_x cluster, respectively [13,14].

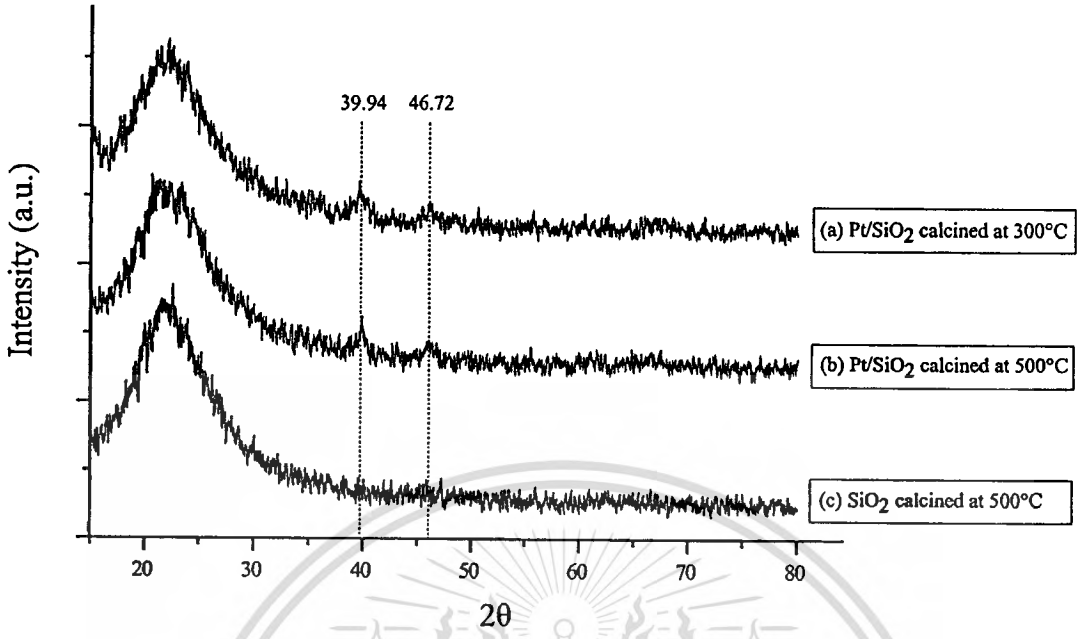

Figure 5.1 XRD patterns of (a) Pt/SiO_2 calcined at 300°C, (b) Pt/SiO_2 calcined at 500°C, and (c) SiO_2 calcined at 500°C.

After reduction at 500°C, it is found that the Pt (111), Pt (200) and Pt (220) are evidently observed in both Pt/SiO_2 catalysts which are calcined at 300°C and 500°C, as shown in Figure 5.2. The higher intensity of Pt (111) of the Pt/SiO_2 calcined at 500°C is observed, as compared to that at 300°C. This suggests that larger Pt (111) surface would be obtained from the reduction of PtO_x specie formed by calcination at 500°C.

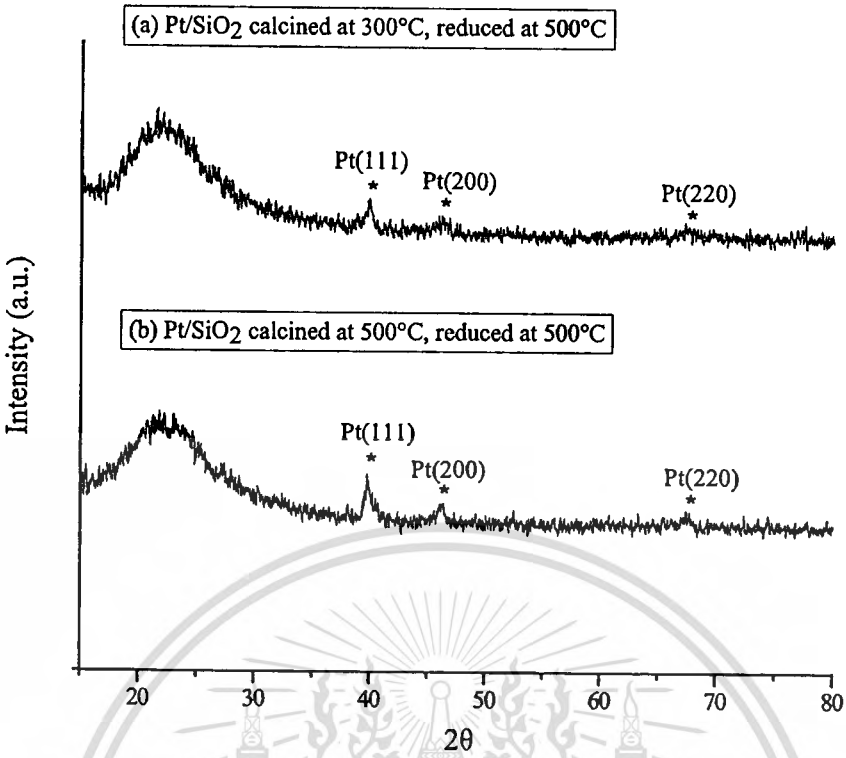

Figure 5.2 XRD patterns of (a) Pt/SiO_2 calcined at 300°C, reduced at 500°C and (b) Pt/SiO_2 calcined at 500°C, reduced at 500°C.

5.3.1.4 Morphology

The catalyst morphology obtained from a transmission electron microscope is shown in Figure 5.3. It can be seen that the PtO_x obtained from calcination at 500°C shows lower dispersion, as compared to that the PtO_x formed after calcination at 300°C. This reveals that the interaction between PtO_x and the SiO_2 is relatively weak, the PtO_x species can be agglomerated during the calcination process. As higher calcination temperature is employed, the PtO_x agglomeration is noticeably enhanced [15, 16].

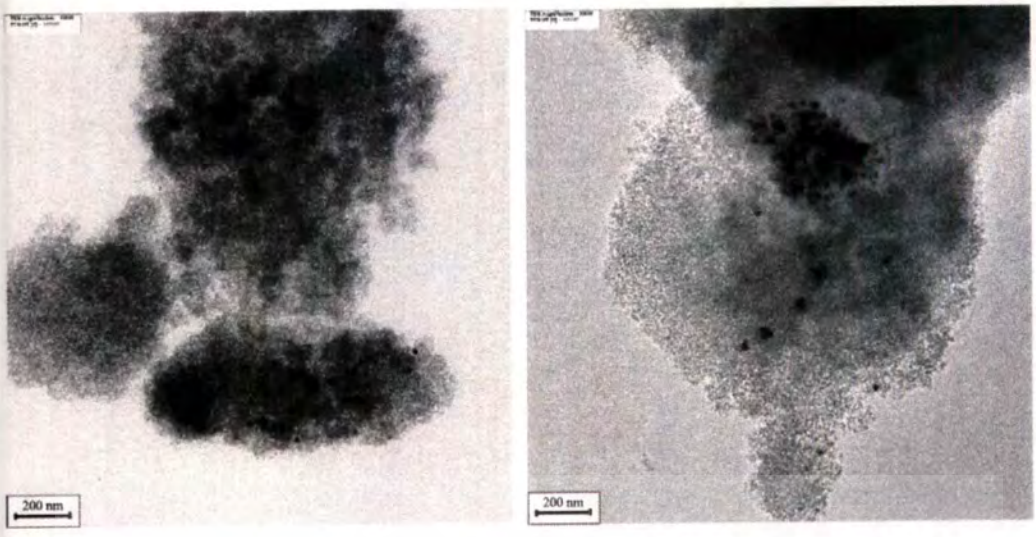

(a) Pt/SiO_2 calcined at 300°C (b) Pt/SiO_2 calcined at 500°C

Figure 5.3 TEM images of (a) Pt/SiO_2 calcined at 300°C and (b) Pt/SiO_2 calcined at 500°C (scale 200 nm).

It is noted that the PtO_x formed can be partially embedded into the SiO_2 framework during the calcination process, as shown in Figure 5.4.

Figure 5.4 TEM image of PtO_x embedded into the SiO_2, scale 7 nm. (This picture is obtained from Pt/SiO_2 calcined at 300°C).

After reduction at 500°C, the Pt metal is formed in the Pt/SiO_2, as previously shown by XRD. It is in line with the XRD that the larger Pt metal surface is observed from the reduction of the PtO_x obtained after calcination at 500°C, as seen in Figure 5.5. As the agglomerate PtO_x is subjected to be reduced, the larger Pt metal surface is reasonably obtained.

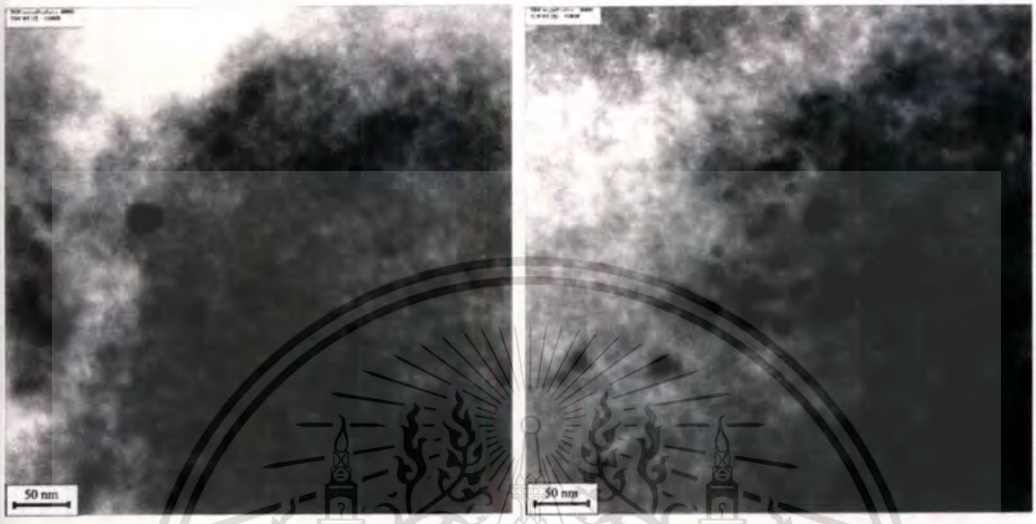

(a) Pt/SiO_2 calcined at 300°C, reduced at 500°C (b) Pt/SiO_2 calcined at 500°C, reduced at 500°C

Figure 5.5 TEM images of (a) Pt/SiO_2 calcined at 300°C, reduced at 500°C and (b) Pt/SiO_2 calcined at 500°C, reduced at 500°C (scale 50 nm).

5.3.1.5 Reducible metal species

TPR of Pt/SiO_2 catalysts calcined at 300°C and 500°C are shown in Figure 5.6. It is found that a major reduction peak is observed in both samples at low temperature about 100-200°C and at high temperature about 450-500°C.

The low temperature reduction peak is referred to the reduction of surface PtO_x to Pt metal (at 100-250°C) [13,17,18,19]. As the Pt metal can be created during calcination especially at high temperature as 500°C; therefore, it would chemisorp oxygen retained in the calcination atmosphere. Such surface platinum oxide specie would be easily reduced, as seen the lower reduction temperature (~100°C) is obtained as compared to that of the reduction of the PtO_x (~230°C) obtained from calcination at 300°C.

The high temperature reduction peaks (450-500°C) may be due to the reduction of PtO_x which are embedded into the silica after calcination process, as previously observed by

TEM (Figure 5.4). No reduction peak is observed in bare SiO_2 suggesting that no reducible species presented in the support. It can be seen in Figure 5.6 that, with the same Pt loading (1wt.%), the peak area for the reduction of surface PtO_x decreases and the reduction for embedded PtO_x increases with an increase in calcination temperature. It is suggested that the calcination at high temperature (500°C) provides low available surface PtO_x species, but high content of embedded PtO_x. In other words, more surface PtO_x is formed when calcined at low temperature (300°C). Therefore, it can be concluded that the active Pt metal surfaces formed over SiO_2 are regulated by calcination temperature.

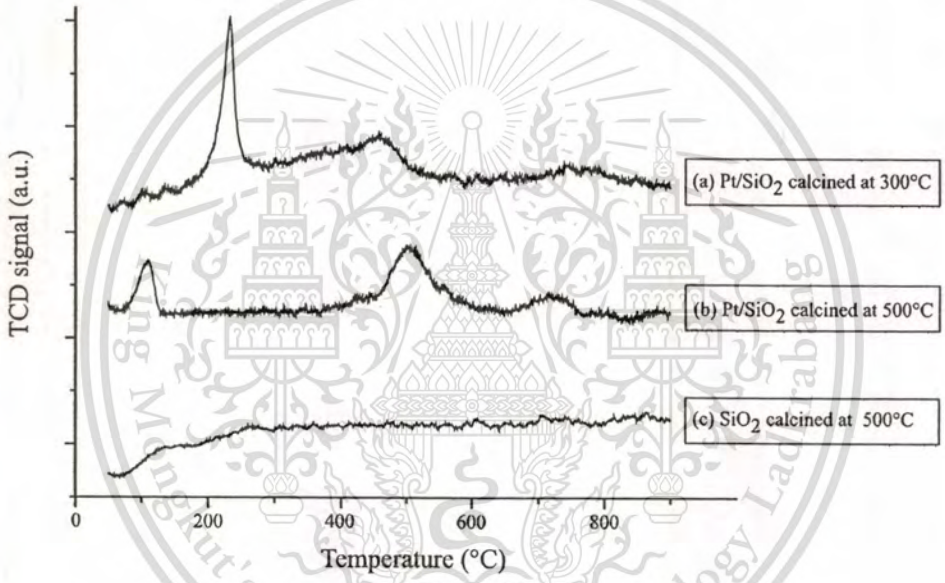

Figure 5.6 TPR of (a) Pt/SiO_2 calcined at 300°C, (b) Pt/SiO_2 calcined at 500°C and (c) SiO_2 calcined at 500°C.

5.3.1.6 The retained chlorine species

From the elemental analysis, chlorine was retained in the Pt/SiO_2 after calcination (Table 5.1). The TGA (in air zero) of the non-calcined Pt/SiO_2 is performed, as shown in Figure 5.7, to speculate the formation of such chlorine specie. It is found that the weight losses are observed at 95°C, 290°C, and 460°C. The first weight loss at 95°C is due to the desorption of water out of the SiO_2 framework. In the presence of air, it has been reported that the $H_2PtCl_6 \cdot 6H_2O$ can be decomposed to either PtO_x and $PtCl_4$ species [20]. The latter forms at 25-280°C (Eq.(5.1)). The $PtCl_4$ is further decomposed to $PtCl_2$ at 280-350°C (Eq.(5.2)). Finally, the $PtCl_2$ is decompsed to Pt at 350-530°C (Eq.(5.3)).

$$H_2PtCl_6 \cdot 6H_2O \xrightarrow{25-280^\circ C} PtCl_4 + 2HCl + 6H_2O \quad (5.1)$$

$$PtCl_4 \xrightarrow{280-350^\circ C} PtCl_2 + Cl_2 \quad (5.2)$$

$$PtCl_2 \xrightarrow{350-530^\circ C} Pt + Cl_2 \quad (5.3)$$

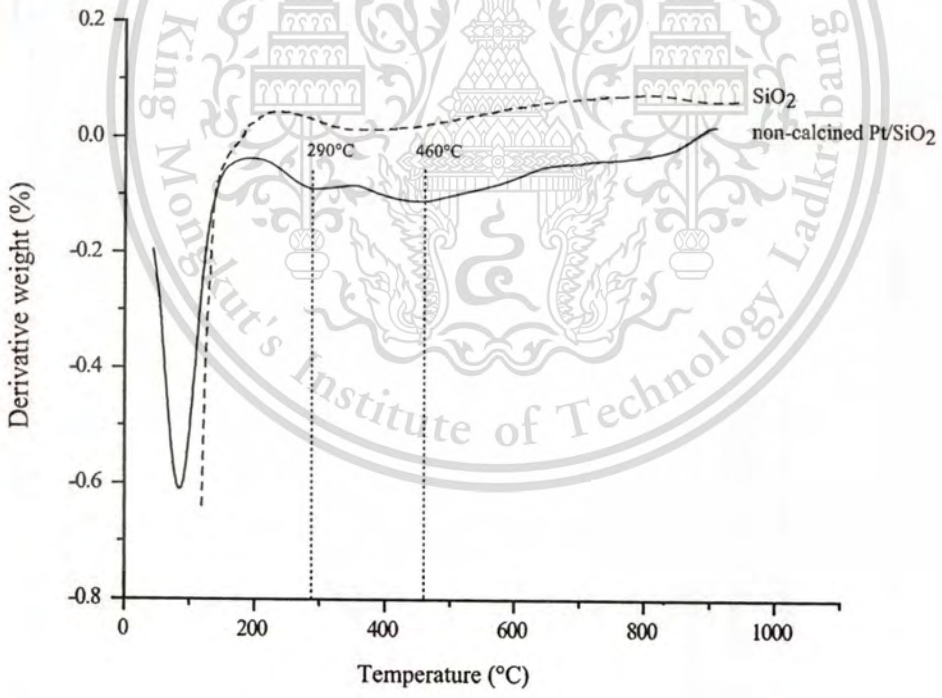

Figure 5.7 TGA (in air) of non-calcined Pt/SiO_2 (1wt.%).

Accordingly, the weight loss at 290°C and 460°C, shown in Figure 5.7 may be attributed from the decomposition of H_2PtCl_6 to $PtCl_2$, and $PtCl_2$ to Pt, respectively. It is possible that the $PtCl_2$ may well be retained as chlorine species in the Pt/SiO_2 after calcination at 300°C and 500°C.

The retained $PtCl_2$ in the Pt/SiO_2 calcined at 300°C and 500°C is also examined by Cl_2-TPD-MS experiment in the continuous flow of 2%H_2 in Ar, as shown in Figure 5.8. It is found that the similar Cl_2 desorption peak is observed at 325°C in both catalysts (Figure 5.8(a)-(b)). This peak presumably reveals the decomposition of $PtCl_2$. However, the additional Cl_2 desorption peaks is observed in the Pt/SiO_2 calcined at 300°C. As compared to the decomposition of the Pt precursor shown in Figure 5.8(c), this would be derived from the incomplete decomposition of the Pt precursor after calcination at 300°C.

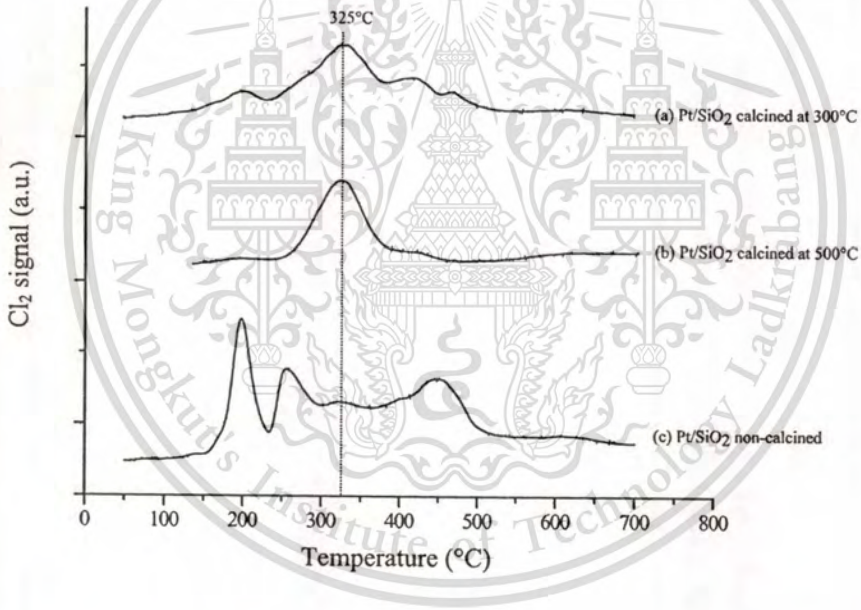

Figure 5.8 MS signal of Cl_2 desorption from the reduction of (a) Pt/SiO_2 calcined at 300°C, (b) Pt/SiO_2 calcined at 500°C, and (c) Pt/SiO_2 non-calcined.

The decomposition of $PtCl_2$ obtained after calcination at 300°C and 500°C can yield Cl_2, as shown in Figure 5.8. In order to investigate the chlorine specie retained after reduction at 500°C, the ESR spectrometry is performed, as shown in Figure 5.9. It is found that before reduction (Figure 5.9(a)-(b)), no ESR signal is observed since the platinum (II) ion does not exhibit an ESR signal. After the $PtCl_2$ is reduced at 500°C (Figure 5.9(c)), the ESR signal at g = 2.01 is observed due to the Pt^+ ion attached to platinum atom at the metal-support interface [21,22]. This reveals that the reduction at 500°C cannot completely yield metallic platinum. Some of Pt^{2+} is reduced to Pt^+ that is likely retained in the catalyst as PtCl.

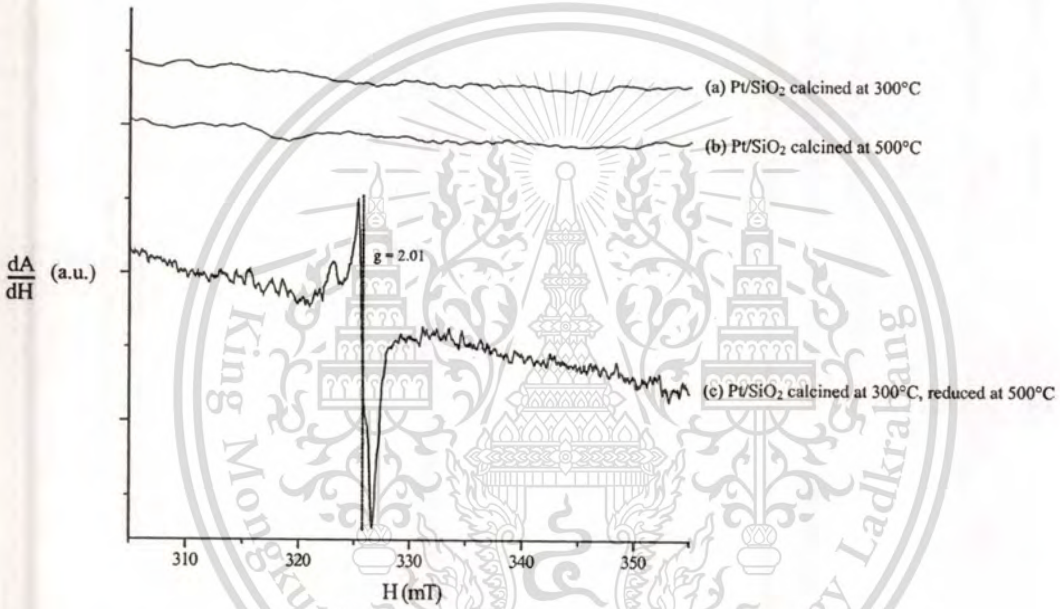

Figure 5.9 ESR spectra of (a) Pt/SiO_2 calcined at 300°C, (b) Pt/SiO_2 calcined at 500°C, and (c) Pt/SiO_2 calcined at 300°C, reduced at 500°C.

The existence of the PtCl left after H_2 reduction at 500°C is also defined by K-edge XANE spectrometry, as shown in Figure 5.10. In consistent with XRF and Cl_2-TPD-MS, the higher chlorine content is still observed in the Pt/SiO_2 that is calcined at 300°C (Figure 5.10(a)), as compared to that of the Pt/SiO_2 calcined at 500°C (Figure 5.10(b)).

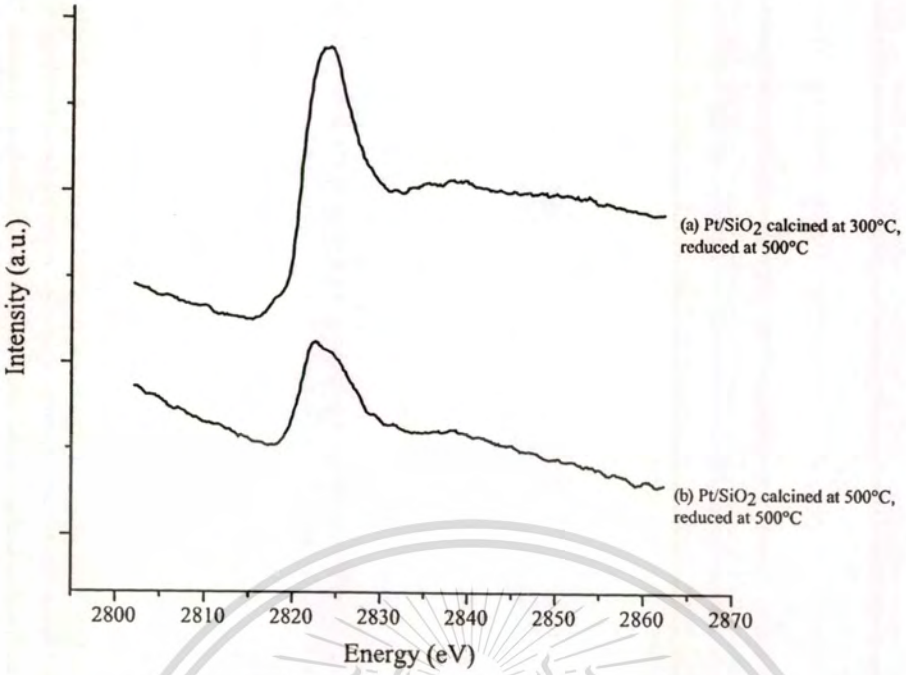

Figure 5.10 Cl K-edge XANES spectra of (a) Pt/SiO_2 calcined at 300°C, reduced at 500°C and (b) Pt/SiO_2 calcine at 500°C, reduced at 500°C.

Moreover, the H_2 reduction of Pt/SiO_2 at higher temperature can partially eliminate chlorine in the catalyst, as observed by XANE in Figure 5.11. It is likely that as the Pt/SiO_2 is subjected to be reduced at higher temperature, larger amount of PtCl is proportionally converted to Pt metal and releases Cl_2 and/or HCl leading to lower the PtCl content.

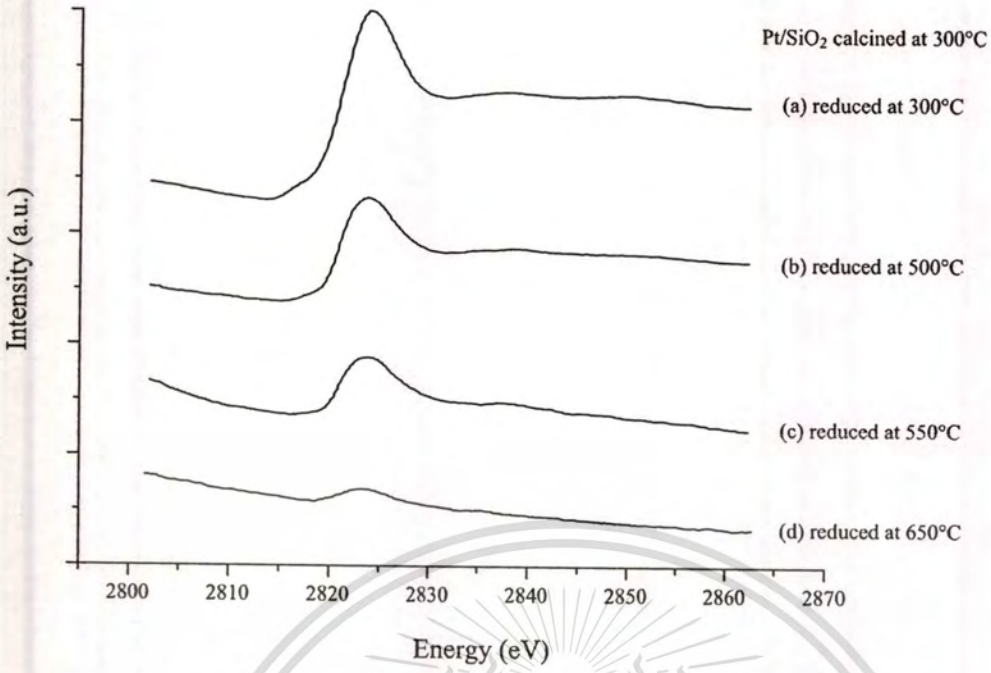

Figure 5.11 Cl K-edge XANES spectra of Pt/SiO_2 calcined at 300°C, reduced at 300-650°C.

5.3.1.7 Acidity of the catalyst

The NH_3-TPD of the Pt/SiO_2 catalysts reduced at 500°C is shown in Figure 5.12. It can be seen that the weak acid site of silica is observed by ammonia desorption peak at 175°C. Such acid sites would be contributed from the silanol group [23]. However, the additional acidity would be generated after Pt loading. This may be due to the electron deficiency of the Pt metal surface which causes by PtCl species retained after calcination and reduction, as previously observed by ESR and XANES.

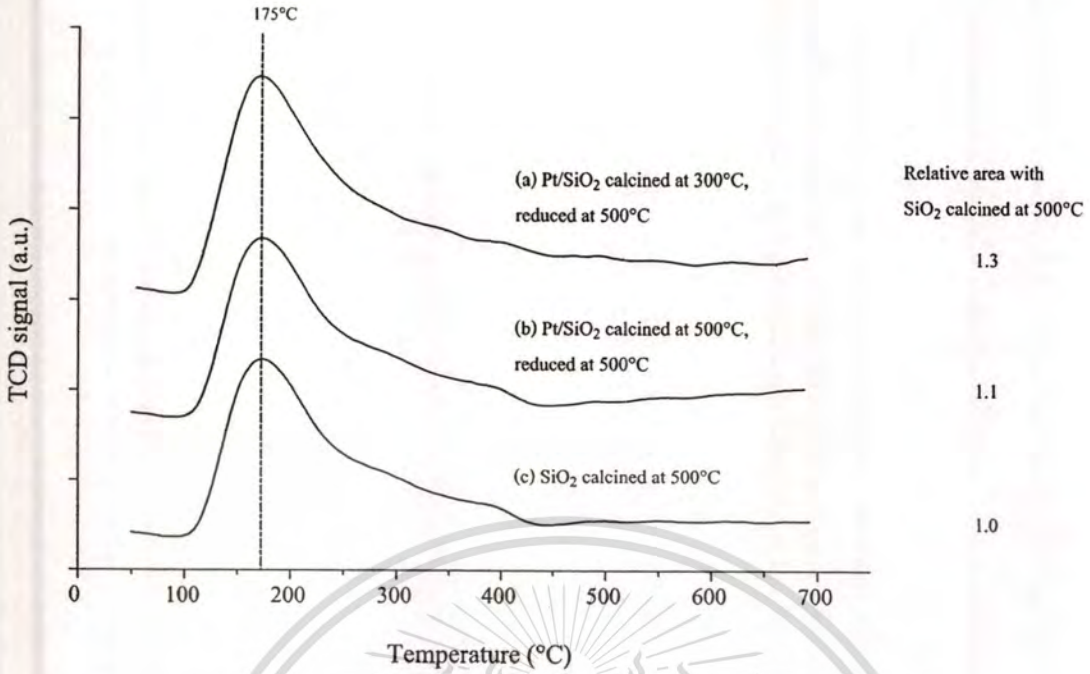

Figure 5.12 NH_3-TPD of (a) Pt/SiO_2 calcined at 300°C, reduced at 500°C, (b) Pt/SiO_2 calcined at 500°C, reduced at 500°C, and (c) SiO_2 calcined at 500°C.

The Pt/SiO_2 calcined at 300°C and reduced at 500°C (Figure 5.12(a)) shows acidity higher than that of the Pt/SiO_2 calcined at 500°C and reduced at 500°C (Figure 5.12(b)). This corresponds to the Cl content in those catalysts (Figure 5.10). As the higher amount of Cl is retained, the higher acidity (electron deficiency) would be obtained. It is noted that the only one desorption peak is observed from NH_3-TPD. The strong base as ammonia may interact with silanol and electron deficient Pt metal surface in a similar manner. Therefore, NH_3 cannot discriminate the two acid species on the catalyst surface.

A Lewis base molecule, as pyridine is used instead of NH_3. The results of pyridine-TPD are shown in Figure 5.13. It can be seen that the acid site of silanol group is detected by pyridine desorption peak at 155°C. The additional acidity that would be formed from electron deficient Pt species is evidenced by pyridine desorption peak at 500°C. In corresponds to the NH_3-TPD, the acidity of Pt/SiO_2 catalyst is decreased with a decrease in chlorine content.

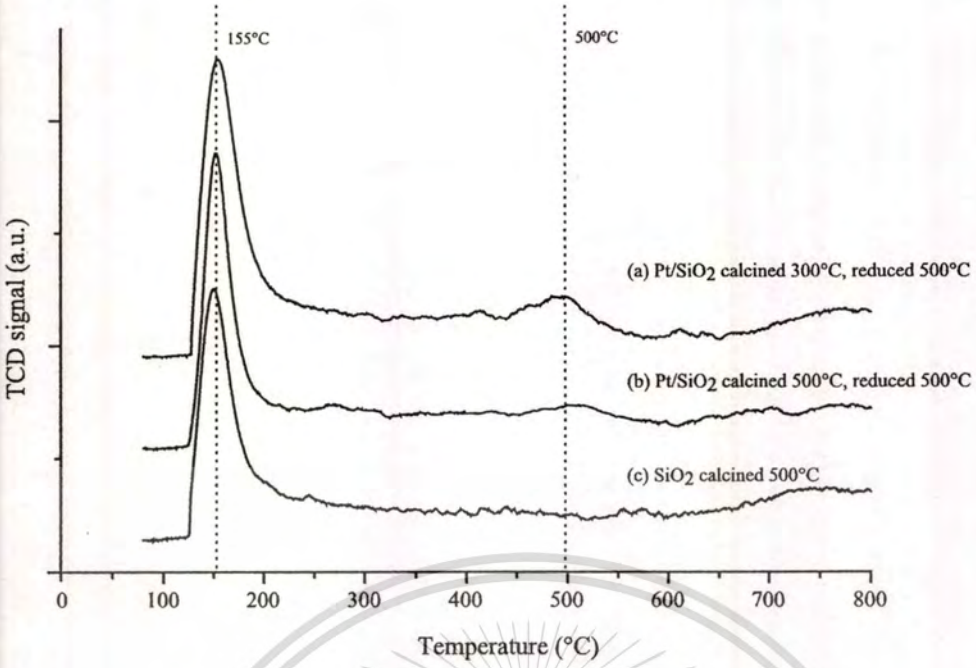

Figure 5.13 Pyridine-TPD of (a) Pt/SiO_2 calcined at 300°C, reduced at 500°C, (b) Pt/SiO_2 calcined at 500°C, reduced at 500°C, and (c) SiO_2 calcined at 500°C.

5.3.2 Activity testing

The catalytic activity of the Pt/SiO_2 obtained from calcination at 300°C and 500°C for *n*-pentane transformation at 500°C is examined. Before running the reaction, the H_2 reduction at 500°C is required for creating Pt metal surface and removing the chlorine specie. The results are shown in Table 5.2. It is found that the higher activity (12.8%) is obtained when the Pt/SiO_2 is calcined at 300°C, as compared to that obtained from the Pt/SiO_2 which is calcined at 500°C (1.71%). This is in line with the amount of available Pt metal surface which acts as active sites, as observed by TPR (Figure 5.6). As the Pt/SiO_2 with the high content of Pt metal surface is employed, the high *n*-pentane conversion would be obtained.

Table 5.2 Catalytic activity of Pt/SiO_2 calcined at 300°C and 500°C.

Calcination temperature (°C)	300	500
Reduction temperature (°C)	500	500
Reaction temperature (°C)	500	500
Contact time (g h/mol)	49.8	49.8
Conversion (%)	12.8	1.71
Selectivity (%)		
methane	1.21	-
ethane	2.05	-
propane	1.93	-
n-butane	1.19	-
cyclopentane	20.4	-
isopentane	3.05	-
cyclopentene	6.99	-
isopentene	38.0	60.2
1-pentene	8.18	16.4
cyclopentadiene	15.2	23.4
C_6	1.83	-

It can be seen in the Table 5.2 that various products are formed. Methane, ethane, propane, and *n*-butane would mainly come from hydrogenolysis; cyclopentane, cyclopentene, and cyclopentadiene would be formed by cyclization; isopentane, and isopentene (2-methyl-2-butene) would be formed by isomerization; 1-pentene would be formed by dehydrogenation; and C_6 would be formed by oligomerization. However, the main products are isopentene and cyclic C_5. It is noted that no reaction at 500°C is taken place over bare SiO_2. Only silanol group cannot activate *n*-pentane.

Accordingly to the catalytic activity, the Pt/SiO_2 calcined at 300°C is selected to examine the effect of contact time, reaction and reduction temperature, H_2 partial pressure, and effect of feed structure, as discussed below.

5.3.2.1 Effect of contact time

Effect of contact time for *n*-pentane transformation over Pt/SiO_2 calcined at 300°C is shown in Figure 5.14. It is found that all products (shown in Table 5.2) are observed despite the reaction is performed at low contact time. This reveals that hydrogenolysis, isomerization, cyclization, and dehydrogenation take place in parallel.

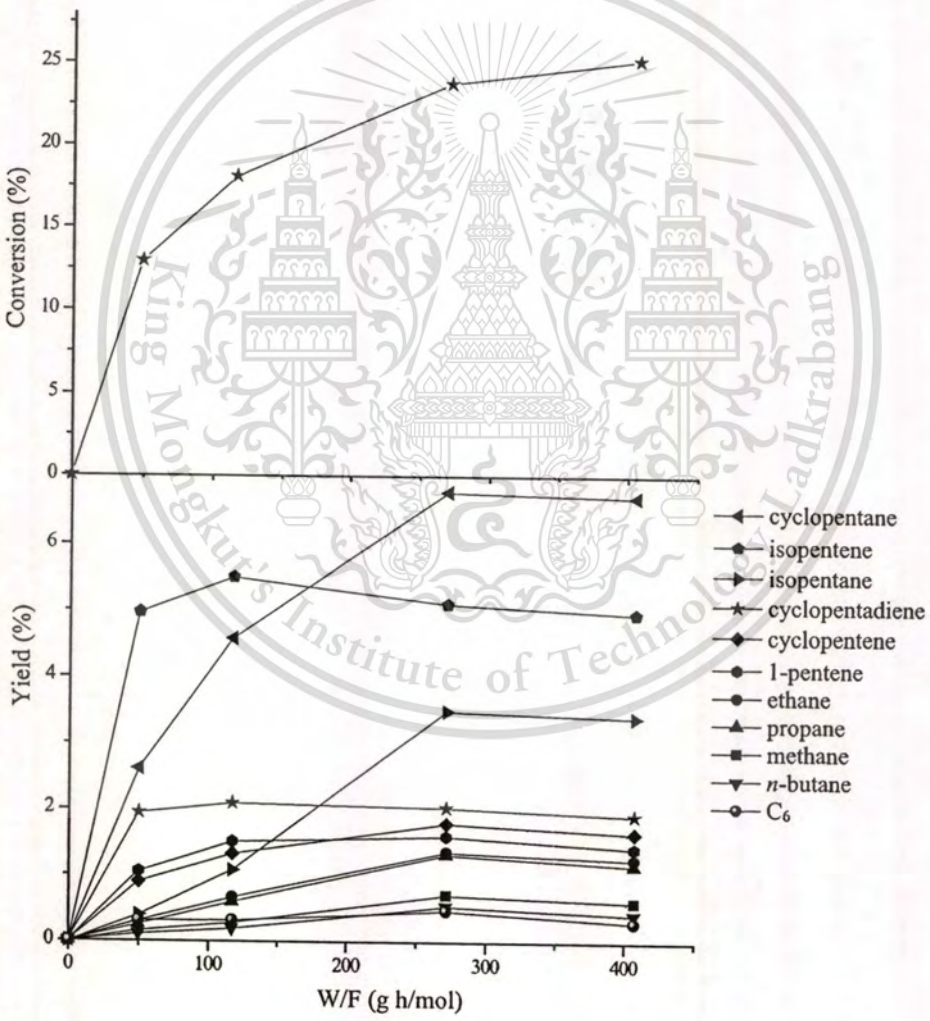

Figure 5.14 Effect of contact time for *n*-pentane conversion over Pt/SiO_2 (1wt.%) calcined at 300°C, reaction temperature 500°C.

An isomerized product (i.e., isopentene) is observed as a main product. This is probably due to the effect of the acidity from the chlorine specie retained in the Pt/SiO_2 catalyst (as observed by NH_3-TPD and pyridine-TPD) that promotes isomerization. However, such acidity would also promote hydrogenolysis (C-C clevage) producing smaller paraffinic products, as observed in Table 5.2. On the other hand, the Pt metal surface can cyclize the adsorbed *n*-pentane to cyclopentane, cyclopentene and cyclopentadiene.

As contact time is increased, yield of isopentene, cyclopentene and cyclopentadiene decrease (5.04, 1.67 and 1.94%, respectively) together with an increase in isopentane and cyclopentane yield (2.69 and 6.07%, respectively). This reveals that at high contact time hydrogenation of the produced olefins can be promoted. Moreover hydrogenolyzed products (i.e., methane, ethane, propane, and *n*-butane) are also boosted in parallel.

According to the product distribution, the reaction pathway for *n*-pentane conversion over Pt/SiO_2 catalyst is proposed in Figure 5.15. *n*-Pentane would be dissociatively adsorbed (C-H bond breaking) over the Pt metal surface in three possible configurations (I, II, and III). The adsorbed *n*-pentane would be either consecutively hydrogenolyzed, isomerized, cyclized, or dehydrogenated to C_5 olefins. The intermediate I can be either hydrogenolyzed to ethane and propane or isomerized to isopentene and isopentane. The intermediate II gives a similar product as intermediate I, but it can be additionally hydrogenolyzed to methane and *n*-butane. The intermediate III can be hydrogenolyzed to methane and *n*-butane; moreover, it can be also cyclized to cyclopentane, cyclopentene, and cyclopentadiene. In addition, some of the olefinic products can be further hydrogenated to saturated hydrocarbons.

It is noted that the yield of methane and *n*-butane are almost similar. This is also the case for ethane and propane yield. Hence, it is likely that these products are derived from direct mono-molecular hydrocracking of *n*-pentane, but from a different intermediate. Since, the ethane-propane show higher yield, as compared to that of methane-*n*-butane couple, cracking to ethane-propane is preferred presumably due to the higher stability of intermediate I and II, as compared to that of intermediate III (Figure 5.15). Moreover, small of 1-pentene is observed presumably from dehydrogenation of intermediate II and III. However, 2-pentene is not observed. It may strongly adsorb on the Pt metal surface and undergo further reaction before leaving as a product.

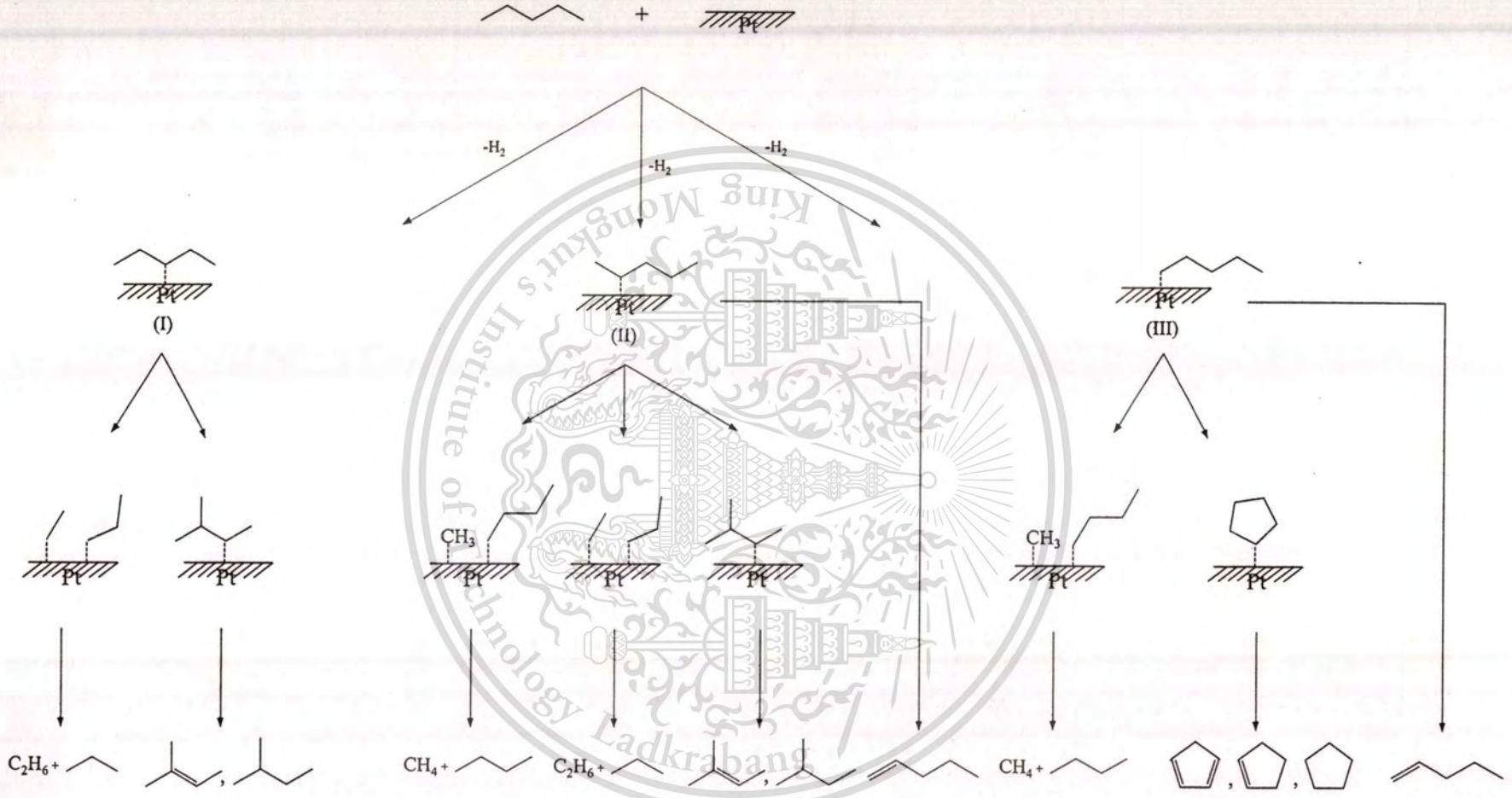

Figure 5.15 Proposed reaction pathway for *n*-pentane conversion over Pt/SiO_2 catalyst.

5.3.2.2 Effect of reaction temperature

An effect of reaction temperature on *n*-pentane conversion over Pt/SiO_2 is shown in Figure 5.16 and Table 5.3. As the temperature is increased, the higher conversion of *n*-pentane is observed with an increase in hydrogenolyzed products and a decrease in isomerized and cyclized products. This reveals that the higher reaction temperature can promote hydrogenolysis activity.

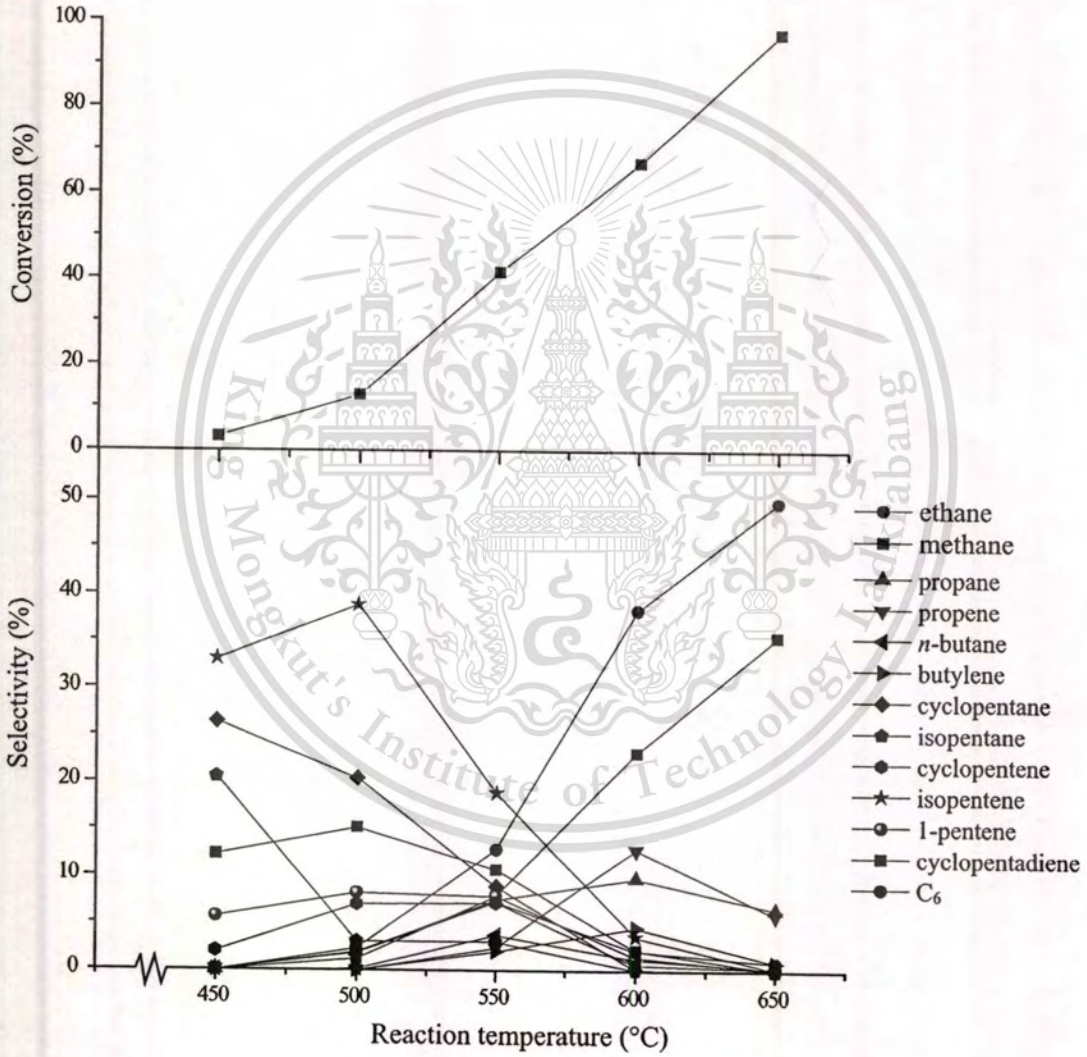

Figure 5.16 Effect of reaction temperature for *n*-pentane conversion over Pt/SiO_2 (1wt.%) calcined at 300°C, W/F = 49.8 g h/mol.

Table 5.3 Product distribution obtained from *n*-pentane conversion at 450-650°C over Pt/SiO_2 (1 wt.%) calcined at 300°C, W/F = 49.8 g h/mol.

Reaction temperature (°C)	450	500	550	600	650
Conversion (%)	3.08	12.8	41.6	67.0	97.1
Selectivity (%)					
methane	-	1.21	7.81	23.1	35.4
ethane	-	2.05	12.9	38.3	49.8
ethylene	-	-	-	-	-
propane	-	1.93	7.47	9.76	6.48
propylene	-	-	2.38	12.8	5.90
n-butane	-	1.19	3.75	1.23	0.21
butylene	-	-	2.01	4.56	0.88
cyclopentane	26.4	20.4	8.88	0.14	-
isopentane	20.5	3.05	3.05	0.10	-
cyclopentene	2.03	6.99	7.15	0.66	0.22
isopentene	33.1	38.0	18.8	3.59	0.14
1-pentene	5.66	8.18	7.87	1.45	0.05
cyclopentadiene	12.3	15.2	10.7	2.19	0.08
C_6	-	1.83	7.24	2.12	0.87

It can be seen in Table 5.3 that as the temperature is increased (> 500°C), the hydrogenolyzed products (methane-*n*-butane and ethane-propane) are not observed in a stoichiometric ratio (1:1), as discussed previously. Moreover, ethane and methane are mainly observed in the hydrogenolyzed products, as compared to propane and *n*-butane. This may be due to excessive hydrogenolysis of *n*-pentane to ethane and methane which are additionally promoted at very high temperature. Such reaction can be taken place by secondarily hydrogenolysis of the ethylidyne, propylidyne, and butylidyne intermediates, as shown in Figure 5.17. Moreover, propylidyne and butylidyne intermediates can be dehydrogenated to propylene and butylene due to a higher electron density that provides a stronger interaction with the Pt metal surface, whereas ethylidyne is relatively more electron deficient. Hence, dehydrogenation to ethylene is somewhat inhibited.

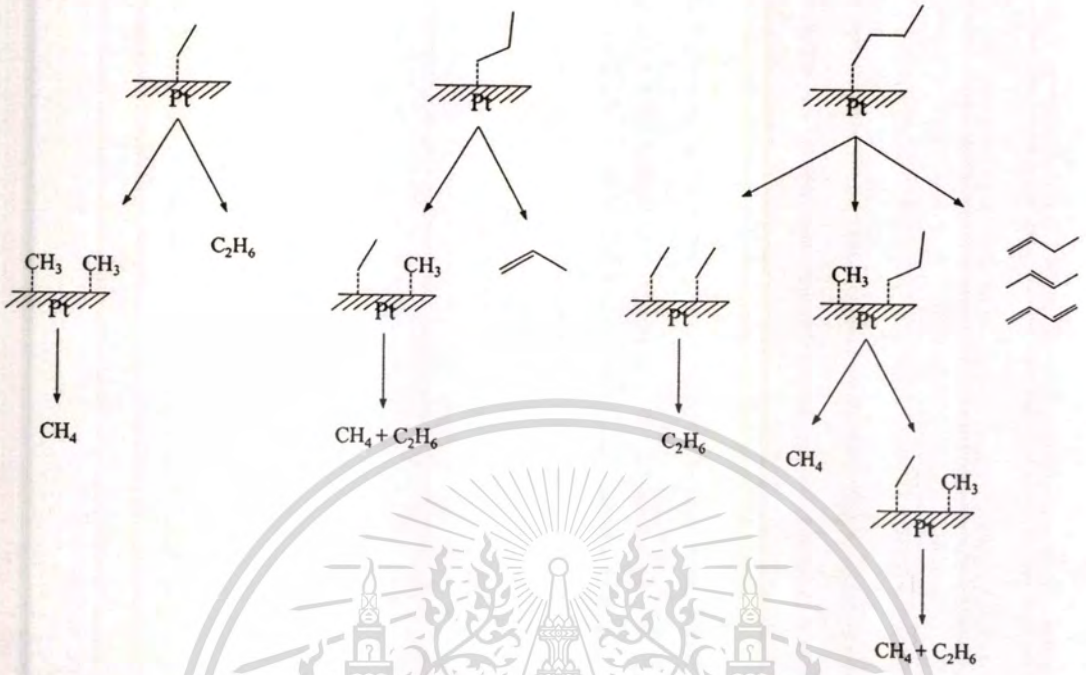

Figure 5.17 Secondarily hydrogenolysis.

As mentioned previously that C_6 can be formed by oligomerization over the electron deficient Pt metal surface, this reaction is also enhanced by increasing reaction temperature (450-550°C), as seen in Table 5.3. However, at very high temperature (600-650°C), the C_6 is almost vanished due to the higher hydrogenolysis activity.

For cyclization and isomerization, the appropriate reaction temperature seems to be not higher than 500°C to avoid undesirable hydrogenolyzed products.

As, cyclization and isomerization are parallel reactions, isopentene and isopentane are always produced as well as the cyclic C_5. According to the proposed reaction pathway shown in Figure 5.15, *n*-pentane adsorption via Intermediate III configuration is the only route for production of cyclic C_5. Hence, the larger Pt metal cluster that improved *n*-pentane adsorption may be required for cyclization. Therefore, the effect of reduction temperature (which is able to increase the metal cluster size) and the effect of H_2 partial pressure (which relates to electronically of Pt metal surface) are examined.

5.3.2.3 Effect of reduction temperature

An effect of reduction temperature on *n*-pentane conversion over Pt/SiO_2 is shown in Figure 5.18. As the Pt/SiO_2 is subjected to be reduced at higher temperature, an increase in cyclopentane, cyclopentene and cyclopentadiene (cyclic-products) selectivities with a decrease in isopentene and isopentane selectivities (iso-products) can be observed. This is because the Pt metal cluster is increased from reduction at high temperature (> 500°C) [12, 16]. Therefore, the electron density of Pt metal surface would be proportionally enlarged and facilitate *n*-pentane adsorption particularly for the least electron deficient species, i.e., intermediate III (Figure 5.15) that a precursor for cyclic C_5. As the intermediate III is facilitated, hydrogenylysis to methane and *n*-butane is also promoted (2.5% selectivity).

In addition, H_2 reduction at higher temperature can decrease an amount of chlorine specie (Figure 5.10) which leads to the acidity of Pt metal surface. Such acidity is well known to promote isomerization and hydrogenolysis. As the chlorine content is decreased, the acidity would be proportionally suppressed. Therefore, isomerization and hydrogenolysis activity are lowered when Pt/SiO_2 is reduced at higher temperature.

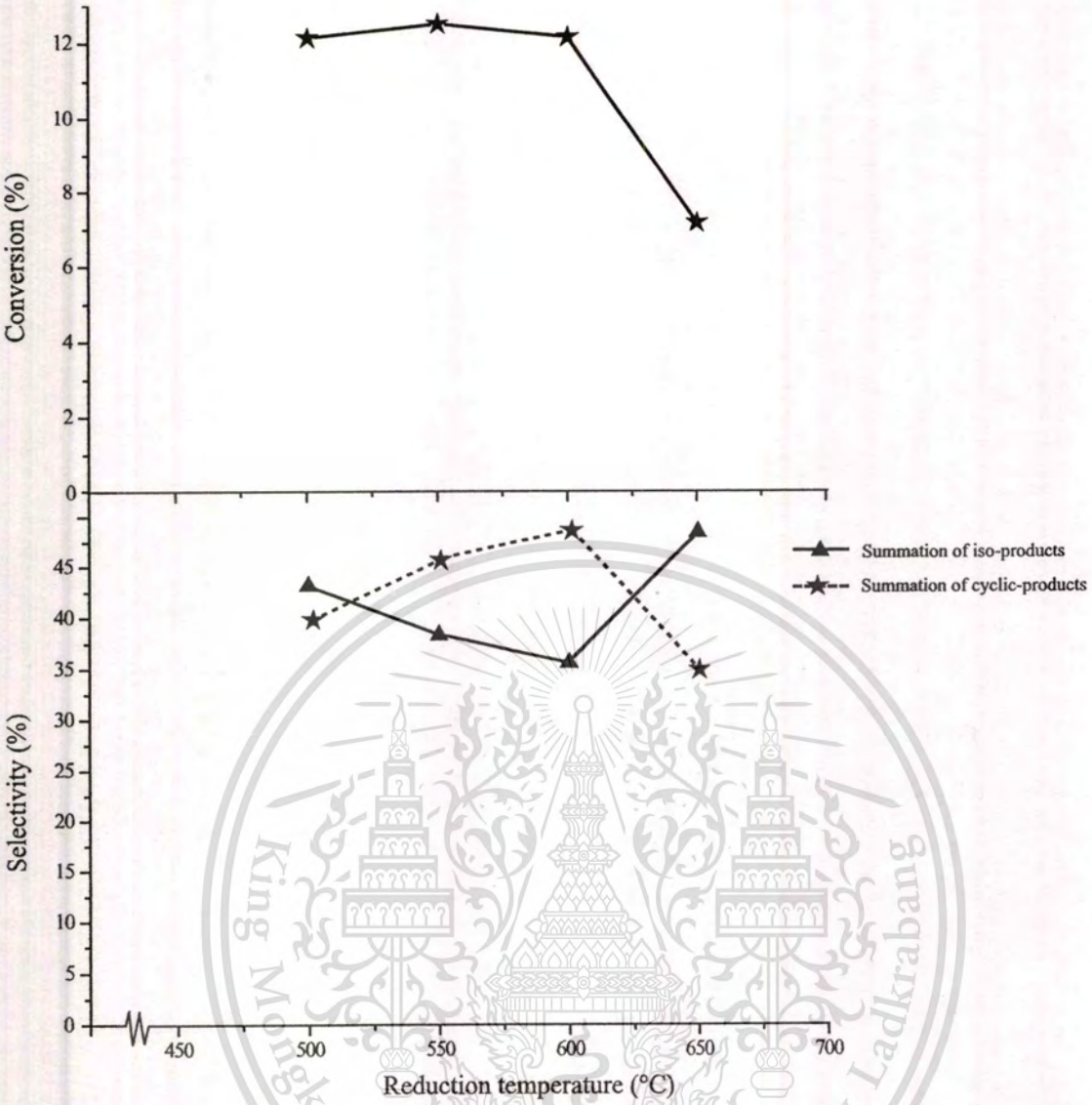

Figure 5.18 Effect of reduction temperature for *n*-pentane conversion over Pt/SiO_2 (1 wt.%) calcined at 300°C, W/F = 49.8 g h/mol, reaction temperature 500°C. (Other products: methane, ethane, propane, and *n*-butane ~ 10%, 1-pentene ~ 10% and C_6 ~ 2 %).

In a support manner, TEM images of Pt/SiO_2 reduced at various temperatures are shown in Figure 5.19. It is found that the larger Pt metal cluster is obtained for the Pt/SiO_2 reduced at higher temperature, as expected.

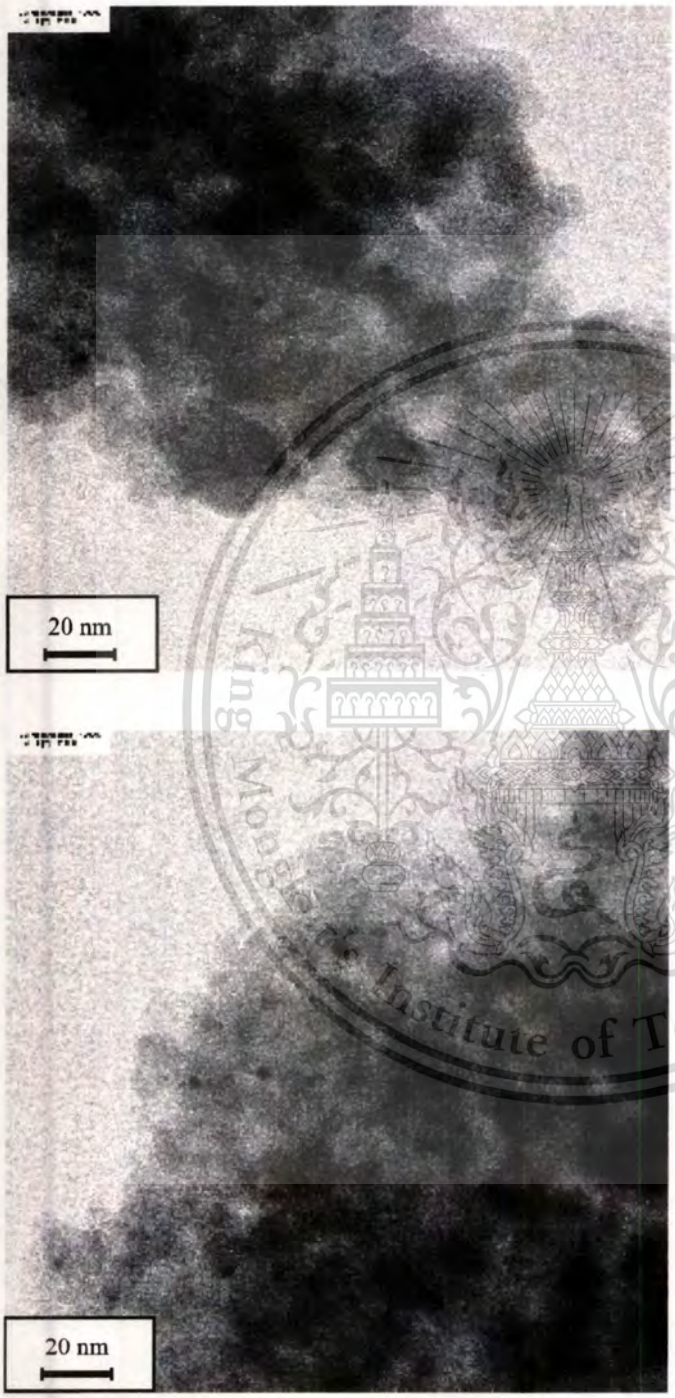

Reduction temperature: 300°C
n-Pentane conversion: -
BET surface area: 345 m^2/g

Reduction temperature: 500°C
n-Pentane conversion: 12.3%
BET surface area: 340 m^2/g

Figure 5.19 TEM images and surface area of Pt/SiO_2 calcined at 300°C, reduced at 300-650°C.

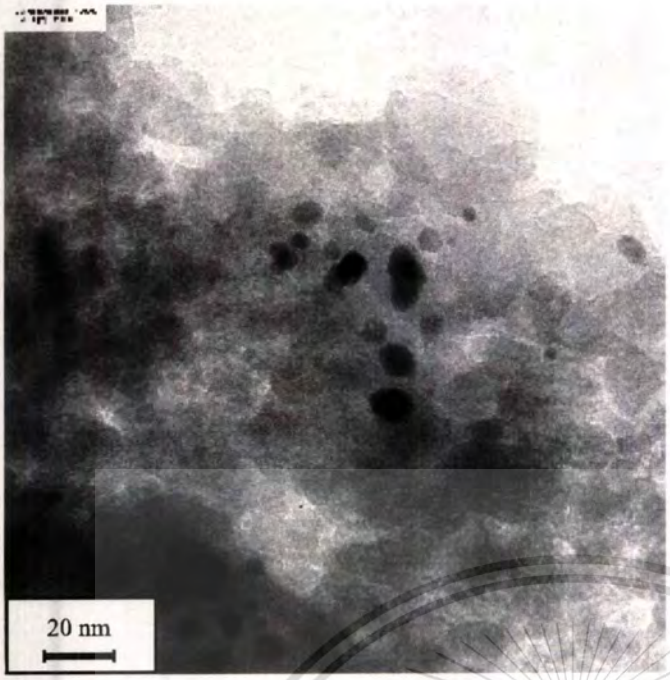

Reduction temperature: 550°C

n-Pentane conversion: 12.6%

BET surface area: 337 m^2/g

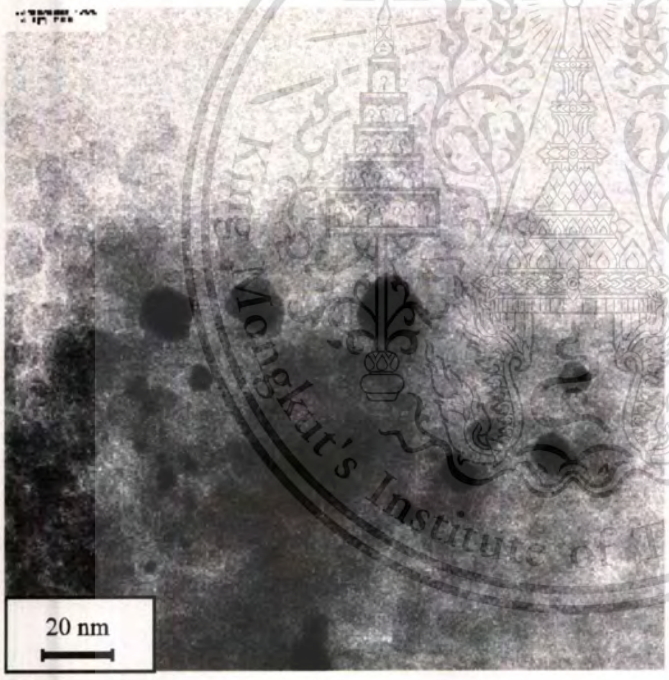

Reduction temperature: 600°C

n-Pentane conversion: 12.1%

BET surface area: 330 m^2/g

Figure 5.19 TEM images and surface area of Pt/SiO_2 calcined at 300°C, reduced at 300-650°C (continued).

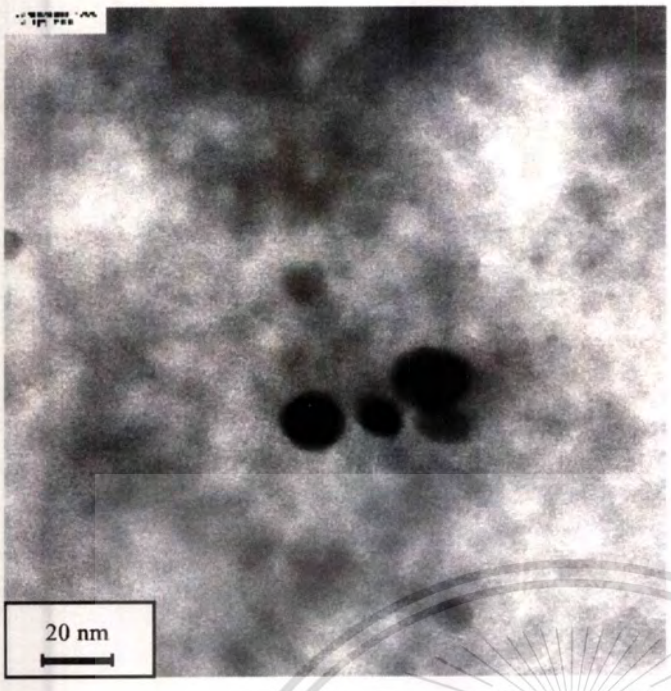

Reduction temperature: 650°C

n-Pentane conversion: 7.0%

BET surface area: 260 m^2/g

Figure 5.19 TEM images and surface area of Pt/SiO_2 calcined at 300°C, reduced at 300-650°C (continued).

For all cyclic C_5, cyclopentane shows higher content, as compared to that of cyclopentene and cyclopentadiene. This is because the catalyst also promotes the hydrogenation of cyclopentene and cyclopentadiene to cyclopentane at operating condition.

However, reduction at 650°C gives the very large Pt metal cluster that gives lower activity in *n*-pentane conversion, as compared to that of the reduction at low temperature (Figure 5.18). This may be due to the loss of surface area from the destruction of SiO_2 framework, as observed by BET surface area shown in Figure 5.19. Hence, the available Pt metal surface would also become lower, as the observed cyclization products are decreased.

5.3.2.4 Effect of H_2 partial pressure

An effect of H_2 partial pressure on *n*-pentane conversion over Pt/SiO_2 is shown in Figure 5.20. It is found that as the H_2 partial pressure is decreased, a lower *n*-pentane conversion is obtained. This reveals that the H_2 is required for the reaction, likely to increase the electron density of the Pt metal surface by dissociative chemisorption. As the electron density of the Pt metal surface is enhanced, the adsorption and activation of *n*-pentane is proportionally promoted. The H_2 also plays role for cleaning surface of Pt by reacting/competing with the adsorbed species to form certain less adsorptive products. This provides available vacant sites for further adsorption of the coming hydrocarbon feed to be activated on the Pt metal surface. When H_2 partial pressure is reduced, the products can retain on the Pt metal surface inhibiting next adsorption and also react to form secondary products.

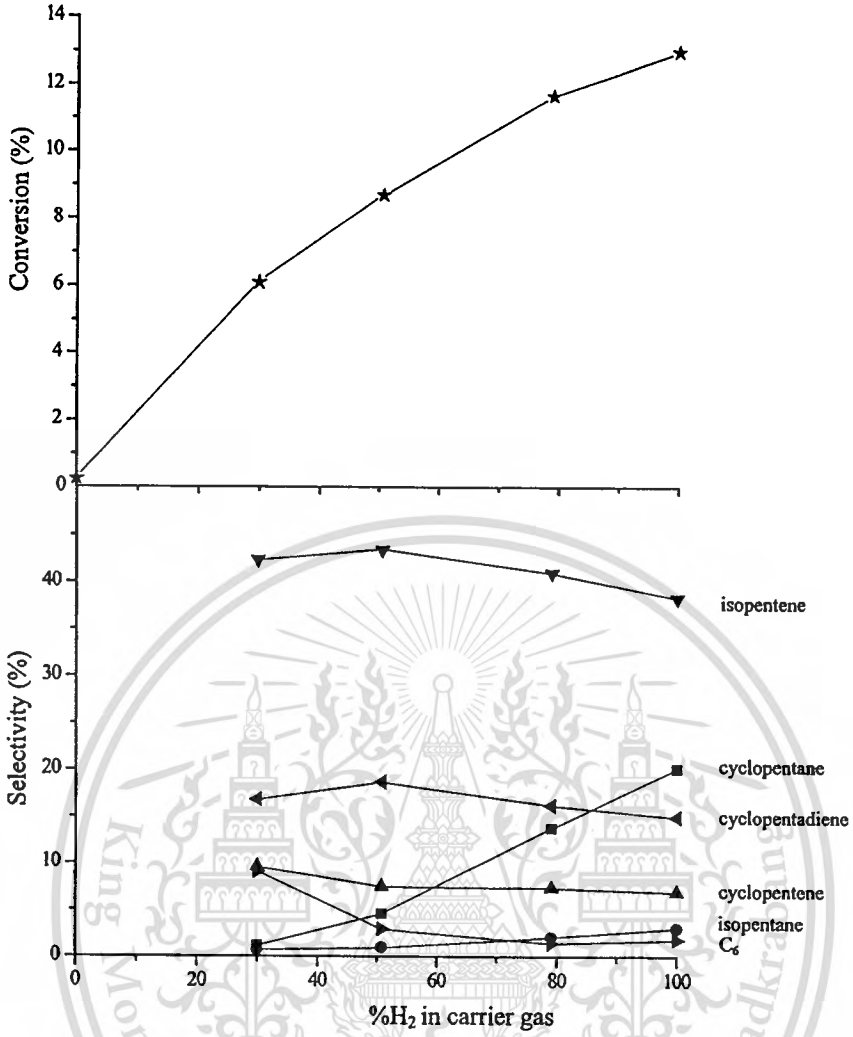

Figure 5.20 Effect of H_2 partial pressure for *n*-pentane conversion over Pt/SiO_2 (1wt.%) calcined at 300°C, W/F = 49.8 g h/mol, reduction/reaction temperature 500°C. (Other products: methane, ethane, propane, and *n*-butane ~ 10% and 1-pentene ~ 10%).

However, isopentene, cyclopentene, and cyclopentadiene selectivities are almost similar. This reveals that isomerization and cyclization are still promoted. It is observed that only cyclopentane is decreased while C_6 is increased, as a decreased in H_2 partial pressure. This is because the hydrogenation to cyclopentane is suppressed proportionally to the H_2 partial pressure. In similar manner, the oligomerization to C_6 is enhanced because more olefins are formed at low H_2 partial pressure.

The oligomerization of the olefins can also lead to coke deposited on the Pt metal surface which causes catalyst deactivation. TGA of the used Pt/SiO_2 from the reaction with the different H_2 partial pressure (Figure 5.21) shows that higher coke content is obtained when the H_2 partial pressure is decreased. It is found that the three weight loss peaks are observed at 60°C, 200°C, and 330°C are observed. The first peak is attributed from water desorption, while the second and the third peaks may attribute from the desorption of light and hard cokes, respectively. When the reaction is performed in carrier gas with 100%H_2, the only light coke (200°C) is observed with 1.37 wt.%. As the H_2 partial pressure is decreased, the higher coke content is observed particularly for the hard coke (330°C). This is in line with the results in Figure 5.20 that, as the H_2 partial pressure is decreased, the oligomerized hydrocarbons (i.e., C_6) and coke would be promoted.

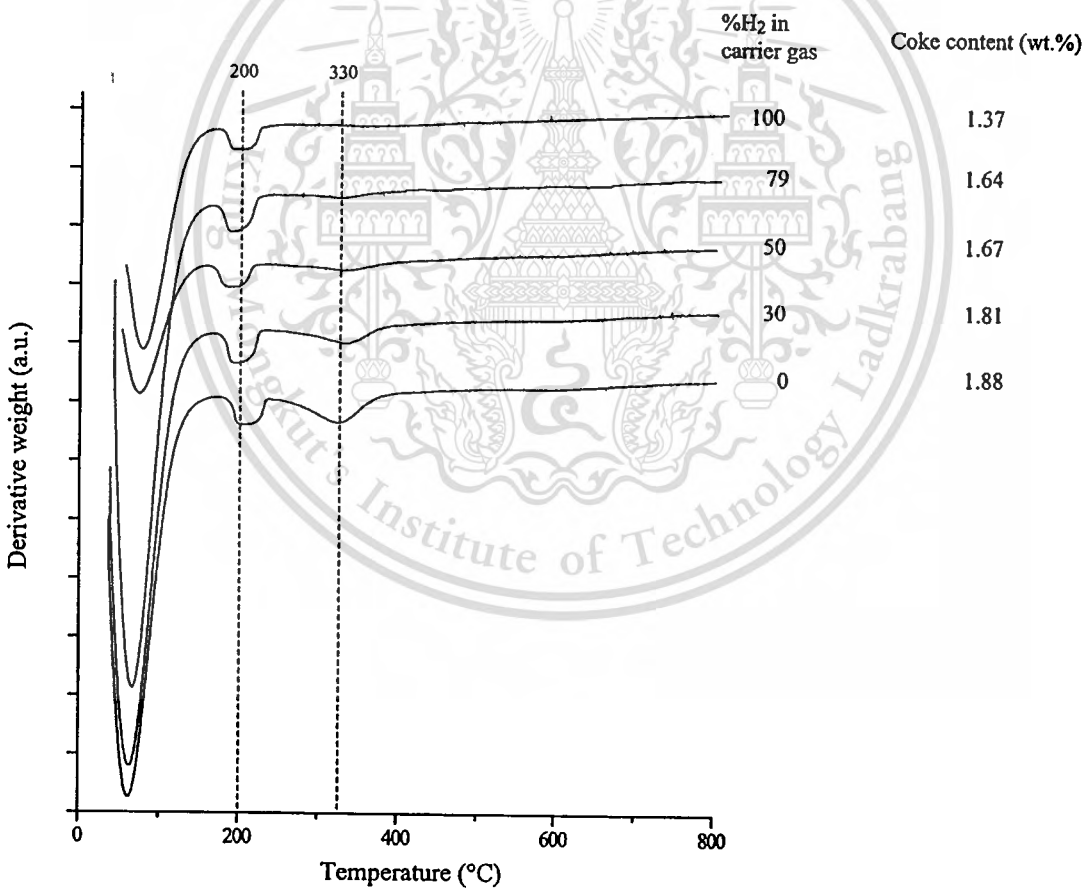

Figure 5.21 TGA (in air) of used Pt/SiO_2.

The results of the TPD-MS experiment of the used Pt/SiO_2 catalysts ($30\%H_2$) also support the existence of the light and hard coke, as shown in Figure 5.22. It can be seen that the mass number of 27 and 42 atomic unit are mainly observed from the desorption at 200°C. This may be the fragment of *n*-pentane or isopentane which are parts of light coke. When this catalyst is heated up to 330°C, the mass number at 53, 67, 76 and 88 atomic unit are additionally detected. This can be attributed to the high molecular weight compound that is decomposed from the hard coke in the catalyst.

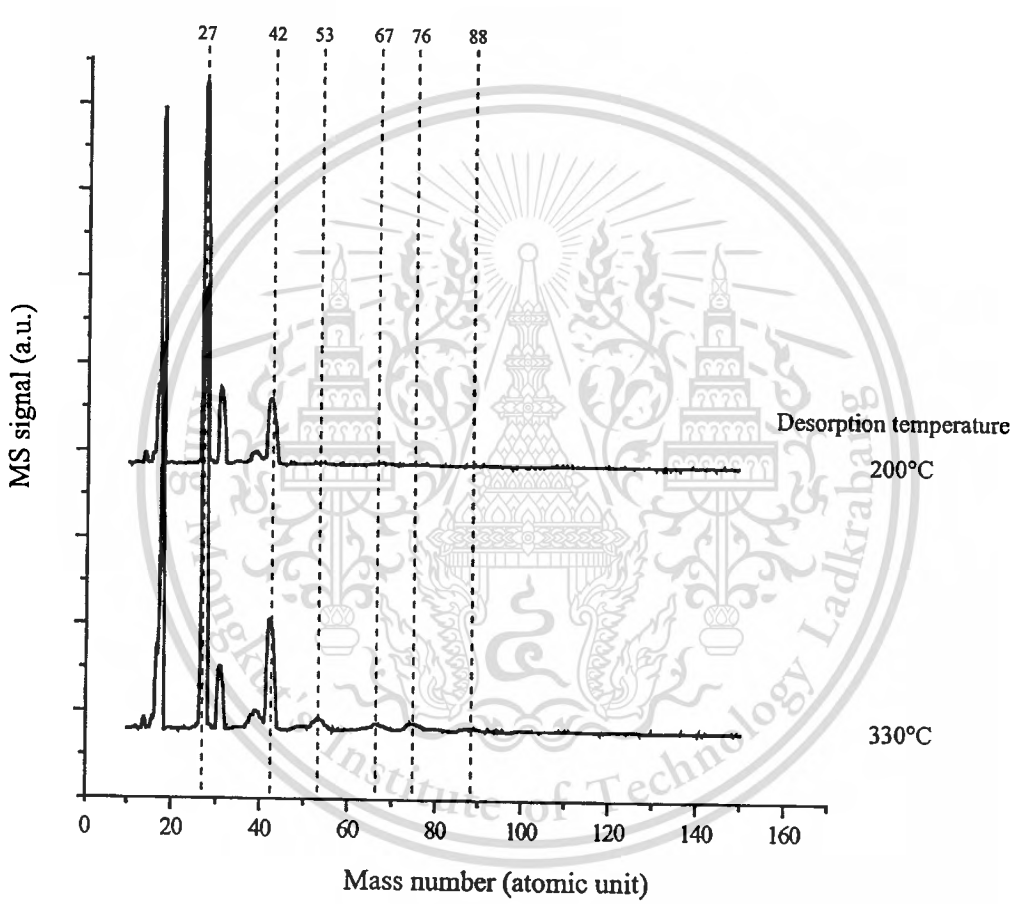

Figure 5.22 TPD-MS of coke formed over Pt/SiO_2 after *n*-pentane conversion at $30\%H_2$ in carrier gas.

5.3.2.5 Effect of feed structure

Since the adsorbed species appear to play significant role on product selectivity, conversion of isopentane, cyclopentane and *n*-pentane over Pt/SiO_2 is comparatively studied in this section. The reaction is carried out in H_2 as carrier gas for 4 hours, then H_2 is replaced by flow of He to investigate the effect of H_2 on different feed. The results are shown in Figure 5.23.

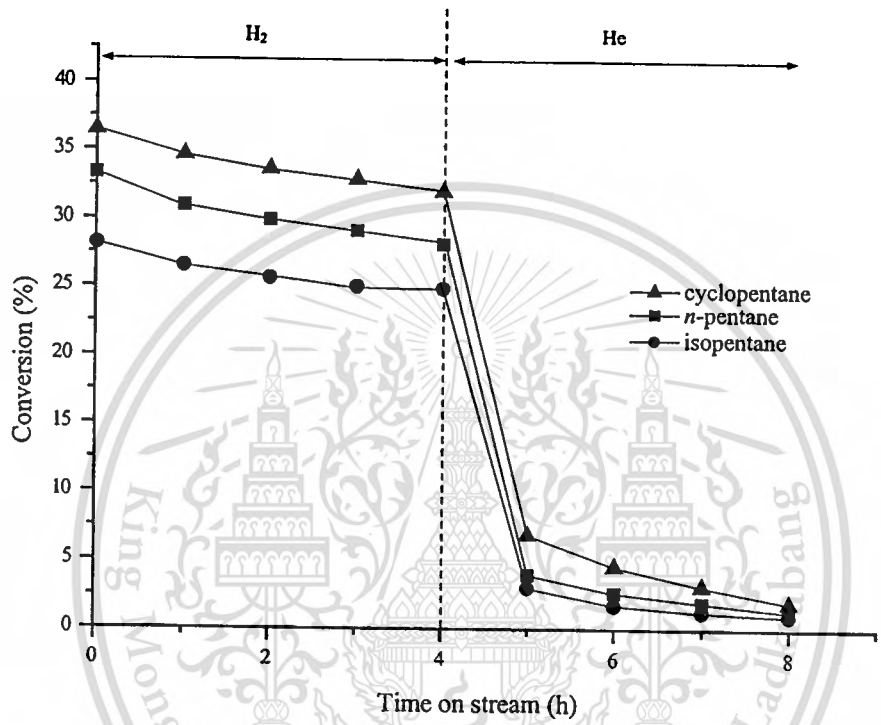

Figure 5.23 *n*-pentane, isopentane, and cyclopentane conversion over Pt/SiO_2 calcined at 300°C, reduction/reaction temperature 500°C, W/F = 521 g h/mol.

It is found in Figure 5.23 that cyclopentane shows higher conversion (37%), as compared to that of *n*-pentane (33%) and isopentane (28%). This is due to the preferential adsorption of cyclopentane over Pt metal surface. Cyclopentane that possesses the lowest vapor pressure (250 mmHg @ 20°C) would be easily adsorbed on the Pt surface, as compared to that of *n*-pentane (440 mmHg @ 20°C) and isopentane (570 mmHg @ 20°C). After switching the carrier gas to He, all pentanes conversion is decreased because H_2 is required to promote the dissociative adsorption of hydrocarbon on the Pt metal surface and cleaning the surface for the available active site, as previously discussed. Without H_2, it is difficult for pentanes to be

adsorbed and activated; therefore, the reaction is markedly suppressed. It is noted that the severe catalyst deactivation is observed due to the coke formation.

The product selectivities of isopentane, cyclopentane and *n*-pentane conversion are shown in Figure 5.24. Isopentane (Figure 5.24(a)) is readily dehydrogenated to isopentene (50%) suggesting that C-H bond breaking is mainly activated for isopentane. Isopentane shows lower adsorption on the Pt metal surface (Figure 5.23), as compared to that of *n*-pentane and cyclopentane. The steric hindrance by branching of isopentane may well retard the C-C bond activation over Pt surface. Hence, hydrogenolysis, isomerization and cyclization which are structure sensitive reaction become less facilitated. Only small amount of *n*-pentane and hydrogenolyzed product are obtained form isopentane conversion. The slightly observed cyclopentene (3%) and cyclopentadiene (0.5%) may be attributed form the cyclization of the *n*-pentane that can be competitively adsorbed on Pt metal surface. Without branching, the C-C bond of *n*-pentane (Figure 5.24(b)) can be easily to activate and isomerization/cyclization can be promoted as seen by iso and cyclic products yield.

In case of cyclopentane (Figure 5.24(c)), the ring opening (C-C hydrogenolysis) is the major reaction for converting cyclopentane to *n*-pentane (45%). As cyclopentane can highly adsorbed on the Pt metal surface, C-C activation would be proportionally enhanced. However, C-H activation can be also promoted as seen by dehydrogenated product, cyclopentene (32%). No cracked products are totally observed because the formed *n*-pentane may not able to competitively adsorb over the Pt surface. The observed 1-pentene (18%) may well be produced in parallel with *n*-pentane from cyclopentane disclosure.

After switching the carrier gas to He, the C_6 and C_5 olefins selectivities from all pentanes (Figure 5.24(a)-(c)) is increasingly observed with a decrease in all pentanes conversion (Figure 5.23). This is because the adsorbed products cannot desorb from the Pt metal surface leading to the formation of secondary products as C_6 and high molecular weight product that may be evolved to coke deposited, as previously observed. Moreover, as the Pt metal surface is fully adsorbed, less active sites are available for further adsorption and activation. Therefore, all structure sensitive reaction (hydrogenolysis, isomerization, and cyclization) is inhibited. However, the structure insensitive reaction, such as dehydrogenation can still be promoted, as seen by small amount of isopentene, 1-pentene, and cyclopentene.

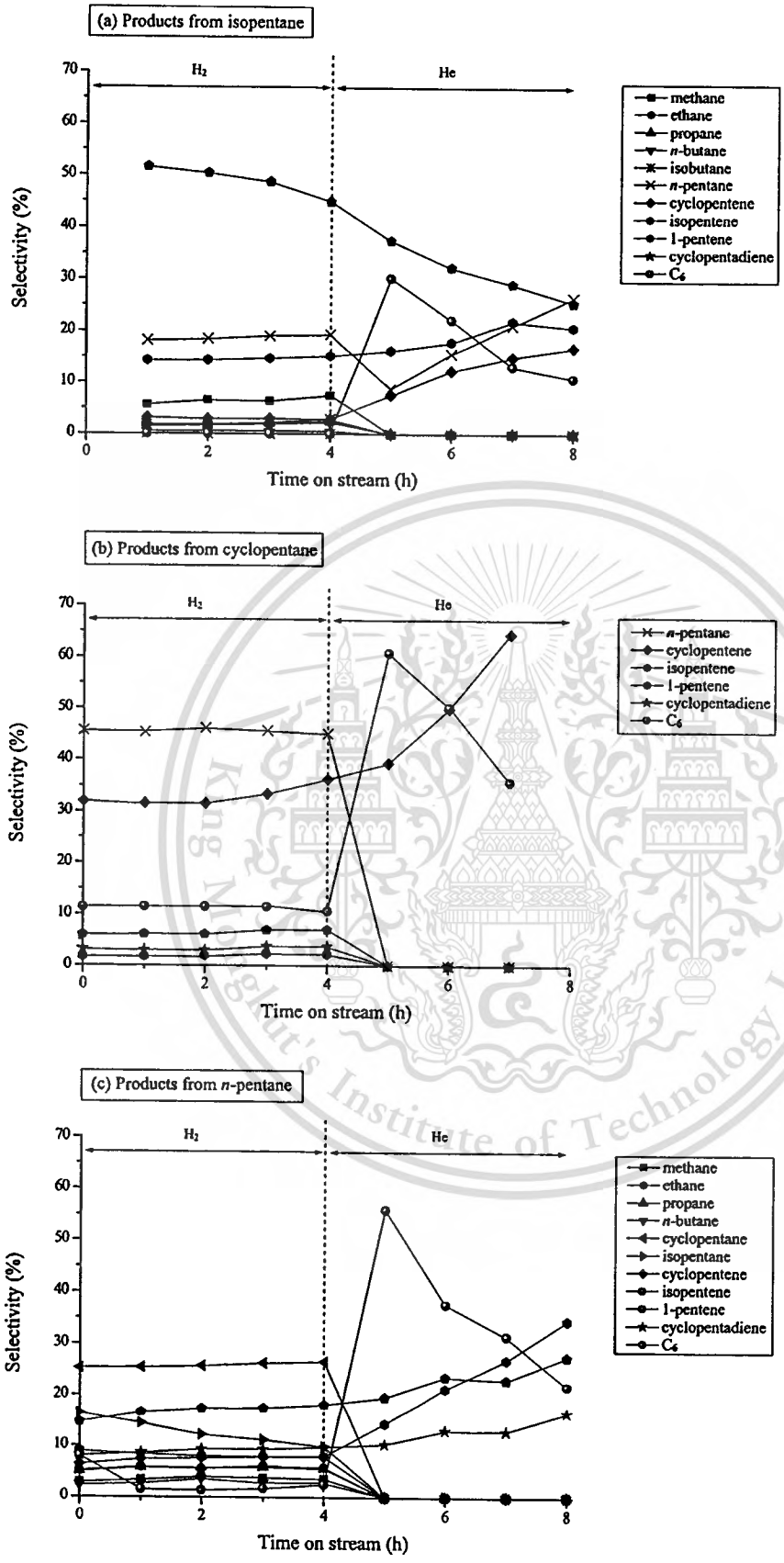

Figure 5.24 Products from isopentane, cyclopentane, and *n*-pentane conversion over Pt/SiO_2 calcined at 300°C, reduction/reaction temperature 500°C, W/F = 521 g h/mol.

5.4 Conclusion

The cyclic olefins, as cyclopentene and cyclopentadiene can be obtained from *n*-pentane conversion over Pt/SiO_2 catalyst at 500°C. H_2 Reduction at 500-650°C can produce larger Pt metal cluster that possesses higher electron density for *n*-pentane adsorption and cyclization. Therefore, the cyclic olefins are increasingly obtained with temperature up to 600°C. In addition, the H_2 is required in the reaction to promote the electron density of the Pt metal surface. Moreover, the H_2 would keep the Pt metal surface clean by facilitating desorption of products. Without H_2, the adsorbed product can further oligomerize to high molecular weight that can be evolved to coke causing the catalyst deactivation.

TPR and TEM suggest that some of PtO_x can be highly embedded into the SiO_2 framework after calcination at high temperature (500°C). To obtain high available Pt metal surface, Pt/SiO_2 calcined at low temperature (300°C) is employed. However, after calcination and reduction, some of Cl species can be retained in the catalyst, likely in the form of PtCl located at the inter phase between the Pt metal and SiO_2 support. As Cl is highly retained in the catalyst, an electron deficient Pt metal surface (acidity) is proportionally obtained. Such acid site promotes isomerization and hydrogenolysis of *n*-pentane to other undesirable products. The H_2 reduction at high temperature (500-650°C) can lower an amount of such chlorine specie leading to reduce isomerization and hydrogenolysis activity. Therefore, H_2 reduction at high temperature (before reaction) is required.

Cyclization, isomerization, hydrogenolysis and dehydrogenation of *n*-pentane take place in parallel. Various products are simultaneously produced. However, hydrogenolysis can be avoided by keeping the reaction temperature not higher than 500°C. Moreover, the secondarily hydrogenolysis can be promoted at high reaction temperature (600°C) producing a large number of ethane and methane.

The feed structure plays important role on the activity and product selectivity. Isopentane shows lower adsorption over Pt metal surface, as compared to that of *n*-pentane and cyclopentane. This leads to low conversion of isopentane. The hydrogenolysis, isomerization and cyclization are not facilitated because the C-C bond activation of isopentane is retarded by its branch structure. Instead, the dehydrogenation is the major reaction for converting isopentane to isopentene via C-H bond activation. Cyclopentane is feasibly adsorbed over Pt metal surface and readily activated. The C-C bond activation is preferred leading to the ring disclosure creating *n*-pentane as main

product. In the absence of H_2, all C-C bond activation cannot be taken place. However, only C-H bond can be activated converting *n*-pentane, isopentane, and cyclopentane to 1-pentene, isopentene, and cyclopentene, respectively.

5.5 References

[1] Graulich, W., Swodenk, W., and Theisen, D. 1972. **Hydrocarbon process.** 51: 71-75.

[2] Nippon Zeon Co., JP 29165,1974.

[3] Honicke, D., and Griesbaum, K. 1982. **Chem. Ing. Tech.** 54: 497.

[4] Griesbaum, K., Honicke, D., and Olson, M. 1998. "Cyclopentadiene and cyclopentene." in Ullmann's Encyclopedia of Industrial Chemistry. Weinheim: Wiley-VCH.

[5] Brown, H.C. and Mandal, A.K. 1980. **Synthesis.** 153-155.

[6] http://en.wikipedia.org/wiki/Cyclopentadiene

[7] http://en.wikipedia.org/wiki/Hexachlorocyclopentadiene

[8] Metcalf, R.L. 2002. "Insect Control." in Ullmann's Encyclopedia of Industrial Chemistry. Wienheim: Wiley-VCH.

[9] Meyer, W. 1976. **Hydrocarbon process.** 55(9): 235-238.

[10] Tamm, P.W., Mohr, D.H., and Wilson, C.R. 1987. in Catalysis. Amsterdam: Elsevier.

[11] Hagen, J. 2006. **Industrial Catalysis.** Weinheim: WILEY-VCH Verlag GmbH & Co. KGaA.

[12] Gates, B.C. 1992. **Catalytic chemistry.** New York: John Wiley & Son.

[13] Zhang, C., He, H., and Tanaka, K. 2006. "Catalytic performance and mechanism of a Pt/TiO_2 catalyst for the oxidation of formaldehyde at room temperature." **Applied Catalysis B: Environment.** 65: 37-43.

[14] Vazquez-Zavala, A., Ostoa-Montes, A., Acosta, D., and Gomez-Cortes, A. 1998. "Characterization of structure and catalytic activity of Pt–Sn catalysts supported in Al_2O_3, SiO_2 and TiO_2." **Applied Surface Science.** 136: 62-72.

[15] Ruppert, A.M. and Paryjczak, T. 2007. "$Pt/ZrO_2/TiO_2$ catalysts for selective hydrogenation of crotonaldehyde: Tuning the SMSI effect for optimum performance." **Applied Catalysis A: General.** 320: 80-90.

[16] Satterfield, C.N. 1993. **Heterogeneous catalysis in industrial practice.** Singapore: McGraw-Hill.

[17] Zexiang, L., Shengfu, J., Hui, L., and L. Chengyue. 2008. "Preparation and characterization of Pt-Sn/SBA-15 catalysts and their catalytic performances for long chain alkane dehydrogenation." **Chinese Journal of Chemical Engineering.** 16: 740-745.

[18] Panagiotopoulou, P., Christodoulakis, A., Kondarides, D.I. and Boghosian, S. 2006. "Particle size effects on the reducibility of titanium dioxide and its relation to the water-gas shift activity of Pt/TiO_2 catalysts." **Journal of Catalysis.** 240: 114-125.

[19] Liang, H., Zhang, Y. and Liu, Y. 2008. "Three-dimensionally ordered macro-porous Pt/TiO_2 catalyst used for water-gas shift reaction " **Journal of Natural Gas Chemistry.** 17: 403-408.

[20] Radivojevic, D., Seshan, K., and Lefferts, L. 2006. "Preparation of well-dispersed Pt/SiO_2 catalysts using low-temperature treatments." **Applied Cayalysis A: General.** 301: 51-58.

[21] Salama, T.M., Kohki Ebitani, H., Hattori, H., and Kita, H. 1994. "Electron paramagnetic resonance studies of reduced platinum supported on Ttanium oxide : effect of hydrogen adsorption-desorption on paramagnetic Platinum (I) and Titanium (III) species." **Chemistry of Materials.** 6: 21-26.

[22] Hulzinga, T. and Prins, R. 1983. "Electron spin resonance investigation of platinum supported on Al_2O_3 and TiO_2." **Journal of Physical Chemistry.** 87: 173-176.

[23] Heitmann, G.P., Dahlhoff, G., and Holderich, W.F. 1999. "Catalytically Active Sites for the Beckmann Rearrangement of Cyclohexanone Oxime to ε-Caprolactam." **Journal of Catalysis.** 15: 12-19.

CHAPTER 6

CONVERSION OF C_5 TO LIGHT HYDROCARBONS

6.1 Introduction

The Pt metal is highly active for converting various hydrocarbons by the reaction involving hydrogenation-dehydrogenation, cyclization, isomerization, and hydrogenolysis [1,2]. Among these metal catalyzed reactions, hydrogenolysis is structure sensitive and requires high activation energy, as compared to others. It is always carried out at temperature higher than 350°C [3]. For hydrogenolysis, the platinum surface is able to adsorb hydrogen [3], not only the gas phase H_2 but also the hydrogen atoms of the hydrocarbon molecules. Therefore, the C-H dissociative adsorption of hydrocarbons, which leads to the formation of the akylidyne intermediates, would be easily promoted. Such intermediate is further dissociated (C-C bond breaking) to smaller akylidyne before combining with the surface hydrogen and leaving the surface as smaller paraffinic hydrocarbons [4,5].

Platinum supported titania, in particular, has been reported to favor C-C bond hydrogenolysis [4,5]. As a result of calcination or reduction temperature, the strong metal-support interaction (SMSI) can be enhanced [6,7,8]. The SMSI readily modifies the chemical properties of the Pt metal cluster and particularly reduces an ability of the Pt metal to absorb hydrogen [9, 10]. Therefore, the hydrogenolysis activity and selectivity of the Pt/TiO_2 is largely dependent upon the heat treatment.

In this chapter, the hydrogenolysis activity of Pt/TiO_2 is tested using *n*-pentane, isopentane, and cyclopentane as modeled feeds. The effect of feed structure on the activity and selectivity are discussed to validate an ability of Pt/TiO_2 for C_5 conversion. The effect of heat treatments, i.e., calcination and reduction, is examined and discussed. The nature of Pt active species responsible to the observed activity is shown as well as the effect of contact time, reaction temperature, and H_2 partial pressure.

6.2 Experimental

The commercial P25 (Degussa) TiO_2 was used as a support. The Pt/TiO_2 catalyst was prepared by incipient wetness impregnation of TiO_2 with an aqueous solution of H_2Cl_6Pt, as previously shown in Chapter 3. The sample was subsequently dried at room temperature, and then calcined at 300°C, and 500°C for 5 h.

The metal loading was determined by XRF spectrometer (Siemens model SRS3400). The surface areas (BET) of catalysts were determined by N_2 adsorption (Autosorb-1). The catalyst structure and crystallinity are determined by an X-ray diffractometer (Siemens model D8). The morphology was observed by TEM (JEOL model JEM-2010). Temperature programmed reduction (TPR) and temperature programmed NH_3/pyridine desorption experiments were performed in a quartz micro-reactor. The H_2 consumption and NH_3/pyridine desorption were recorded by an on-line TCD detector (VICI model TCD2-NIFED). The electronic state of the Pt, Cl and Ti were determined by X-ray absorption near edge structure (XANES) and electron spin resonance (ESR) spectrometer. XANES measurement was carried out at the beamline BL8 of the Siam Photon Laboratory. Fluorescence mode XAS was performed to obtain Chlorine K-edge spectra and Platinum M-edge spectra which were calibrated with potassium chloride (edge energy at 2822 eV) and platinum foil (edge energy at 2122 eV), respectively. ESR is performed using an X-band JEOL, model JES-RE2X spectrometer (frequency of 8.8-9.6 GHz). The sample temperature is kept constant at about 77 K. The line position is calibrated with DPPH.

The *n*-pentane transformation was carried out at 300°C and ambient pressure. Before the reaction, the catalysts were activated in air (13 ml/min) at corresponding calcination temperature (300°C and 500°C). After that, the catalysts were reduced by H_2 (15 ml/min) at 300°C for 2 h. The temperature was set at 300-550°C, and a saturated vapor of *n*-pentane (at -5°C), isopentane (at -5°C) or cyclopentane (at 3.5°C) was carried by hydrogen/helium (a total flow of 15 ml/min) through a fixed bed reactor made with a quartz tube (O.D. = 8 mm). The products from the reaction were analyzed by an on-line gas chromatograph (BUCK Scientific, Model 910) with FID detector using HP-PLOT column (ϕ = 0.53 mm, L = 30 m).

For coke characterization, TPD-MS of the coked catalysts was performed in a quartz reactor and the coke content was analyzed by TGA (Perkin Elmer model TGA Pryis 1). The details of each experimental procedure are mentioned thoroughly in Chapter 3.

6.3 Results and discussion

6.3.1 Catalyst characterization

6.3.1.1 Elemental analysis

The platinum content in the impregnated Pt/TiO_2 are determined by an XRF spectrometer. It is found that the platinum loading is approximately 1 wt.%. Moreover, chlorine is found to retain in the catalyst, as observed in Table 6.1. The chlorine content is decreased with an increase in calcination temperature.

Table 6.1 The elemental analysis and surface area of Pt/TiO_2 used in this study.

Catalyst	Calcination temperature (°C)	Pt (wt.%)	Cl (wt.%)	BET surface area (m^2/g)
TiO_2	-	-	-	52
Pt/TiO_2	300	0.98	2.23	50
Pt/TiO_2	500	0.98	1.02	45

6.3.1.2 Surface area

Surface area of TiO_2 and Pt/TiO_2 catalysts are determined by nitrogen adsorption technique using Brunauer-Emmet-Teller (BET) as model equation. The calculated surface area for the Pt/TiO_2 calcined at 300°C and 500°C is also summarized in Table 6.1. All Pt/TiO_2 catalysts possess surface area similar to that of the support (about 50 m^2/g).

6.3.1.3 Structure

The XRD patterns of TiO_2 and Pt/TiO_2 calcined at 300°C and 500°C are shown in Figure 6.1. It is found that each sample exhibites strong sharp peaks of anatase at 25, 38, 48, 54, 55, 63, 69, 70, and 75° [11,12] and rutile at 27, 36 and 42° [13] suggesting the mixture of such two phases. However, as the catalyst is calcined at higher temperature, a decrease in its crystallinity is observed. This is presumably because the incorporation of Pt species creates defect of TiO_2 support during calcination. No peaks corresponding to the PtO_x and other Pt species are observed in the Pt/TiO_2 catalysts suggesting that the small platinum species would be highly dispersed on the TiO_2 support.

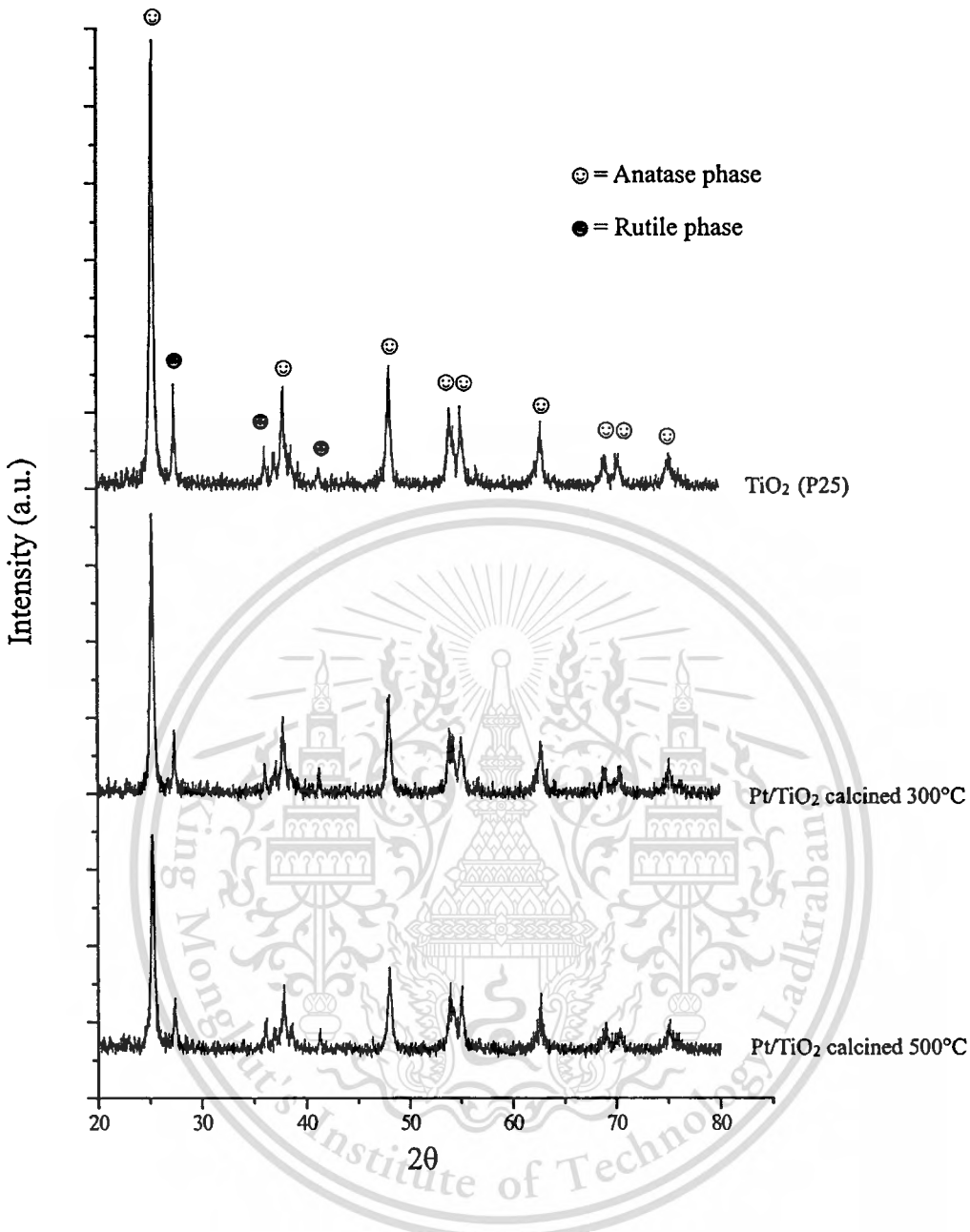

Figure 6.1 XRD patterns of TiO_2 and Pt/TiO_2 catalysts.

After reduction at 300°C and 500°C, no peaks of metallic Pt are observed (Figure 6.2) despite literatures suggest that Pt metal can be formed [6,9,13]. This suggests that small Pt metal clusters may well be obtained. In addition, slightly lower crystallinity of the support, as compared to the fresh support, is also observed after reduction at higher temperature. This reveals that H_2 reduction would also promote the defect on the support.

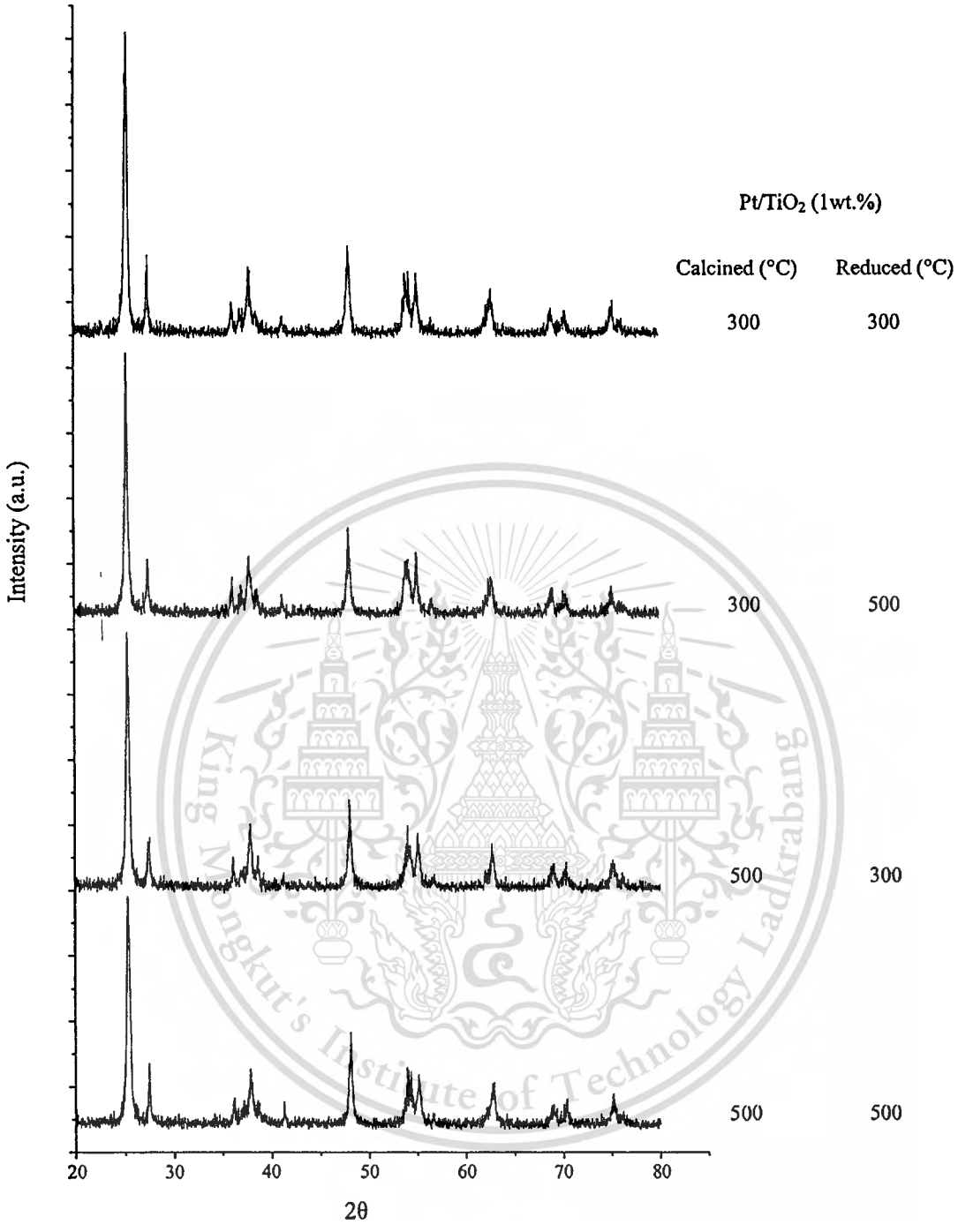

Figure 6.2 XRD patterns of Pt/TiO_2 calcined at 300°C and 500°C, reduced at 300°C and 500°C.

6.3.1.4 Morphology

The catalyst morphology is obtained from transmission electron microscope, as shown in Figure 6.3. It can be seen that a high dispersion of Pt species is obtained after the Pt/TiO_2 catalysts are calcined at 300°C and 500°C. In both cases, the small cluster size of Pt species (~1 nm) is observed in consistent with the suggestion from XRD results. This reveals that the interaction of the Pt species and TiO_2 support would be relatively strong.

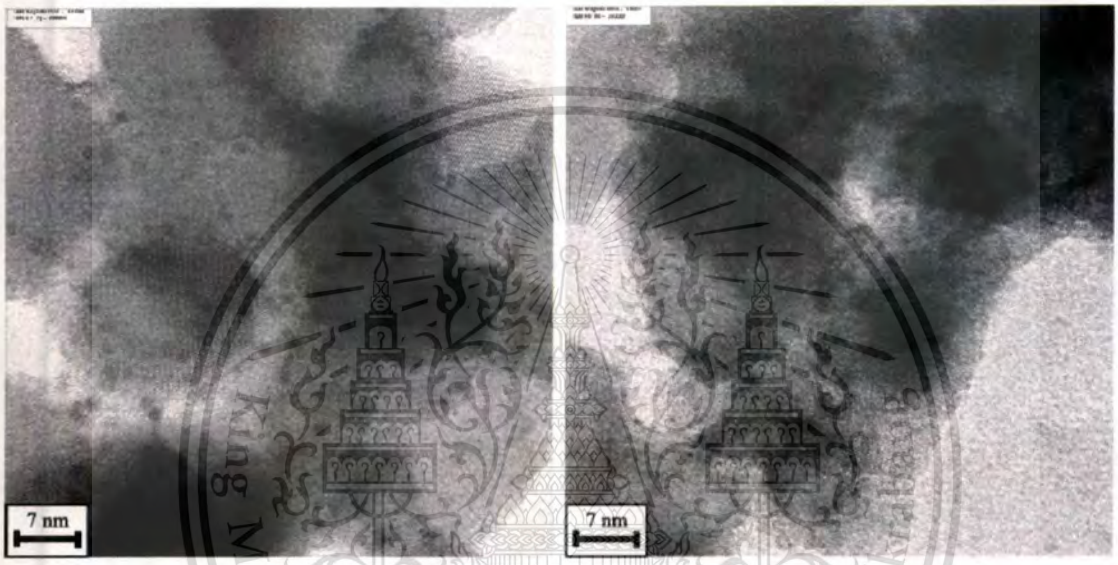

(a) Pt/TiO_2 calcined at 300°C (a) Pt/TiO_2 calcined at 500°C

Figure 6.3 TEM images of (a) Pt/TiO_2 calcined at 300°C and (b) Pt/TiO_2 calcined at 500°C (scale 7 nm).

After reduction at 300°C and 500°C, the relatively small platinum clusters are retained, as shown in Figure 6.4. Moreover, there is no significantly difference in the size of such platinum cluster obtained from both reduction temperatures suggesting that the dispersion of platinum can be maintained.

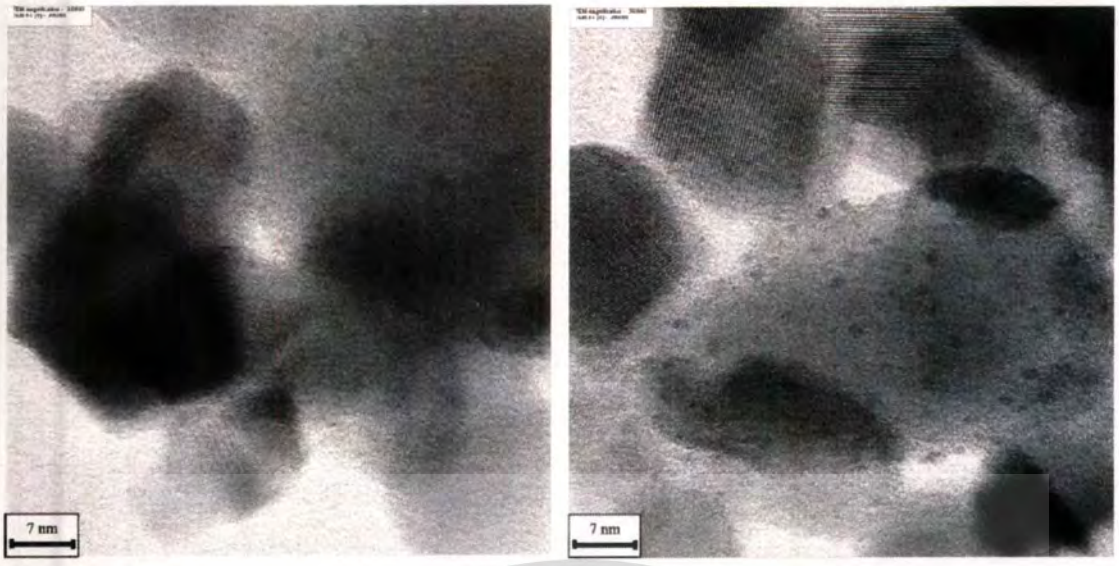

(a) Pt/TiO_2 calcined 300°C, reduced 300°C (b) Pt/TiO_2 calcined 300°C, reduced 500°C

Figure 6.4 TEM images of (a) Pt/TiO_2 calcined at 300°C, reduced at 300°C and (b) Pt/TiO_2 calcined at 300°C, reduced at 500°C (scale 7 nm).

6.3.1.5 Reducible metal species

TPR profiles of Pt/TiO_2 calcined at 300°C and 500°C are shown in Figure 6.5.

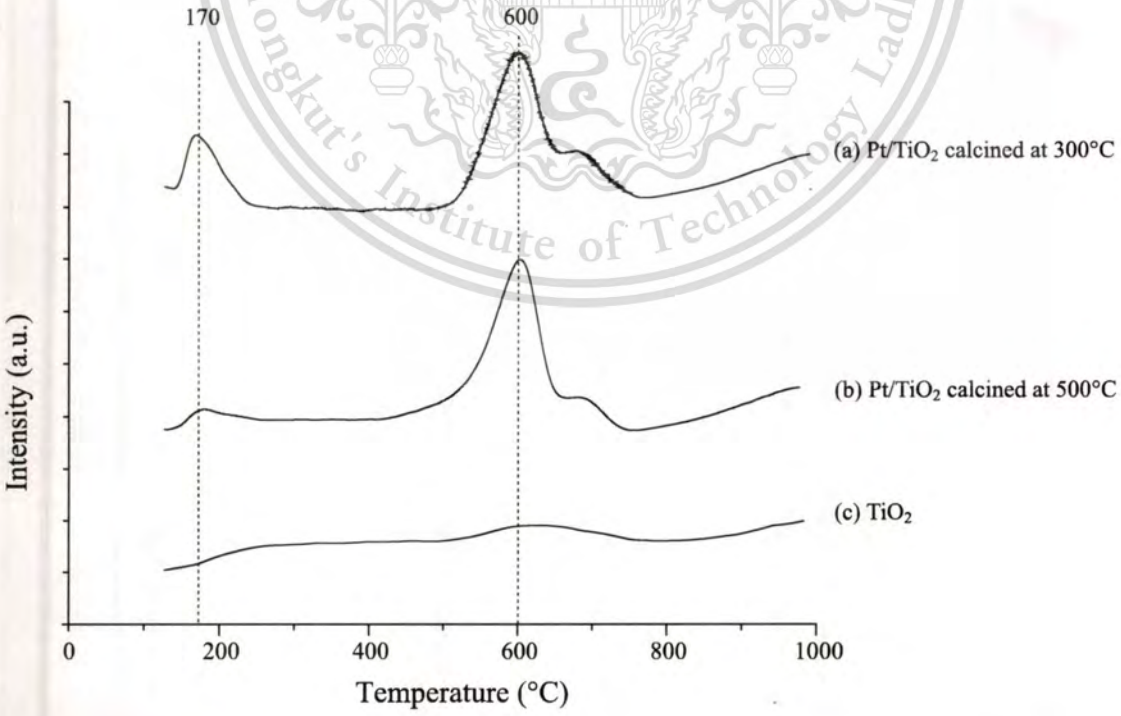

Figure 6.5 TPR of (a) Pt/TiO_2 calcined at 300°C, (b) Pt/TiO_2 calcined at 500°C, and (c) TiO_2.

In Figure 6.5, it is found that the reduction peaks are observed at 170°C and 600°C. The former peak is attributed to the reduction of the PtO_x to metallic Pt [13,14] while, the latter peak is attributed to the reduction of the support (TiO_2) [13,14], as shown by an ESR of the Ti^{3+} (g = 1.96 [12,15]) obtained when the support is reduced at 600°C (Figure 6.6).

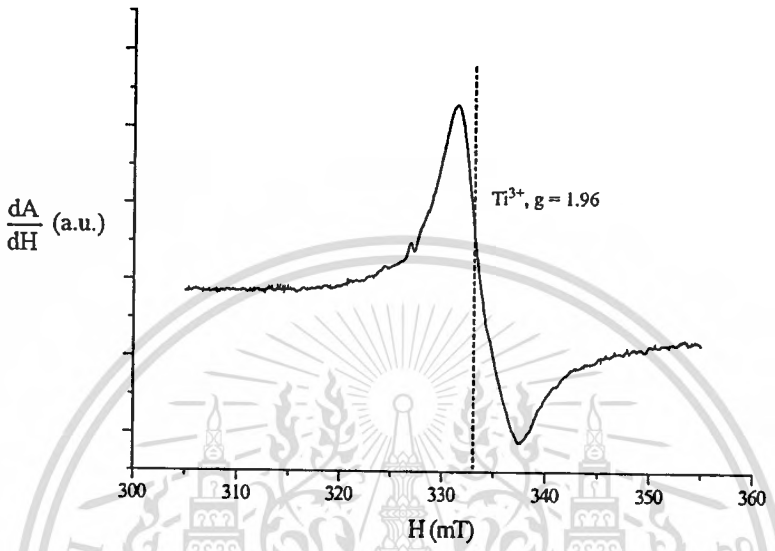

Figure 6.6 An ESR signal showing Ti^{3+} obtained from reduction of TiO_2 at 600°C.

It can be seen in Figure 6.5 that reduction of the PtO_x (170°C) obtained from calcination at 300°C shows higher intensity than that of the calcination at 500°C. This reveals that the amount of surface PtO_x in the catalyst calcined at 300°C is higher than that of calcined at 500°C. This corresponds to the literatures that the Pt precursor can be decomposed during calcination to Pt ion, likely Pt^{2+} specie [7] that can diffuse into the surface of TiO_2 support [16,17]. As the catalyst is calcined at higher temperature (500°C), Pt species would be proportionally more embedded [7]. Therefore, the surface PtO_x is decreased (as seen by lower H_2 consumption at 170°C) when the catalyst is calcined at 500°C. The embedded Pt species may be reduced at high temperature, as observed as shoulder peak at 700°C (Figure 6.5).

The presence of Pt species also facilitates the reduction of the support [18, 19], as observed higher reduction peak of support in the Pt/TiO_2 catalysts (Figure 6.5). This is because Pt promotes H_2 spill over on the support. Corresponding to the XRD in Figure 6.2, the defect of the support is enhanced after the Pt/TiO_2 is reduced at higher temperature.

To examine the oxidation state of the Pt species in the catalysts, the Pt/TiO_2 calcined at 300°C and 500°C are qualitatively examined by Pt M-edge XANE spectrometry. It is found from the results shown in Figure 6.7 that the edge energy of the Pt in the catalysts calcined at 300°C and 500°C are observed at 2128 eV. This number is exactly referred to the edge energy of the Pt^{4+}. Therefore, it is likely that the surface PtO_2 are located on the TiO_2 surface.

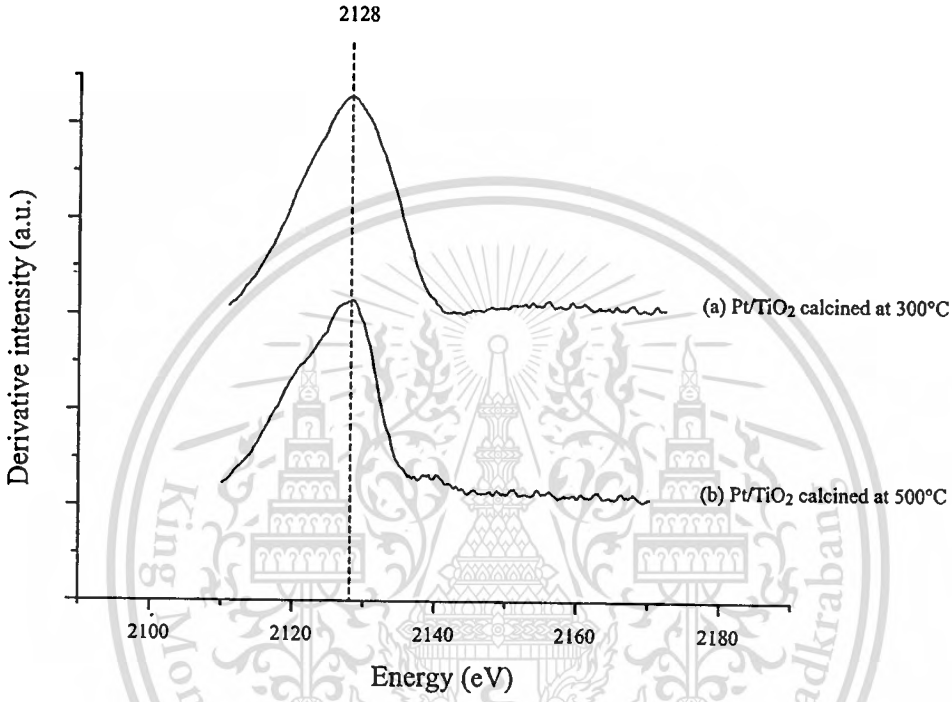

Figure 6.7 Pt M-edge XANE spectra of (a) Pt/TiO_2 calcined at 300°C, (b) Pt/TiO_2 calcined at 500°C.

6.3.1.6 The retained chlorine species

From the elemental analysis (Table 6.1), chlorine specie was retained in the Pt/TiO_2 after calcination. As the catalyst is calcined at higher temperature, the lower chlorine content is obtained. This corresponds to the TGA (in air) of the non-calcined Pt/TiO_2 shown in Figure 6.8 that the weight losses presumably from the decomposition of the chlorine species are observed at 300°C, 560°C, and 650°C.

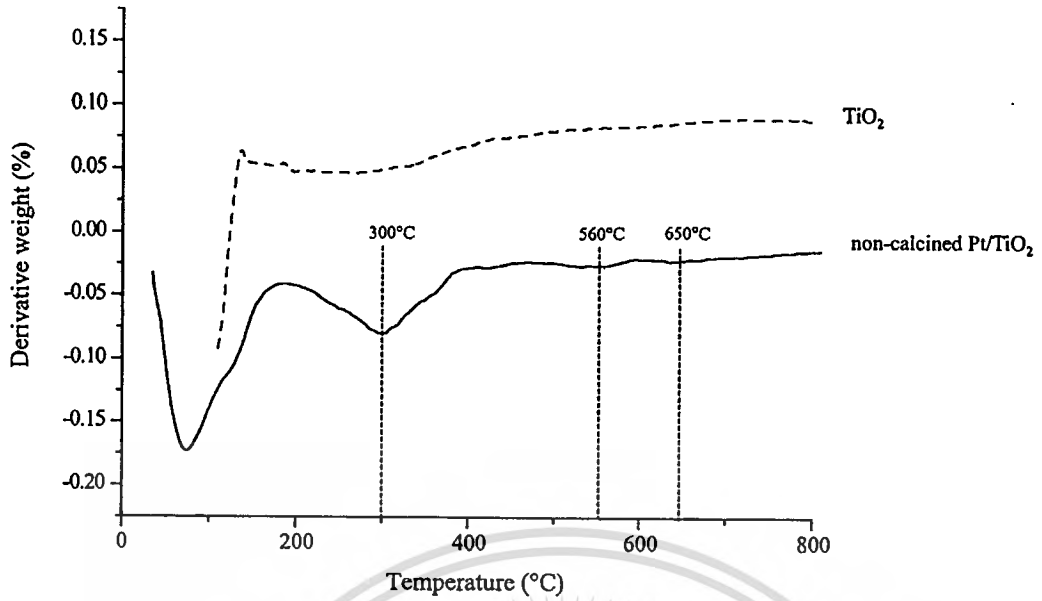

Figure 6.8 TGA (in air) of non-calcined Pt/TiO_2 (1 wt.%).

It has been reported that the Pt precursor ($H_2PtCl_6 \cdot 6H_2O$) can be decomposed during calcination to either PtO_x or $PtCl_4$ species [13,14,20]. The latter is feasible at 25-280°C [20] (Eq.(6.1)). The $PtCl_4$ is further decomposed at 280-350°C to $PtCl_2$ [20] (Eq.(6.2)) which can be degraded at 350-530°C to the Pt metal (Eq.(6.3)).

$$H_2PtCl_6 \cdot 6H_2O \xrightarrow{25-280^\circ C} PtCl_4 + 2HCl + 6H_2O \quad (6.1)$$

$$PtCl_4 \xrightarrow{280-350^\circ C} PtCl_2 + Cl_2 \quad (6.2)$$

$$PtCl_2 \xrightarrow{350-530^\circ C} Pt + Cl_2 \quad (6.3)$$

The Cl_2-TPD-MS experiment in the continuous flow of air of the Pt/TiO_2 catalysts are examined, as shown in Figure 6.9. In consistent with TGA, it is found that the Cl_2 desorption peaks of the non-calcined Pt/TiO_2 are observed at 300°C, 560°C, and 690°C. Accordingly to Eq.(6.1)-(6.3), the Cl_2 desorption peaks at 300°C and 560°C (Figure 6.9) are attributed from the decomposition of $PtCl_4$ (Eq.(6.2)) and $PtCl_2$ (Eq. (6.3)), respectively. The last desorption peak at 690°C is presumably attributed from the decomposition of chlorine species which strongly interacts with the support.

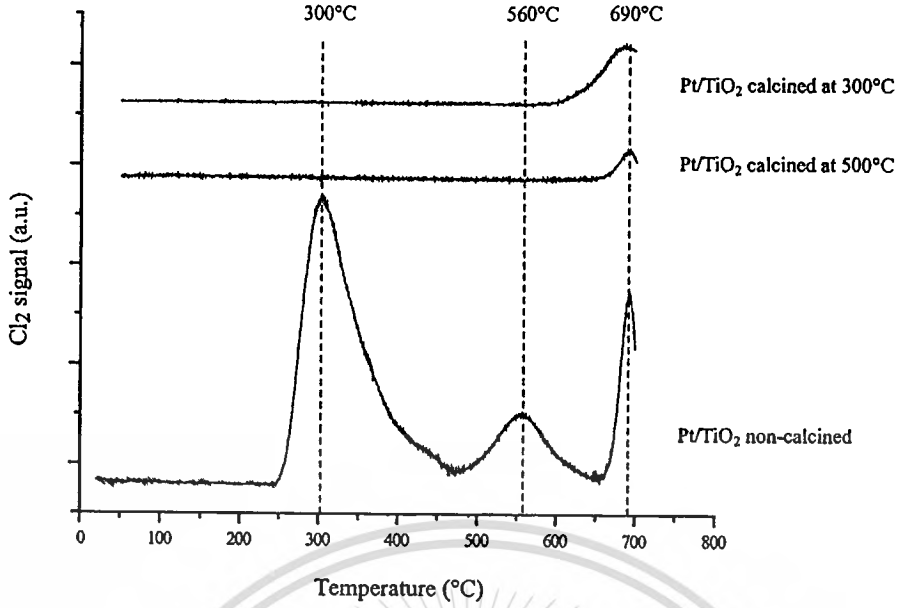

Figure 6.9 MS signal of Cl_2 desorption from the oxidation of Pt/TiO_2 catalysts.

After calcination at 300°C and 500°C, there is no Cl_2 desorption peaks at 300°C and 560°C (Figure 6.9) supporting that the H_2PtCl_6, $PtCl_4$, and $PtCl_2$ species can be decomposed during calcination. However, the chlorine species can be retained in the catalyst [21] shown as Cl_2 desorption peak at 690°C. As the catalyst is calcined at higher temperature (500°C) lower content of chlorine species is retained, as compared to that of the calcination at 300°C (Figure 6.9).

Effect of H_2 reduction (for creating the Pt metal as active site) on the retained chlorine content are examined by Cl K-edge XANE spectrometry, as shown in Figure 6.10. It is found that reduction at higher temperature can also reduce chlorine content in the catalyst presumably by converting the retained chlorine species (i.e., platinum-chlorine complex) to the Pt metal and HCl [20]. Moreover, the retained chlorine species shows the pre-edge resonance (Figure 6.10) suggesting that such chlorine specie retained after reduction is located far apart from each other. Consequently, the chlorine species would be highly dispersed in the catalyst.

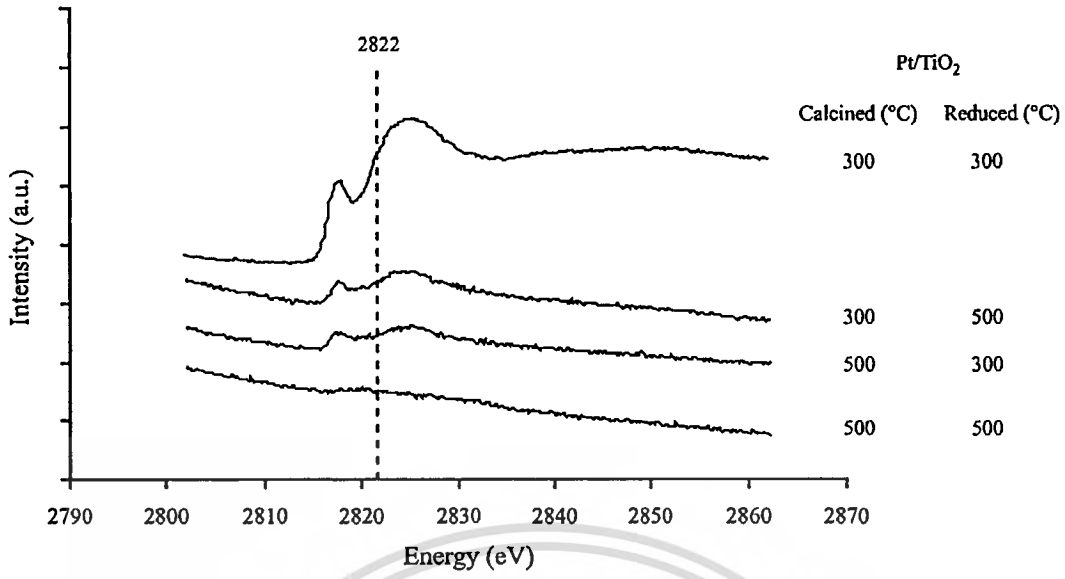

Figure 6.10 Cl K-edge XANE spectra of Pt/TiO_2 calcined at 300°C and 500°C, reduced at 300°C and 500°C.

6.3.1.7 Acidity of the catalyst

The Pt/TiO_2 catalysts calcined at 300-500°C and reduced at 300-500°C are subjected for pyridine TPD and the results are shown in Figure 6.11. It is found that the pyridine desorption peaks are observed at 200°C and around 550°C. The former and the latter peaks would be attributed from the desorption of pyridine on TiO_2 support and on the acid site created by the retained chlorine species, likely in the form of $PtCl_x$ and/or $TiCl_x$. The Pt/TiO_2 calcined at 300°C and reduced at 300°C whose possesses the highest chlorine content shows higher acidity, as compared to that of the others. Therefore, as the high content of the chlorine species are retained in the catalyst, high acidity would be proportionally obtained. However, with the highly dispersed chlorine species (Figure 6.10) and highly dispersed Pt metal (Figure 6.4), there would be the case for the adjacent sites between the chlorine species and Pt metal. Consequently, the Pt metals presumably behave an electron deficient.

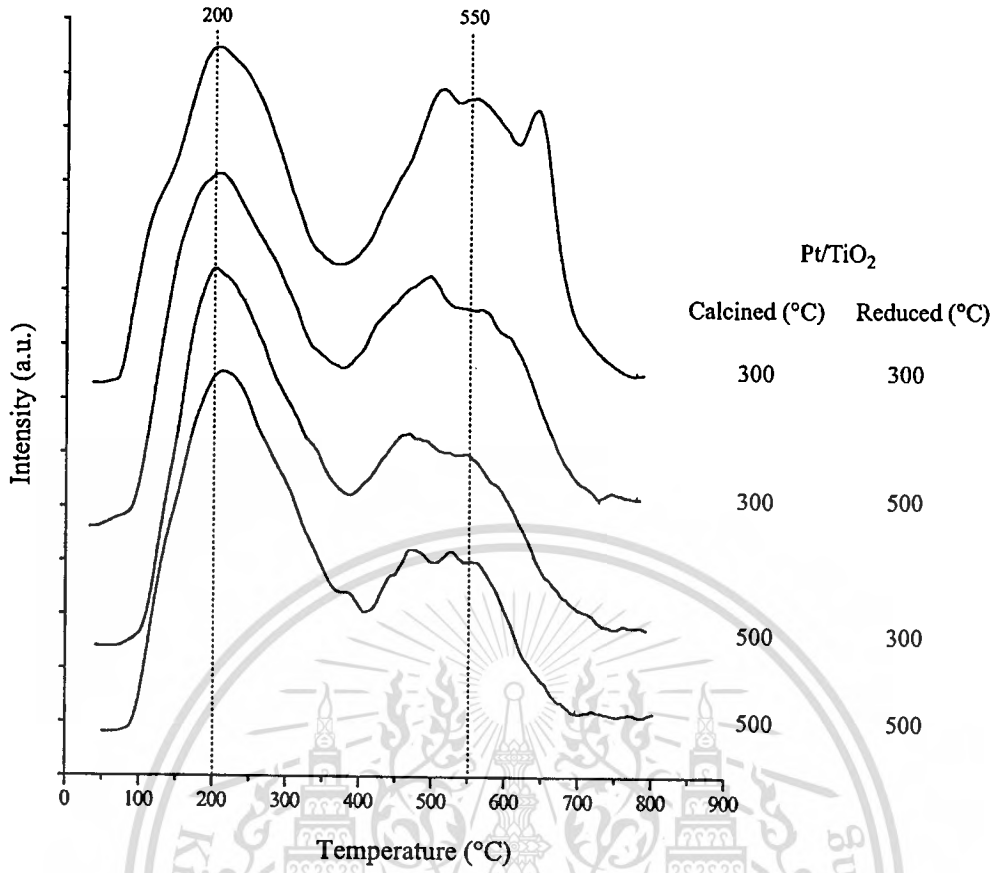

Figure 6.11 Pyridine-TPD of the Pt/TiO_2 calcined at 300°C and 500°C, reduced at 300°C and 500°C.

The retained chlorine content is not significantly affected by the timing of reduction period. In Figure 6.12, it can be seen that the acidity generated by the chlorine species is almost similar whether the calcined Pt/TiO_2 is subjected to reduce by H_2 for 1.5 or 6 hours. This reveals that after reduction the chlorine species are relatively stable in the catalyst.

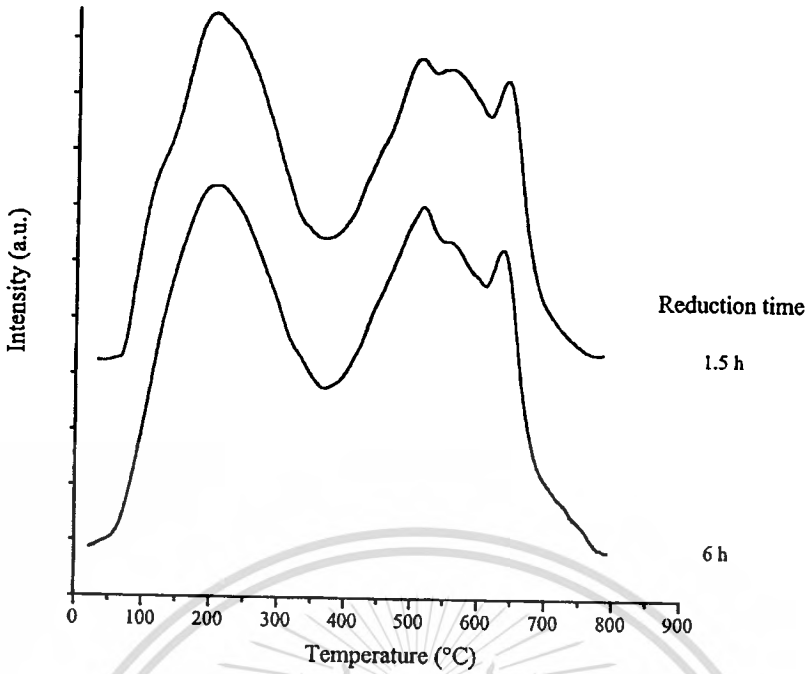

Figure 6.12 Pyridine-TPD of the Pt/TiO_2 calcined at 300°C, reduced at 300°C for 1.5 h and 6 h.

6.3.2 Activity testing

The catalytic activity of the Pt/TiO_2 calcined at 300°C and 500°C for *n*-pentane hydrogenolysis at 300°C is shown in Table 6.2. It is found that the higher activity (23.93%) for *n*-pentane hydrogenolysis is obtained when the Pt/TiO_2 is calcined at 300°C, as compared to that obtained from the Pt/TiO_2 calcined at 500°C (1.57%). As mentioned previously, some of Pt species can be embedded into the support after calcination. With the higher calcination temperature, the higher content of embedded Pt species is obtained. From TPR (Figure 6.5), the available surface Pt metal (active site) of the Pt/TiO_2 calcined at 300°C is relatively high, as compared to that of the Pt/TiO_2 calcined at 500°C. Consequently, the Pt/TiO_2 calcined at 300°C shows higher hydrogenolysis activity, as compared to that of the Pt/TiO_2 calcined at 500°C. However, the same selectivity is observed (Table 6.2) suggesting that the surface Pt metal is still the active site for converting *n*-pentane in both cases. It is noted that no activity at 300°C is observed over bare TiO_2.

Table 6.2 Catalytic activity of Pt/TiO_2 calcined at 300°C and 500°C for *n*-pentane hydrogenolysis at 300°C.

Calcination temperature (°C)	300	500
Reduction temperature (°C)	300	300
Reaction temperature (°C)	300	300
Contact time (g h/mol)	271	271
Conversion (%)	23.9	1.57
Selectivity (%)		
methane	25.7	25.5
ethane	22.4	23.6
propane	22.4	23.5
n-butane	28.0	26.1
cyclopentane	0.31	0.30
isopentane	1.17	1.00

It can be seen in the Table 6.2 that the saturated hydrocarbons from C_1 to C_5 are observed as products. Methane, ethane, propane and *n*-butane (light hydrocarbons) would be formed by hydrogenolysis. Cyclopentane and isopentane would be formed by cyclization and isomerization, respectively. The Pt/TiO_2 shows higher activity for hydrogenolysis, as compared to cyclization and isomerization.

Effect of reduction temperature is shown in Table 6.3. It is found that Pt/TiO_2 reduced at 500°C shows lower activity (2.53%), as compared to that of the reduction at 300°C (23.9%). The lower in activity after reduction at higher temperature (500°C) is not attributed from the agglomeration of Pt metal (Figure 6.4), i.e., the similar Pt dispersion is obtained whether the Pt/TiO_2 is reduced at 300°C or 500°C. On the other hand, such lower activity may be attributed from the lower of Pt metal surface due to strong metal support interaction (SMSI) that is normally taken place after the Pt/TiO_2 is subjected to reduce at high temperature (~500°C) [22,23]. The SMSI facilitate the reduction of the support to Ti^{3+} [8,10,18] generating film of TiO_x covering the Pt metal surface [18,19]. As the Pt/TiO_2 is reduced at higher temperature, the higher content of

TiO_x film is proportionally generated. Therefore, the available Pt metal sites obtained after reduction at 500°C shows lower content, as compared to that of the reduction at 300°C. Consequently, its catalytic activity is proportionally reduced, as observed in Table 6.3.

Table 6.3 Effect of reduction temperature of Pt/TiO_2 calcined at 300°C for *n*-pentane hydrogenolysis at 300°C.

Reduction temperature (°C)	300	500
Calcination temperature (°C)	300	300
Reaction temperature (°C)	300	300
Contact time (g h/mol)	271	271
Conversion (%)	23.9	2.53
Selectivity (%)		
methane	25.7	6.23
ethane	22.4	6.33
propane	22.4	6.11
n-butane	28.0	6.09
cyclopentane	0.31	24.5
isopentane	1.17	50.8

The Pt/TiO_2 reduced at 300°C shows a high selectivity to hydrogenolysis products, while the reaction over Pt/TiO_2 reduced at 500°C gives isomerized and cyclized products. This reveals that the different active site is presented after the catalysts are reduced at different temperature. Reduction at 300°C would create the only Pt metal surface, while reduction at 500°C also creates the TiO_x film covering Pt metal surface, as schematically shown in Figure 6.13. For the latter case, *n*-pentane can be readily hydrogenolyzed to light hydrocarbons over the available Pt metal surface. On the other hand, over the TiO_x film which is a Lewis acid, *n*-pentane can be isomerized/cyclized to isopentane/cyclopentane. Therefore, it is found that its isopentane/ cyclopentane selectivities is higher than that of the reaction over Pt metal. However, isomerization/cyclization is slower than hydrogenolysis. The catalyst with high content of TiO_x

film would show low *n*-pentane conversion. Consequently, the Pt/TiO_2 reduced at 500°C gives lower conversion, as compared to that of the Pt/TiO_2 reduced at 300°C.

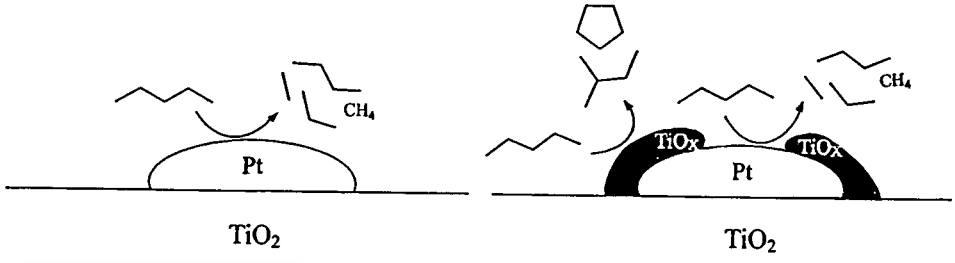

(a) Pt/TiO_2 calcined at 300°C, reduced at 300°C

(b) Pt/TiO_2 calcined at 300°C, reduced at 500°C

Figure 6.13 Proposed active sites obtained after Pt/TiO_2 calcined at 300°C is reduced at (a) 300°C and (b) 500°C.

From the catalytic activity presented in Table 6.2 and 6.3, the Pt/TiO_2 calcined at 300°C and reduced at 300°C is selected for testing hydrogenolysis of *n*-pentane. The effect of reaction temperature, contact time, H_2 partial pressure, and feed structure are examined over this catalyst. The results are given and discussed as followed.

6.3.2.1 Effect of reaction temperature

An effect of reaction temperature on *n*-pentane conversion over Pt/TiO_2 is shown in Figure 6.14. It is found that, as the temperature is increased (300-400°C), the higher conversion of *n*-pentane is observed. This reveals that higher reaction temperature promotes hydrogenolysis activity. However, a decrease of *n*-butane at higher reaction temperature may be due to secondarily hydrogenolysis of the produced *n*-butane to methane-propane and/or two ethanes, as seen by an increase in these product selectivities.

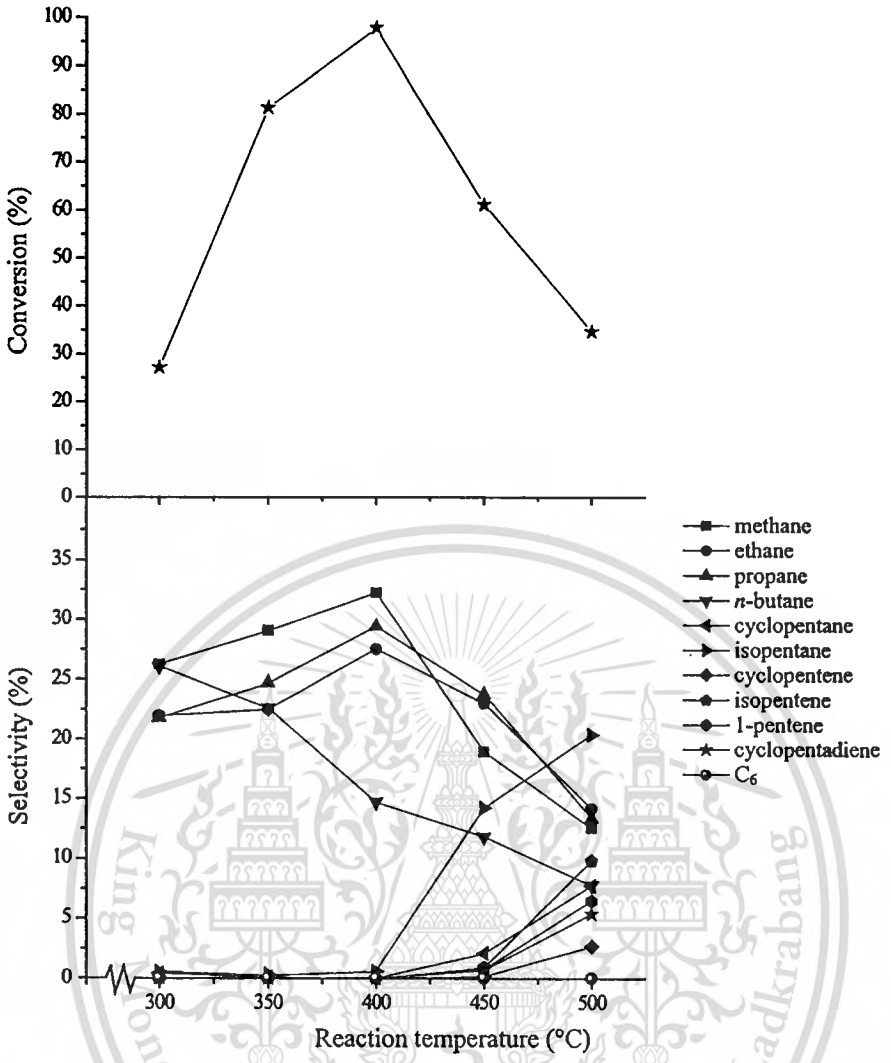

Figure 6.14 Effect of reaction temperature for *n*-pentane conversion over Pt/TiO_2 (1 wt.%) calcined at 300°C, W/F = 271 g h/mol.

However, as the reaction temperature is higher than 400°C (Figure 6.14), a decrease in catalytic activity is observed. This is because the SMSI creates the TiO_x covering the Pt metal surface, as mentioned previously. In consistent with the previous results (Table 6.3), the isomerization/cyclization selectivities are increased, while hydrogenolysis activity is decreased. This is because, as the reaction is performed in H_2 at higher temperature, more TiO_x film covering the Pt metal surface would be generated promoting more isomerized/cyclized products. Furthermore, the dehydrogenation to C_5 alkene over Pt metal can be promoted at higher temperature despite such active site is almost covered by TiO_x.

It is noted that there is no significantly change in surface area of catalyst despite the reaction is preformed at 500°C (~ 45 m^2/g) suggesting that a decrease in activity is not mainly formed by the destruction of support.

6.3.2.2 Effect of contact time

An effect of contact time for *n*-pentane hydrogenolysis over Pt/TiO_2 at 300°C is shown in Figure 6.15. Over the Pt metal surface, methane, ethane, propane, and *n*-butane are observed as main products despite the reaction is performed at low contact time. This reveals that hydrogenolysis of *n*-pentane to these products takes place in parallel. As the contact time is increased, all hydrogenolyzed products is increase with an increase in *n*-pentane conversion suggesting that no further reaction of these products is taken place over the catalyst. However, little of cyclopentane and isopentane are observed due to the slightly TiO_x generating at the metal-support interface.

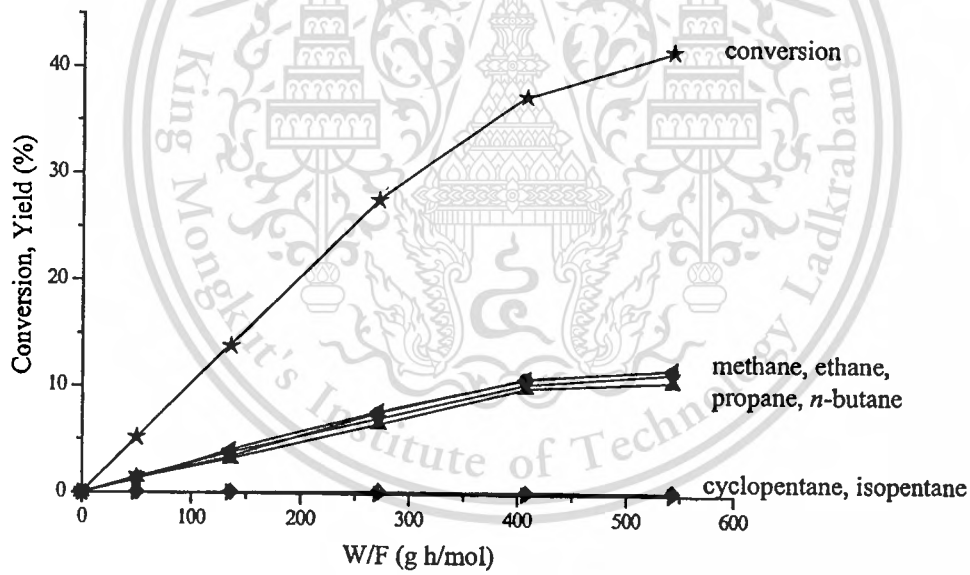

Figure 6.15 Effect of contact time for *n*-pentane hydrogenolysis over Pt/TiO_2 (1 wt.%) calcined at 300°C, reduction/reaction temperature at 300°C.

In Figure 6.15, it is found that the yield of methane and *n*-butane are almost similar. This is also the case for ethane and propane yield. Therefore, it is likely that these products are produced from direct mono-molecular cracking of *n*-pentane. As seen in Figure 6.16, the product selectivities of methane, ethane, propane and *n*-butane are almost 25 mol% suggesting

that such hydrogenolysis of *n*-pentane over this catalyst is not selective. Therefore, the probability for *n*-pentane hydrogenolysis to methane and *n*-butane is equal to that of producing ethane and propane.

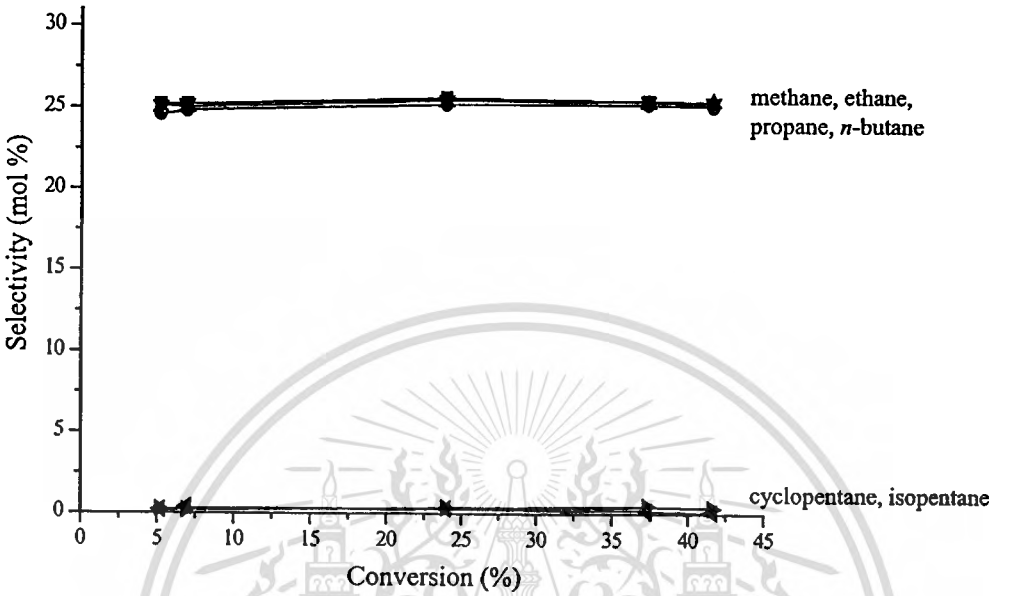

Figure 6.16 Product selectivity from *n*-pentane hydrogenolysis over Pt/TiO_2 (1wt.%) calcined at 300°C, reduction/reaction temperature at 300°C.

The activation of *n*-pentane over Pt/TiO_2 catalyst is shown in Figure 6.17. With the small metal cluster (Figure 6.4) and high electron deficiency (Figure 6.11), the *n*-pentane would be dissociatively adsorbed (C-H bond breaking) over the Pt metal in three possible configurations (I, II, and III). Over limited surface or small Pt cluster, such intermediate would be readily hydrogenolyzed to smaller akylidyne. The intermediate I can be hydrogenolyzed to ethane and propane. The intermediate II gives either a similar product as intermediate I, or methane and *n*-butane. While, the intermediate III can be only hydrogenolyzed to methane and *n*-butane. From Figure 6.17, the probability for producing methane and *n*-butane is equal to that for ethane and propane, as previously observed in Figure 6.16.

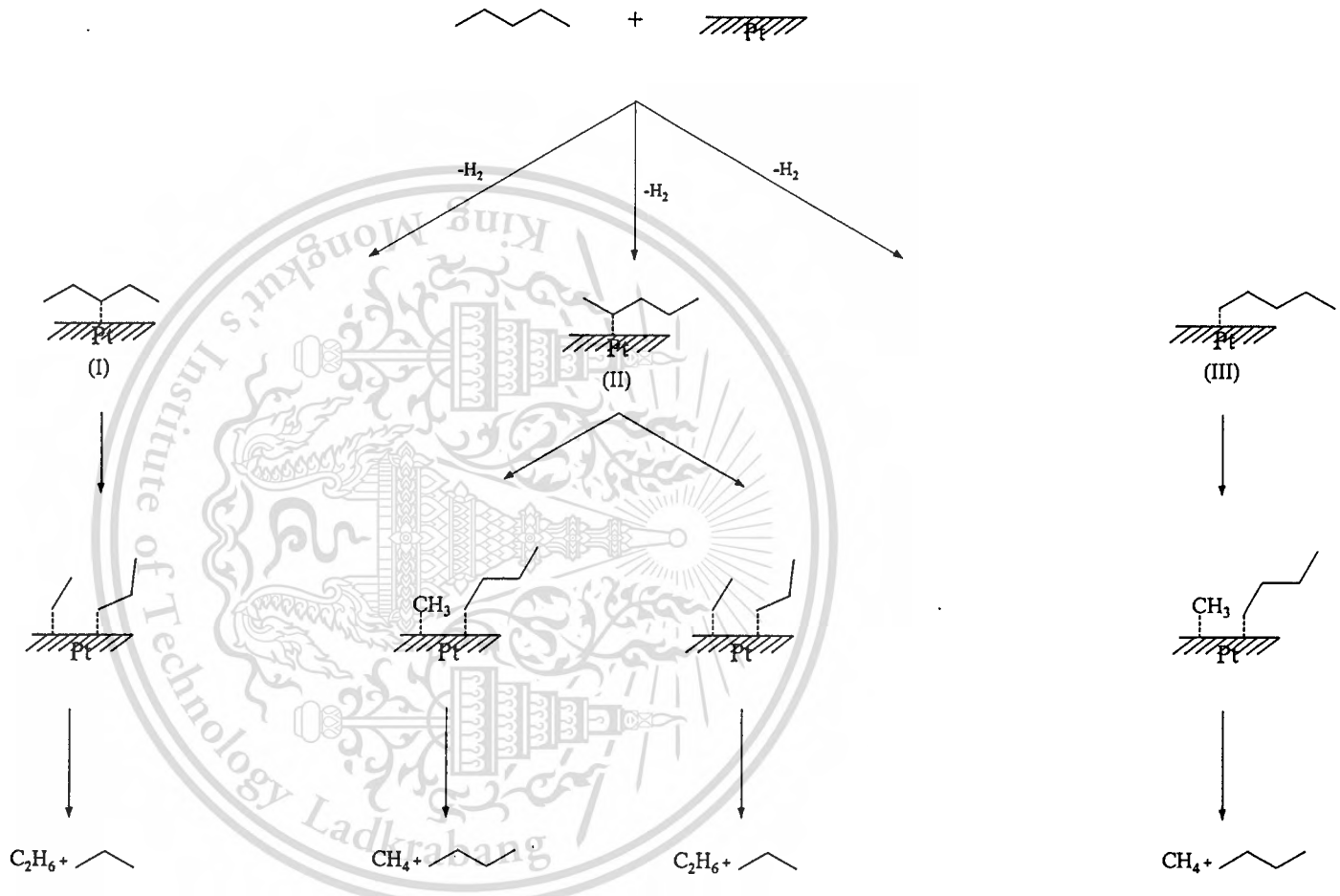

Figure 6.17 Proposed reaction pathway for *n*-pentane conversion over Pt/TiO_2 catalyst.

6.3.2.3 Effect of H_2 partial pressure

An effect of H_2 partial pressure on *n*-pentane hydrogenolysis over Pt/TiO_2 is shown in Figure 6.18. It is found that as the H_2 partial is decreased, lower *n*-pentane conversion is obtained. This reveals that the H_2 is required for the reaction, likely to increase the electron density of the Pt metal by its dissociative chemisorption. As the electron density of the Pt metal surface is increased, the adsorption and activation of *n*-pentane would be enhanced.

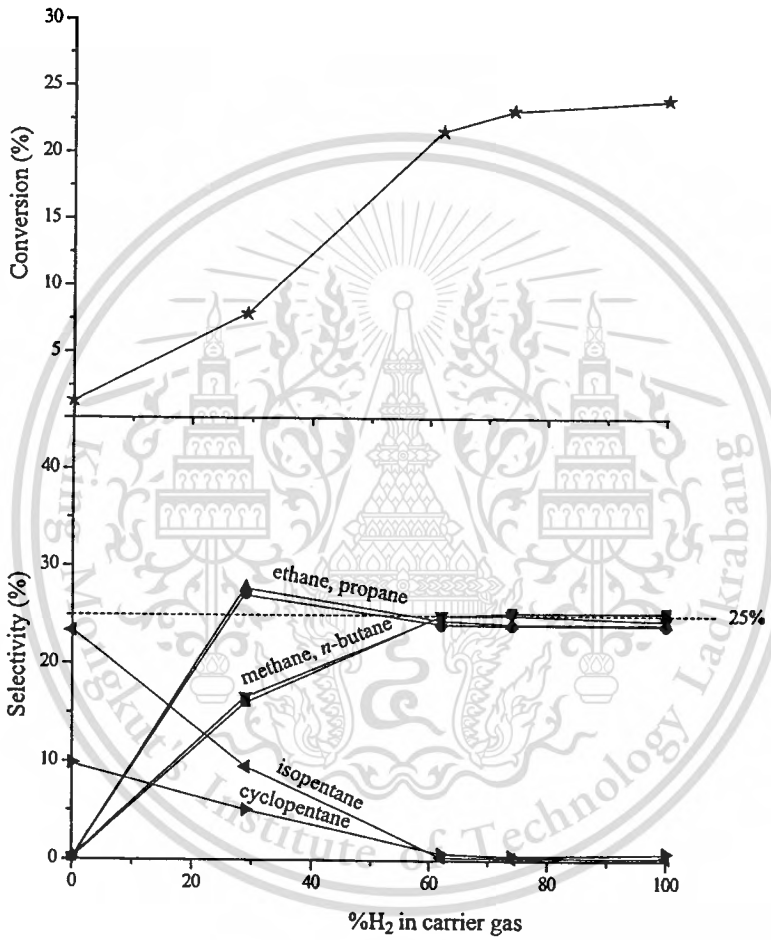

Figure 6.18 Effect of H_2 partial pressure for *n*-pentane conversion over Pt/TiO_2 (1wt.%) at 300°C, W/F = 271 g h/mol, reduction/reaction temperature 300°C. (Other products at 0%H_2 in carrier gas : isopentene (~40%), 1-pentene (~5%), cyclopentene (~10%), cyclopentadiene (~10%)).

As seen in Figure 6.18, the product selectivity is altered from non-selective hydrogenolysis to more selective ethane-propane hydrogenolysis, when the H_2 partial pressure is decreased. This is because the lower H_2 partial pressure reduces the electron density of the Pt metal surface. Therefore, adsorption accordingly to the intermediate I configuration, which possesses the highest electron density is preferred. As the intermediate I is highly promoted, hydrogenolysis to ethane-propane would be proportionally obtained.

In the absence of H_2, all of *n*-pentane cannot be converted to hydrogenolyzed products because of no available H atom on the Pt metal surface to combine with the akylidyne intermediate. However, such intermediate can isomerize to isopentane and cyclopentane, as main products.

The catalyst stability, when the reaction is performed at different H_2 partial pressure, is shown in Figure 6.19. It is found that full H_2, as carrier gas, shows higher stability than that of others. This is because the H_2 plays role for cleaning surface of Pt metal by dissociative chemisorption and reacting with the adsorbed species to form certain less adsorptive products. This provides available Pt sites for further coming hydrocarbon feed to be activated. When the H_2 partial pressure is reduced, the products can be retained on the Pt metal surface and subsequently oligomerized to the high molecular weight compounds or coke on the surface causing lower stability, as observed in Figure 6.19.

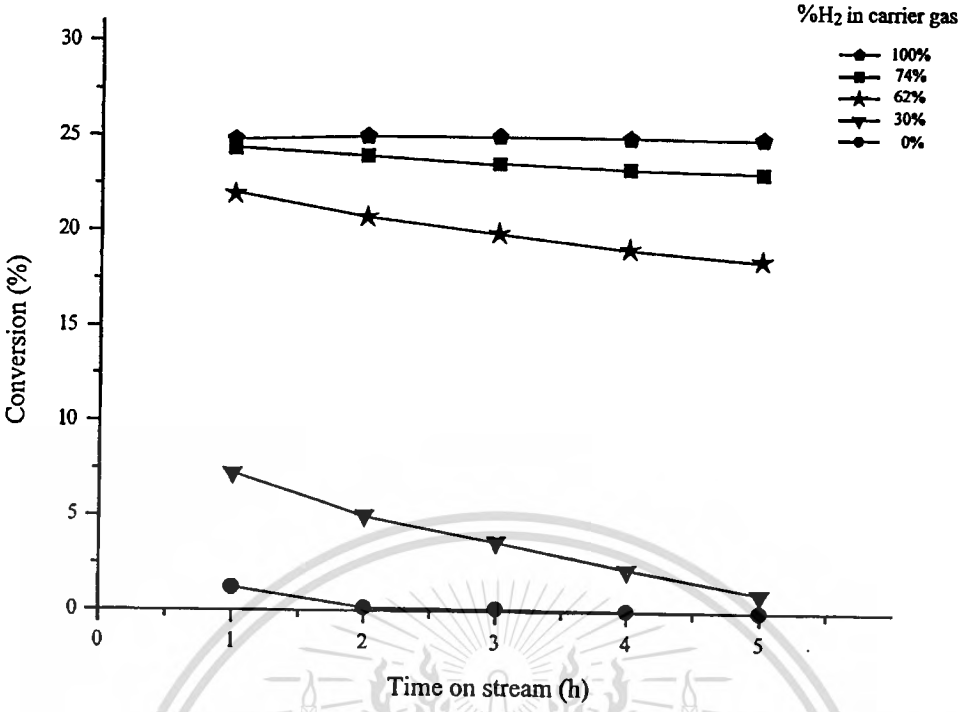

Figure 6.19 Conversion of *n*-pentane over Pt/TiO_2 (1 wt.%) at 300°C in various H_2 partial pressures (W/F = 271 g h/mol).

In consistent with the observed stability, TGA of the used Pt/TiO_2 from the reaction with different H_2 partial pressure is shown in Figure 6.20. It is found that higher coke content is obtained when the H_2 partial pressure is decreased. There are three weight loss at 60°C, 200°C, and 600°C. The first peaks is attributed from water desorption. The second and the third peaks may attribute from the desorption of the light and hard cokes, respectively. When the reaction is performed at 100%H_2 in carrier gas, both cokes can be slightly formed (0.67 wt.%). As the H_2 partial pressure is decreased, higher content of such cokes is observed. In the absence of H_2 (0%H_2 in carrier gas), high content of light coke is formed and further oligomerized over Pt metal surface to higher molecular weight coke. Therefore, it can be desorbed/decomposed at temperature higher than 200°C.

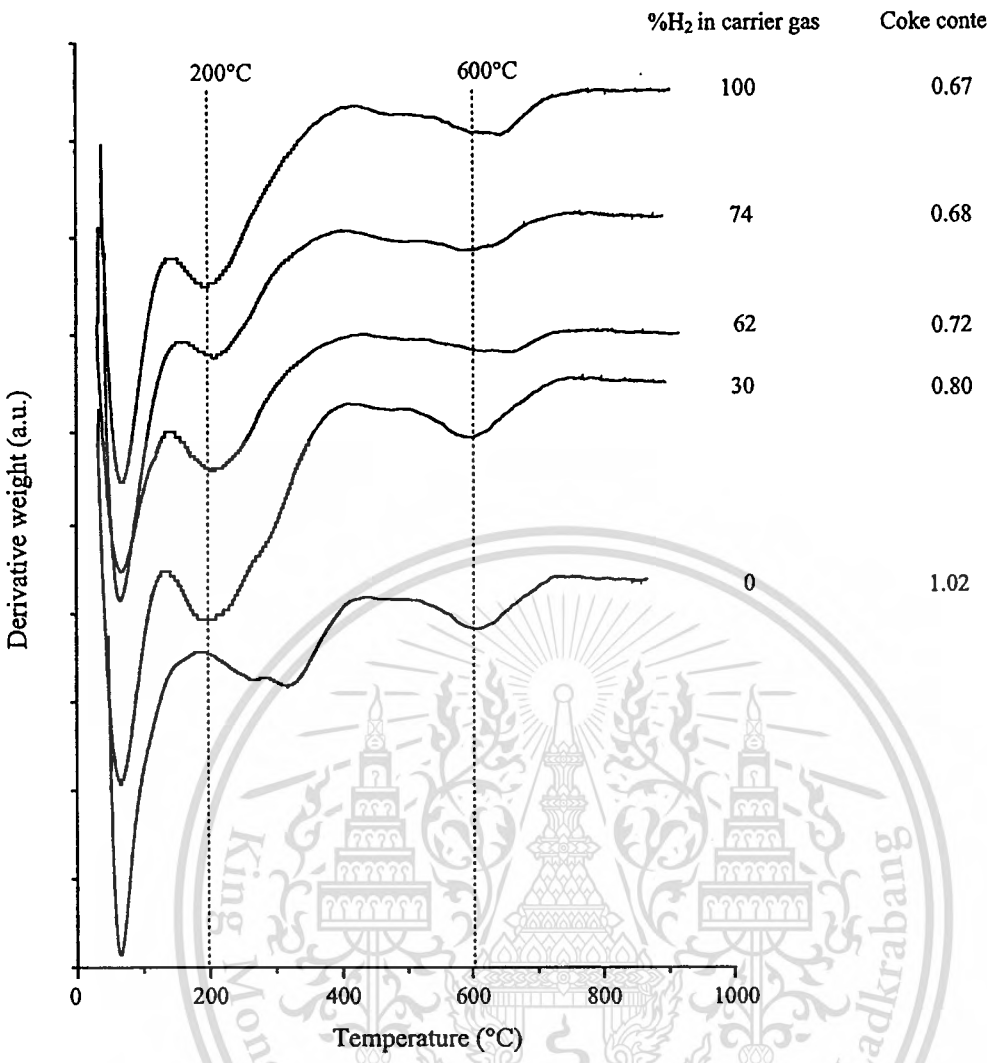

Figure 6.20 TGA (in air) of used Pt/TiO_2.

The TPD-MS experiment of the used Pt/TiO_2 catalyst (30% H_2 in carrier gas) is examined to speculate the existence of the light and hard cokes. As seen in Figure 6.21, the light coke which is desorbed at 200°C shows the mass number mainly at 27 and 42 atomic unit. These may be the fragment of *n*-pentane or isopentane which are parts of light coke. In consistence with TGA, desorption at 600°C shows the mass number additionally at 53, 67, 76, 80, and 88 atomic unit. This attributes to the aromatics fragment that is decomposed from the hard coke in the catalyst. It is noted that the mass number at 35 and 36 atomic unit found especially from the desorption at 600°C may be attributed to the desorption of chlorine species retained in the catalyst.

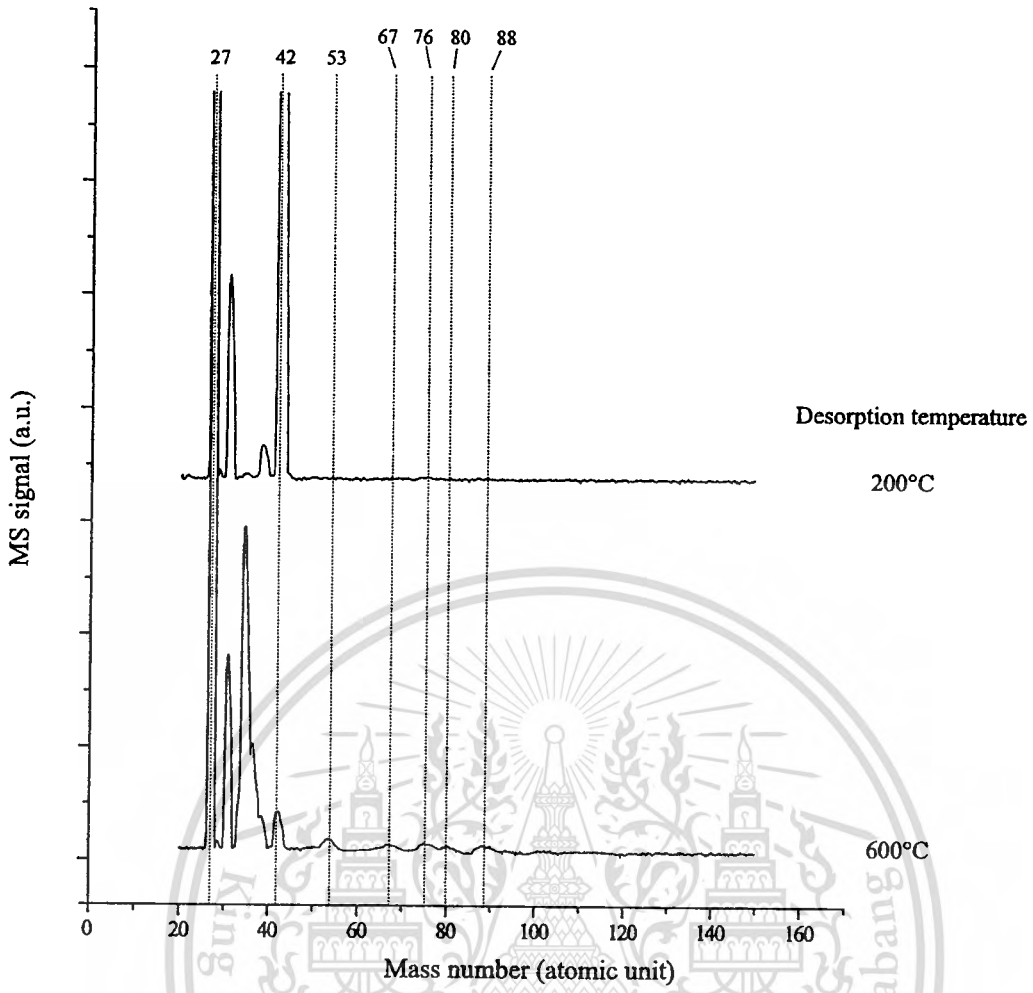

Figure 6.21 TPD-MS of coke formed over Pt/TiO_2 after *n*-pentane conversion at 30% H_2 partial pressure.

6.3.2.4 Effect of feed structure

As known from the previous sections, the Pt/TiO_2 possesses high activity for *n*-pentane hydrogenolysis to light hydrocarbons at 300°C. Other pentane isomers, i.e., isopentane and cyclopentane are examined in this section to study the effect of feed structure on such hydrogenolysis. The reaction is performed in H_2 as carrier gas for 4 hours, then H_2 is replaced by flow of He. The results are shown in Figure 6.22.

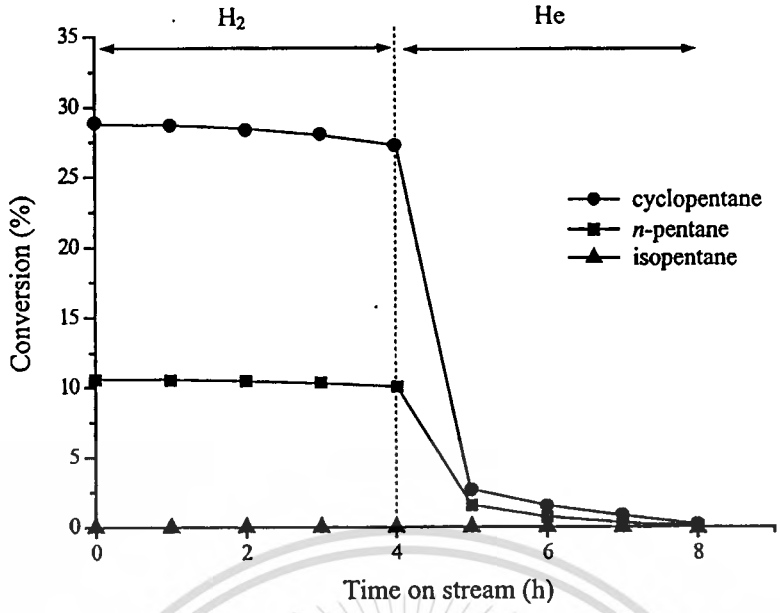

Figure 6.22 *n*-Pentane, isopentane, and cyclopentane conversion over Pt/TiO_2 (1 wt.%) calcined at 300°C, reduction/reaction temperature 300°C, W/F = 407 g h/mol.

It is found in Figure 6.22 that cyclopentane shows higher conversion (28%), as compared to that of *n*-pentane (11%) and isopentane (0%). This is because cyclopentane can be highly adsorbed over Pt metal surface. Cyclopentane that possesses the lower vapor pressure (250 mmHg @ 20°C) would be easily adsorbed on the Pt surface, as compared to that of *n*-pentane (440 mmHg @ 20°C) and isopentane (570 mmHg @ 20°C). In case of isopentane, it is not able to adsorb over the Pt metal surface, presumably due to its branch structure that is too steric to be interacted with the small Pt metal cluster (Figure 6.4). Therefore, no conversion of isopentane is observed.

After switching the carrier gas to He, both *n*-pentane and cyclopentane conversion is markedly decreased. This is because the H_2 is required to promote the dissociative adsorption of hydrocarbon on the Pt metal surface and cleaning the surface for the available Pt metal site. Without H_2, pentanes adsorption is not favored. Subsequently, it cannot be activated and converted to products. Moreover, as the Pt metal cannot be cleaned, the accumulation of the high molecular weight hydrocarbon would be taken place causing the catalyst deactivation, as observed in Figure 6.22.

The product selectivities of cyclopentane and *n*-pentane conversions are shown in Figure 6.23. It is found that cyclopentane is readily hydrogenolized to *n*-pentane with 100% selectivity (Figure 6.23(a)). This suggests that the ring opening by C-C hydrogenolysis is mainly activated for cyclopentane over Pt/TiO_2 catalyst. However, the produced *n*-pentane cannot be further reacted even if *n*-pentane can be also hydrogenolyzed over this catalyst to light hydrocarbons (Figure 6.23(b)). This is because the produced *n*-pentane cannot be competitively adsorbed with cyclopentane. As *n*-pentane is not able to adsorb and be activated, its conversion is not facilitated.

After switching the carrier gas to He, cyclopentane is mainly converted to cyclopentene, while *n*-pentane is mainly converted to C_5 olefins (isopentene, 1-pentene, cyclopentene, and cyclopentadiene). This corresponds to the proposed reaction pathway in Figure 6.17 that C-H dissociation is the primary step to create the akylidyne intermediate. The hydrogenolysis of such intermediate is not facilitated in the absence of H_2 due to no available H atom to combine and release out as hydrogenolyzed products. This leads to coke formation, as mentioned previously. Moreover, for hydrogenolysis which is a structure sensitive reaction, such coke can retard the C-C bond activation and further decrease hydrogenolysis activity. However, the structure insensitive reaction, such as dehydrogenation (C-H activation) can still be promoted, as observed by small amount of C_5 olefins.

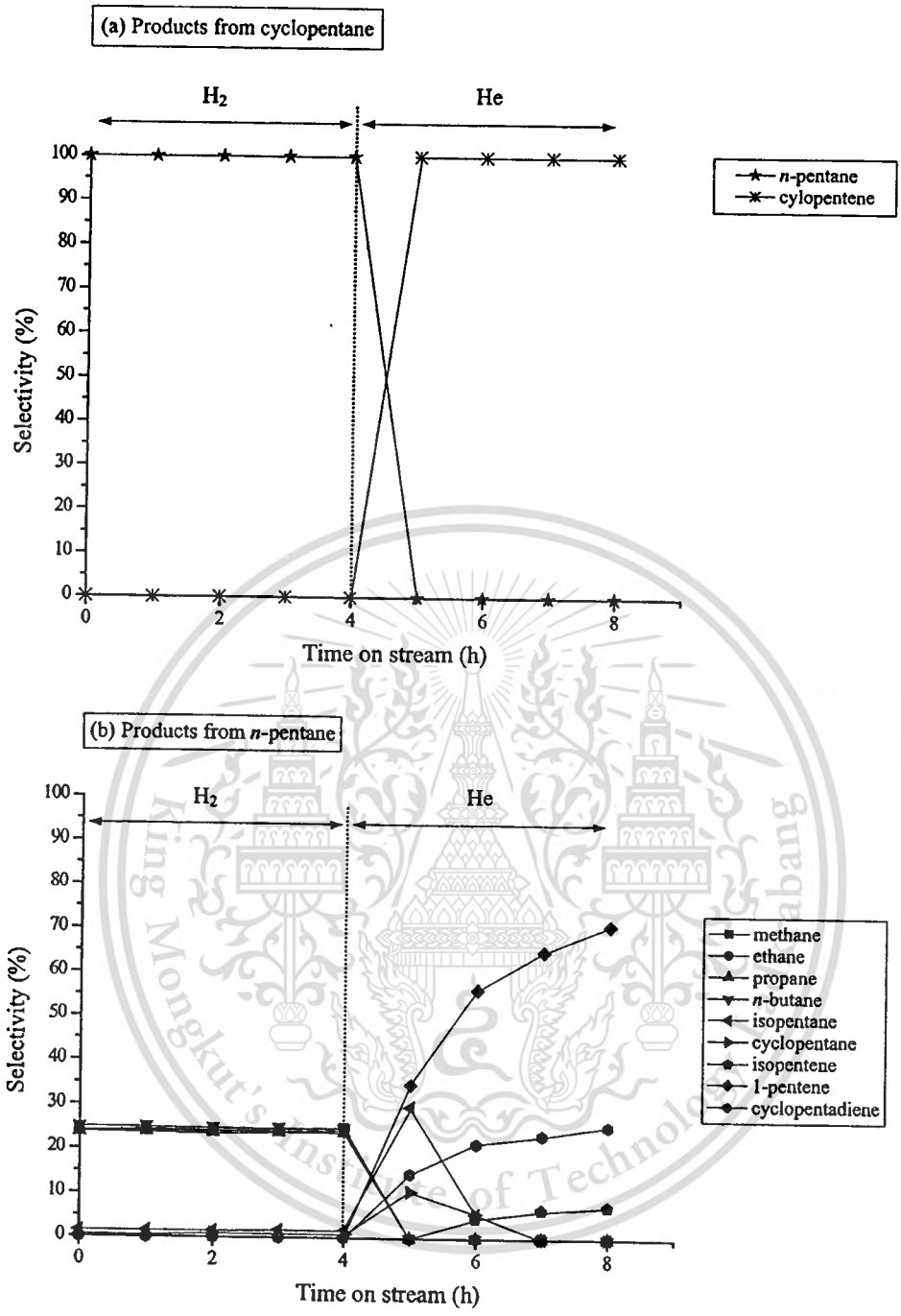

Figure 6.23 Products from (a) cyclopentane and (b) *n*-pentane conversion over Pt/TiO_2 (1 wt.%) calcined at 300°C, reduction/reaction temperature 300°C, W/F = 407 g h/mol.

6.4 Conclusion

The Pt/TiO_2 catalyst shows high hydrogenolysis activity for converting *n*-pentane to light hydrocarbons (methane, ethane, propane and *n*-butane) at 300°C. By impregnation method, Pt species are highly dispersed over TiO_2 support causing small metal cluster after reduction. The H_2 is required in the reaction to promote the electron density of the Pt metal surface and keep the Pt metal surface to be clean by facilitating desorption of products. With the small metal surface, the C-C rearrangement reactions (isomerization and cyclization) are not facilitated.

Some of platinum ions can diffuse into the TiO_2 framework after calcination at high temperature (500°C). To obtain high available Pt metal surface, Pt/TiO_2 calcined at low temperature (300°C) is employed. However, after reduction or reaction (in H_2) at high temperature (500°C), the strong metal support interaction (SMSI) facilitates the formation of TiO_x film covering the Pt metal surface leading to the lower in hydrogenolysis activity. Therefore, H_2 reduction and the hydrogenolysis reaction must be also performed at low temperature (300°C). Nevertheless, the TiO_x film can promote isomerization and cyclization of *n*-pentane but its activity is lower than that of the hydrogenolysis activity of Pt metal surface.

The chlorine species can be retained in the catalyst, especially the Pt/TiO_2 calcined and reduced at low temperature (300°C). Such species would make the Pt metal surface to be an electron deficient (possesses acidity). Over this catalyst, non-selective hydrogenolysis of *n*-pentane is promoted. However, the lower in H_2 concentration can improve the ethane and propane selectivity because their intermediate can be more stabilized.

The feed structure plays important role on the activity and product selectivity. Isopentane with its branch structure cannot adsorb over the small Pt metal surface. No conversion of isopentane is observed at the condition studied. In contrast, cyclopentane can highly adsorbed and be hydrogenolyzed to *n*-pentane. The *n*-pentane product cannot competitively adsorb with cyclopentane; therefore its further reaction is not facilitated. In the absence of H_2, the C-C activation is prohibited but the C-H activation can be promoted converting *n*-pentane and cyclopentane to 1-pentene and cyclopentene, respectively.

6.5 References

[1] Gates, B.C. 1992. **Catalytic chemistry.** New York: John Wiley & Sons.

[2] Satterfield, C.N. 1993. **Heterogeneous catalysis in industrial practice.** Singapore: McGraw-Hill.

[3] Hagen, J. 2006. **Industrial Catalysis.** Weinheim: WILEY-VCH Verlag GmbH & Co. KGaA.

[4] Davis, B.H. 1999. "Alkane dehydrocyclization mechanism." **Catalysis Today.** 53: 443-516.

[5] Bent, B.E. 1996. "Mimicking aspects of heterogeneous catalysis: generating, isolating, and reacting proposed surface intermediates on on single crystals in vacuum." **Chemical Review.** 96: 1361-1390.

[6] Ruppert, A.M. and Paryjczak, T. 2007. "$Pt/ZrO_2/TiO_2$ catalysts for selective hydrogenation of crotonaldehyde: Tuning the SMSI effect for optimum performance." **Applied Catalysis A: General.** 320: 80-90.

[7] Lin, C., Chao, J., Liu, C., Chang, J. and Wang, F. 2008. "Effect of calcination temperature on the structure of a Pt/TiO_2 (B) nanofiber and its photocatalytic activity in generating H_2." **Langmuir.** 24: 9907-9915.

[8] Hulzinga, T., and Prins, R. 1983. "Electron spin resonance investigations of platinum supported on Al_2O_3 and TiO_2." **Journal of Physical Chemistry.** 87: 173-176.

[9] Chien, S., Kuo, M., Lu, C. and Lu, K. 2004. "Spectroscopic studies of NO reduction on Pt/TiO2 catalysts." **Catalysis Today.** 97: 121-127.

[10] Salama, T.M., Ebitani, H.K., Hattori, H., and Kita, H. 1994. "Electron paramagnetic resonance studies of reduced platinum supported on titanium oxide: Effect of hydrogen adsorption-desorption on paramagnetic Pt (I) and Ti (III) species." **Chemistry of Materials.** 6: 21-26.

[11] Suriye, K., Lobo-Lapidus, R.J., Yeagle, G.J., Praserthdam, P., Britt, R.D., and Gates B.C. 2008. "Probing defect sites on TiO_2 with $[Re_3(CO)_{12}H_3]$: Spectroscopic characterization of the surface species." **CHEMISTRY: A European Journal.** 14: 1402-1414.

[12] Suriye, K., Praserthdam, P., and Jongsomjit, B. 2005. "Impact of Ti^{3+} present in titania on characteristics and catalytic properties of the Co/TiO_2 catalyst." **Industrial and Engineering Chemistry Research.** 44: 6599-6604.

[13] Liang, H., Zhang, Y., and Liu, Y. 2008. "Three-dimensionally ordered macro-porous Pt/TiO_2 catalysts used for water gas shift reaction." **Journal of Natural Gas Chemistry.** 17: 403-408.

[14] Panagiotopoulou, P., Christodoulakis, A., Kondarides, D.I., and Boghosian, S. 2006. "Particle size effects on the reducibility of titanium dioxide and its relation to the water-gas shift acivity of Pt/TiO_2 catalysts." **Journal of Catalysis.** 240: 114-125.

[15] Watterich, A. Hofstaetter, A., Wuerz, R., and Scharmann, A. 1996. "Ti^{3+} centers in reduced $ZnWO_4$: Ti single crystals." **Solid state Communications.** 100: 513-518.

[16] Li, Q., Wang, K., Zhang, S., Zhang, M., Yang, J., and Jin, Z. 2006. "Effect of photocatalytic activity of CO oxidation on Pt/TiO_2 by strong interaction between Pt and TiO_2 under oxidizing atmosphere." **Journal of Molecular Catalysis A: Chemical.** 258: 83-88.

[17] Zhang, M., Jin, Z., Zhang, Z., and Dang, H. 2005. "Study of strong interation between Pt and TiO_2 under oxidizing almosphere." **Applied Surface Science.** 250: 29-34.

[18] Vishwanathan, V. and Narayanan, S. 1993. "Evidence for strong metal support interaction (SMSI) in Rh/TiO_2 system." **Catalysis Letter.** 21: 183-189.

[19] Haller, G.L., Resasco, D.E. 1989. "Metal-support interation: Group VIII metal and reducible oxides." Advances in Catalysis. 36: 173-235.

[20] Radivojevic, D., Seshan, K., and Lefferts, L. 2006. "Preparation of well dispersed Pt/SiO_2 catalysts using low temperature treatments." **Applied Catalysis A: General.** 301: 51-58.

[21] Zhou, Y., Wood, M.C., and Winograd, N. 1994. "A time of flight SIMS study of the chemical nature of highly dispersed Pt on alumina." **Journal of Catalysis.** 146: 82-86.

[22] Brumberger, H., Delaglio, F., Goodisman, J., Phillips, M.G., Schwarz, J.A., and Sen, P. 1985. "Investigation of the SMSI catalyst Pt/TiO_2 by small-angle scattering." **Journal of Catalysis.** 92: 199-210.

[23] Kelley, M.J., Short, D.R., Swartzfager, D.G. 1983. "In situ TEM and ISS studies of supported metal 'SMSI' catalysts." **Journal of Molecular Catalysis.** 20: 235-249.

CHAPTER 7

CONCLUSIONS AND SUGGESTIONS

7.1 Conclusions

This thesis has studied the conversion of C_5 hydrocarbons, i.e., *n*-pentane, cyclopentane, and isopentane. Using a particular designated catalyst, such C_5 are readily converted to desired products. Over GaZSM-5 and ZnZSM-5, pentanes can be catalyzed to aromatics (CHAPTER 4). Over Pt/SiO_2, pentanes can be cyclized to cyclic olefins (CHAPTER 5). Over Pt/TiO_2, pentanes can be hydrogenolyzed to light hydrocarbons (CHAPTER 6). This section would summarize the results obtained from each chapter as follow:

In CHAPTER 4, the aromatics can be obtained over the shape selective GaZSM-5 and ZnZSM-5 catalysts at 500°C. With the pore restriction of HZSM-5, the activities are in the order of cyclopentane (26%) > isopentane (13%) > *n*-pentane (10%). However, after Ga loading by impregnation, the higher activity are obtained from the Ga active sites (GaO^+ and GaH_2^+) which are located outside and inside the pore leading to isopentane (47%) > cyclopentane (37%) > *n*-pentane (29%). With the dehydrogenation activity of GaO^+ and GaH_2^+, *n*-pentane and isopentane are primarily converted to branch hydrocarbon pool that is cracked to C_1-C_4. The formed C_1-C_4 are oligomerized to aromatics pool that are further cracked to BTX and C_{9+} alkyl aromatics. While, cyclopentane is primarily converted to cyclic hydrocarbon pool that is further cracked to C_{9+} indane derivatives. The formed C_{9+} indane derivatives are further cracked to C_1-C_4 and BTX. Over ZnZSM-5, the reaction path way seems to be similar as over GaZSM-5 but the loss of active site by evaporation is likely observed. The aromatics formation can be improved by lowering the Si/Al ratio of the catalyst. However, the aromatics are decreased when the reaction is operated at high temperature. Moreover, reduction of GaZSM-5 at 550°C creates the most active gallium specie, i.e., GaO^+ and GaH_2^+. The product selectivity remains unchanged although the different gallium active sites are employed suggesting that the reaction pathway over GaZSM-5 depends on the structure of C_5, irrespective to the type of gallium species. In addition, higher coke formation is obtained in the reaction with low H_2 concentration.

In CHAPTER 5, the cyclic olefins, i.e., cyclopentene and cyclopentadiene can be obtained from *n*-pentane conversion over Pt/SiO_2 catalyst at 500°C. Larger Pt metal cluster obtained from H_2 reduction at 500-650°C promotes *n*-pentane adsorption and cyclization. The H_2

is required to enhance the electron density of the Pt metal surface. Moreover, the H_2 also keeps the Pt metal surface clean by facilitating desorption of products. To obtain high available Pt metal surface, the Pt/SiO_2 catalyst would be calcined at low temperature (300°C). This is because some of PtO_x can be embedded into the SiO_2 framework after calcination at high temperature. However, after calcination and reduction some of chlorine species can be retained in the catalyst leading the Pt metal surface to be an electron deficient and possess acidity. This acid site promotes undesired reactions, such as isomerization and hydrogenolysis. Nevertheless, the chlorine species can be decreased by reduction at higher temperature causing the suppression of any undesired reactions. In the mechanistic point of view, cyclization, isomerization, hydrogenolysis, and dehydrogenation of *n*-pentane take place in parallel. However, the hydrogenolysis can be avoided by keeping the reaction temperature not higher than 500°C. The feed structure plays important role on the activity and product selectivity. Isopentane shows lower adsorption over Pt metal surface, as compared to that of *n*-pentane and cyclopentane leading to low conversion of isopentane. The hydrogenolysis, isomerization and cyclization are not facilitated because the C-C bond activation of isopentane is retarded by its branch structure. However, the dehydrogenation is the major reaction for converting isopentane to isopentene via C-H bond activation. Cyclopentane is feasibly adsorbed over Pt metal surface. The C-C bond activation is preferred leading to the ring disclosure creating *n*-pentane as main product. In the absence of H_2, all C-C bond activation cannot be taken place. However, only C-H bond can be activated converting *n*-pentane, isopentane, and cyclopentane to 1-pentene, isopentene, and cyclopentene, respectively.

In CHAPTER 6, hydrogenolysis of *n*-pentane to light hydrocarbon is a model reaction to test the hydrogenolysis activity of Pt/TiO_2. By impregnation, Pt species are highly dispersed over TiO_2 support causing small metal cluster after reduction. With the small metal surface, the Pt/TiO_2 shows high hydrogenolysis activity at 300°C. In addition, the H_2 is required in the reaction to promote the electron density of the Pt metal surface and keep the Pt metal surface to be clean by facilitating desorption of products. It is found that some of platinum ions can diffuse into the TiO_2 framework after calcination at high temperature (500°C). Therefore, to obtain high available Pt metal surface, Pt/TiO_2 calcined at low temperature (300°C) is employed. However, after reduction or reaction (in H_2) at high temperature (500°C), the strong metal support interaction (SMSI) facilitates the formation of TiO_x film covering the Pt metal surface leading to the lower in hydrogenolysis activity. In addition, the chlorine species can be retained in the

catalyst, especially the Pt/TiO_2 calcined and reduced at low temperature ($300^{\circ}C$). Such species would make the Pt metal surface to be an electron deficient. Over this catalyst, non-selective hydrogenolysis of *n*-pentane is promoted. However, the lower in H_2 concentration can improve the ethane and propane selectivity because their high stable intermediate can be facilitated. The activity and product selectivity are affected by the feed structure of C_5. Isopentane with its branch structure cannot adsorb over the small Pt metal surface. No conversion of isopentane is observed. In contrast, cyclopentane can highly adsorbed and be hydrogenolyzed to *n*-pentane. The *n*-pentane product cannot competitively adsorb with cyclopentane; therefore its further reaction is not facilitated. In the absence of H_2, the C-C activation is prohibited but the C-H activation can be promoted converting *n*-pentane and cyclopentane to 1-pentene and cyclopentene, respectively.

7.2 Suggestions

7.2.1 In this thesis, the continuous flow experiment is performed to obtain the catalytic activity of the catalyst. However, the pulse experiment should be incorporated. With the accurate feed content in each pulse, the initial conversion over the fresh catalyst and the turnover number are obtained. Moreover, the transient behavior of the active sites can be studied using this technique.

7.2.2 Despite the flow experiment has attempted to determined the catalytic activity of the active sites, there is lack of *in situ* studied. This system can exhibit their local catalytic activity and a true active species may well be revealed. Thus, an *in situ* investigation of the nature of metal species obtained at different temperature treatments (calcination and reduction) should be studied using XPS and/or EXAFS techniques.

7.2.3 With the feed structure that can effect to the reaction pathway, other hydrocarbon feeds, i.e., alkyl cyclopentane, larger linear and cyclic alkanes should be examined to generalize the aromatization, cyclization and hydrogenolysis over the catalysts.

7.2.4 The biomass conversion to valuable hydrocarbons can be presumably applied using the specified catalysts. The Pt/TiO_2 may well be suitable for elimination of oxygenated function by C=O or C-O- hydrogenolysis to give the petrochemical grade paraffinic hydrocarbons. The aromatics and cyclic olefins can be further obtained from aromatization and cyclization of such hydrocarbons over the GaZSM-5 and Pt/SiO_2 catalysts, respectively.

APPENDIXES

APPENDIX A

EXPLOSIVE LIMITS IN AIR

Lower Explosive Limit (LEL): The lowest concentration (percentage) of a gas or a vapor in air capable of producing a flash of fire in presence of an ignition source (arc, flame, heat). At a concentration in air below the LEL there is not enough fuel to continue an explosion.

Upper Explosive Limit (UEL): The Highest concentration (percentage) of a gas or a vapor in air capable of producing a flash of fire in presence of an ignition source (arc, flame, heat). Concentration higher than UEL are "too rich" to burn.

Table A1 Explosive limit of pentanes in air.

Name	$T_{freezing}$ (^{o}F)	$T_{boiling}$ (^{o}F)	LEL (vol.%)	UEL (vol.%)
n-Pentane	-201.51	96.93	1.4	7.8
Isopentane	-255.82	82.11	1.4	7.6
Cyclopentane	-136.91	120.65	1.4	9.4

Source: Carl L. Yaws, 1997. "Handbook of Chemical Compound Data for Process Safety." Elsevier Science & Technology Books.

APPENDIX B

Standard X-ray diffraction pattern of ZSM-5 zeolite

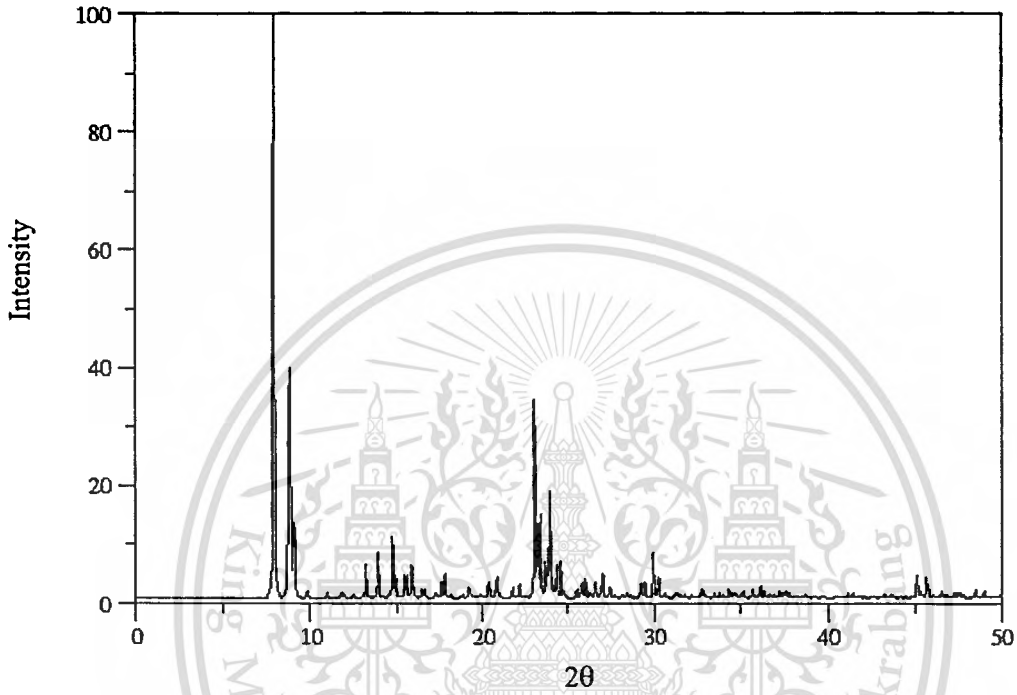

Figure B1 Standard X-ray diffraction pattern of ZSM-5

Source: http://izasc-mirror.la.asu.edu/cgi-bin/collection1.py

APPENDIX C

MOLECULAR DIAMETER OF SOME HYDROCARBONS

Table C1 Molecular diameter of some hydrocarbons.

Name	Structure	Diameter (Å × Å)
n-Pentane		6.92 × 3.07
Isopentane	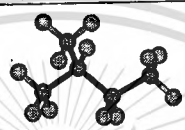	5.63 × 3.17
Cyclopentane		4.26 × 4.26
Benzene		4.96 × 4.96
Toluene		5.88 × 4.29
m-Xylene	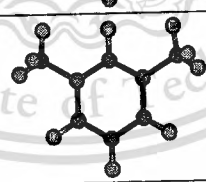	6.64 × 4.95
p-Xylene		6.95 × 4.29
Ethylbenzene	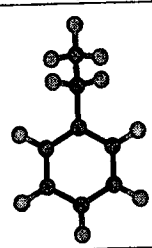	6.16 × 4.29

Name	Structure	Diameter (Å × Å)
1-ethyl-3-methyl-Benzene	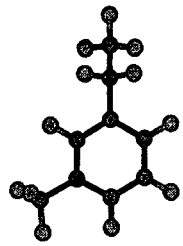	6.88 × 5.50
1,2,3-trimethyl-Benzene	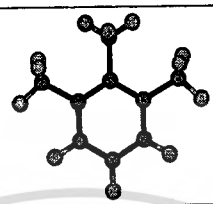	6.75 × 5.41
2-ethyl-1,3-dimethyl-Benzene		6.81 × 6.75
2,3-dihydro-4-methyl-1H-Indene	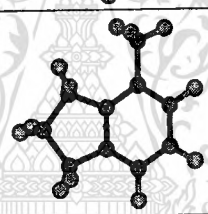	6.72 × 5.92
1,2,3,4-tetrahydro-Naphthalene	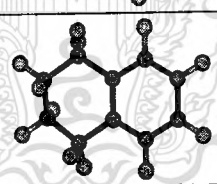	7.25 × 4.94
Naphthalene	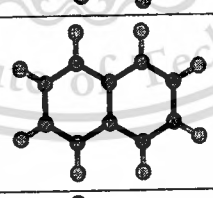	6.75 × 4.98
1-methyl-Indane	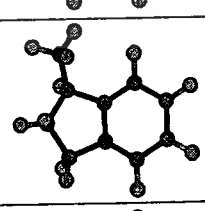	7.33 × 5.46
Indane	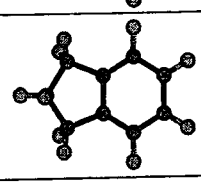	6.73 × 4.99

Note: These molecular diameters are derived from the optimized structure using the density functional theory B3LYP calculation with 6-31G(d,p) basis set. All atoms in the model are allowed to fully relax and the calculations are performed by using the Gaussian 03 program. The details of the program are written in Frisch, M. J. T., G. W., Schlegel, H. B., Scuseria, G. E., Robb, M. A., Cheeseman, J. R., Montgomery, J. A., Jr., Vreven, T., Kudin, K. N., Burant, J. C., Millam, J. M., Iyengar, S. S., Tomasi, J., Barone, V., Mennucci, B., Cossi, M., Scalmani, G., Rega, N., Petersson, G. A., Nakatsuji, H., Hada, M., Ehara, M., Toyota, K., Fukuda, R., Hasegawa, J., Ishida, M., Nakajima, T., Honda, Y., Kitao, O., Nakai, H., Klene, M., Li, X., Knox, J. E., Hratchian, H. P., Cross, J. B., Adamo, C., Jaramillo, J., Gomperts, R., Stratmann, R. E., Yazyev, O., Austin, A. J., Cammi, R., Pomelli, C., Ochterski, J. W., Ayala, P. Y., Morokuma, K., Voth, G. A., Salvador, P., Dannenberg, J. J., Zakrzewski, V. G., Dapprich, S., Daniels, A. D., Strain, M. C., Farkas, O., Malick, D. K., Rabuck, A. D., Raghavachari, K., Foresman, J. B., Ortiz, J. V., Cui, Q., Baboul, A. G., Clifford, S., Cioslowski, J., Stefanov, B. B., Liu, G., Liashenko, A., Piskorz, P., Komaromi, I., Martin, R. L., Fox, D. J., Keith, T., Al-Laham, M. A., Peng, C. Y., Nanayakkara, A., Challacombe, M., Gill, P. M. W., Johnson, B., Chen, W., Wong, M. W., Gonzalez, C., Pople, J.A. 2004. **Gaussian 03**, *reVision E.01*, Gaussian, Inc.: Wallingford, CT.

AUTHOR BIOGRAPHY

Name Mr. Nipat Peamaroon

Birth Date January 20, 1979

Birth Place Lopburi, Thailand

Education

Year Institution Degree/diploma

1997 King Mongkut's Institute of Technology North Bangkok
Certificate in Technical Education (Electrical and Electronics)

2001 King Mongkut's Institute of Technology North Bangkok
Bachelor of Engineering (Chemical Engineering)

2004 Kasetsart University
Master of Science (Chemistry), major in Physical Chemistry

2004 Ramkhamhaeng University
Bachelor of Science (Mathematics)

Scholarships

1) Higher Education Development Scholarship, Rambhai Barni Rajabhat University (2006-2011)

2) Research Assistant Scholar, Siam Cement Group Company (2008)

3) Teaching Assistant Scholar, Department of Chemistry, King Mongkut's Institute of Technology Ladkrabang (2009-2010)

Publications

1) Peamaroon, N. and Sooknoi, T. 2009. "Aromatization of cyclopentane over GaZSM-5 and ZnZSM-5 catalyst." (oral) in The Pure and Applied Chemistry International Conference 2009. Phitsanulok: Naresuan University.

2) Peamaroon, N. and Sooknoi, T. 2009. "Effect of H_2/steam on Ga active sites in GaZSM-5 for isopentane transformation." 122-126. in The 6th International Symposium on Advance Material in Asia-Pacific Rim. Bangkok: Chulalongkorn University.

3) Peamaroon, N. and Sooknoi, T. 2010. "*n*-Pentane conversion over Pt/SiO_2: Effect of calcination temperature." 781-783. in The Pure and Applied Chemistry International Conference 2010. Ubon Ratchathani: Ubon Ratchathani University.

4) Peamaroon, N. and Sooknoi, T. 2011. "Aromatization of cyclopentane over ZSM-5 catalysts: A proposal of reaction pathway." Petroleum Science and Technology Journal. In press.

Work Experience

Year situation Institute

2004 Special lecturer at Faculty of Industrial Technology, Thepstri Rajabhat University

2004-present Lecturer at Faculty of Science and Technology, Rambhai Barni Rajabhat University